Hot Mix Asphalt
Recycling
PRACTICES AND PRINCIPLES

Mohamad Mohajeri

Hot Mix Asphalt **Recycling**

PRACTICES AND PRINCIPLES

PROEFSCHRIFT

ter verkrijging van de graad van doctor
aan de Technische Universiteit Delft,
op gezag van de Rector Magnificus prof. ir. K.C.A.M. Luyben,
voorzitter van het College voor Promoties,
in het openbaar te verdedigen op 28 Januari 2015 om 10:00 uur

door

Mohamad Mohajeri
MSc, University of Tehran
geboren te Shahre Rey, Tehran, Iran

Dit proefschrift is goedgekeurd door de promotor:
Prof. dr. ir. A.A.A. Molenaar
Copromotor:
Ir. M.F.C. van de Ven

Samenstelling promotiecommissie:

Rector Magnificus,	Technische Universiteit Delft, voorzitter
Prof. dr. ir. A.A.A. Molenaar,	Technische Universiteit Delft, promotor
Ir. M.F.C. van de Ven,	Technische Universiteit Delft, copromotor
Prof. dr. A. Scarpas,	Technische Universiteit Delft
Prof. dr. ir. H. E. J. G. Schlangen,	Technische Universiteit Delft
Prof. dr. P.C. Rem,	Technische Universiteit Delft
Prof. dr. G. Airey,	University of Nottingham
Prof. dr. G. Thenoux,	Pontificia Universidad Catolica de Chile
Prof. dr. ir. K. Van Breugel,	Technische Universiteit Delft, reserve lid

Published and distributed by:
Mohamad Mohajeri
Section of Road and Railway Engineering
Faculty of Civil Engineering and Geosciences
Delft University of Technology
P.O. Box 5048, 2600 GA Delft, the Netherlands
E-mail: mohajeri_me@yahoo.com
ISBN 9789461864215
Printing: Wohramann Print Service, Zutphen, the Netherlands
©2015 by Mohamad Mohajeri

All rights reserved. No part of this publication may be reproduced, stored in a retrieval system or transmitted in any form or by any means, electronic, mechanical, photocopying, recording, or otherwise without the prior permission of the proprietor.

To my wife, Elham
and my wonderful kids Parmis and Arvin

ACKNOWLEDGEMENT

With completion of this thesis I approach the end of my journey in obtaining my PhD. In the very beginning, the only thing mattered to me was the end of this journey. At this moment, when I am almost there, and the things that matter to me is the journey itself and the people and the parties who made it possible for me. I take this opportunity to say "THANKS" to all those who accompanied me through unforgettable part of my life.

My work was mainly sponsored by Delft University of Technology and it was conducted in the Road and Railway Engineering section in the Faculty of Civil engineering. It was also partly sponsored by Gebr. Van der Lee contracting company and I wish to express my gratitude to this company not only because of making available necessary funds but also because of their big support in making their laboratory equipment, technical personnel and asphalt production facilities (batch plant and double drum mixer) available to this project. Without this it would have been impossible to do important parts of my research. Their support went well above what can be expected from a sponsoring body. Therefore a wholeheartedly thank especially mr Eddy van der Lee, director of Gebr van der Lee contracting company, for this great support offered to me.

At this moment of accomplishment, I pay homage first of all to my promoter Professor Andre Molenaar and my daily supervisor Associate Professor Martin van de Ven for their guidance, coaching and mentoring in my research. Andre and Martin, I appreciate the freedom you provided me in my research as well as the efforts you made to keep my rabbit mind on track. Otherwise I would have been lost in my journey and would have ended up nowhere. You were always available if I had issues even other than my PhD project. I have been always moved by your international and humanistic approach towards Master and PhD students. You made the science of "Black Asphalt Pavements" in our department, interestingly colorful and pleasant by gathering students from all over the world. I was lucky to know great people like you as the very first impressions of the Dutch nation. That made me optimistic about this society.

I also like to acknowledge Mark Oostveen because of his interest in providing practical and technical supports at Gebr van der Lee's company during my experiments in their construction projects and asphalt plants. I learned a lot on hot mix asphalt regulations from Dr. Eyassu Hagos as the head of R&D and his assistant Girum Mengiste. They also provided great help in conducting the heavy tasks of sampling and sample preparation in the lab as well as in the field. I would like to extend my thanks to Mimoun, Sander, Jacqueline,

Dominique and other production and QC personnel of Gebr. Van der Lee's company.

I acknowledge with gratitude the contribution of Professor Schlangen to my research by helping me with the Nano-indentation tests in the Microlab. He and His PhD student Quantao helped me a lot in sample preparation and doing the tests parallel to their own research. I also acknowledge Wim Verwaal for his help in conducting the Nano CT scanning of my bitumen samples.

I like to thank Alexander Schmets and Sayedah Nahar and Professor Scarpas for their enthusiasm and cooperation on conducting AFM on the morphology of RA the blending zone. The results of their research are not included in this thesis but I have learned a lot by working with them.

Most of the results described in this thesis would not have been obtained without the support and collaboration of the laboratory staff at the Road and Railway Research Laboratory of TU Delft. I gratefully acknowledge Jan Moraal, Jan- Willem Bientjes, Marco Poot, Dirk Doedens, and Jacqueline Barnhoorn for their help and support during my research in our section. I am also grateful to the Associate Professors in our section, ir Lambert Houben, Dr Rien Huurman and ir Ad Pronk for their openness in providing any kind of help and support.

It is not possible to work in the lab without sharing knowledge and equipment with other PhD colleagues. I acknowledge Dr. J. Qui for sharing me that precious experience on extracting and recovery of bitumen. I acknowledge Ning Li for his help in conducting the direct tension and compression test. I gratefully acknowledge the contribution that Ahmadullah Chacho and Girum Mengiste had made to my thesis during their MSc studies. Words of thanks are also extended to my former PhD colleagues, many of them have already their PhD degrees, and present PhD fellows Dr. Gang Liu, Dr. Dongxing Xuan, Dr. Milliyon Woldekidan, Dr. Diederik van Lent, Dr. Maryam Miradi. Dr. Sadegh Akbarnejad, Dr. Yue Xiao, Dr. Alem Alemgena, , Dr. Mingliang Li, Dr. Wim van den Bergh, Dr. Maria Moldova, Dr. Oscar Arias-Cuevas, Chang, Dongya, Yuan, Shaoguang, Nico, Maider, Jingang, Pungky and PengPeng. I enjoyed every moment of their companion during coffee breaks, social events, laboratory activities and I enjoyed all those happy moments playing table tennis with my professional Chinese friends.

I would like to thank my Iranian friends and family who made my stay in the Netherlands more joyful: Zahra, Nader, Shadi, Nazi, Mahnaz, Reza, Ali, Alieh, Mehdi, Azadeh, Shahnam, Mona, Sanaz, Somi, Kamran, Farid, Marjan, Ashkan, Zohreh, Soheil, Kianoush, Mohammadreza, Elnaz, Shahram, Mehranoosh, Vahid, Firoozeh and many others whom I have to spend a whole

page to list them. I specially thank Sara Fekri for her artistic design of the cover page on this book.

I have to extend my gratitude to many of my Dutch friends who supported me and my family in the Netherlands from the very beginning. I have to acknowledge Anya, Peter and the Family van Zwol–Schröder.

It's my fortune to gratefully acknowledge the support of some special individuals. Words fail me to express my appreciation to Abdol Miradi. Beside his support as the head of the laboratory, he helped me a lot in getting settled down in Delft with my family. He and his lovely wife and his daughter, Maryam, and Nasim, hosted us in our arrival to Delft. Their family supports allowed me to be more focused on my PhD project. Abdol and Maryam made us feel home in Delft and made a perfect family network for us during these years. They have been our advisors in all aspects of our life in Delft. They should write a book of "*how to start a living in the Netherlands for dummies*".

It is not just enough to say thank you to my parents, Shahla and Sayad, for their endless love throughout my life. They taught me to be patient and to stay encouraged during every up and down in my life. I should extend my love and thanks to my parents in law Eshagh and Tahereh for their encouragements and support. My wife and I were lucky to be brought up in two large families with our lovely siblings; Maryam, Mostafa, Mojtaba, Elham, Elhaeh, Elnaz and Behnaz. Thank you all for sharing me your love when I was thousands of kilometers away from you.

A journey is more joyful and easier when you travel together with a dedicated partner. Therefore, finally but most importantly, I have to thank my wife, Elham. Words are short to express my gratitude for her love, patience, assistance, and supports. We got married at the end of my bachelor study and she was the only one who kept me motivated the whole way through my PhD. She is the one who is always keeping the compass and pointing to the mountaintops. She sacrifices her studies and her profession temporarily to allow me following my dreams. Thank you for bringing up two wonderful kids, Parmis and Arvin, whom have filled my life with playfulness and love. When I started my PhD, Parmis just started learning how to read and write. She was always exited to know how many pages my book would count when completed. Thank you Parmis to motivate me in writing such a thick book ☺☺☺.

Mohamad Mohajeri

9 December 2014

SUMMARY

Hot mix asphalt recycling has become common practice all over the world since the 1970s because of the crisis in oil prices. In the Netherlands, hot recycling has advanced to such an extent that in most of the mixtures more than 50% of reclaimed asphalt (RA) is allowed. These mixtures with such a high RA content are produced in a batch plant to which a parallel drum is attached. In this drum RA is pre-heated to approximately 130°C. Since 2007 another hot mix recycling techniques became available in which RA is mixed in cold and moist condition in contrary to conventional methods. It is a so called double barrel drum mixer. In this method virgin aggregates are superheated in the inner drum and mixed with cool and moist RA and fines and virgin bitumen in the outer drum. In both cases, double drum and partial heating methods, the virgin aggregates have to be pre-heated to higher temperatures than with mixtures without RA in order to achieve a mixing temperature of around 170°C. Dependent on RA amount, moisture, pre-heating, etc. in the batch plant the virgin aggregates have to be pre-heated to around 300° C and in the double barrel drum to around 500°C. These high temperatures have led to concerns about the quality of the produced mixtures. Since 2008, a new Dutch specification system for asphalt mixtures is in place in line with the European standards (EN13108 series). The new regulation gives contractors freedom to select their own material such as bitumen grade and the amount of recycling; however, in return it makes them responsible for the quality of the mixture. The mixture should fulfill the requirement of fundamental performance characteristics of the mixtures such as resistance to fatigue and permanent deformation.

In this research two major questions have been investigated. One of the questions is whether these high temperatures have a negative effect on the bituminous binder, while the other important question is whether the RA binder will blend totally with the virgin binder that is added.

The focus of this research was on four objectives. The first objective was to develop a laboratory mixing method to simulate the real recycling process in the field. The second objective was to assess the effect of the double barrel drum on the mixture quality in comparison with conventional batch plant. Third, it was aimed to measure the blending degree between two binders. And finally, to increase the understanding of the mechanism behind blending RA binders with virgin bitumen, with focus on their micro structure.

To cover all research topics, this dissertation is organized in two parts in which the first part is devoted to laboratory and field mixture evaluation while

the second part is presenting the exploratory research on the fundamental aspects of blending.

Research in part 1 is conducted in two phases, laboratory simulation and field experimentation. The conventional partial warming recycling method (PW) the upgraded double drum mixing method (UPG) were simulated in the lab and the quality of mixtures were compared with the standard mixing method (SM) in the lab at different RA content and different moisture content. This research showed that higher percentages of RA results in higher stiffness and lower fatigue life. However in the UPG method with 4% moisture and 60% RA, the mixture became remarkably lower in stiffness and durable against fatigue. This might be because of the lack of blending or the effect of foaming of bitumen. It was concluded that the UPG method could not effectively be simulated in the lab.

In the next experimental phase of the study, three identical mixtures were produced with 50% RA and 4.3% bitumen. One mixture was produced in a batch plant (BB) while the second one was mixed using a double drum mixer by the same contractor (A). The third mixture was produced in the laboratory (L) using a lab pugmill mixer. The comparison between three mixtures shows that mixture L has a higher stiffness than A and BB. Mixture BB has as slightly higher stiffness than A. Furthermore, mixture A has the lowest stiffness which is most probably due to the system of cold and moist RA feeding into the double drum system.

Besides the 4PB fatigue and stiffness test, monotonic uniaxial tension (UT) and compression (UC) tests were performed to be used in material modeling and to determine a fatigue endurance limit. The limit value of the stress ratio parameter (R_{limit}) was determined which is useful in the determination of the endurance limit in a three-dimensional state. It shows that different mixing methods lead to different endurance limits. It turns out that the plant produced mixture has a higher endurance limit than the laboratory mixture.

In this research an infrared thermography method was used in every material preparation stage. The temperature homogeneity of the mixtures in the lab and in the field was investigated. It proved to be a useful method in visualizing the temperature exchange during mixing and compaction.

In Part 2, the effect of superheating aggregates is studied by simulating RA and real aggregates with glass beads and artificial aged binder. The stage extraction method was evaluated in this research with respect to size and shape of aggregates.

The blending and diffusion mechanism between old and new bitumen is studied at the microstructure level by means of Nano indention and Nano-CT

scanning. The morphology of different types of bitumen was detectable by these techniques; however the blending zone couldn't be characterized.

SAMNEVATTING

Hergebruik van asfalt (HMA recycling) is in de jaren 1970 in opkomst gekomen als gevolg van de olie crisis in die tijd. Hergebruik van asfalt in Nederland heeft zich inmiddels zodanig ontwikkeld dat in de meeste mengsels meer dan 50% geregenereerd asfalt (RA) is toegestaan. Deze mengsels met een dergelijk hoog RA gehalte worden geproduceerd in een batch plant met een parallel trommel. In deze parallel trommel wordt RA voorverwarmd tot ongeveer 130°C en het wordt samen met het nieuw toe te voegen materiaal in de batch plant bij een temperatuur van ca 170°C gemengd. Sinds 2007 is in Nederland een nieuwe HMA recycling techniek beschikbaar waarin de onverwarmd en vochtig RA gemengd wordt met andere nieuwe materialen. Deze nieuwe techniek wordt de dubbele drum menger (double barrel) genoemd. In deze methode wordt nieuw aggregaat oververhit in de binnentrommel en gemengd met vochtig RA en het nieuwe bitumen in de buitenste trommel. Zowel bij de double drum als bij de batch plant met parallel trommel, moeten de nieuwe aggregaten worden voorverwarmd tot hogere temperaturen dan met mengsels zonder RA om een mengtemperatuur van ongeveer 170° C bereiken. Bij de batch plant moet het nieuwe aggregaat tot ongeveer 300° C worden voorverwarmd terwijl dit bij de double drum ongeveer 500° C is afhankelijk van RA gehalte, vochtgehalte, voorverwarming temperatuur van RA, etc...

De hoge voorverwarming temperatuur van nieuw aggregaat heeft geleid tot zorgen bij klanten over de kwaliteit van het geproduceerde mengsel.

Sinds 2008 is, een nieuw Nederlands specificatie systeem voor asfalt in gebruik dat in overeenstemming is met de Europese normen (EN13108-serie). Aannemers zijn volgens de nieuwe regeling vrij om hun eigen materiaal zoals bitumen en de hoeveelheid RA te selecteren (behalve voor SMA en ZOAB); ze zijn daarmee volledig verantwoordelijk voor de kwaliteit van het mengsel. Het mengsel moet voldoen aan de vereiste functionele eigenschappen zoals weerstand tegen vermoeiing en permanente vervorming.

Twee belangrijke onderwerpen zijn onderzocht in dit project. Een er van is of de hoge voorverwarmings temperatuur invloed heeft op de eigenschappen van het bitumineuze bindmiddel, terwijl de andere belangrijke vraag is of het RA bindmiddel volledig zal mengen met het nieuwe bitumen dat wordt toegevoegd. De focus van dit onderzoek lag op vier doelstellingen om het probleem te bestuderen vanuit verschillende aspecten. Het eerste doel was om een laboratorium mengmethode te ontwikkelen om het echte proces in de meng installatie zo goed mogelijk te simuleren. Het tweede doel was om de kwaliteit van het mengsel uit de double drum te beoordelen en te vergelijken met het batch plant mengsel. De derde doelstelling was om de mate van

blending tussen twee bindmiddelen te bepalen. En ten slotte is onderzoek gedaan naar het mechanisme achter de mogelijke blending tussen het RA bindmiddel en het nieuwe bitumen op basis van hun micro-structuur.

Dit proefschrift bestaat uit twee delen; het eerste deel (Part 1) gaat over de evaluatie van een lab gemengd asfalt en hetzelfde mengsel uit praktijk. In het tweede deel worden de fundamentele aspecten van blending bestudeerd. Het onderzoek in Part 1 is uitgevoerd in twee fasen, te weten een laboratorium simulatie en experimenten in de praktijk. De conventionele (SM) methode, de methode met gedeeltelijke opwarming van de RA (PW) en de double drum mengmethode (UPG) zijn gesimuleerd in het laboratorium en de kwaliteit van de mengsels is vergeleken met de standaard mengmethode (SM) zoals die in het laboratorium wordt toegepast voor verschillende RA percentages en verschillende vochtgehalten. Aangetoond werd dat een hoger RA percentage leidt tot een hogere stijfheid en een lagere vermoeiingslevensduur. Echter in de UPG methode met een vochtgehalte van 4% en een RA gehalte van 60% had het mengsel een opmerkelijk lagere stijfheid en een hogere weerstand tegen vermoeing. Dit kan zijn vanwege de onvolledige blending of het effect van schuimvorming van bitumen. Uiteindelijk was de conclusie dat de double drum methode niet goed kan wordenin het lab kan worden gesimuleerd.

In de volgende experimentele fase van de studie werden drie identieke mengsels geproduceerd met een RA gehalte van 50% en een bitumengehalte van 4,3%. Eén mengsel werd geproduceerd in een batch plant (BB) terwijl hetzelfde mengsel ook werd geproduceerd in een double drum menger (A) door dezelfde aannemer. Het derde mengsel werd geproduceerd in het laboratorium (L) met een lab menger. Uit een vergelijking tussen de drie mengsels blijkt dat mengsel L een hogere stijfheid heeft dan mengsels A en BB. Mengsel BB heeft een iets hogere stijfheid dan A. Dat mengsel A de laagste stijfheid heeft wordt waarschijnlijk veroorzaakt door de toevoeging van koude en vochtige RA in de double drum menger. Monotone uni-axiale trek- en drukproeven zijn uitgevoerd ter bepaling van de treksterkte (UT) en druksterkte (UC). Daarnaast zijn 4 puntsbuigproeven (4PB) uitgevoerd ter bepaling van de mengselstijfheid en vermoeiingsweerstand. De resultaten zijn gebruikt om de zogenaamde “fatigue endurance limit” (FEL) te bepalen.

Een grenswaarde voor de verhouding van aanwezige spanning tot toelaatbare spanningsparameter (Rlimit) is bepaald, welke bruikbaar is voor de bepaling van de FEL in een driedimensionale toestand. Aangetoond is dat de verschillende mengmethoden leiden tot verschillende FEL waardes. Het blijkt dat het in de asfaltmenginstallatie geproduceerde mengsel een hogere FEL waarde heeft dan het in het laboratorium gemengde materiaal.

Een infrarood thermografie methode is gebruikt tijdens het onderzoek voor elke materiaal voorbereidingsfase. Zowel de (in)homogeniteit van de

temperatuur van het mengsel in het laboratorium als in het veld zijn onderzocht. Het bleek het een uitermate nuttige methode is voor het visualiseren van de temperatuur uitwisseling tijdens het mengen en verdichten.

In Part 2 is de mogelijke invloed van oververhitting van aggregaten op de mate van blending en bitumeneigenschappen onderzocht door de RA en echte aggregaten te simuleren met glasparels en kunstmatig verouderd bindmiddel. Met een in fasen uitgevoerde extractie (stage extraction) is onderzocht of er bitumineus tweelagen systeem met verschillende rheologische eigenschappen rond de aggregaatkorrels aanwezig is. Daarbij is tevens rekening gehouden met de grootte van de korrels. Zo'n tweelagensysteem kon niet eenduidig worden vastgesteld maar er is een verschil in rheologische eigenschappen van de bitumen teruggewonnen van de verschillende aggregaatkorrels.. Het mechanisme van blending en diffusie tussen oud en nieuw bitumen is onderzocht op microstructuur niveau met behulp van Nanoindentation en Nano CT-scanning. Met deze technieken was de morfologie van verschillende typen bitumen detecteerbaar, maar de meng zone kon niet worden gekarakteriseerd.

TABLE OF CONTENTS

SUMMARY I

GENERAL INTRODUCTION 1

i. Hot mix asphalt recycling 1

ii. Problem statement 3

iii. Research objectives 5

iv. Scope and organization of the thesis 5

Part 1- Effect of the HMA recycling process on mixture properties 9

CHAPTER 1. Introduction to Part 1 11

1.1. INTRODUCTION 11

1.2. LITERATURE SURVEY 14

1.2.1. Hot mix recycling facilities 14

1.2.2. Segregation 26

1.2.3. Bitumen aging 27

1.2.4. Temperature 29

1.2.5. Mixing time 30

1.2.6. Type of mixing process (facility type) 30

1.2.7. Residual moisture in aggregate 30

1.2.8. Properties of recycled binder 30

1.2.9. Mix design with RA 31

1.2.10. Blending of RA and virgin binders 33

1.2.11. Effect of extraction and recovery methods on RA Binder 36

1.3. CONCLUSION AND SUMMARY OF THE LITERATURE SURVEY 38

CHAPTER 2. Experimental Design for PART 1 41

2.1. EXPERIMENTAL PLAN 41

2.1.1. Experimental plan of Phase I 42

2.1.2. Experimental plan of Phase II 45

2.2. TESTING METHODS AND INSTRUMENTATION 47

2.2.1. Specific gravity by ultra-pycnometer 47

2.2.2. Extraction and recovery of RA and compacted mixtures 48

2.2.3. Rheological tests on bituminous binder 49

2.2.4. Modelling bitumen viscoelasticity (master curves) 51

2.2.5. Four point bending stiffness and fatigue test *53*
2.2.6. Indirect tensile strength *55*
2.2.7. Indirect tensile stiffness and fatigue test *56*
2.2.8. Uniaxial monotonic direct tension test (UMDTT) *58*
2.2.9. Uniaxial monotonic direct compression test (UMDCT) *59*
CHAPTER 3. Material and Mixture Design 61
3.1. INTRODUCTION 61
3.2. MIXTURE DESIGN PROCEDURE 62
3.2.1. RA Characterization *62*
3.2.2. Determination of combined aggregate gradation *66*
3.2.3. Virgin bitumen grade and quantity determination *69*
3.2.4. Determination of bulk specific gravity *69*
3.2.5. Mixing and sample preparation procedures *74*
CHAPTER 4. Infrared Thermography 85
4.1. INTRODUCTION 85
4.2. EXPERIMENTAL DESIGN 87
4.2.1. Material and TMIT instrumentations *88*
4.2.2. Results and discussion *91*
4.2.3. Conclusions *108*
CHAPTER 5. Analysis of the Mechanical Characterization Test Results 111
5.1. INTRODUCTION 111
5.2. TEST RESULTS OF PHASE I 111
5.2.1. Indirect tensile stiffness modulus test (ITSM) *112*
5.2.2. Indirect tensile strength (ITS) *125*
5.2.3. Fatigue life evaluation *129*
5.2.4. The effect of mixing time and air voids content *135*
5.2.5. Conclusions of Phase I *141*
5.3. TEST RESULTS OF PHASE II 142
5.3.1. Four point bending (4PB) flexural stiffness *142*
5.3.2. 4PB fatigue life *149*
5.3.3. Conclusions of fatigue life results *156*
5.3.4. Uniaxial monotonic direct compression Test (UMDC) *157*
5.3.5. Uniaxial monotonic direct tension test (UMDT) *177*
5.4. THE MATERIAL MODEL 192

5.4.1. Response surface 192
5.4.2. Material model at uniaxial stress state 195
5.4.3. Determining yield surface for fatigue test conditions 196
5.4.4. Relation between yield surface and fatigue life 199
5.4.5. Fatigue endurance limit (FEL) 205
5.4.6. Conclusions and summary of Phase I and Phase II 208
PART 2- Exploratory Studies on Mixing, Blending and Diffusion 213
CHAPTER 6. Introduction to Part 2 215
6.1. PROBLEM STATEMENT 215
6.2. ORGANIZATION OF PART 2 216
6.3. LITERATURE SURVEY 218
6.3.2. Physical and chemical aspects of RA binder 221
6.4. AGING INDEX 222
6.5. MICROSTRUCTURE OF THE RA BINDER 223
6.6. CONCLUSIONS OF THE LITERATURE REVIEW 226
CHAPTER 7. Blending of RA and virgin binder and the effect of superheated aggregates 227
7.1. INTRODUCTION 227
7.2. EXPERIMENTAL DESIGN 228
7.2.1. Mixtures 229
7.3. MATERIALS AND PROCESSES 231
7.3.1. Development of extraction and recovery method 232
7.4. STAGE EXTRACTION 235
7.4.1. Background 235
7.4.2. Extraction test in two layers 237
7.5. MATERIAL 240
7.5.1. Artificial RA binder 240
7.5.2. The rotating cylinder aging test (RCAT) 241
7.5.3. Rheological evaluation of aged binders 242
7.5.4. Glass beads 244
7.5.5. Mixtures 246
7.6. RESULTS AND ANALYSIS 252
7.6.1. Mixture 1 252
7.6.2. Mixture 2 255

7.6.3. Mixture 3 ..... *260*
7.7. CONCLUSIONS 264
CHAPTER 8. Rheological Study on Possible Effects of Diffusion on Blending of RA Binder 267
8.1. INTRODUCTION 267
8.1.1. Background on diffusion *268*
8.2. MLBS SETUP AND MATERIALS 271
8.2.1. Results and discussion on diffusion *276*
8.2.2. Results and discussion on effective shear modulus *284*
8.3. CONCLUSIONS 286
8.4. RECOMMENDATION 287
CHAPTER 9. Morphology of the blending interfaces of RA binder 289
9.1. INTRODUCTION 289
9.2. MORPHOLOGY RESEARCH METHODOLOGY 291
9.3. NANO INDENTATION 291
9.4. NANO COMPUTED TOMOGRAPHY SCANNING 292
9.5. MATERIALS AND SPECIMEN PREPARATION 293
9.5.1. Material Preparation for nano CT scanning *293*
9.5.2. Material preparation for nano indentation and optical microscopy *294*
9.6. EXPERIMENTS AND RESULTS 295
9.6.1. Light polarized microscopy imaging *295*
9.6.2. Nano indentation results *296*
9.6.3. Nano computed tomography imaging results *300*
9.7. CONCLUSIONS 303
CHAPTER 10. General conclusions and recommendations 305
10.1. CONCLUSIONS ON PART 1 305
10.2. CONCLUSIONS ON PART 2 308
10.3. RECOMMENDATIONS 309
BIBLIOGRAPHY 311
APPENDICES 319
Appendix A Volumetric properties of Specimen *319*
Appendix B Details of stiffness values (Phase I) *329*
Appendix C Details of stiffness values (Phase II) *330*



GENERAL INTRODUCTION

i. Hot mix asphalt recycling

Crushed asphalt particles which become available as the result of pavement rehabilitation or from rejected and surplus production, still remain to be of value, primarily because of its quality mineral aggregates and bituminous constituent. They are called Reclaimed Asphalt Pavement (RAP) in the United States or Reclaimed Asphalt (RA) in accordance with EN 13108-8[1].

RA binders, which got hardened and aged, chemically and physically, during production and construction (STA[2]) and service life (LTA[3]), can still be reused in new mixtures by means of rejuvenation or blending with very soft bitumen. This process is called asphalt recycling which comprises handling, sorting and mixing of reclaimed asphalt into a new mixture in a hot, warm or cold mixing process. This is known and implemented for almost a century. The first recorded recycling project dates back to 1915 [1] though it was not widely used till the 1970`s when the bitumen price strongly increased as the result of the oil crisis. Ever since, asphalt recycling has become attractive for both road authorities and contractors because of economic and environmental reasons.

In the Netherlands, especially, shortage of new mineral aggregates (coarse crushed stones) and limitations set to waste landfills, contributed to a rapid evolutionary change in the asphalt recycling industry after the oil crisis in 1970. The Dutch government firstly focused on cold feed with the batch plant and after that warm feed using a parallel drum. The MARS (in the late 1980`s) and Renofalt (1976) projects were developed by industry and supported by the Dutch government and aimed to recycle 100% RA. RA was

[1]EN13108-8 Bituminous Mixtures- Material Specifications- Part 8: Reclaimed asphalt)

[2]Short Term Aging

[3]Long Term Aging

preheated by a Microwave in the MARS project and by means of steam processing in the Renofalt project.

However, these processes became less attractive because it was much easier to equip conventional batch plants with a parallel drum dryer (for drying and preheating RA). The cost of a parallel drum installation was very soon compensated for the contractors by replacing 50% expensive new material with RA in all types of HMA mixtures except surface layers. At this moment 38 batch plants in the Netherlands are equipped with the parallel drum dryer to preheat RA to 130°C prior to mixing.

Since 2007 another mixing facility became available to the Dutch market being the Double Barrel Drum Mixer (patented by ASTEC). Contrary to conventional batch plants, it is a continuous process in which cold RA is being introduced directly to superheated virgin material in an outer drum. This study is partly devoted to studying the mixture quality of double drum produced mixtures in comparison with mixtures which are produced in the conventional way with a parallel drum.

In 1990, the Dutch government recognized RA as a "normal" building material and it was incorporated in the Dutch Standard (RAW). The effect of economy and government legislation on the amount of RA usage is demonstrated clearly in Figure 1.1. The annual production of hot and warm mix asphalt is plotted together with the amount of RA used in it.

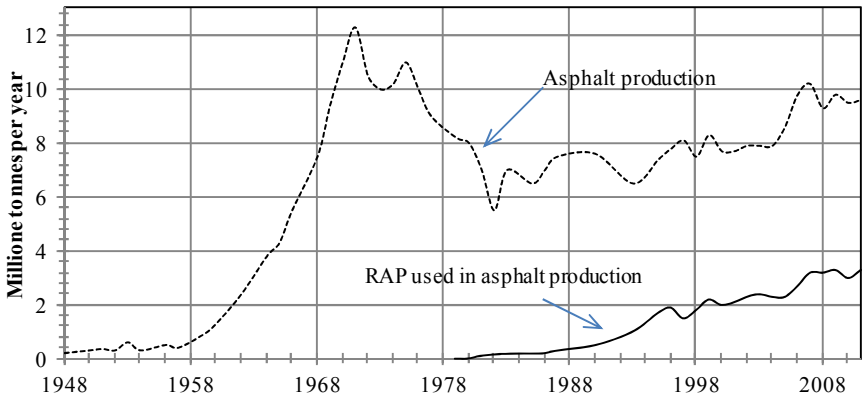

Figure 1.1: Asphalt production (hot and warm mix) and amount of RA used in asphalt mixtures [[2], [3]]

This chart also demonstrates three distinctive periods. *First*, after World War II, the HMA production increased rapidly from 0.2 million tons (in 1954) to

12 million tons per year (in 1970). *Next*, in the 1970`s, because of the global economy and oil crisis, the production almost halved to 6 million ton in (1982). *The third* period (1980-2011) is characterized with an increase of reusing RA which becomes available because of pavement maintenance and rehabilitation operations. Nowadays, at least 80% of the available RA in the Netherlands is used in new hot and warm mix production. It makes Netherlands in this field one of the most active countries in Europe (see Table 1.1 below).

Table 1.1Recycling of RA in Europe [3]

Country	***RA available in 2011 (million tons)***	***Amount of available RA used in asphalt production (%)***
Denmark	0,6	80
Germany	14	84
Netherlands	4	83
Sweden	1,1	70

ii. Problem statement

Since 1990, RA is recognized in the Netherlands as a normal construction material and it is allowed to mix up to 50% RA with virgin materials to produce recycled HMA for base courses using conventional modified batch plants. Furthermore, road authorities used to prescribe the mix design and material properties. Since 2008, a new Dutch specification system for asphalt mixtures is in place in line with the European standards (EN13108 series). According to the new regulations, road authorities are not prescribing the material and the procedure anymore, but fundamental performance characteristics of the mixtures such as resistance to fatigue and permanent deformation must fulfill the specified requirements. It implies that contractors are responsible to do everything themselves in achieving a CE marking certification for each mixture design. On one hand the new regulations give contractors the freedom to use their own mixture designs including as much as possible RA in their mixtures, on the other hand, contractors have to proof the performance level of the mixtures by means of type testing to be done in accordance with EN13108-19.

As it was explained earlier, the most common way of HMA recycling in the Netherlands is based on the method of RA partial warming in which RA is preheated to maximum 130°C in a parallel drum and is then mixed with preheated virgin material (in a pug mill mixer) to achieve a mixture temperature between 160-180°C.

Mixing of higher RA contents implies higher preheating temperatures of the virgin aggregates. This issue becomes more crucial when more than 50% cold RA is used in a double barrel drum mixer, because virgin aggregates have to be superheated up to 500°C. Mixing superheated aggregates with a high amount of moist RA has raised some questions about the quality of such mixtures. Although asphalt recycling has been one of the most researched topics in this discipline, there are still significant uncertainties about the quality of recycled mixtures.

The viscoelastic behavior of bituminous materials (including hot recycled mixtures) is primarily determined by the time and temperature dependent properties of the bituminous binder. Several models are available to predict asphalt concrete behavior from binder or mastic properties. Chemical and physical issues in terms of *blending* between RA and virgin binder (or any rejuvenator), pose a challenge for designers to predict the mixture properties. Although designers are using blending charts to predict viscosity characteristics of the binder of the recycled mixture from the RA binder and added virgin binder, there are still doubts about their applicability for all kind of recycled mixtures because of the unlikely assumption of 100% blending between RA and virgin binder.

Furthermore, there is still relatively little knowledge on the properties of the aged RA binder with respect to its chemical and physical interaction with virgin[1] binder. Moreover, the complexity of the bitumen micro-structure makes it extremely difficult to explain the mechanism of blending.

The final point to emphasize here is that the RA handling circumstances (including moisture and preheating temperature) are not considered in standard laboratory mixing methods which are widely used to estimate the properties of mixtures produced in a real plant.

In summary, this research program was initiated to address the following problems.

- There is uncertainty about the performance level of hot recycled mixtures containing high amounts of RA produced with the double barrel technique.

[1]Fresh bitumen

- Laboratory mixing methods as currently applied seem to be not realistic enough in simulating real plant mixing techniques
- There are no measures of the efficiency of the mixing process of different recycling plants.
- The applicability of current mix design methods has to be examined rigorously.

iii. Research objectives

The main goal of this study is to explore different aspects of high RA contents in recycled HMA with regards to RA handling conditions like moisture content and preheating temperatures.

In order to achieve this goal, the following objectives are identified:

1- To develop an effective laboratory mixing method to simulate the real recycling process in the field.
2- To assess the effect of the double barrel drum recycling process on the properties of a mixture in comparison with the conventional batch plant.
3- To explore techniques to develop an appropriate way for measuring the degree of blending between two binders.
4- To increase the understanding of blending RA binders with virgin bitumen, with focus on their microstructure.

iv. Scope and organization of the thesis

This dissertation consists of two separate parts which allow to coherently presenting all the research results and conclusions. Part 1 is devoted to laboratory and field mixture evaluation, while Part 2 presents the exploratory research on fundamental aspects of blending. An overview of the structure of the research and thesis is illustrated in Figure 1.2.

General Information.

Before starting with Part 1 and Part 2, *general information* is provided to give a background to asphalt recycling issues. Also the main research objective and its main goal are defined.

PART 1

All experiments and observations related to recycled mixture properties are explained and presented in this part. This part itself consists of 5 chapters. They are described below as follows;

Chapter 1 presents an extensive literature survey on the effect of RA on the quality of hot recycled mixtures. Also, an overview of available recycling facilities is given. At the end of this chapter the main objectives and questions are formulated which are addressed in Part 1.

Chapter 2 gives the experimental design and research methodology. A two phase approach is followed by performing experiments at laboratory scale of recycled mixtures and plant produced mixtures to evaluate their properties.

Chapter 3 presents the materials used and procedures followed in both phases of the experiments. The three mixing methods (PW, UPG and SM) used in the first phase (laboratory simulation) are explained. Then the preparation of three full scale mixtures used in the second phase is explained. Two of them were plant produced mixtures, one from batch plant and one from double drum plant. The third mixture was prepared from the same material in the laboratory mixer.

Chapter 4 gives analyses of temperature distributions during the process of hot recycled mixture production in the double drum mixer. An extensive thermal observation made during the paving of a recycled mixture is also presented.

Chapter 5 covers the measurement results obtained for materials tested in Phase 1 and Phase 2 separately. It provides a summary of results and conclusions considering the literature review, thermo-graphic analysis and the results of the experiments performed on the hot recycled mixtures in each of the two phases.

Part 2:

All of the experiments and methods used to obtain a fundamental understanding of blending and diffusion between two binders are covered in this part. A fundamental investigation on the effect of superheating of aggregates on binder properties is also reported. This part consists of 4 chapters;

Chapter 6 gives an introduction on blending of RA and virgin binder in recycled mixtures. An extensive literature review is included in this chapter which explores available techniques for measuring and observing the degree of blending.

Chapter 7 explains the experimental design and the results of the fundamental investigation on the effect of superheating of aggregates on binder properties.

Chapter 8 covers the tests carried out to explore possible diffusion during blending of RA binder and virgin bitumen by means of the Dynamic Shear Rheometer.

Chapter 9 provides the exploratory study on the morphology of bitumen in the blending zone of RA binder and virgin bitumen by means of nano indentation, nano- CT scanning, and optical microscopy.

General conclusions: this last part of the dissertation presents a concise summary of the dissertation and outlines the most important achievements of the research.

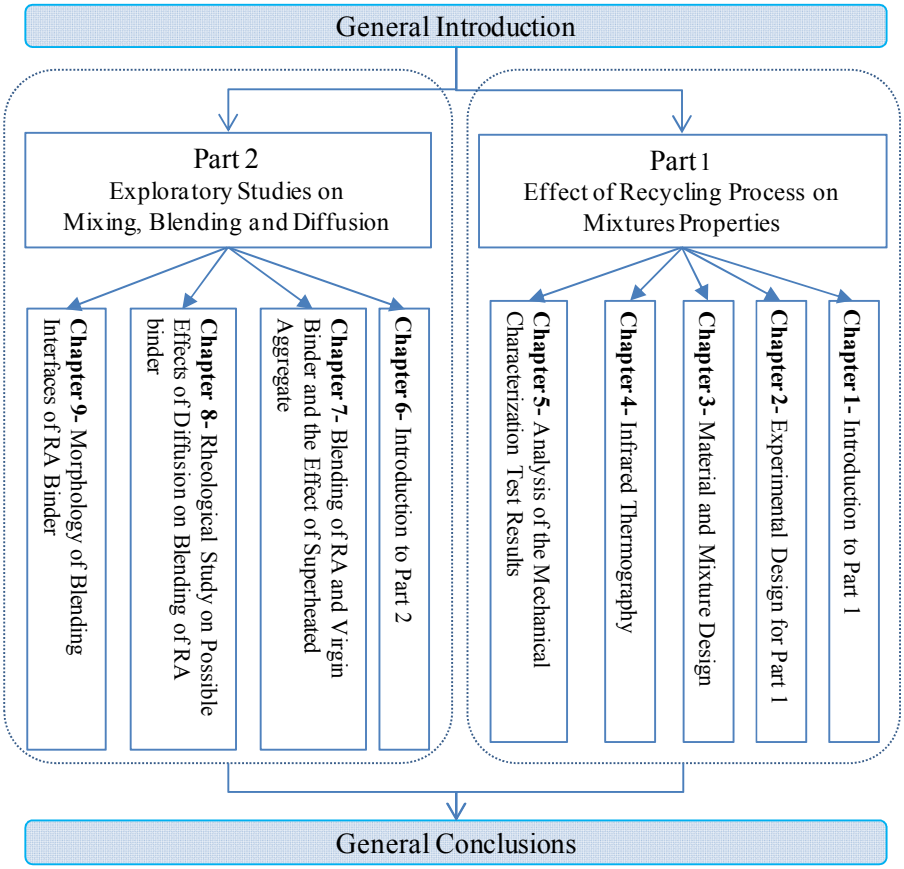

Figure 1.2 Structure of the research and the dissertation

PART 1



EFFECT OF THE HMA RECYCLING PROCESS ON MIXTURE PROPERTIES

CHAPTER 1



INTRODUCTION ON PART1

1.1. Introduction

This part of the study is focusing on the quality aspects of hot mixed asphalt containing a high amount of reclaimed asphalt in relation to the type of mixing process and RA handling conditions.

As discussed earlier, in the Netherlands, recycling of asphalt at the highest possible level is inevitable because of environmental issues and economic interests. As a result, reclaimed asphalt was officially identified as a secondary aggregate and more than 80 percent of these available aggregates (4 million tons per year) are reused in new mixtures. At the moment it is common practice to add a total amount of 50% RA in the base course, binder course and dense wearing course mixtures in a batch plant facility equipped with a parallel drum to preheat the RA. Almost all hot mixing facilities (around 38 central batch plants) are equipped with such a parallel drum in which RA is preheated to 130°C prior to being mixed with the virgin materials in the pug mill mixer. Mixing should result in final temperatures between 160-180°C of the mixed components.

Other types of mixing facilities have been developed by modifying existing drum mixers. Since 2007 a double barrel drum mixer with the capability of mixing RA into new mixtures became available to the Dutch market. Handling RA is quite different in the double drum mixing facility compared to the conventional batch plants with a parallel drum. Virgin aggregates are superheated up to 500°C in the inner drum and then they are mixed with cold moist RA in the outer drum during a short mixing time of no more than 30 seconds.

The RA in the double barrel drum mixer is not directly exposed to the hot gas which is the case in the parallel batch plant drum dryer, however, it is in direct contact with superheated aggregates.

As the result of new regulations (since 2008), using more than 50% RA has become attractive to contractors. However, increasing the RA content in both

mixing processes (double drum and batch + parallel drum) also poses a challenge to contractors. The RA preheating temperature in a parallel drum cannot exceed 130C because of safety and environmental issues and because of the fact that at higher temperatures the RA particles start to stick too much together. In the double drum unit the RA is only fed in cold conditions while the target mixing temperature is 160-180°C. Preheating of virgin aggregates to higher temperatures is one of the possibilities to reach these target mixing temperatures. Furthermore, occasionally a higher moisture content occurring in the RA is another factor that pushes up the preheating temperature of the virgin aggregates in the double drum mixer. It is presumed that exposure to either flames or superheated aggregates might have consequences to the RA binder quality because of burning or extra aging. Including 70% RA in the mixture means in general that 70% of the binder comes from the RA. It indicates the important role of the RA binder quality in the mixture.

Besides having a 170°C final overall mixture temperature to ensure a low enough binder viscosity for mixing and compaction, it should also be ensured that the RA binder is blended with the virgin soft binder during the mixing process. It is also presumed in this research that the capability of each mixing method in activating the RA binder to have a better blended binder in the final mixture might influence the properties of the mixture.

The use of high amounts of RA also poses a challenge to mix designers. Although the mixture properties might be affected by the RA handling conditions during the mixing process, there is only one standard laboratory mixing method available to verify material properties before construction. In the standard laboratory mixing method, RA and the virgin aggregates are equally preheated at 170°C for quite a long time prior to mixing. Furthermore, a mixing time of 3 minutes as used in the lab is very unrealistic compared to the short mixing times of 30-45 seconds in the real plants. Therefore it seems that the mixture designed and made following this lab method might not be an appropriate representation of the mixture produced by a real plant. This poor simulation of reality could end up with misleading results when characterizing the mixture by means of tests on lab prepared specimens.

Another challenge in the design of recycled mixtures is to determine the grade of the soft virgin bitumen with respect to the rheological properties of the RA binder, RA percentage and mixture requirements. Several blending charts and models are available for designers to determine the virgin binder properties needed. They are based on the assumption that the RA and virgin binder will fully blend. However, the question is whether these charts are applicable in the mix design because the assumption of full blending might not be valid.

In summary, there are primarily three major issues with regard to producing hot mixtures containing high amounts of RA being:

- mixture design,
- mixing process and
- mixture properties.

To address these three research issues two assumptions were made:

- A number of RA handling conditions are identified which will affect the mixture properties but in this research it is assumed that the following are the most important conditions; RA content, moisture content of the RA, preheating conditions and mixing time.
- Available mix design methods are not appropriate in predicting mixture properties delivered off plant.

This part of the dissertation is devoted to evaluate the validity of these assumptions for double drum mixing methods. It also includes a literature survey in which the critical points of the current knowledge including substantial findings as well as theoretical and methodological contributions to hot mix asphalt recycling are considered. The literature review is also focused on the three major issues; mixture design, mixing facilities and mixture properties.

After the literature survey, the design of the experimental program is explained. This program is primarily based on the two-phase experimental plan; laboratory studies and field investigations.

Heat exchange during laboratory mixing and real plant mixing is playing a pivotal role in determining the quality and the homogeneity of the mixture. Therefore a full section is devoted in this part to thermo-graphic analyses in the lab and at real plants.

After reporting the result of experiments and their analysis, conclusions and a summary from both experiment phases are presented at the end of the dissertation.

1.2. Literature survey

1.2.1. Hot mix recycling facilities

The primary purpose of a HMA facility is to properly proportion, blend, and heat aggregates and mix them with bitumen to produce a HMA that meets the requirements of the job mix formula [4]. The first mechanical asphalt mixers were developed in Paris in 1854. They were quite basic and it took 4 hours to produce only one batch. The whole facility consisted of iron trays in which aggregates were dried by operators above open coal fires. The skills of operators mostly determine the mixture quality. The Cummer Company opened the first central hot mix production facilities in the U.S. in 1870 [5]. In 1901, Warren brothers developed the first asphalt facility including all basic features we have today, except a cold feed and pollution control equipment. (See Figure 1.1). Significant improvements took place by adding a cold feed system in the 1920s and vibrating screens in the 1930s. However, all asphalt plants (basically batch plants) in the 1950s consisted of a dryer, screening tower and a mixer; they were extremely dusty and dirty. By utilizing plants with a baghouse[1] system, the plants became a bit cleaner. In this period, the use of storage silos became well-known. Prior to that, asphalt mixtures were directly loaded to trucks.

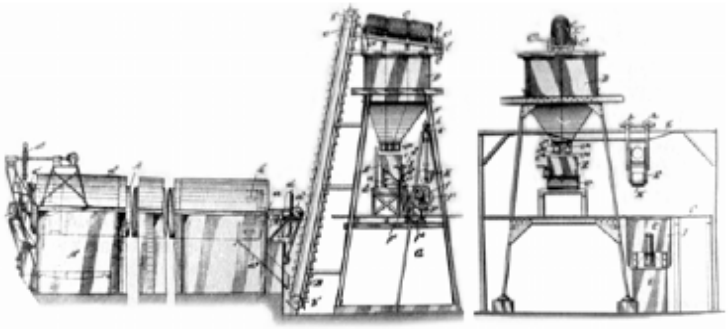

Figure 1.1 Warren Brothers Patent Application Drawing: Original Batch Plant built in 1901 [6]

The other major change in the late '60s was the addition of surge bins and storage bins. Prior to that, everything was loaded right from the plant into the truck and bins for storing the mix for short periods of time added surge capacity. In the 1970s asphalt recycling became important because of the oil

[1]Fabric filter dust collector

embargo. Moreover, the development of the drum mix facilities helped the popularity of asphalt recycling. Before the development of the drum mix facility, engineers did not know how to recycle in a batch plant [4].

Hot mix recycling facilities are basically modified forms of normal hot mix asphalt plants with an extra process of introducing RA. This is needed because it is not possible to dry reclaimed material along with virgin material at the same temperature. Therefore, RA is mixed with preheated virgin aggregates half way of the drum mixing facility or RA is added to the pug mill mixer or weigh box in the batch plants.

Typically, three types of asphalt recycling and mixing facilities came available to the market. They are listed below:

Parallel drum mixer: Here the aggregate flow is in the direction of the exhaust gases or away from the burner. For that reason it is called "parallel". RA is mostly introduced half way along the drum [7].

Batch plants: These types of plants are usually coupled with a counter-flow drum dryer or parallel drum or both of them. In the Netherlands, typically a parallel drum dryer is used together with the batch plant. In the United States double drum dryers have also been used in batch plant facilities.

Counter-flow drum mixers: Here the material flows in the opposite direction of the gas flow. They can be categorized in three types [8] being, single drums, double drums and triple drums.

Although all of these methods have the same objective to proportion and mixing aggregates with bituminous binders, each of these methods might however affect the final quality of the mixture in several ways due to their unique features. The virgin and RA binder are prone to extra hardening due to short term aging during the drying and mixing period. The way the aggregates are handled, particularly RA, mostly depends on the type of recycling facility. Bituminous binders lose their volatile components while they are exposed to the hot gas stream and superheated virgin aggregates. Oxidation of the binder in bitumen tanks and storage silos are also important factors that could affect the mixture quality, albeit they are beyond the scope of this research. Homogeneity in temperature, bitumen content and aggregate gradation is another important factor, which is partly determined during material handling and mixing in the plant.

For this purpose, a detailed comparison between different types of facilities with focus on RA handling and mixing conditions will be provided in this chapter. In this comparison, emphasis is placed on the batch plant and double drum mixer (counter-flow double drum).

1.2.1.1. Hot recycling in a parallel drum mixer

It is called *parallel* because, all material is flowing in the same direction as the hot gas stream. In this type of mixing plant all virgin materials are added in the same drum continuously. Materials get dried and preheated as they are exposed directly to open flames and hot gas. They flow downward to the end of the drum where bitumen and fillers come in.

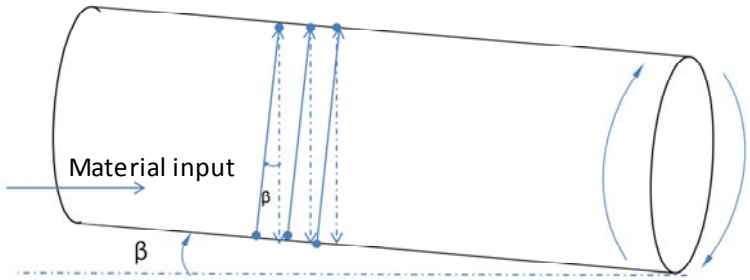

Figure 1.2 Concept of material movement in a drum mixer: drum rotates

The concept of material movement due to the drum rotation and its inclined angle is demonstrated in Figure 1.2. The diameter of the drums is varying between 1.8-3m.

This type of drum mixers can produce up to 120 tons per hour depending on the drum size and the moisture content of the aggregate. In modified types of drum mixers, RA is introduced in the middle of the drum, as far as possible from the open flame (see Figure 1.3). The same figure also shows clearly the heat exchange between cold RA, virgin material and exhaust gas. Gas and virgin material reach temperature peaks of 760°C, and 260°C, respectively, just before RA introduction. The heat exchange occurs via conduction, convection and radiation.

1.2.1.2. HMA recycling using a batch plant

The batch process encompasses a series of operations carried out over a period of time on a separate, identifiable parcel of material [9]. As the name implies, this type of plant produces a single batch of material at a time. This is then repeated to produce the required quantity. A pre-set amount of proportioned aggregate and bitumen is mixed in batches that may vary from 500 kg to 5 tons. The plant capacity is determined by both the type of mixture and the batch size. Mixing times vary with the type of mixture. A 2.5 tons batch for example, requiring a mixing cycle time of 60 s, will give a maximum plant capacity of 150 tons per hour.

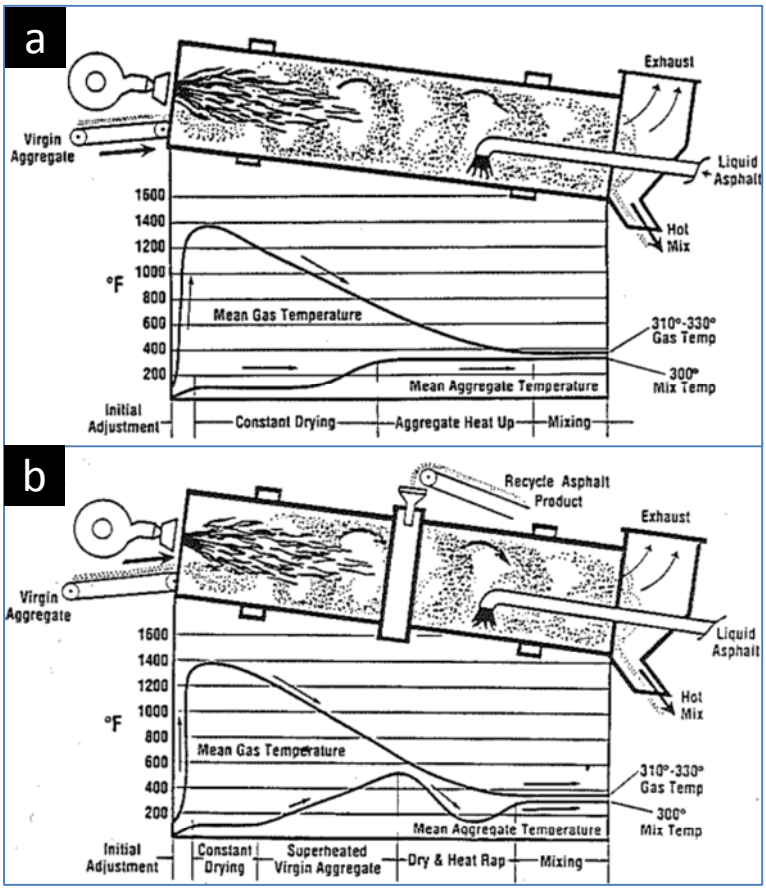

Figure 1.3 Exhaust Gases and Aggregate Temperature profile comparison for Parallel drum mixer; (a) without RA and (b) with 50% RA [4]

This plant is very flexible in terms of changing from one mixture type to another without difficulties. This feature makes it favorable for handling the often small quantities of different mixtures that exist in the Netherland. These plants have capacities ranging from 100 to over 400 tons per hour [10]. The major components of a batch plant are; the cold-feed system, the bitumen supply system, the aggregate dryer, mixing tower and emission-control system [8]. As mentioned before the first patented batch plant was registered by the Warren brothers in 1901 and since then the structure of this kind of plant remained almost the same except the cold feed system.

Figure 1.4 illustrates the arrangement of a typical batch plant with a cold RA bin on it in order to feed the cold RA to the virgin materials in the pug mill.

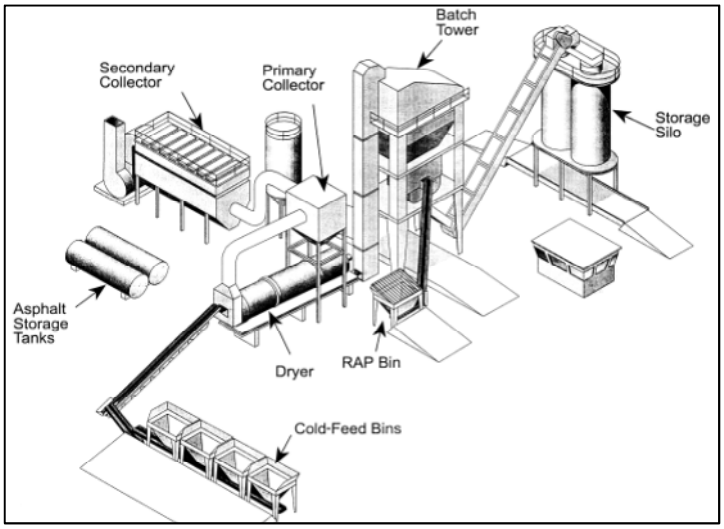

Figure 1.4 Major components of a batch plant

Three types of aggregate dryers were developed in order to work with batch plants:

- the long rotating cylinder,
- the tower dryer in which the aggregate is slowly passing downwards whilst hot gases are forced upwards through it,
- the short drum type of batch dryer which is the forerunner of the batch-heater mixer.

A Batch plant operation system is usually performed in the following 7 steps [11] ;

- cold aggregate storage,
- proportioning,
- drying and heating in a counter-flow drum dryer
- screening in the batch tower,
- hot aggregate storage,
- measuring and mixing of aggregate and bitumen,
- discharge of the mixture into a truck, storage silo or surge bin.

Almost all batch plants can be modified for recycling purposes. A number of changes have to be made in several parts. The most important part is the RA preheating and feeding system. Five methods of RA handling in batch plants

have been identified by Brock [12] and Kandhal [13]; they are shown in Figure *1.5.*

In Method 1 and 2 superheated virgin aggregates as well as RA is transported to the screen by an elevator. Because of moisture in the RA, a large quantity of steam releases from the hot bins.

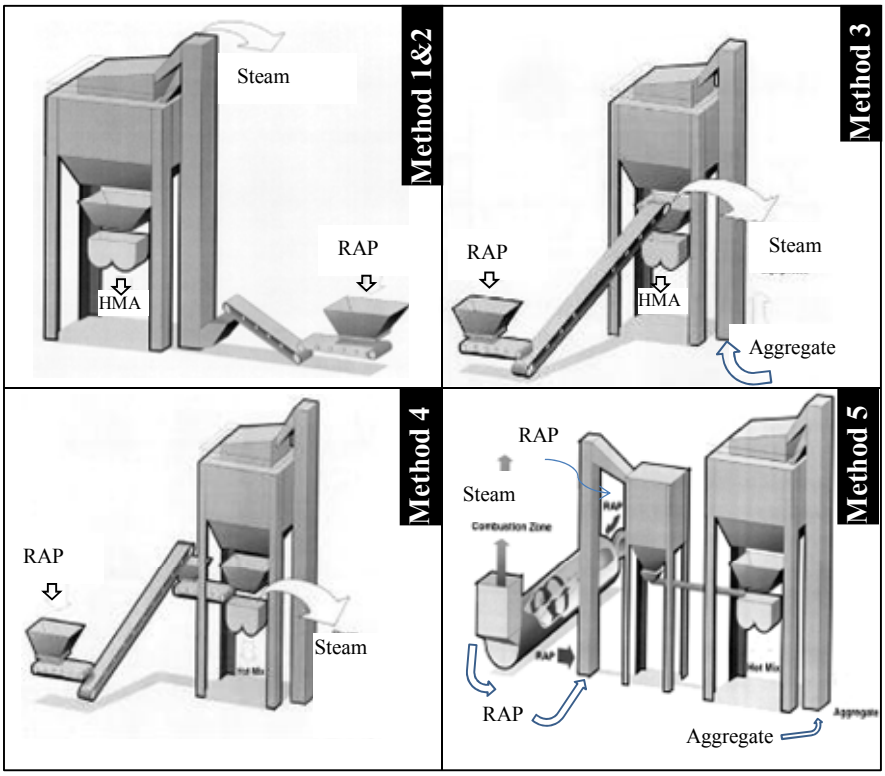

Figure 1.5 Different methods of RA introduction in HMA batch plants [12] [13]

In method 2, RA is stored in a separate bin (fifth bin) prior to mixing. In method 3 RA is introduced directly to the weighing hopper in the middle of superheated virgin material from the hot bins in such a way that RA is sandwiched between the superheated virgin aggregates which results in more heat exchange. A temperature shock might happen to RA binders because of the sudden exposure to superheated aggregates while they get in touch in the weighing hopper. When moist RA is used an "explosion" of steam will occur in the weighing hopper.

Method 4 is more advanced than the previous methods. RA is fed to a separate scale before being transported to the weighing hopper. Then it is added gradually to the pugmill in a period of 20-30 seconds. This method has a better control over steam generation.

In all the 4 methods mentioned above, RA is introduced in a cold and moist condition which usually leads to significant steam generation. The question now is whether these methods are able to release all of the moisture of the RA or not. Furthermore, the amount of RA and its moisture content are determining the preheating temperature of virgin aggregates (see Figure 1.6) which might be as high as 450˚C when 50% RA with 5% moisture is added.

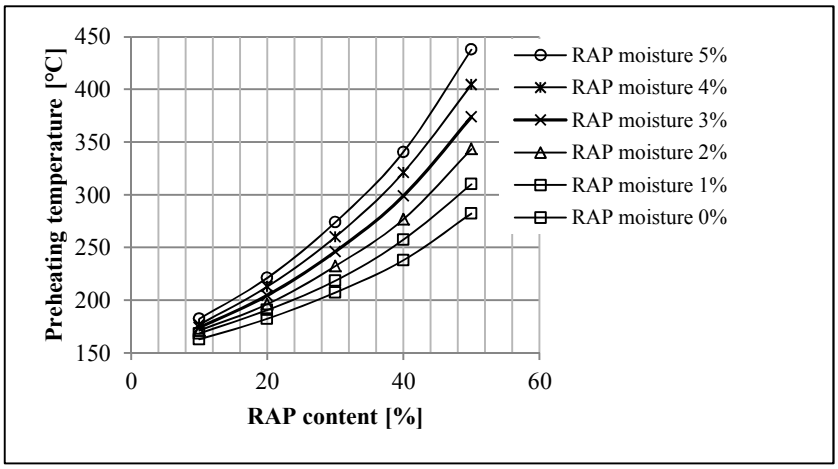

Figure 1.6 Required aggregate temperature in relation to the amount of cold added RA and its moisture content.

To overcome this problem, a RA preheating parallel drum dryer is added to most batch plants (Method 5). RA is preheated at 130˚C before conveying to a separate bin in the batch tower. It has its own weighing hopper in the tower as well. After weighing in the hopper, the RA is fed to the pugmill alongside virgin material. In some plants, the RA drum dryer is installed at the same height as the batch tower because warm RA may cause problems in elevators by sticking to the paddles. The last method (Method 5) is the most common method in the Netherlands. To date, 38 batch plants from a total of 44 active plants in the Netherlands are equipped with a parallel drum dryer which allows using 50% RA.

1.2.1.3. Hot recycling in a double drum mixer

A more recent development in drum-mix plant design is the counter-flow drum-mix plant. Its design represents an effort to improve the heat transfer process inside the drum and to reduce plant emissions. In the counter-flow drum-mix plant, the heating and drying of the aggregate are accomplished in a manner similar to that of a conventional batch plant dryer. The double drum mixer is an improved form of counter-flow drum mixers. It was developed by Astec in 1987.

With a double-barrel system, the mixing chamber is folded back around the aggregate drying drum. This mixing unit doesn't rotate. Virgin materials are introduced in the inner drum and they flow in an opposite direction of the hot gas stream. As is shown in Figure 1.7, the heated and dried aggregate is discharged from underneath the burner downward into the non-rotating outer shell or drum. This occurs at the lower end of the mixing unit [8].

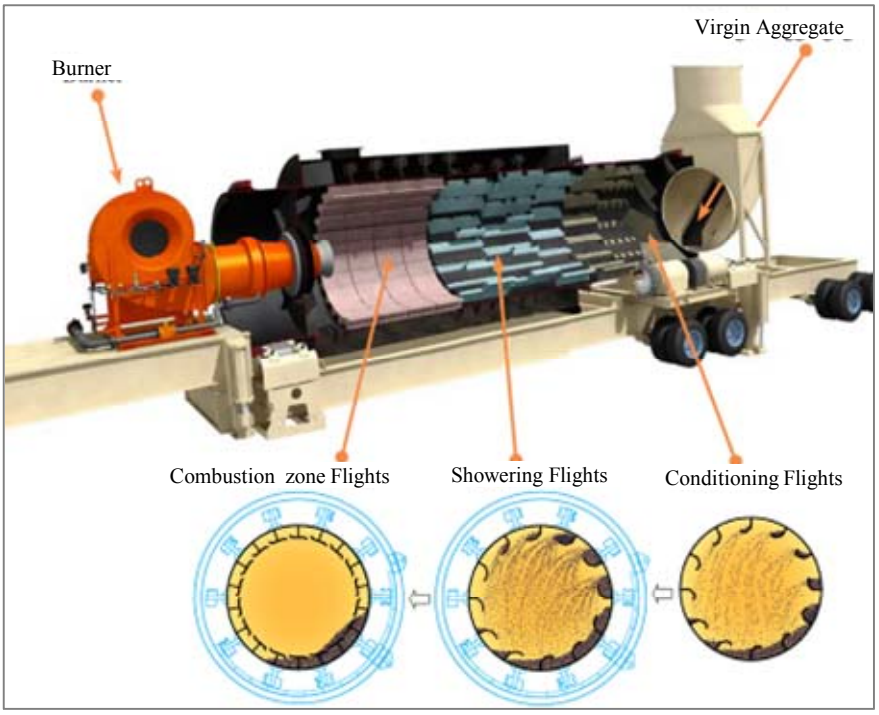

Figure 1.7 Inner drum of the Astec double barrel drum mixer with three different types of flights. [14]

Three different types of flights force the material forward through the drying chamber. They are especially designed for three separate functions which are shown in Figure 1.8 [14];

- *Conditioning flights* which break up any clumps or sticky material when the aggregate first enters.
- *Showering flights* which make sure that the material is veiled evenly through the hot gas stream.
- *Combustion flights* which prevent aggregate from impinging on the flame while spreading the material to maximize radiant heat transfer.

Shortly after the new aggregate enters the mixing chamber, RA is added to the external drum. This material falls into the shell and quickly blends with the superheated new aggregate. Heat transfer from the hot new aggregate to the ambient-temperature RA begins immediately. As with the conventional counter-flow drum mixer, any moisture in the RA and any hydrocarbon emissions that develop during the heating process are drawn back into the dryer unit by the exhaust fan.

The moisture is carried into the emission-control equipment, similar to what happens with the moisture released by the new aggregate during the heating and drying process. The hydrocarbon emissions from the RA are incinerated by the burner. Once the RA has entered the outer shell, any additives, such as mineral filler, needed in the mix are deposited into the mixing area. The baghouse fines are also introduced into the outer shell at the same location as the filler.

Because the flow of air in the area between the inner drum and the outer shell is minimal, there is no tendency for the added materials to be sucked out of the mixing chamber into the aggregate dryer section of the drum-mix plant.

Sequential mixing happens in the outer shell to make a good mix on a consistent basis. Ingredients are added to the hot dry aggregate in an order that allows better temperature equalization and even distribution of all particles throughout the mix. This is illustrated in Figure 1.8:

When all of the aggregate materials (virgin and RA) are in the outer shell, the bitumen is added to the mixture. On most double-barrel plants, the binder can be added in one of the two possible locations. If *RA is not added* to the mixture, the bitumen is mostly introduced as quickly as possible but shortly before the baghouse fines and mineral filler have been charged into the exterior drum. If RA is used in the mixture, the addition of the binder is delayed to make sure that enough heat transfer can take place between the superheated new aggregate and the reclaimed material [1].

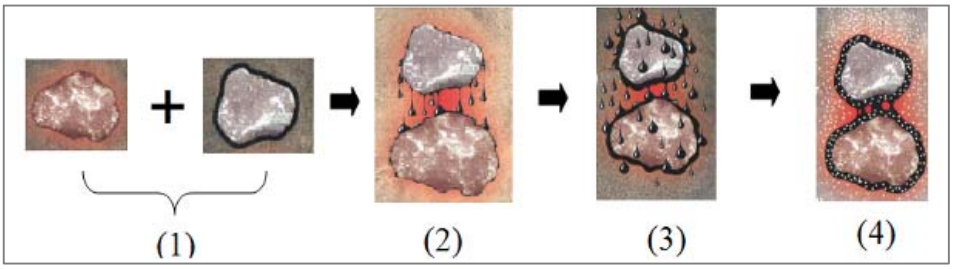

Figure 1.8 Sequential mixing in the outer shell of the double barrel mixer

Mixing takes place by a series of paddles attached to the outside of the inner drum (the virgin aggregate dryer) (see Figure 1.9). The paddles are set at the proper angle to push the combination of new aggregate, bag house fines and mineral filler, RA, and bitumen uphill, blending these materials together as they travel in the narrow space between the outside of the rotating inner drum and the inside of the non-rotating outer drum. Mixing occurs only in the lower quarter-portion of the circumference of the outer shell; the mixture is not carried over the top of the inner drum. In addition to the heat transfer that takes place by direct contact between the new aggregate and the other mix components (90%), further heating occurs as all the materials come in contact with the inner drum and by radiation of heat from the inner drum into the outer shell (which is 10% of the total heat transfer) [14].

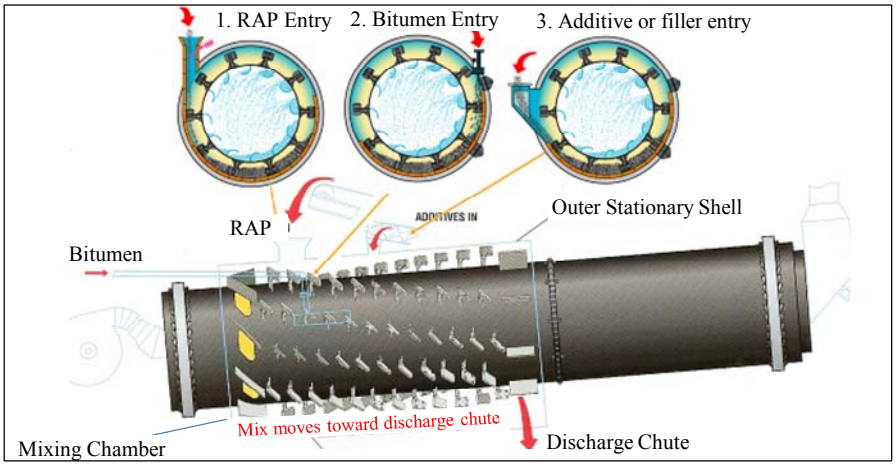

Figure 1.9 Mixing process in outer shell with mixing paddles at different stages [14]

Depending on the size and production capacity of the double-barrel plant, mixing and blending of all of the mixture components typically occurs in a

time period which is not longer than 60 seconds. Upon completion of the mixing process, the HMA material is delivered into a discharge chute for transport to a silo.

The recycling process in the double drum mixer can be summarized in 9 steps as is shown in Figure 1.9 [14]:

- virgin aggregate enters the inner drum,
- hot air enters the inner drum,
- aggregate moves through the inner drum,
- heated aggregate enters the outer shell,
- RA enters the outer shell,
- liquid bitumen enters the outer shell,
- baghouse fines enter the outer shell,
- virgin aggregate, RA, fines and liquid bitumen are mixed in the outer shell,
- finished mixture exits the outer shell.

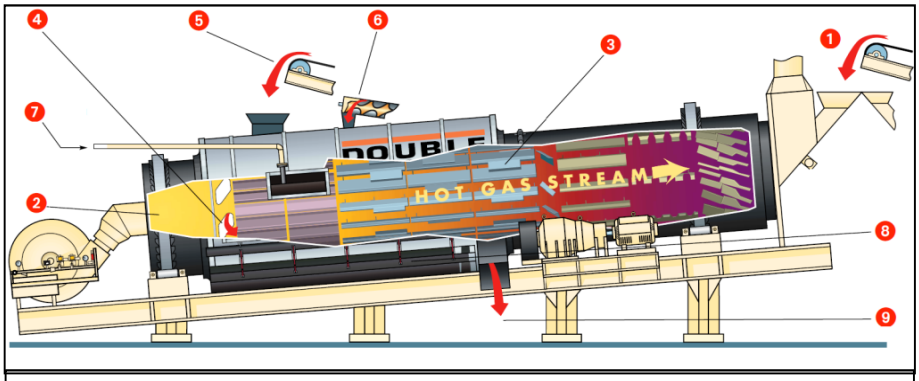

1- virgin aggregate
2-burner
3-showering flights
4- discharging superheated virgin aggregares
5- RAP
6- filler and additives
7- bitumen
8- mixing flights
9- discharge shut of HMA

Figure 1.10 The detail of Astec double barrel drum mixer [14]

1.2.1.4. Moisture handling in plants

In the double drum mixer, virgin aggregates are discharged immediately to the mixing chamber after drying and preheating in the inner drum. It is claimed that double drum mixers are capable of removing more internal moisture than

other plants by superheating the virgin aggregates. For example, when a mixture with 50% RA is supposed to be produced, the surface temperature of virgin aggregates may be as high as 500-600ºC, which allows a quick evaporation of virgin aggregate moisture prior to mixing with RA and virgin bitumen.

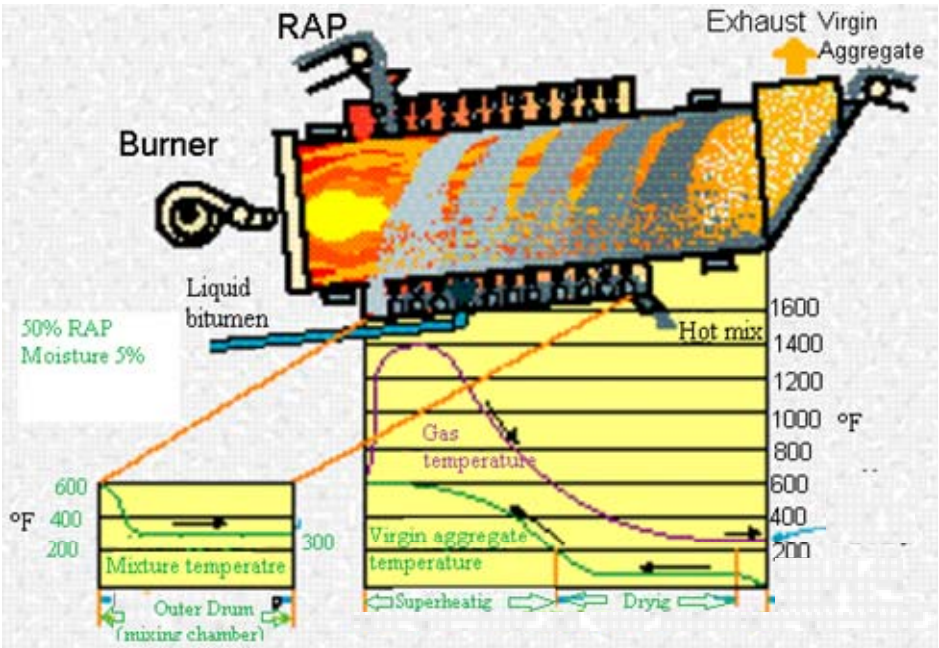

Figure 1.11 Temperature profile in the double drum mixer [14]

It is reasonable to assume that almost all moisture in the virgin aggregate is evaporated in the inner drum, though there is still some uncertainty about complete removal of the RA moisture while it mixes with superheated virgin aggregates. The question however is whether this likely residual moisture in RA will affect the mixture properties. To answer this question, one has to distinguish between moisture in the RA and the virgin aggregates because RA aggregates have their own binder coating prior to mixing. Once the RA aggregate is brought in contact with superheated virgin aggregates, the RA moisture starts to evaporate. However, it is uncertain if the complete removal of RA moisture takes place. It is claimed that RA moisture may cause some foaming effect of the virgin binder and may even decrease the viscosity of the RA binder during the mixing period. Nevertheless, no evidence is found in the literature to support this hypothesis.

To get a better understanding about the heat transfer and moisture handling in a double drum mixer, a temperature profile of the material in the inner drum and mixing chamber is presented in Figure 1.11.

1.2.2. Segregation

One of the most common defects occurring during hot mix asphalt operations and pavement construction is segregation. Part of the segregation might occur because of the way of aggregate feeding, drying (or preheating), mixing and discharging.

Segregation of asphalt mixtures is defined as the non-uniform distribution of aggregate with different sizes, or in limited cases, specific gravities [15]. Thus, segregation involves a higher concentration of coarse materials in a specific area and fines in another area. Three types of HMA segregation have been identified [16] :

Gradation segregation is the state of non-uniformity in the distribution of different sizes of aggregates in the final mixture on the pavement. It can occur at one or several stages during production, hauling and paving.

Agglomeration of coarse aggregate is typically associated with high air voids and low bitumen contents; these conditions may cause moisture damage as well as other durability distresses such as fatigue cracking, pothole formation, and raveling. It is shown that very coarsely segregated materials also have a substantially reduced tensile strength and fatigue life [17]. Conversely, agglomeration of fine aggregates is associated with high bitumen contents, making them susceptible to rutting.

Temperature segregation is the state of non-uniformity in temperature of aggregates just before compaction of the asphalt layer. It occurs because of heat loss at the surface of the material during transportation and paving. This type of inhomogeneity also may cause less compaction in cold areas compared to warmer areas.

Non uniformity in bitumen content (bitumen drainage), is a common problem in stone mastic asphalt mixtures (SMAs) and other mixtures with high bitumen content (but also stone skeleton mixtures with high voids content like PAC) It causes non-uniformity in the thickness of binder films which may make the mixture susceptible to durability distresses such as aging, fatigue failures. The rich bitumen parts of the mixture are also susceptible to permanent deformation.

Based on studies and articles [15] [16] [17] [18] several sources of segregation have been identified and they are shown in Figure 1.12.

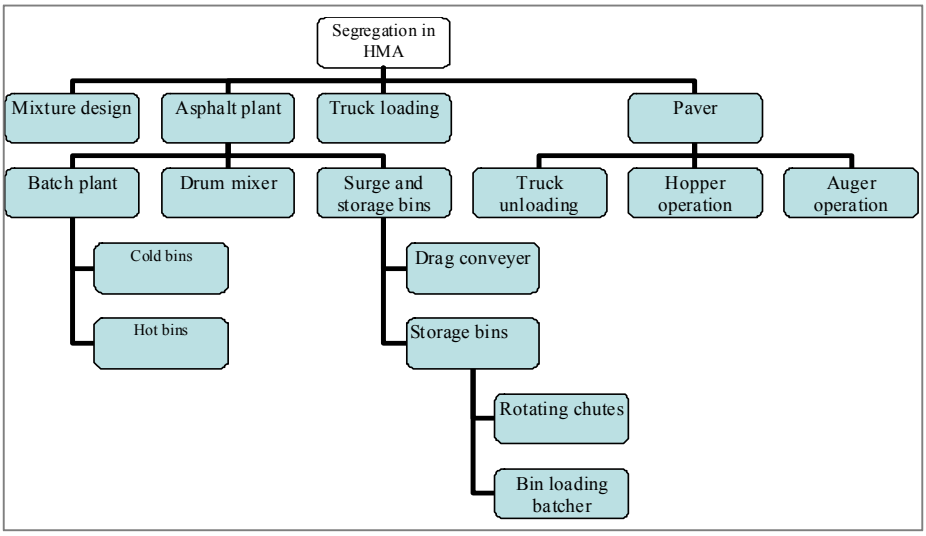

Figure 1.12 Different stages where gradation segregation might occur [18]

Most of the potential places for segregation are identified in the asphalt plant. Segregation can occur at numerous points in a hot mix asphalt plant. These will vary depending on whether it is a drum mixer or a batch plant. However there are also other sources of segregation in temperature and gradation which may be caused by trucks and paver during construction.

1.2.3. Bitumen aging

Short term aging during HMA production may substantially influence the mixture quality in all aspects in several stages prior to paving (and during paving). Aging will vary with the type of facilities and the procedures. Generally bitumen will be influenced by oxygen, ultraviolet radiation and by elevated temperatures. Steric hardening of bitumen is identified as “curing” and it is believed that it will increase the load spreading capability of the structure as it increases the stiffness of the material [10].

Ageing can be separated in short-term and long-term aging [4]. Long term aging refers to the oxidation of the bitumen during the service life of the asphalt mixture while short-term aging refers to the loss of volatiles and oxidation of the bitumen during the construction phase.

In Figure 1.13 the general trend of the effect of aging during production and the service period on the viscosity in the form of the ratio of the viscosity of aged to un-aged binder, is illustrated.

There are a number of circumstances under which hardening occurs. Hardening of bitumen may even occur during bitumen storage in tanks for hours or even days however it is not as crucial as hardening during the mixing process.

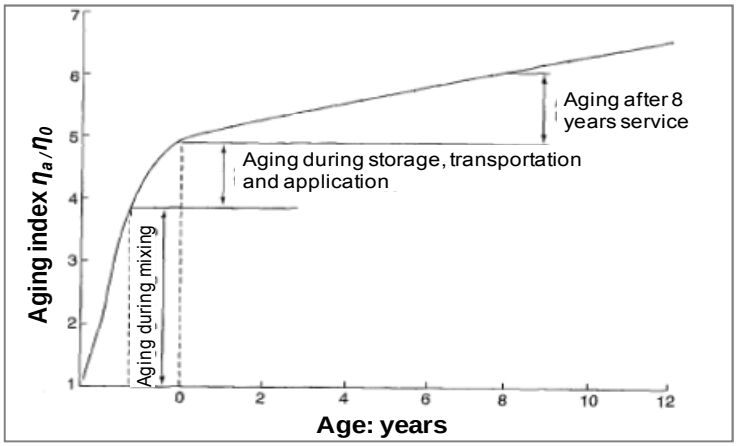

Figure 1.13 Short term aging in comparison with long term aging during service life [10]

Several factors as listed below are identified and reported as reasons for hardening and aging of bitumen during mixing and service life [19] [20] [10] such as: volatilization, photo-oxidation, photo-chemical reactions, polymerization, steric or physical hardening, exudation of oils, action by water, absorption by solids, absorption of components at a solid surface, chemical reactions, microbiological deterioration.

However the main factors causing hardening of bitumen during mixing are oxidation and volatilization.

1.2.3.1.1. Oxidation

Vallerga [19] has defined "oxidation" as the reaction of oxygen with bitumen. He also believes that the oxidation rate depends on the character of the bitumen and the temperature. When in contact with the oxygen in the atmosphere, bitumen, as an organic substance, becomes oxidized. Polar groups containing oxygen are formed and these tend to associate into micelles of higher molecular weight thereby increasing the viscosity of the bitumen. Polar hydroxyl, carbonyl and carboxylic groups are formed, resulting in larger and more complex molecules that make the bitumen harder and less flexible [10].

1.2.3.1.2. Volatilization

Volatilization as a function of temperature is the evaporation of the lighter fractions from bitumen. It is the major factor contributing to short term aging during production but has less effect during the service life of a pavement. The level of aging is primarily determined by temperature and the period during which virgin bitumen and RA binder are exposed to high temperatures. Brock [21] points out that light oils which remain in the bitumen after the refinery process, are the main source of volatile fractions during the mixing process. When crude oil is distilled in a refining process, light fractions are separated from heavy fractions. Light oils (gasoline, kerosene, etc.) rise to the top of the distillation column and heavy fractions fall to the bottom, however they are never fully separated. Since bitumen is basically the residue from the refining process, the amount of light fractions left in bitumen depends on the factors mentioned above and on the final viscosity desired in the final bitumen.

1.2.4. Temperature

Higher mixing temperatures may substantially increase the degree of hardening of the bitumen. The effect of high mixing temperature on the softening point is illustrated in Figure 1.14. An increase of 5.5ºC in mixing temperature results for a standard mixing time of 30 s in an increase of 1ºC in the softening point of the bitumen [22].

Bitumen and gas stream temperature at the point of bitumen injection are both critically influential with respect to the removal of light fractions of bitumen.

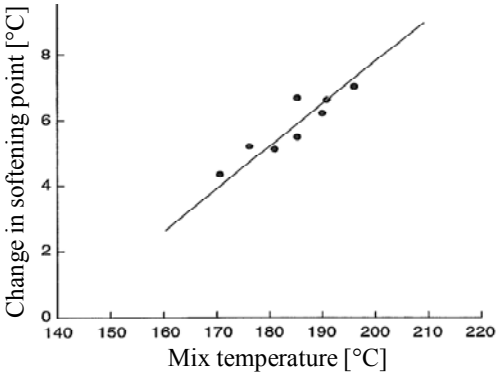

Figure 1.14 Relationship between the production temperature of the mixture and change in softening point [22].

1.2.5. Mixing time

Although a longer mixing time is beneficial in producing a more homogeneous mixture, it also significantly contributes to short term aging. For relatively short wet-mix times (28 to 35 seconds), the penetration of average bitumen will decrease up to 30 percent compared to the virgin bitumen. For longer wet-mix times (up to 45 seconds), the penetration of the bitumen may drop below 60 percent of the original value, while the viscosity of the binder material may increase up to 4 times its original value.

1.2.6. Type of mixing process (facility type)

The type of mixer used also affects the amount of hardening during mixing. It has been recognized for some time that the amount of hardening in a drum mixer is often less than in a conventional batch mixer [23].

This is probably the result of shorter bitumen/aggregate mixing times and the presence of steam in the drum, which limits the amount of oxygen during mixing. However, the multiplicity of different designs of drum mixers means that variation in the amount of hardening between different designs of plant is almost inevitable.

1.2.7. Residual moisture in aggregate

The aggregate moisture can vary depending on mineralogy, gradation of aggregates, climatic conditions at the time the plant is operating and pre-possessing of the aggregate (storage, drainage, etc.). Generally, moisture levels of 5 percent result in approximately 10 percent steam by volume in the gas stream while moisture content as high as 15 percent results in 35 percent steam by volume in the gas stream [21]. Moisture problems can be overcome to a large extent by sheltering the stockpiles and good drainage.

1.2.8. Properties of recycled binder

As mentioned when discussing binder hardening, bitumen is exposed to short-term and long-term aging. During construction (short-term), bitumen is exposed to hot gas and hot aggregates. This may result in substantial changes in viscosity and rheological properties of the mixture binder. RA binder properties are also changed during the service life of the pavement so the quality of the RA binder also depends on the amount of aging developed during the service life of a pavement [24]. The air voids content in the mixture is one of the influential factors on long term aging of bitumen by

permitting more oxygen in the voids. Recovered binder from porous HMA has shown to be significantly stiffer than from regular, dense, HMA [25].

1.2.9. Mix design with RA

The use of processed RA in hot mix asphalt pavements is now standard practice in most countries and is referenced in ASTM D3515 and NEN-EN 13108-8. The primary steps in the design of mixes include:

- the determination of material properties of RA and new materials,
- the selection of an appropriate blend of RA and virgin aggregate to meet the gradation requirement,
- the selection of an appropriate bitumen blend to satisfy specified viscosity and/or penetration requirements,
- the need to add a recycling or rejuvenating agent to soften the existing binder, and the need to comply with mechanical properties.

In the European standard (EN13108-8) it is suggested to use the log-pen rule for determining the penetration grade of the added bitumen with respect to the penetration of the RA binder and the percentage of added recycled material. The penetration and softening point of the blended mixture are predicted by means of the following equations (see EN13108-8);

$$log[pen_{mix}] = a\ log[pen_1] + b\, log[pen_2] \qquad (1.1)$$

$$T_{mix} = aT_1 + bT_2 \qquad (1.2)$$

Where:

Pen_{mix} = calculated penetration of the mixture

Pen_1, Pen_2 = penetrations of both binders comprising

a , b = mass proportions of each bitumen in the mixture *(a + b =1)*

T_{mix} = calculated softening point of the mixture

T_1, T_1 = softening point of each individual binder in the mixture.

In ASTM D4887, procedures for selecting the quality of bitumen or recycling agent are given. This specification includes a viscosity blending chart (at 60°C) which enables the designer to determine the percentage of recycling or rejuvenating agent (or soft bitumen) to add to the total binder in order to achieve a desired value of absolute viscosity for the recycled bitumen (Figure 1.15). This blending chart is based on the equation which is expressing mixing theory for binary liquids;

$$ln\,\eta_{mix} = x_1\,ln(\eta_1) + x_2\,ln(\eta_2) \qquad (1.3)$$

Where:

η_{mix} = viscosity of the mixture of two binary liquids

η_1, η_2 = viscosity of both liquids

x_1, x_2 = volume percentage of both liquids

In this equation which was primarily suggested by Arrhenius in 1887 for binary liquids, the interaction between two liquids (chemically or physically) was not taken into account. In 1949, Grunberg presented a modified form of the Arrhenius equation [26] by adding an interaction parameter (G_{12}) to it.

$$ln(\eta_{mix}) = x_1\,ln(\eta_1) + x_2\,ln(\eta_2) + x_1 x_2 G_{12} \qquad (1.4)$$

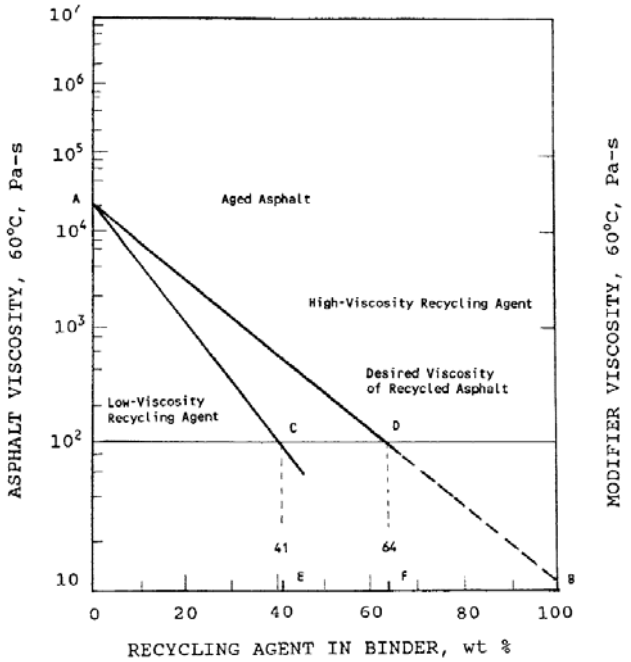

Figure 1.15 Viscosity blending chart (60 C) prescribed in ASTM D 4887 [27]; the right vertical axis is used for rejuvenator or virgin bitumen, the left vertical axis is used for RA binder viscosity

Another form of the Arrhenius equation is presented in 1980 by estimating the viscosity of a mixture of two liquids based on a log-log relationship with the log-log viscosity of each individual liquid and the mass percentage in the whole mixture [1].

$$ln[ln(\eta_{mix})] = x_1 ln\,[ln(\eta_1)] + x_2\, ln\,[ln\,(\eta_2)] \qquad (1.5)$$

All these methods are based on the assumption of 100% blending between two binders or a binder and rejuvenator, which are unlikely in the real mixtures.

1.2.10. Blending of RA and virgin binders

An important issue in hot mix or warm mix asphalt recycling is the amount of blending between aged RA binder and virgin binder added to it. Is the RA binder blending totally or partially with the virgin binder? Or does the RA act like black rock and does blending not occur?

Apparently the way how the RA binder is mixing with the virgin binder depends on the production process used. In the double drum mixer, the order of adding materials is; (1) heating virgin aggregates (2) adding RA (3) adding virgin bitumen (4) adding fines. Therefore the old binder, firstly, melts off totally (or partially) by exposure to superheated aggregates. Before adding virgin bitumen, virgin aggregate is coated by a thin layer of recycled binder. Then new bitumen is added and probably blended with recycled bitumen.

Independent of what actually happens; the level of blending will affect both the performance of the produced HMA and the economic competitiveness of the recycling process. If the designer assumes that the materials blend completely but it is actually behaving as a black rock, the binder will not be stiff enough and a far too low amount of bitumen is used. In contrast, if it is assumed that RA does not blend with the virgin bitumen when it is actually blending, then the added binder will be stiffer than expected and a rich mix will result. The problem can be further complicated if one considers that the blending process may take some time to occur and is influenced by the rejuvenating agent; this is reported by Carpenter and Wolosick [28].

A limited number of studies have investigated the blending process between aged and virgin bitumen [29] [30] [31] [32].

Another investigation [30] was carried out in 2001 to evaluate the blending process between aged and virgin bitumen. In that investigation an artificial RA was produced by aging a normal mixture in the oven at extended time and elevated temperature. This mixture then was manually crushed and milled to

achieve the artificial RA aggregates in the laboratory. One HMA mixture was produced by using 50% of artificial RA.

A second HMA containing the same aggregate was produced with identical aggregates and volumetric properties. The bitumen of the second mixture was pre-blended with 50% RA binder and 50% virgin bitumen. Bitumen from both mixtures were extracted and recovered for testing. Both mixtures had the same binder and void contents. In addition, both mixtures were tested for laboratory fatigue and rutting performance. Results of laboratory testing showed that the recycled HMA exhibited better fatigue and rutting performance than the virgin HMA. Eventually it was concluded from these results that aged and virgin binders might not fully blend because of the concentration of aggregates which cause less blending interface between recycled and virgin material. Therefore, inhomogeneous mixing/blending of the virgin and RA binder was expected to result in areas with soft binder. This resulted in an overall softer binder than regular HMA because of the softer part of mixture becoming dominant during loading.

An experimental program was conducted by Stephen [32] to evaluate the effects of blending between RA and virgin binders on the resulting SuperPave grade. To validate that RA does not act as a black rock and has an effect on the overall blend, 11 mixes were prepared with the same gradation, RA percentage (15%), and binder. The difference between the prepared samples was the RA preheating time before being added to the virgin aggregates and binder. Another mixture was also prepared with virgin aggregates and binder with no RA binder. The preheating time of RA varied from zero to 540 minutes. It was assumed that if the preheating time didn't influence the properties of the mixture then it acts as black rock. In contrast, if long heating times facilitate the blending between aged and virgin binders, an increase in the mix strength should be detected because in a poor blended mixture, the soft binder would be dominant during loading. The relation between the indirect tensile strength and unconfined compression strength on one hand and the RA preheating time is presented in *Figure* 1.16. It shows that the preheating time can activate RA binder to interact with virgin bitumen. The prolonged preheating time may also increase the stiffness because of aging which is not mentioned in the results. Therefore this study doesn't provide enough evidence of increased blending due to increased preheating times.

In addition, when comparing the mix with no preheating to the mix made with virgin materials, an increase in strength is immediately observed upon adding the RA to the virgin materials even without any preheating.

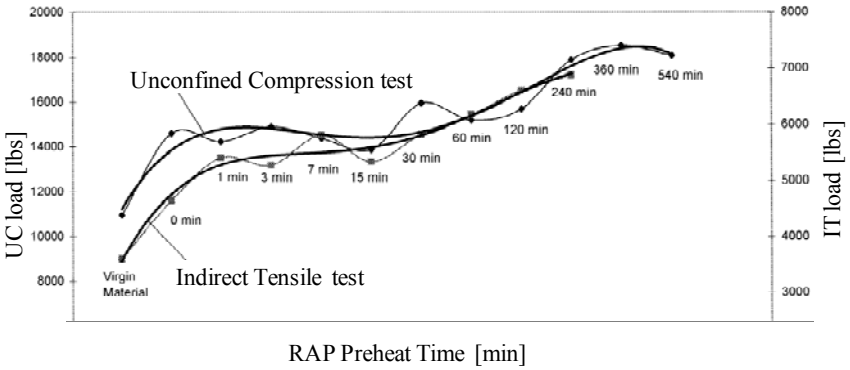

Figure 1.16 Effect of RA preheating time on unconfined compression and indirect tensile strength [32].

The idea that bitumen films on coarse aggregates would be more available for blending with virgin aggregates than bitumen film around fine aggregates was also investigated. After being lightly heated and spread in a flat pan at one stone layer thickness, an HMA containing 40% RA was placed in a drum mixer with steel ball bearings and mixed for four minutes. The binder was then recovered from the coarse aggregate pieces and compared to binder recovered from fine aggregates. Using a Dynamic Shear Rheometer (DSR) the G^* of recovered binders was then determined. Results indicated that variation in the binder stiffness did not relate to the asphalt coating of the coarse and fine aggregates. In fact, for a virgin HMA, large differences in bitumen stiffness were detected between recovered fractions. The stiffness of the thin layer of binder coating the aggregates is mainly controlled by its exposure to heat and air during production, which is a random process and does not relate to whether the aggregate is coarse or fine.

Huang et al [31] conducted a study to investigate the blending between aged and virgin binders in HMA containing RA. The aggregate in the RA material was limestone, which was fractionized so that only material passing through a 4.75mm sieve was used. Virgin aggregates larger than 4.75mm were used to make it possible to separate them from fine RA aggregates. To assess the blending due to pure mechanical mixing, RA materials were blended with virgin aggregates only (i.e., no virgin binder was added). After mixing, the RA and virgin aggregates were separated again with the 4.75mm sieve.

It was found that only 11% of RA binder was transferred to the virgin aggregates. Huang concluded that pure mechanical mixing as conducted in [31] is not sufficient to guarantee a certain percentage of aged binder that can

be removed from the RA and that can be available for use as effective bitumen for coating both virgin aggregates and recoating the RA particles.

The process of diffusion allows rejuvenating the aged binder and may facilitate its separation from the RA materials and its effective contribution to the coating of virgin and RA aggregates. One has to consider also the fact that only minus #4 (4.75mm) RA was used in this study, which would result in more bitumen available in the fine fraction of the mixture. This is done with a longer mechanical mixing time than what is used in typical laboratory situations or at the plant and at a higher temperature.

Actual mixing between RA materials and virgin bitumen and aggregates can be demonstrated by the level of blending between aged and virgin bitumen around RA aggregates. In this case, Huang et al. conducted staged extractions to obtain bitumen from various layers coating the RA aggregates. Results indicated that after blending, the outside layers of bitumen around RA aggregates were much softer than the inside layers of binder. In terms of percentages, about 60% of the aged binder did not blend with the virgin binder while 40% of the outside binder was a blend between aged and virgin binders. Although the authors mentioned that the mixtures used in that study do not reflect common HMA normally used in practice, it was evident that 100% of RA was not effectively blended in the mixture. Therefore he suggested that further investigation is required to measure the amount of blending.

1.2.11. Effect of extraction and recovery methods on RA Binder

Binder extraction and recovery of aged bitumen is necessary to determine the amount of bitumen content and measure its rheological properties. The circumstances under which the recovery and extraction take place might influence the rheological properties by chemical changes or extra hardening. There have been also valuable efforts to estimate RA's binder viscosity [31] by estimating it using GPC without binder recovery. This was done by correlating different GPC measurement results with the results of viscosity measurements.

Different methods, equipment and solvents for extraction of bitumen can have significant effects on the properties of the extracted bitumen. Figure 1.17 illustrates a fast extraction apparatus using Methylene Chloride to extract bitumen using a centrifuge. Figure 1.18 shows a rotary evaporator which is based on NEN-EN 12697-3.



Figure 1.17 "InfraTest" fast automatic extraction apparatus, b.) Soaking of the bituminous sample in a sieve drum. [33]

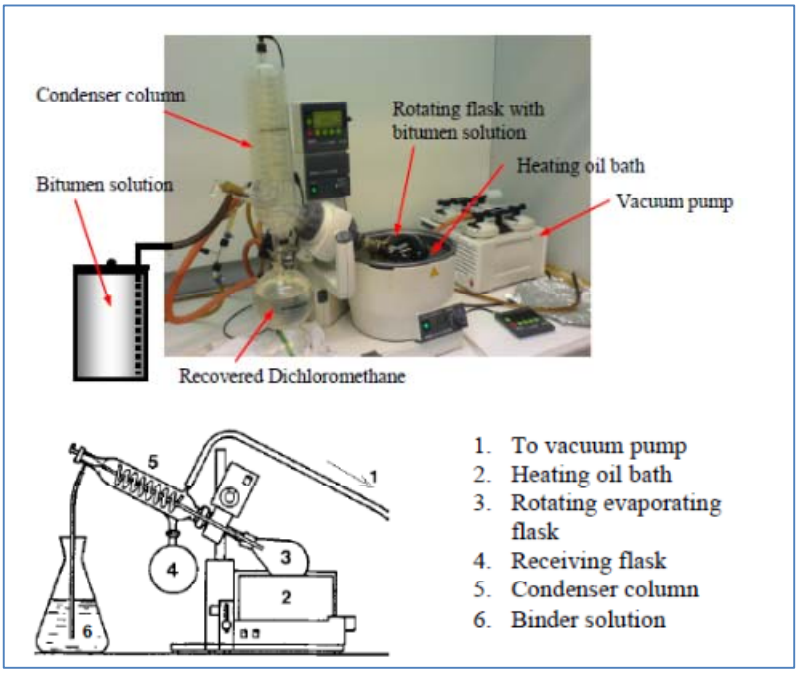

Figure 1.18 Rotary evaporator used in the recovery of bitumen (Büchi Rotavapor R-200) [33]

Hagos [33] evaluated the effect of solvent extraction and rotatory evaporing recovery method on the physical properties of bitumen by measuring them

before and after extraction and recovery treatment. Applying the extraction and recovery methods shown in Figure 1.17 and Figure 1.18, he concluded that a decrease of about 10% in penetration and an increase of about 2.5% in softening point after recovery took place.

ASTM D2 172, *Quantitative Extraction of Bitumen from Bituminous Paving Mixtures,* has been the accepted procedure for extraction for many years. The procedure allows five methods. Method A, (centrifuge extraction), and Method B (reflux extraction) are the most commonly used methods. Methods C and D are variations of the reflux extraction that are not commonly used. Method E is the vacuum extraction. Previous research has indicated that Method B (reflux) appears to cause some hardening of the bitumen [34]. The vacuum method has not been used as widespread as the other methods. Given the fact that reflux extraction can cause extra hardening and the vacuum method is seldom used in the Netherlands, the centrifuge method (Method A) is therefore used in this PhD research for extraction of RA binder.

1.3. Conclusions and summary of the literature survey

The main points of the literature survey are:

1. Almost all hot mixing plants can be modified for asphalt recycling. However the circumstances under which RA is introduced and mixed with virgin bitumen depends on the type of unit and can have a significant influence on the mixture properties.
2. Three major mixing facilities are identified, being; batch plant, parallel drum mixer, and counter drum mixer. The double drum is a modified form of counter-flow mixer in which the mixing chamber is folded around the drum dryer.
3. Adding RA into a parallel drum mixer causes severe exposure of RA and virgin binder to the hot gas stream which will result in extra aging.
4. The most important part in hot recycling in batch plants is the preheating and feeding system. Five types of modification of batch plants have been used for RA preheating and feeding system. A cold RA feeding system is used in four of them while in the fifth method a drum dryer is employed to preheat the RA prior to mixing. A method similar to the fifth method is widely used in the Netherlands for HMA recycling.

5. In cold feeding systems, thermal energy is transferred via virgin aggregates; this implies that the level of preheating should be selected in accordance with the RA content and its moisture content.
6. Cold and moist RA is exposed to superheated virgin aggregates in the mixing chamber. However, this exposure is happening gradually. Immediate mixing after RA introduction may reduce the effect of the heat shock on the RA and the virgin binder.
7. In general the mixing period in a double drum is slightly longer than in a batch plant. It also depends on the rotating speed of the inner drum.
8. Segregation may occur during mixing, storage and construction in three types; aggregate segregation, temperature segregation and segregation in bitumen content. Almost all types of segregations may cause serious durability problems during the service life of a pavement.
9. Two forms of aging are identified; short term and long term aging. Short term aging is associated with mixing and handling of the hot mixture. Oxidation and volatilization of bituminous binders while they are exposed to hot gas and superheated aggregates are the main factors responsible for binder hardening during production and construction.
10. Increasing the mixing time of RA and virgin material may improve the homogeneity of the mixture but it may also contribute to extra aging of the binder.
11. The quality of the RA binder depends on the source and the type of handling during crushing and stockpiling. Depending on the quality of the RA, the binder still possesses volatile fractions which could evaporate during a prolonged preheating time of RA and will result in binder hardening. Increasing the preheating time can stabilize the homogeneity of the RA temperature and that contributes to mixing, however, it may also cause extra aging of RA binder
12. Designs for the grade of the added bitumen in recycled mixtures are primarily based on penetration, softening point, and viscosity blending equations. The viscosity blending chart is based on the Arrhenius equation and is used for blending of RA with soft binder as well as rejuvenator. The Log pen rule is mainly developed for pen grade bitumen. Each blending rule assumes total blending between two binders or a binder and a rejuvenator. Total blending however will not occur in real practice.

13. When applying solvent extraction and recovery methods, one has to take into account the possible presence of some residual solvent and filler which could affect the binder properties.
14. The level of interaction and the extent of blending between virgin bitumen and RA binder still require substantial study.
15. The properties of recycled mixtures with high amounts of RA are significantly affected by the increase of binder stiffness which in turn is depending on the amount of RA and the way of RA handling.

CHAPTER 2

EXPERIMENTAL DESIGN ON PART 1

2.1. Experimental plan

As explained earlier, the focus in Part 1 is on experiments with hot recycled mixtures prepared in the laboratory and in the field with real mixing plants. In the general introduction of this dissertation, four objectives were identified to be addressed in Part 1 which is separately discussed in two parts of this dissertation. Two of those objectives will be studied in a two phase experimental program in part 1, namely;

- To develop an effective laboratory mixing method to simulate the real recycling process in the field as good as possible.
- To assess the effect of the double drum recycling process on mixture properties in comparison with the conventional batch plant and standard laboratory mix design.

The organization of both study phases and their interrelation are shown in Figure 2.1. The experimental design of each phase will be explained here-after.

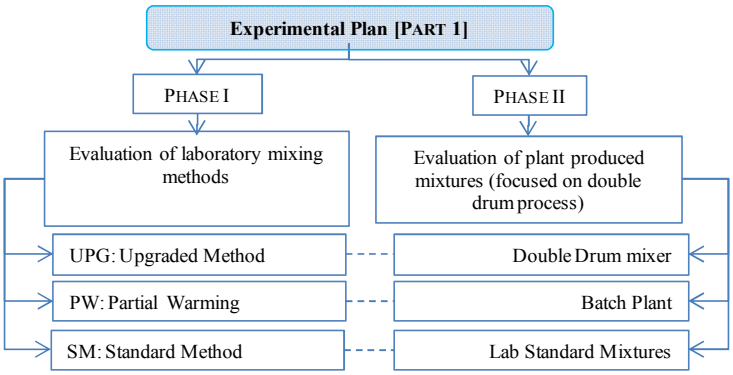

Figure 2.1 Overview of the experimental plan of PART 1.

2.1.1. Experimental plan of Phase I

Mixing methods in the laboratory are considered to be a scaled down model of what happens in real plants. In HMA mixture designs without RA, preheating of all material at 170°C (see EN 12697-35) prior to mixing with a lab pug mill mixer or pan mixer seems to be adequate in simulating the real plant. This method is called here after the Standard Method (SM). However, a number of factors still have to be taken into account while simulating real plant hot mix asphalt in the lab. Standard mixing methods which are described in most of the norms are based on the concept of preheating, mixing and storing (aging) all material at one fixed temperature. Although this presumption is not likely to introduce a big difference between lab and plant produced mixtures made from virgin materials, the introduction of RA in cold and moist conditions requires additional factors to be taken into account. The two additional factors, RA preheating and moisture conditions are depicted together with others in Figure 2.2.

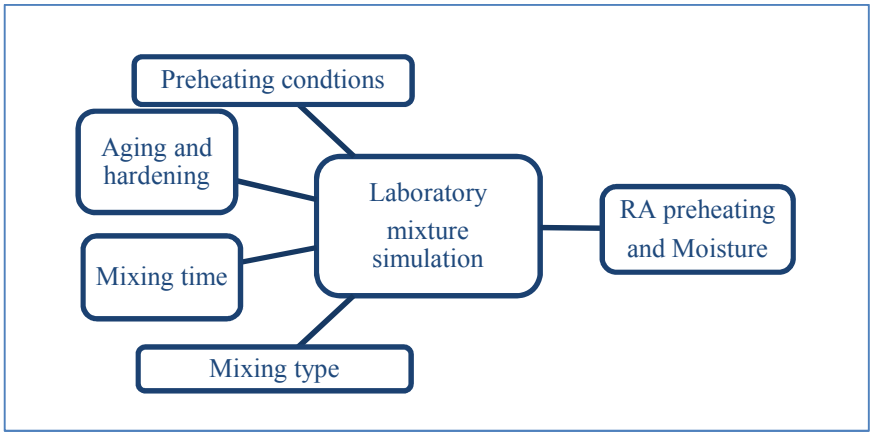

Figure 2.2 Factors which are simulated in laboratory mixing methods

Two more laboratory mixing methods are developed in this research to modify the standard way of mixing in the lab with respect to the addition of cold and moist RA. The Partial Warming method (PW) is simulating the partial heating of RA at 130°C while the Upgraded Method (UPG) is developed to mimic the double drum process.

The three mixing methods examined in "Phase I" are summarized in Table 2.1. Similar to real plants, preheating temperatures of aggregate were set according to RA content and its moisture (see Table 2.2 and Figure 2.3 for comparison).

Table 2.1 Mixing method simulation and conditioning

Mixing method	***Related actual plant***	***Preheating conditions and temperatures (°C)***		***RAP***	
		Virgin Aggregate	RAP	Moisture content [%]	Yield in the mixture [%]
SM	Standard mixing procedure in Lab	170	170	No	0, 30, 60
PW	Batch plant with parallel drum	240~330 (depending on RA content)	130	No	30, 60
UPG	Double drum mixer	290~515 (depending on RA content and its moisture)	23	0%, 4%	30, 60

RA contents of 30% and 60% are used in the SM, PW and UPG method. Mix designs are identified with their variables as digits following the initials of mixing methods. For example SM30 means mixtures produced with the SM method with 30% RA. Moisture contents of 0% and 4% were also involved in the UPG method, hence they are coded as UPG0 and UPG4 preceding the number indicating the RA content. For example UPG460 implies 4% moisture and 60% RA. The organization of the mixture designs and the system of mixture identification are shown in Figure 2.4.

Table 2.2 Preheating temperature of different mixing methods, RA content and moistures

Mixing method	***Preheating temperature of virgin aggregates***		***Preheating temperature of RA***
	Before mixing with 30% RA	Before mixing with 60% RA	
SM	170°C	170°C	170°C
PW	240°C	330°C	130°C
UPG0	290°C	430°C	25°C
UPG4	345°C	515°C	25°C

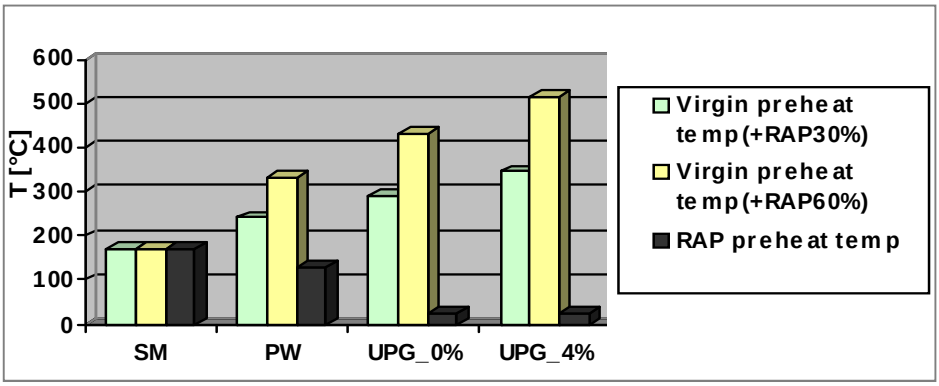

Figure 2.3 Comparison of preheating conditions of virgin aggregates and RA for different mixing methods (the target mixture temperature is 170°C)

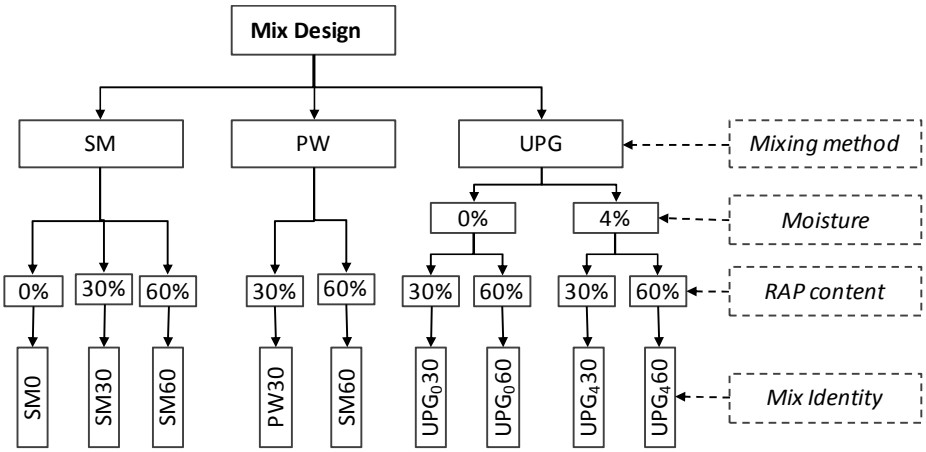

Figure 2.4 Structure of the mixture designs considering three mixing methods, three levels of RA content and two levels of moisture content (for UPG)

One mixture type is produced in 9 versions (see also Figure 2.4) being: SM0 (No RA), SM30, SM60, PW30, PW60, UPG030, UPG060, UPG430, and UPG460. A ten liter Hobart mixer was used for mixing the aggregates. Cylindrical samples were produced by means of Gyratory and Marshal Compaction. Prepared samples were used to measure the indirect tensile strength, stiffness and fatigue life.

Because the initial mixtures were compacted to voids contents of approximately 3%, extra series of mixtures containing 60% RA were similarly tested during a master thesis by Chacho [35]. He tested SM60*, PW60*, UPG060* and UPG460* at higher air voids of around 5% which is more comparable to the voids contents achieved in practice. Chacho's work therefore allowed evaluating the effect of higher air voids on the fatigue and stiffness characteristics. His mixtures are distinguished in sample coding with an extra * sign at the end of the mixture codes.

2.1.2. Experimental plan of Phase II

In this phase, experiments were developed to evaluate mixtures produced by means of the batch plant and double drum mixer in comparison with laboratory mixtures using the same material. Similar to Phase I, only one base course mixture (AC22)[1] was investigated which contained 50% RA. They are identified as "A", "BB", and "L" in this thesis corresponding to the mixtures produced respectively in Astec double drum (A), batch plant (BB) and laboratory mixer (L).

As it was explained earlier in the literature review the RA is introduced in the double drum while cold and moist; the moisture content in the stockpile was approximately 4%. In the batch plant, RA is preheated at 130°C in a parallel drum prior to be mixed with the virgin materials. The target temperature of the final mixture was set to 170°C hence the virgin aggregate temperature is adjusted to meet this target temperature. For the LAB samples RA and virgin materials were all preheated at 170°C. Similar sources of material including RA, crushed stone, filler and virgin bitumen were used for the production of all mixtures except for a special mixture "B" with 25% PRA (reclaimed material from crushed porous asphalt) and 25% RA.

A shear box compactor was used to produce compacted blocks which were cut into beams and cylinders. Facilities and mixing devices in this phase are shown in Figure 2.5.

[1] Asphalt Concrete with maximum aggregates size of 22mm.

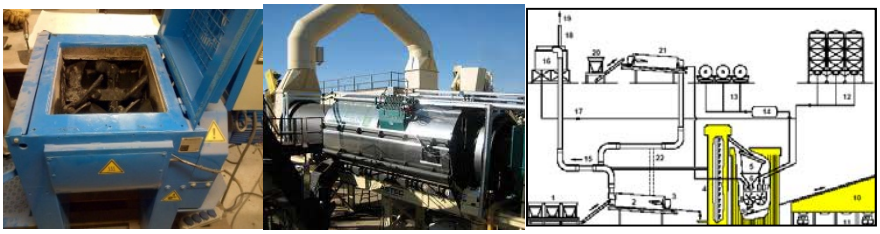

Figure 2.5 Mixing facilities used in phase II (from left to right: Laboratory mixer, Astec double drum mixer and Batch plant equipped with parallel drum dryer)

Beams and cylinders are used to evaluate the material stiffness, tensile strength and fatigue life. The experimental plans of Phase I & II are depicted in Figure 2.6.

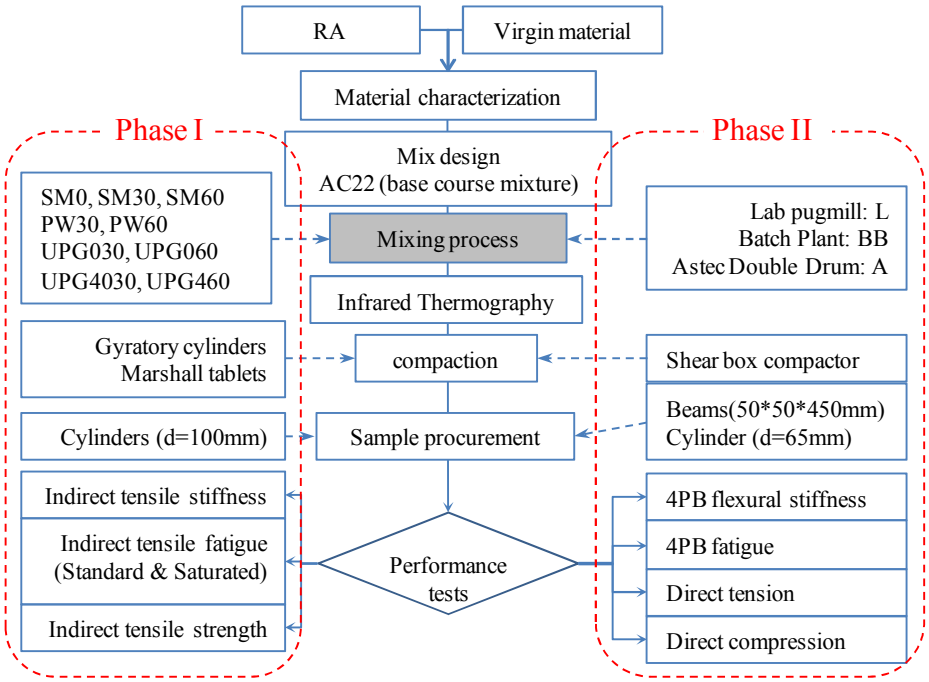

Figure 2.6 General overview of the experimental plan of Phase I and Phase II.

2.2. Testing methods and instrumentation

A number of instruments and test methods were used in characterizing the materials and measuring the performance related properties of the procured specimens. Figure 2.6, shows the tests carried out during Phase I and II according to the testing methods listed in Table 2.3.

Table 2.3 Testing methods used during material preparation in both phases of experiments (Phases I&II)

Properties/procedures	***Method***
Bitumen/ binder penetration	EN 1426, Bitumen and bituminous binders-Determination of needle penetration
Extraction of RA binder	EN 12697-1, Bituminous mixtures — Test methods for hot mix asphalt — Part 1 Soluble binder content.
Recovery of RA binder	EN 12697-3, Bituminous mixtures — Test methods for hot mix asphalt — Part 3: Bitumen recovery: Rotary Evaporator
Bulk density	EN 12697-6, Bituminous mixtures — Test methods for hot mix asphalt — Part 6: Determination of bulk density of bituminous specimens.
Theoretical maximum density	EN 12697-5, Bituminous mixtures — Test methods for hot mix asphalt — Part 5: Determination of the maximum density.
Specific gravity of particles	Gas Pycnometery (Ultrapycnometer 1000)

Although most of these testing methods are explained in the European norms, their measuring principles are explained below for the sake of completeness.

2.2.1. Specific gravity by ultra-pycnometer

Measuring the bulk density of aggregates is essential for determining the theoretical maximum density of the mixture and other volumetric properties such as air void content. In this research an Ultra-pycnometer 1000 (Figure 2.7) is employed to measure the bulk specific gravity of the crushed stones, sands and fillers.

It measures the true volume of solid materials based on the principle of Archimedes for gas displacement (preferably Helium gas because of its smaller atoms). Helium gas can penetrate into pores as small as 10^{-10} m which

enhances the accuracy of the volume measurement. The sample holder can contain only a small amount of particles. The specific gravity is obtained by averaging the results of three repeated measurements. This method is used in this research because of its accuracy and the speed of measuring several types of aggregates and particles.



Figure 2.7 Ultra-pycnometer 1000 used for specific density of particles

2.2.2. Extraction and recovery of RA and compacted mixtures

In order to be able to determine the grade of the virgin bitumen and the amount of virgin bitumen to be used in the mixture, it is necessary to know the properties of the RA binder as well as the RA bitumen content. Also the aggregate gradation of RA should be known.

In order to extract the binder, a solvent based extraction method is applied in this research according to EN 12697-1 using Dichloromethane (Methylene Chloride) as the solvent. Approximately 2kg of air dried RA is washed with solvent on several sieve sizes to be collected later. The solution is circulated until it is clear. Then the solution is brought into a distillation recovery setup according to EN12697-3 called "Rotatory evaporator". The purpose is to separate the bitumen from the solvent. In this method the Rotatory evaporator flask is operating under vacuum. An oil bath maintains the temperature in the flask at different temperatures (85, 150°C) and different vacuum pressures (85 and 2kPa), in three phases during the process. The equipment used in the extraction and recovery process is shown in Figure 2.8.



Figure 2.8 Centrifugal extraction and Rotatory evaporator setup [36]

2.2.3. Rheological tests on bituminous binder

A Dynamic Shear Rheometer (DSR) is used in this research to characterize the binder properties. In addition, empirical binder tests like needle penetration (EN 1426) and ring and ball tests were performed. The DSR is used to measure the rheological properties of bituminous binders over a range of temperatures and loading times (frequency). Bitumen is a thermoplastic, visco-elastic material which behaves as an elastic solid at low temperature (or high loading frequency) and as a viscous fluid at high temperature (or low frequency). The shear modulus (G*) obtained in the linear visco-elastic range is commonly used for creating master curves. These master curves are extensively used in Part1 and Part2 of the dissertation to compare RA binder properties as well as those of other bitumen involved in the experiment. An AR2000ex DSR, with a torque capacity of 0.2 Nm, is used in this research (see Figure 2.9). It is equipped with an environmental test chamber (ETC[1])

In the test a thin layer of binder is sandwiched between two circular plates. The lower plate is fixed while the upper plate oscillates by applying a sinusoidal shear strain or stress across the sample at a given angular frequency (ω). The DSR can be applied either in the stress or strain controlled mode. It measures continuously the required torque in response to the applied strain.

In this research the DSR is mainly used to determine G^* and the phase angle δ and to describe the visco-elastic properties under sinusoidal shear loading conditions (see Figure 2.10)

[1]ETC is a test cabinet with an accurate temperature control system based on electrical heating and gas cooling (using a Nitrogen storage vessel) [37]

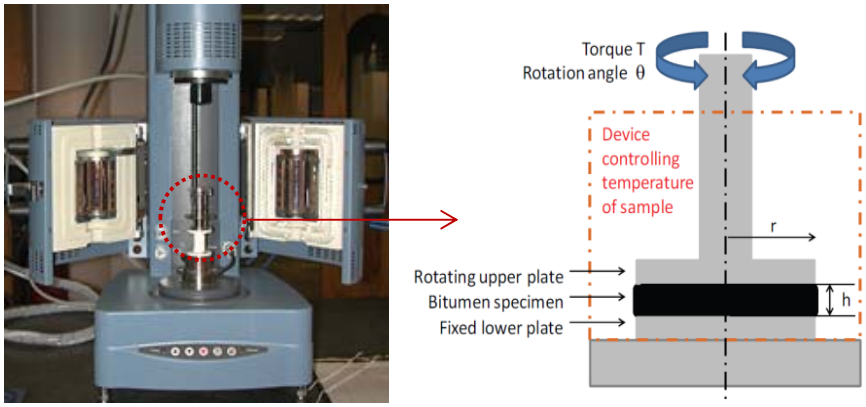

Figure 2.9 Right: concept of the DSR [37], Left: Dynamic Shear Rheometer used in this research (AR2000),

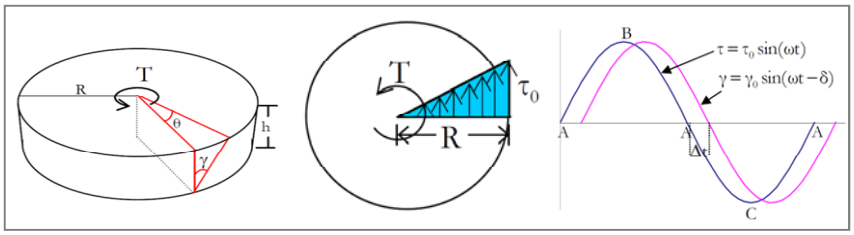

Figure 2.10 Oscillatory loading in DSR and viscoelastic behaviour of bitumen ($\tau_o = \tau_{max}$; $\gamma_0 = \gamma_{max}$) [38]

The following equations are used for obtaining the fundamental material properties (in the figure 2.10 you give γo and τ_o as maximum values)

$$\gamma_{max} = \frac{\theta_R}{h} \text{ and } \tau_{max} = \frac{2T}{\pi R^3} \qquad (2.1)$$

$$|G^*(\omega)| = \frac{\tau_{max}}{\gamma_{max}} \qquad (2.2)$$

$$G^*(\omega) = |G^*(\omega)| \cdot \cos\delta + i\,|G^*(\omega)| \cdot \sin\delta = G' + iG'' \qquad (2.3)$$

$$\delta = \omega\Delta t = a\tan {}^{G''}/_{G'} \qquad (2.4)$$

The following relations are used to determine the shear compliance in a DSR test [38].

$$|J^*(\omega)| = \frac{\gamma_{max}}{\tau_{max}} \qquad (2.5)$$

$$J^*(\omega) = |J^*(\omega)| \cdot \cos\delta + i\,|J^*(\omega)| \cdot \sin\delta = J' + iJ'' \qquad (2.6)$$

Where:

R = radius of the cylindrical sample [mm]

h = height of the cylindrical sample [mm]

T = is the applied Torque [N.mm]

θ = rotation [rad]

τ_{max} = maximum shear stress [MPa]

γ_{max} = maximum shear strain [-]

i = complex notation

Δt = phase lag between the stress and strain signals [s]

δ = phase angle of the material for a given frequency, ω,[º]

$|G^*|$ = magnitude of the complex shear modulus [MPa]

G' = storage shear modulus [MPa]

G'' = loss shear modulus [MPa]

$|J^*|$ = magnitude of the complex creep compliance [MPa]

J' = storage creep compliance [MPa]

J'' = loss creep compliance [MPa]

2.2.4. Modelling bitumen viscoelasticity (master curves)

Bitumen is a time-temperature dependent visco-elastic material. This characteristic allows the creation of G* and δ master curves. Master curves are built using the time-temperature super positioning (TTS) principle. To create master curves, frequency sweep tests on the binder at a number of temperatures need to be available. The data obtained at different temperatures are shifted such that a master curve is obtained at the set reference

temperature (see Figure 2.11). The WLF[1] model is used to shift G* and δ values. This model is presented in the following equation.

$$\log \propto_T = \frac{C_1(T - T_R)}{C_2 + T - T_R} \qquad (2.7)$$

Where:

α_T = shift factor (horizontal) at temperature T [-]

T_R = reference temperature [°C]

C_1, C_2 = constants [-]

The Arrhenius equation is also widely used for the determination of the shift factor [39] [40] [41] [42]; this is done by means of the following equation

$$\log \propto_T = \frac{\Delta H}{2.303R}\left(\frac{1}{T} - \frac{1}{T_R}\right) \qquad (2.8)$$

Where:

ΔH = activation energy [KJ/mol]

R = gas constant

T_R = reference temperature [Kelvin]

In this research the WLF model is used for creating bitumen master curves and Arrhenius is used in mixture master curves.

Once curves are shifted, a mathematical model is used to fit all shifted curves into one master curve. In this research an S-curve model is employed to fit the data. The following equations are expressing the model parameters [43]:

$$G^* = G^*_{min} + S(G^*_{max} - G^*_{min}) \qquad (2.9)$$

$$\delta = \delta_{max} - S(\delta_{max} - \delta_{min}) \qquad (2.10)$$

$$S = [1 + ({}^{\omega_c}/_{\omega'})^k]^{\frac{-m_e}{k}} \qquad (2.11)$$

$$\omega' = \propto_T . \omega \qquad (2.12)$$

Where:

G^* = complex modulus [MPa]

[1] Williams-Landel-Ferry

G^*_{min} , G^*_{max}	=	complex modulus for $\omega \rightarrow 0$ and $\omega \rightarrow \infty$ [MPa]
δ	=	phase angle [°]
δ_{min} , δ_{max}	=	phase angle for $\omega \rightarrow \infty$ and $\omega \rightarrow 0$[°]
k, m_e	=	shape parameters [-]
$\propto_T$	=	shift factor [-]
ω	=	frequency [rad/s]
ω'	=	reduced frequency [rad/s]
ω_c	=	location parameter [rad/s]

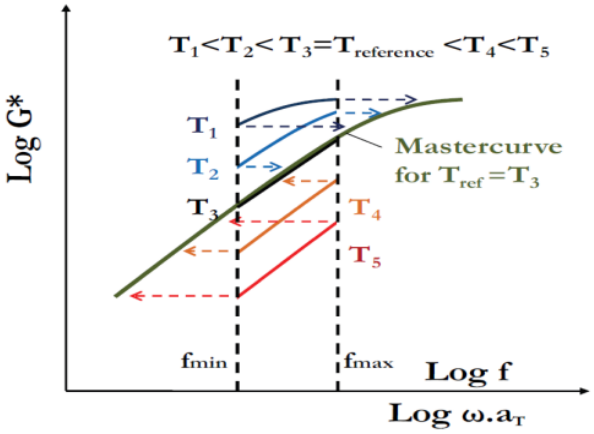

Figure 2.11 Schematic of master curve generation method using TTS character of bitumen [37]

2.2.5. Four point bending stiffness and fatigue test

Stiffness and fatigue properties of asphalt mixtures are crucial factors in mechanistic-empirical pavement design systems [44] . In the Netherlands, the 4 point bending test is employed for decades to evaluate the mechanical properties of asphalt mixtures based on European Norms NEN-EN 12697-24 & 26. The four point bending test is designed to characterize the behaviour of mixtures under fatigue loading by continuously measuring the flexural stiffness during a cyclic test. This test setup consists of inner and outer clamps which are holding a rectangular beam (typically 50×50×450mm) in a horizontal position. The sample is exposed to cyclic bending with free rotation in all clamps (see Figure 2.12)

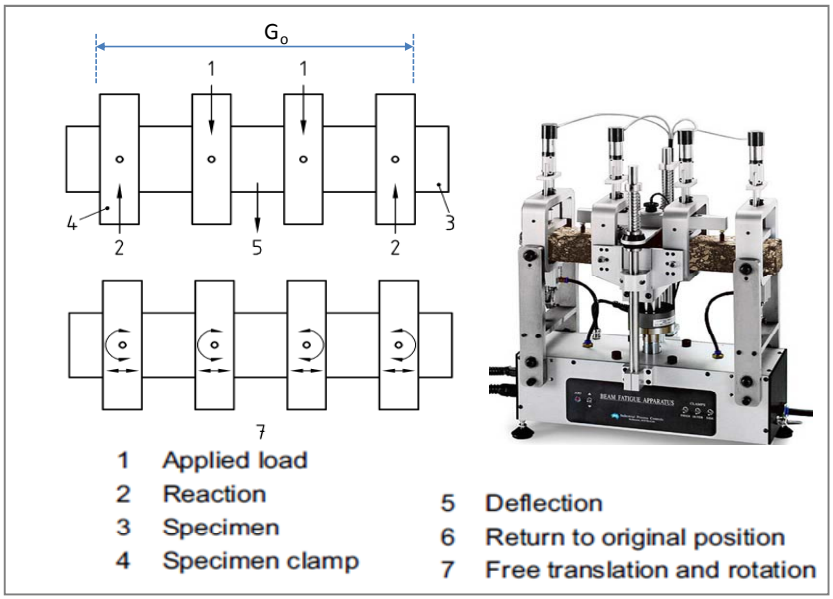

Figure 2.12 Basic principles of 4PB test as described in EN 12697-24

The outer clamps are fixed while the inner clamps move in the vertical direction causing bending deflection in the beam.

The applied load, deflection and phase lag between the load and displacement are measured when a sinusoidal loading is applied on the specimen. The following equations are employed in calculating the influencing parameters:

$$\sigma_t = \frac{PG_0}{wh^2} * 10^6 \qquad (2.13)$$

$$\varepsilon_t = \frac{12\delta h}{3{G_0}^2 - 4{G_i}^2} * 10^6 \qquad (2.14)$$

$$S = {}^{\sigma_t}/_{\varepsilon_t} * 10^3 \qquad (2.15)$$

$$\varphi = 360fs \qquad (2.16)$$

Where:

σ_t = maximum tensile stress [kPa]

G_0 = outer gauge length [typically 355.5mm]

P = peak force [kN]

W = beam width [mm]

h = beam height [mm]

ε_t = maximum tensile strain [µm/m]

δ = peak deflection at the center of the beam [mm]

S = flexural stiffness [MPa]

φ = phase angle [°]

s = time lag between peak deformation and peak force [s]

f = load frequency [Hz]

The flexural stiffness value which is determined after 100 conditioning load pulses is used in this research as the initial stiffness of the material in creating a master curve. The fatigue life is also determined; it is defined as the number of load repetitions at which the stiffness of the mixture under strain control conditions reaches half of its initial value.

2.2.6. Indirect tensile strength

The Indirect tensile strength test is carried out according to EN 12697-12. In this test the cylindrical test specimen is brought to the specified test temperature, placed in the compression testing machine between the loading strips, and loaded diametrically along the direction of the cylinder axis with a constant speed of displacement until it breaks.

The indirect tensile strength is the maximum tensile stress calculated from the peak load (see Figure 2.13) applied at break and the dimensions of the specimen with the following equation:

$$ITS = \frac{2P}{\pi DH} \qquad (2.17)$$

Where:

ITS = indirect tensile strength, expressed in [MPa]

P = peak load, expressed in [N]

D = diameter of the specimen, expressed in [mm]

H = height of the specimen, expressed in [mm]

This test was done on cylindrical samples according to EN 12697-12 at 5°C. This temperature was selected in order to estimate an appropriate stress level for the stress controlled fatigue tests that were performed at that temperature.

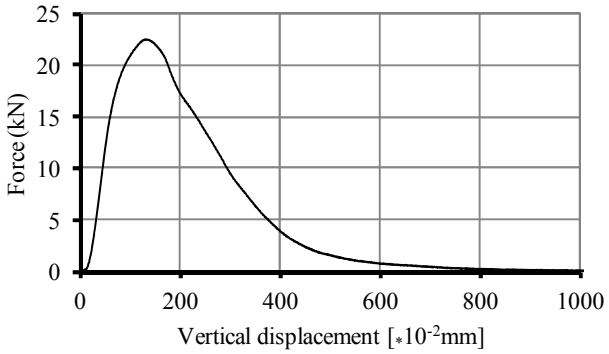

Figure 2.13 Typical force-displacement result in ITS test

2.2.7. Indirect tensile stiffness and fatigue test

This method was used to obtain indirect tensile stiffness values at different temperatures and loading times on cylindrical samples in Phase I of the experiments. Stiffness values were measured according to EN 12697-26 (see Figure 2.14). Stiffness values are determined after 5 conditioning pulses and a rest period of 3000ms; the stiffness values are calculated with equation (2.18).

The results were then used to create complex modulus master curves at the defined reference temperatures.

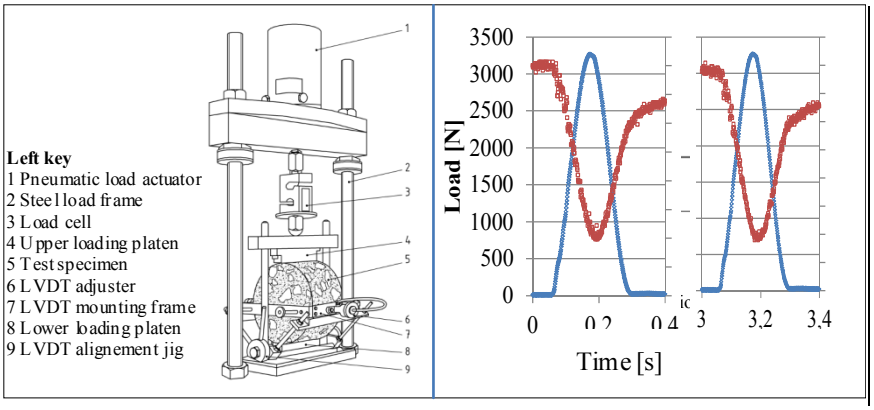

Figure 2.14 Instrumentation and haver sine loading of indirect tensile cyclic test [45].

$$E_r = \frac{F(0.27+\upsilon)}{l.\Delta d} \qquad (2.18)$$

Where;

F = maximum applied load (repeated load) [N]

υ = Poisson's ratio

l = height of the specimen [mm]

Δd = total recoverable (resilient) horizontal deformation [mm]

E_r = resilient modulus [MPa]

During the tests, the Poisson's ratio values shown in Table 2.4 were assumed at different temperatures. These values were determined during the ACRe project by Erkens (2000).

Table 2.4 Assumed Poisson's ratio values

Temperature (°C)	***5°C***	***10°C***	***15°C***	***23°C***	***35°C***
Poisson's ratio	0.22	0.24	0.27	0.32	0.4

In order to characterize the behavior of different mix designs, the ITT fatigue tests were also conducted on cylindrical samples. Cylindrical shaped samples were exposed to repeated haversine shaped compressive loads through the vertical plane. This loading develops a relatively uniform tensile stress over the middle 2/3 part of the specimen perpendicular to the direction of the applied load and along the vertical diametric plane, which causes the specimen to fail by splitting along the central part of the vertical diameter. After ITT stiffness tests, fatigue tests were done at one temperature of 20°C in a continuous cyclic loading test with no rest periods between the cycles. The number of cycles at which the mixture fails under the controlled stress condition, is defined as the fatigue life according to EN 12697-24. Because of the limited number of available specimens, all tests were done at a stress level of 220kPa and a loading frequency of 10Hz. This stress level was determined by trial and error to get a reasonable number of loading cycles for each fatigue test. The mixtures with the higher air voids content (those which are indicated with *) were tested at different stress levels.

2.2.8. Uniaxial monotonic direct tension test (UMDTT)

In order to better understand the damage mechanisms in asphalt concrete it is necessary to establish more fundamental knowledge about the material properties and responses [48]. In Phase II of this research UMDTT was conducted in the displacement controlled mode. The setup has been developed during the ACRe project [49] in the section of Road and Railway Engineering of TUDelft in 2000. The test setup consists of a rigid frame with a 3 hinge loading system enclosed in a temperature cabinet which is capable of maintaining temperatures in a range of -40 to 100°C. A 50 kN hydraulic actuator is maintaining the load and displacement during the test. The installation of cylindrical samples between 3 hinges ascertains the exposure of the sample to a pure uniaxial force and avoids any bending moments in the specimen. A load cell, installed between the two hinges above the specimen, measures the force value. The force and displacement rate are controlled by an internal controller (MTS 407). The radial deformation is measured using a diametric chain extensometer.

Cylindrical specimens of 65×138 mm which were cored from shear box compacted blocks, are glued on both side to aluminum caps by means of a two component glue. Additional plastic rings are also glued to achieve a better load distribution towards the body of the specimen to prevent failure at the caps (see Figure 2.15 for details). This setup and sample preparation was done according to [46] and [47].

The axial deformation of the specimen is controlled by three LVDTs installed between the two caps.

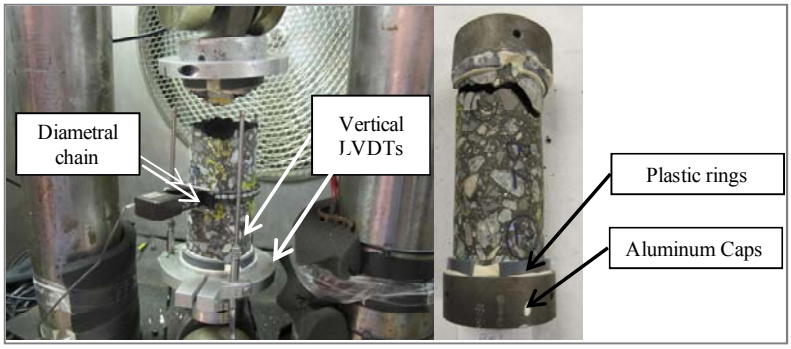

Figure 2.15 Uniaxial Monotonic Direct Tension Test Setup

2.2.9. Uniaxial monotonic direct compression test (UMDCT)

This test setup was also developed at TU Delft during the ACRe project [48] in 2001. It consists of a rigid steel frame with a hydraulic actuator of 150kN mounted on top of the setup. The compression cell is located in a small temperature chamber to maintain the temperature in a range between -5 to 45°C. The frame is placed on a concrete block (see Figure 2.16). The bottom and top plate are kept parallel by means of three massive aluminum bars which are connected to the bottom plates and pass through linear bearings in the top plate [49]. To avoid friction between sample and steel plates, a special plastic foil which is covered with soap is employed on both sides. This friction reduction system improves uniformity in the stress distribution on the sample.

The axial deformation is registered by three LVDTs. The radial deformation is also measured with a radial extensometer chain, similar to the tension test. Data is collected via a data acquisition system at sampling rates ranging from 1 to 1000 Hz. The test data are then collected from the setup to reproduce the loading signals and further analytical charts in Excel sheets. The process of data analysis is explained in chapter 5.

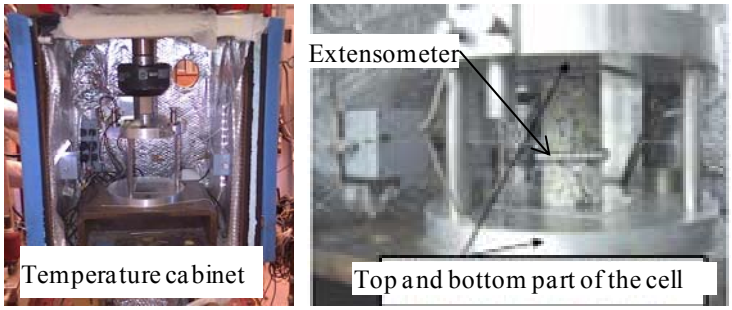

Figure 2.16 Uniaxial Monotonic compression test

CHAPTER 3



MATERIALS AND MIX DESIGN

3.1. Introduction

Based on the research methodology, two series of mixtures with different RA contents had to be prepared for the phase I and phase II studies. The mix design procedure, the sample preparation procedures and material properties in both experiment phases will be explained in this chapter.

Several batches of an AC22[9] base course mixture were produced, each with the same target gradation but containing different amounts of RA. The AC22 is in practice produced with at least 50% RA in base courses. For this reason this type of mixture was selected in this research for both phases of the study.

In Phase I, 9 mixtures were produced using the SM, PW and UPG mixing methods containing 0%, 30% and 60% RA. In the UPG method, RA moisture contents of 0% and 4% were considered. It has to be noted that study "Phase I" was repeated in a master thesis by Chacho [35] which will be reported here as complementary information. In that master study similar mixtures (SM, PW and UPG) with 60% RA but with higher air voids content were produced.

In Phase II, three sets of mixtures containing 50% RA were produced using a batch plant, a double drum mixer, and a laboratory pug mill mixer. The same source of RA and virgin material were used in producing all mixtures except mixture "B" in which two types of RA were used to study the effect of different RA types on the final mechanical properties. The comparison of the mechanical properties between mixture "B" and "BB" is given in chapter 5; both mixtures are produced in a batch plant.

[9]Maximum aggregate size of 22mm

Next to the mixture design, the procedure of mixing and sample preparation is presented (for each phase separately). Furthermore results of initial sample analyses, such as volumetric characterization of samples, are included in this chapter.

3.2. Mixture design procedure

The mixture design procedure can be briefly summarized as follows:

- extraction and recovery of RA binder to characterize the rheological properties of the aged binder;
- determination of the RA binder properties and the grade of bitumen to be added;
- determination of the virgin and RA aggregate properties: gradation and specific gravity;
- determination of the maximum density of the mixture;
- determination of the required amount of virgin aggregate (in relation to RA gradation) and determination of temperature to which virgin aggregate has to be preheated (in relation to the target temperature, RA content and the moisture content of the RA).

3.2.1. RA Characterization

For the purpose of RA characterization RA was sampled from the stockpile in the central asphalt plant. It was crushed and sieved to a nominal size of 0-20 mm. It was air dried in the lab to achieve more control on the moisture content. It should be noted that the RA sampled for Phase I was sieved and fractionized in the lab to have more control on the grading. For the field experiment however, the RA used in the batch plant and drum mixer was as it was in the stockpile without any extra fractioning to fine and coarse fractions. Figure 3.1 illustrates the RA and the virgin aggregate fractions.

For the purpose of RA analysis, each fraction was analyzed with respect to its binder and filler content. Extraction and recovery was done using the method of Rotatory evaporation. The binder extracted from the RA was analyzed with the penetration, ring and ball and DSR test. The gradation of the RA, its bitumen content as well as filler content was determined from residual extracted material. In addition to the whole RA analysis, an analysis of each fraction is also presented. These results were not taken into account in the mixture design but did provide information about the effect of fractionizing in controlling RA properties in practice.

The average RA moisture content of samples taken from the stockpile was 3.2% and the specific gravity of RA aggregates, as measured by Ultra-pycnometer, was 2495 kg/m^3.

The total binder and filler content of the RA were, respectively, 4.3 and 7.8 %m/m by total mass weight. The distributions of this amount of binder and filler to each fraction[10] are shown in Figure 3.2. It is shown that the fractions smaller than 5mm, which constitute 43% of RA, are carrying 57% of the binder and 64% of the filler. These results suggest that it could be beneficial to fractionize RA in asphalt plants, because controlling the bitumen and filler content is of significant importance in reducing variability.

The properties of the RA binder are presented in Table 3.1;

Table 3.1 Extracted RA binder properties

Properties	***Unit***	***Measured values from extracted binder of RA***
Penetration @ 25°C (# @ 15°C)	0.1mm	29
Softening Point, $T_{R\&B}$	°C	59
Penetration Index	( )	-0.8
Density, 25°C, typical	kg/m^3	1035
Binder content	%m/m	4.3
Filler content	%m/m	7.8

The penetration index is calculated by the following equation;

$$PI = \frac{20T_{R\&B} + 500\log P - 1952}{T_{R\&B} - 50\log P + 120} \qquad (3.1)$$

Where:

PI = penetration index

[10] It refers to chunks of RAP aggregates which are screened in order to separate apparent sizes of aggregates. Naturally, each fraction may contain smaller sizes as well. For examplethe RAP fraction of 11-16mm may contain aggregate sizes less than 8 mm as well as filler. It means that each fraction has its own gradation (see Figure 3.3)

$T_{R\&B}$ = softening point [°C]

P = needle penetration at 25°C [0.1 mm]

The complete gradation of RA and the particle seize distribution of all fractions are shown in Figure 3.3. The complete gradation of the RA and related specific gravity values were used in the mixture design procedure.

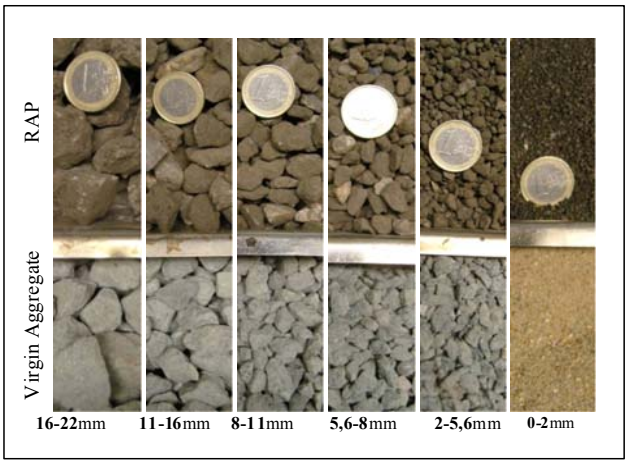

Figure 3.1 RA fractions versus virgin aggregate fractions

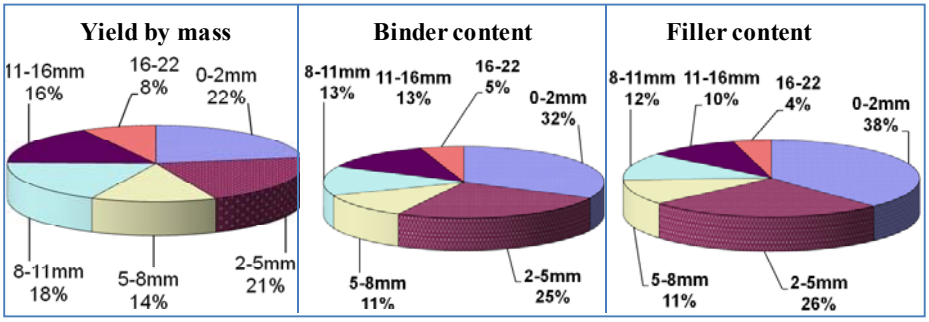

Figure 3.2 Analysis of different fractions of RA (after the extraction of each fraction)

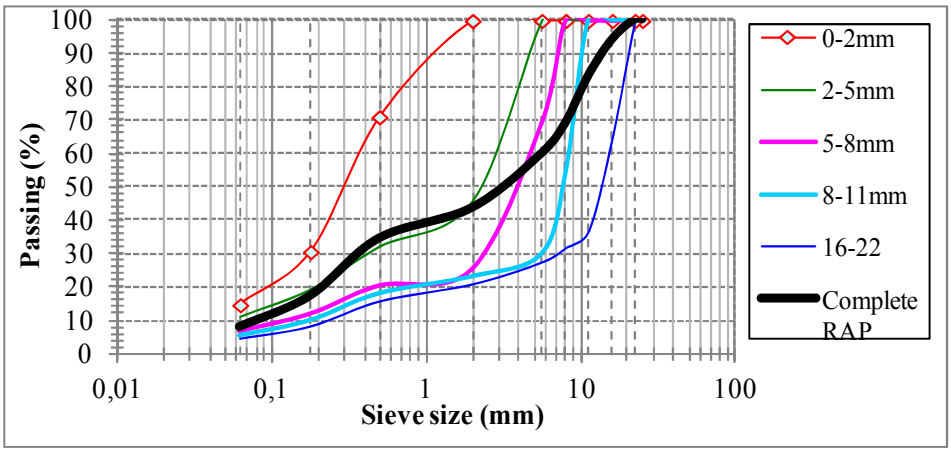

Figure 3.3 Particle distribution of all fractions

3.2.1.1. Properties of the virgin materials

Each material used in this research, (including crushed stone (Norwegian granite) as well as RA), was sampled from the stockpiles at the Gebr. Van der Lee B.V asphalt plant[11]. Two penetration grade bitumens (40/60 and 70/100) supplied by Q8 were used in the experiment. Their nominal properties and the properties measured from the samples are listed in Table 3.2. Wigras 40K was used as filler in all mixtures. The nominal properties of the filler are listed in Table 3.3.

Table 3.2 Properties of virgin bitumen

Properties	***Unit***	***Q8 pen40/60***		***Q8 pen 70/100***	
		Specification range	Measured	Specification range	Measured
Penetration	0.1mm	40-60	50	70-100	90
$T_{R\&B}$	°C	48-56	51	43-51	46
Penetration Index PI.	( )	-1	-0.96	-1	-0.45
Density, 25°C, typical	kg/m3	1035		1029	

[11] Located in Lelystad in the Netherlands

Table 3.3 Properties of the Wigras 40K filler used in the mixtures [50]

Filler properties		
Gradation (passing sieve) 0,125mm 0,063mm		 90-100 (%) 76-86 (%)
Bitumen number[12] (NEN 13179-2)		44-50
Air void % (V/V)		43-47
Density (kg/m^3)		2550 -2750
Calcium Hydroxide category		Ka5
Compositions	% (m/m)	Primary 10 - 35 Secondary[13] 50 - 85 Ca $(OH)_2$ 5 – 15

Table 3.4 Aggregate bulk specific gravities of virgin aggregates

Aggregate Size [mm]	***22,4 - 16***	***16 - 11,2***	***11,2 -8***	***8 - 5,6***	***5,6 -2***	***Sand***	***Filler < 0,063***
specific gravity [gr/mm^3]	2,747	2,777	2,754	2,745	2,789	2,650	2,641

3.2.2. Determination of combined aggregate gradation

Once the RA aggregate gradation (after extraction and recovery) was known, the next step was to determine the bulk specific gravity of the mixture. The combined specific gravity was determined for mixtures containing 0%, 30%, 50% and 60% RA. A fixed target gradation is determined according to the Dutch RAW 2005 standard. This target

[12] Apparent viscosity of a water-filler aggregate mixture, expressed numerically according to NEN 13179-2:2000)

[13] Recycled filler

gradation according to RAW requirements for AC22 is presented in Table 3.5. The desired (target) gradation is also plotted next to the RA gradation (after extraction) in Figure 3.4. Based on the RA content in the mixture, one can calculate the amount of virgin aggregate and filler to achieve the target gradation. In Table 3.6, the calculation of the mass of each virgin aggregate fraction is presented.

Table 3.5 Requirement for AC/22 (RAW 2005) (binder content on 100% aggregate by weight)

	Sieve opening (mm)	***Cumulative % retained in each sieve***		
		Target	Min.	Max.
Gradation Requirements	22.4	1.2	0	6
	16.0	13.5	-	-
	11.2	20	15	40
	8.0	40.2	-	-
	5.6	47.9	-	-
	2.0	57	54.0	60.0
	0.063	94.0	92.0	94.0
	< 0.063	6.0	-	-
Binder Requirements	Binder content			4.0%-5%
	Penetration @ 25°C (# @ 15°C)			40-60

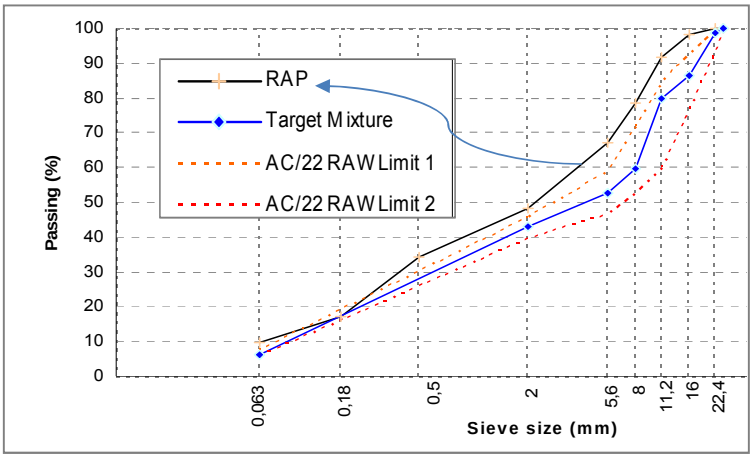

Figure 3.4 Target gradation curve of the mixtures, RA (RAP)

Table 3.6 Determination of added virgin aggregate from each fraction with respect to added RA and target gradation [% m/m]

Fraction Size (mm)	***100% RA***	***0% RA***	***100% Virgin***	***30% RA***	***70% Virgin***	***50% RA***	***50% Virgin***	***60% RA***	***40% Virgin***	***Target [retained mass on screen %***
> C22.4	0.0	0	1.2	0.0	1.2	0	1.2	0.0	1.2	*1.2*
C22.4 - C16	6	0	12.2	**1.8***	**10.4****	3	9.2	3.6	8.6	*12.2*
C16 - C11.2	11	0	6.6	3.3	3.3	5.5	1.1	6.6	0.0	*6.6*
C11.2 - C8	14	0	20.2	4.2	16.0	7	13.2	8.4	11.8	*20.2*
C8 - C5.6	9.2	0	7.0	2.8	4.2	4.6	2.4	5.5	1.5	*7.0*
C5.6 - C2	16.3	0	9.8	4.9	4.9	8.2	1.65	9.8	0.0	*9.8*
Sand (0/2)	35.7	0	37.0	10.7	26.3	17.9	19.15	21.4	15.6	*37.0*
< 0.063	7.8	0	6.0	2.3	3.7	3.9	2.1	4.7	1.3	*6.0*
Total (%)	100	0	100.0	30.0	70.0	50	50	60.0	40.0	*100*
Bitumen	4.3	0	4.5	1.3	3.2	2.2	2.35	2.6	1.9	*4.5*

Calculation Example: * 1.8=0.30×6 ; **10.4=12.2- (0.30×6)

3.2.3. Virgin bitumen grade and quantity determination

Calculations according to the log-pen rule show that if total blending happens during mixing RA with virgin 70/100 pen grade bitumen, the penetration grade will be 63, 50, and 45[dmm] for mixtures containing, 30%, 50%, and 60% RA respectively (see Table 3.7). According to RAW 2005, the binder penetration after recovery should be between 40 and 60 for this type of mixture (AC22). Thus the values obtained just satisfy the mix design requirement. Therefore 70/100 pen bitumen is used in the lab mixtures as well as plant produced mixtures. The amount of added bitumen is calculated with formula 3.2 and given in Table 3.8.

$$a \log Pen_{RAP} + b \log Pen_{virgin} = (a+b) \log Pen_{mix} \qquad (3.2)$$

Where:

a = % of RA

b = % of virgin material

$a+b$ = 100%

Table 3.7 Blended binder properties (according to log-pen rule)

No.	RA binder (%)	Virgin Bitumen (%)	Penetration @ 25°C (# @ 15°C) [0.1 mm]		
			RA binder	Virgin binder (Q8 Pen70/100)	Blended binder
1	30	70	28	90	63
2	50	50	28	90	50
3	60	40	28	90	45

3.2.4. Determination of bulk specific gravity

The purpose of mix design is primarily to proportion the binder and the mineral aggregates in the mixture by their volume. Because it is more feasible to determine the weight of material and convert that into volume by dividing it by its specific gravity values, accuracy in determining the specific gravity of virgin and RA is important in mixture design.

3.2.4.1. Bulk specific gravity (G_{sb})

The specific gravity of each aggregate fraction might be different due to the source and type of aggregates. The specific gravity of the blended aggregate is calculated according to equation (3.3). It is necessary to know the specific gravity of each fraction separately. The specific gravity of the coarse aggregates, filler and sand is already given in Table 3.4. The specific gravity of the RA is also measured with the Ultra-pycnometer. It is considered in the calculations as G_{mm}. It is the combined specific gravity of all the RA ingredients (being aggregate, sand and binder) which are measured all together in the Ultra-pycnometer. In order to determine the bulk specific gravity of RA ($G_{sb(RAP)}$) with equation (3.4) one has to determine the "effective specific gravity (G_{se})" using equation (3.5). Calculation of the combined specific gravity (G_{sb}) is shown in Table 3.9. In this table the retained percentages of virgin aggregate are obtained from Table 3.6.

Table 3.8 Amount of virgin bitumen to be added

RA Content (%)	***RA binder content (P_{bRAP}) (% m/m) "in" 4.3 %***	***Total Binder (%)(m/m "in")*** [14]	***New binder to be added ($P_{b\ NEW}$) (%) (m/m "in")***
30 %	0.30×4.3=1.3	4.3	4.3-1.3=3.0
50%	0.5×4.3= 2.15	4.3	4.3-2.15= 2.15
60 %	0.60×4.3=2.6	4.3	4.3-2.5=1.8

$$G_{sb} = \frac{\left(P_1 + P_2 + P_3 + P_4\right)}{\left(\frac{P_1}{G_1} + \frac{P_2}{G_2} + \frac{P_3}{G_3} + \frac{P_4}{G_4}\right)} \qquad (3.3)$$

[14] In RAW 2005 when bitumen content is shown with "on", it means that all aggregates mass is considered as 100% and bitumen will be added to that value. For example if the bitumen content is 4.5(%)(m/m "on"), the total mass of mixture is 104.5%. On the other hand when it is shown as 4.3(%)(m/m "in"), the total mass of aggregate and bitumen is 100%(m/m) thus aggregate percentage is 95.7%(m/m).

$$G_{sb(RAP)} = \frac{G_{se(RAP)}}{(\frac{P_{ba(RAP)} G_{se(RAP)}}{100 G_{b(RAP)}} + 1)} \qquad (3.4)$$

$$G_{se} = \frac{100 - P_{b(RAP)}}{\frac{100}{G_{mm(RAP)}} - \frac{P_{b(RAP)}}{G_{b(RAP)}}} \qquad (3.5)$$

Where:

$G_{sb(RAP)}$	=	bulk specific gravity of RA aggregate;
$P_{ba\ (RAP}$	=	absorption of RA aggregate;
$G_{b(RAP)}$	=	RA binder specific gravity;
G_{sb}	=	combined bulk specific gravity of the aggregate blend including RA aggregate;
P_1, P_2, P_3, P_4	=	percentage of different aggregate types the mix;
G_1, G_2, G_3, G_4	=	bulk specific gravity of the aggregate types in the mix;
$G_{se(RAP)}$	=	effective specific gravity of RA aggregate determined.

Values which are required for determination of combined specific gravity are listed below:

G_{mm} (theoretical max. spec. gravity) of RA	= 2.493
RA binder content $P_{b(RAP)}$	= 4.3%
Absorption of RA aggregate (P_{ba}) (it is assumed)	= 0.3%
Specific gravity of RA binder $Gb_{(RAP)}$	= 1.035
Effective specific gravity of RA agg. (Gse)	= 2.661
Bulk specific gravity of RA agg. (G_{sb})	= 2.641

Table 3.9 Combined virgin aggregate bulk specific gravity

Mix design (RA content)		***0 % RA***	***30 % RA***	***50 % RA***	***60 % RA***
Sieve (mm)	Bulk Specific gravity	Retained percentage (% m/m)	Retained percentage (% m/m)	Retained percentage (% m/m)	Retained percentage (% m/m)
C22,4 - C16	2.747	13.4	11.6	10.4	9.8
C16 - C11.2	2.777	6.6	3.3	1.1	0
C11.2 - C8	2.754	20.2	16	13.2	11.8
C8 - C5.6	2.745	7	4.24	2.4	1.48
C5.6 - C2	2.789	9.8	4.91	1.65	0.02
River Sand 0/2	2.650	37	26.29	19.15	15.58
Filler < 0.063	2.641	6	3.66	2.1	1.32
RA aggregate	2.641	0	30	50	60
TOTAL		100	100	100	100
Combined bulk Spec. gravity		2.711	2.689	2.674	2.667

3.2.4.2. Theoretical maximum specific gravity of the mixture

Determination of air voids of the mixture requires the value of maximum specific gravity of the mixture (G_{mm})**.** The maximum density is defined as the mass per volume of the mix without air voids. This value could be determined theoretically or via the pycnometer. The theoretical method is explained in EN12697-5 "Determination of the maximum density of hot mix asphalt using mathematical procedure". In this report the maximum specific density is calculated mathematically. The result of maximum density calculations of mixtures containing 0%, 30%, 50%, 60% RA is presented in Table 3.10

$$G_{mm} = \frac{100}{\left(\frac{P_{agg.}}{G_{sb.}} + \frac{P_b}{G_b}\right)} \qquad (3.6)$$

Where:

G_{mm} = maximum specific gravity of the compacted mixture;
P_{agg} = mass percentage of aggregate in the mix;
P_b = mass percentage of binder in the mix;
G_{sb} = bulk specific gravities of the aggregate ;
G_b = bulk specific gravities of the binder.

Table 3.10 Determination of max density (G_{mm})

	00 % RA	30 % RA	50 % RA	60 % RA
P_{agg}	95.5	95.5	95.5	95.5
G_{agg}	2.711	2.689	2.674	2.667
$P_{b(virgin)}$	4.5	3.2	2.3	1.9
$G_{(virgin)}$	1.035 *	1.029**	1.029	1.029
$P_{b(RAP)}$	0	1.3	2.2	2.6
$G_{b(RAP)}$	1.035	1.035	1.035	1.035
G_{mm}	2.527	2.507	2.495	2.490

*Density of 40/60 bitumen
**Density of 70/100 bitumen

-An example of calculations for a mixture with 30% RA is presented below;

$$G_{se} = \frac{100 - 4.3}{\frac{100}{2.493} - \frac{4.3}{1.035}} = 2.661$$

$$G_{sb(RAP)} = \frac{2.661}{\frac{0.3 * 2.661}{100 * 1.035} + 1} = 2.641$$

$$G_{sb} = \frac{(11.6+3.3+16+4.24+4.91+26.29+3.66+30)}{\left(\frac{11.6}{2.741}+\frac{3.3}{2.777}+\frac{16}{2.754}+\frac{4.24}{2.745}+\frac{4.91}{2.789}+\frac{26.29}{2.650}+\frac{30}{2.641}\right)} = 2.689$$

$$G_{mm} = \frac{100}{[\frac{95.5}{2.689}+\frac{3.2}{1.029}+\frac{1.3}{1.035}]} = 2.507$$

3.2.5. Mixing and sample preparation procedures

As it was explained earlier, the experiment was divided in two phases; a lab study (phase I) and a field study (phase II). Although the mixture design process (proportioning of materials) was identical for the studies, the mixing and sample preparation for each phase was different and therefore described separately here.

3.2.5.1. Phase I

Three mixing methods (SM, PW, and UPG) are employed using 30% and 60% RA containing 0% moisture. However, RA with 4% moisture was also used in the UPG method. In addition to mixtures containing RA, a reference mix (SM0) without RA was also prepared using the SM method. As it was explained earlier, a 70/100 pen bitumen was used as virgin bitumen in all mixtures except SM0 which doesn't contain RA. In this reference mixture, Q8 40/60 pen bitumen was used (according to RAW 2005 specifications). A Hobart pan mixer with a capacity of 10 liter and a spiral dough hook (Figure 3.5) were used for all mixtures in Phase I.

Also infrared thermography measurements were done during the mixing process. The mixing setups were enclosed in a specially designed chamber to avoid heat loss. Via this chamber also emissions, vapor and dusts were guided to a ventilating system.

Mixing conditions are explained in detail below;

Standard Method (SM): This mixing method is devised according to EN 12697 “Test methods for hot mix asphalt-Part35: laboratory mixing”.

After proportioning, all virgin aggregates, filler and sand were stored in an oven at 170°C overnight. RA, if used, was proportioned and stored (in aluminum foil) at 170°C for three hours prior to mixing. All mixing equipment was also preheated to the same temperature to avoid heat loss during mixing time. Virgin bitumen was stored at 160°C for 3hours. Virgin aggregates and RA were mixed for 1 minute in the pan mixer, after which virgin bitumen was added and mixing continued for 1.5 minute. Finally,

filler was added to the mixture and an extra 30 seconds of mixing was applied. In total the mixing time was 3 minutes.

Partial Warming (PW): The mixing procedure, mixing time, sequences of material adding, and preheating time of materials are all similar to the SM method except for the preheating temperature of RA which was done at 130°C for 3hrs. The preheating temperature of virgin aggregate was determined by trial and error in order to obtain a mixture temperature of 170°C. Finally two preheating temperatures of 240°C and 330°C were selected for the virgin aggregates used in the PW30 and PW60. Table 3.11 presents a summary of the preheating conditions for all mixtures.

Upgraded Method (UPG): Also in this method, all mixing sequences and mixing times are similar to SM, except for preheating temperatures and moisture conditions. UPG030 and UPG060 stand for 30% and 60% RA content mixtures in which dry RA at ambient temperature was introduced. Similarly, UPG430 and UPG460 stand for 30% and 60% RA content mixtures in which RA at ambient temperature containing 4% moisture was introduced. The preheating temperatures of virgin aggregate are obtained after several trial and error efforts. The finally selected temperatures are listed in Table 3.11.



Figure 3.5 Mixing setup in all mixing methods of Phase I (left; dust collecting chamber and right: IR thermography setup for temperature measurements during mixing of the material in the Hobart mixer)

Table 3.11 Preheating conditions for each mix design

Mix Designs	*Moisture Content in RA*	*Preheating*				*Discharge Temperature T (°C)*
		Virgin aggregate		RAP		
		T (°C)	Time(hr)	T (°C)	Time(hr)	
SM0	0	170	8	170	3	170°C
SM30	0	170	8	170	3	170°C
SM60	0	170	8	170	3	170°C
PW30	0	240	8	130	3	170°C
PW60	0	330	8	130	3	170°C
UPG030	0	290	8	No	No	170°C
UPG060	0	430	8	No	No	170°C
UPG430	4%	345	8	No	No	170°C
UPG460	4%	515	8	No	No	170°C

3.2.5.1.1. Short term aging and compaction

Each mixture was stored in the oven (at 160°C) for half an hour to simulate short term aging that occurs in real plants before transport, paving and compaction. Storing them in the oven also provides a more consistent temperature distribution through the mixture and it makes sure that the mixture is at the right compaction temperature. It was observed that the UPG mixture with moisture was very sensitive to lose its temperature to the environment in the early stages during the mixing process due to moisture evaporation.

The loose mixtures were then compacted by means of a gyratory and Marshall impact compactor. Marshall Compaction was done with 50 blows on each side.

The gyratory compaction was performed according to the RAW 2005 specifications. The Gyratory angle was set to 0.82 degree. A compaction pressure of 600kPa was applied at 30 gyrations per minute. The Servopac gyratory compactor used for compaction is shown in Figure 3.6. The diameter of the mold is 100mm. The cylinders were compacted to the height of 77mm. The compacted cylindrical samples were then stored at room

temperature for 24 hours before placing them in a climate room at 15°C. Then samples were sawn to reduce the height to 50 mm.



Figure 3.6 Gyratory and Marshal Impact compactor used in the research

3.2.5.1.2. Determination of volumetric properties

The volumetric properties of the samples were determined according to "EN 12967-6: "determination of bulk density of bituminous specimens". The relations used in calculating the volumetric properties are also presented in Appendix A. Air voids contents of both gyratory and Marshall samples are also presented in appendix A.

The average voids content of the Marshall and gyratory samples as well as their distribution histogram are plotted in Figure 3.7 and Figure 3.8. The target air voids content of the Gyratory samples was 5%, though, the measured air voids were less than the target. The target air voids was not achieved because it was forgotten to correct the height of the gyrated samples because of the steel plates on the top and the bottom of the samples. Given the fact that low air voids of the samples may mask the difference in mechanical properties between different mixtures, another set of experiments was done with samples that had higher air voids content. They were prepared and tested by Chacho (2012) in his Master thesis study. All preparation procedures were the same except the air voids content of the samples in his study. A summary of his air voids measurements is presented in Figure 3.9. The air voids contents of the latter set of mixtures are higher.

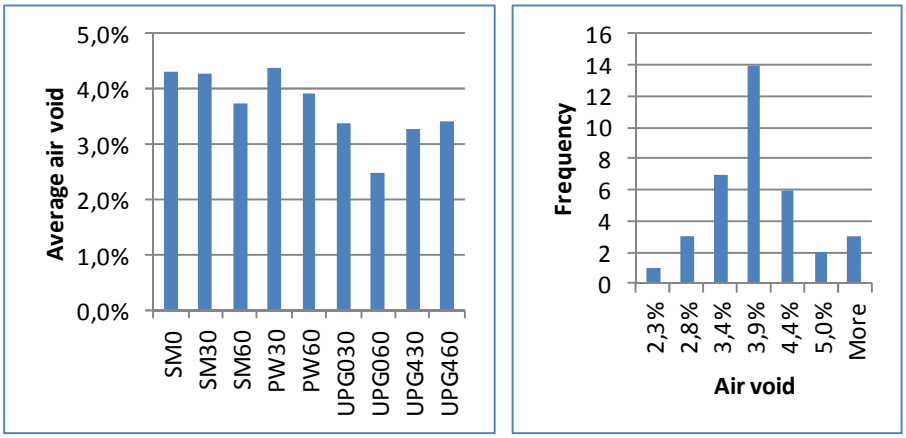

Figure 3.7 Marshall compacted samples (left: average values and right: air voids distribution histogram)

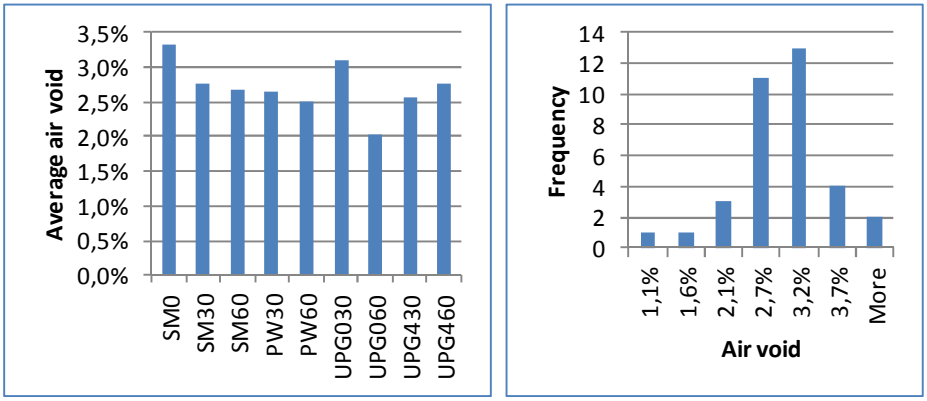

Figure 3.8 Gyratory compacted samples (left: average values and right: air voids distribution histogram)

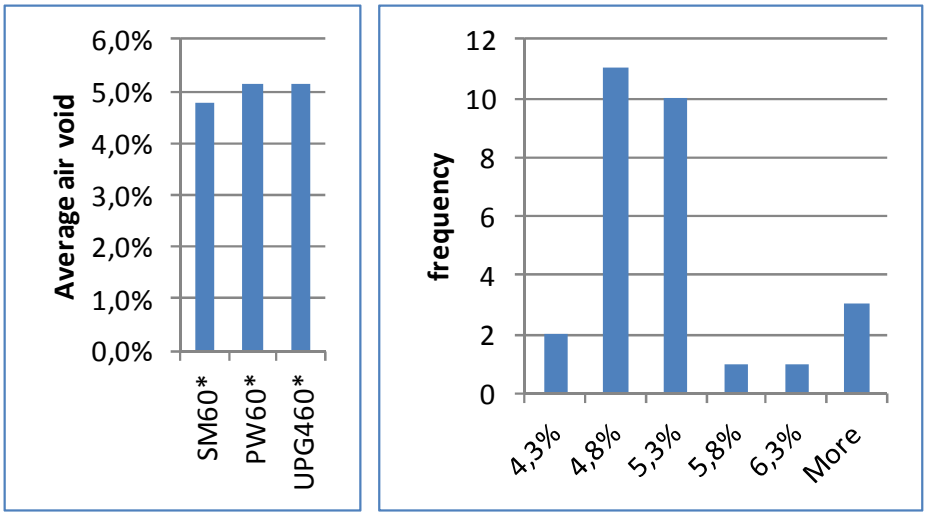

Figure 3.9 Marshal samples compacted by Chacho 2012 (left: average values and right: air voids distribution histogram)

3.2.5.2. Phase II

In phase II, three identical mixtures were produced with 50% RA and 4.3% bitumen content. One mixture was produced in a batch plant while the second one was mixed using a double drum mixer by the same contractor. The third mixture was produced in the laboratory using a 100 liter lab pug mill mixer. All three mixing units were described and illustrated in section (2.1.2). Details of the batch plant and double drum plant are given in Table 3.12.

Table 3.12 Properties of two mixing plant facilities

	Batch Plant	***Double drum***
Brand	Benninghoven BA 200	Astec 9-foot Double Barrel drum mixer
Installation date	1993	2007
Production capacity (t/h)	240	450
Batch size	3 tons	Continuous (max 500ton/hr)
Control system	Miprotek	Astec

The mixing procedures of all facilities are explained here-after.

3.2.5.2.1. Batch plant (BB and B)

As it was explained earlier, a 50% RA (base course RA) containing mixture was produced in a batch plant which is identified as "BB" here after. Another mixture in the batch plant was also produced using 25% porous asphalt RA and 25% base course RA. So the difference between B and BB is the combination of 50% RA in the mixture. Mixture "A" and "L" are also containing only 50% base course RA.

In preparation of "BB" and "B", RA was preheated to 130°C in a parallel drum mixer before introducing it into the pug mill mixer of the batch plant. The virgin aggregates were preheated to 270°C in the counter flow drum dryer of the batch plant. Then they were mixed in the pug mill mixer for 15 seconds. Mixing continued for an extra 15 seconds after adding the virgin bitumen (70/100 pen). A sample size of approximately one ton of produced mixture was transferred from the batch plant to the laboratory, where 8 batches of 30 kg were sampled from it and stored in the oven at 160°C prior to compaction in the shear box compactor. The first block was compacted within 30 minutes. The other blocks were compacted consequently every 40 minutes. According to the maximum density of the mixture with 50% RA, the shear box compactor was set to obtain 5% air voids. 8 blocks of 150×180×450mm were compacted.

3.2.5.2.2. Astec double drum (A)

RA was introduced at ambient temperature and moist conditions. At the time of mixing, the moisture of the RA was 3.5% on average. The virgin aggregates were preheated in the inner drum to 500°C to achieve a 170°C mixture temperature at the discharge point. The same approach of sampling and compaction as for the "BB" samples was applied for the "A" samples. Again 8 blocks of 150×180×450mm were compacted using the shear box compactor.

3.2.5.2.3. Laboratory mix (L)

In the laboratory the same RA and virgin materials were sampled and stored in an oven at 170°. The virgin aggregates were preheated overnight but RA was preheated for 3hrs. The same approach of compaction was applied and 8 blocks of 150×180×450mm were produced.

The shear box was used for compaction of the slabs. The amount of the mixture (required for a slab) was weighed and stored again in the oven to stabilize the temperature at 160°C. Then it was poured in the box and the

surface of the mixture was leveled manually. The utmost effort was done to distribute the sample evenly in the box.

The BB, B, L and A blocks were kept at room temperature for at least 24hr. After that they were kept in a climate room at 15°C. After one week three blocks were used for cutting beams and cylinders. 12 beams of 50×50×450mm were cut from three blocks of each mixing method (4 beams per block). These beams were used in 4PB stiffness and fatigue tests.

Cylindrical samples were also cored; they had a diameter of 65mm and a height of 138mm (see Figure 3.10).

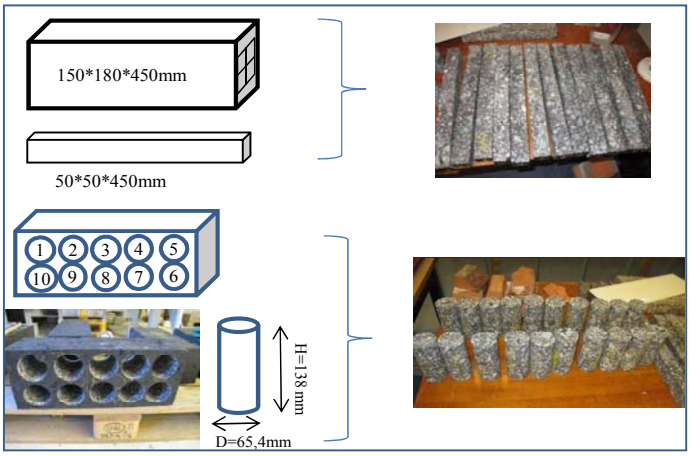

Figure 3.10 Preparation of the beams and cylindrical samples from compacted blocks

Volumetric properties of all specimens were determined according to "EN 12967-6: "determination of bulk density of bituminous specimens". They are presented in detail in Appendix A.

Histograms of the air voids distribution of the beam and cylinder specimens are plotted in Figure 3.11 . These plots were used to select samples with similar air voids for further testing.

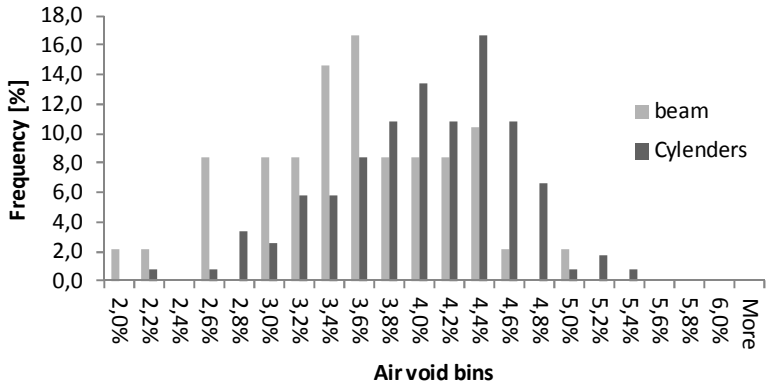

Figure 3.11 Histogram of air voids distribution of beams and cylinders

The air voids data of numerous compacted specimens made it also possible to study the effect of shear box compaction on the homogeneity of the mixture in terms of air voids distribution. The force direction in the shear box compactor is depicted in Figure 3.12 as well as the beam and cylinder specimen location with respect to that direction.

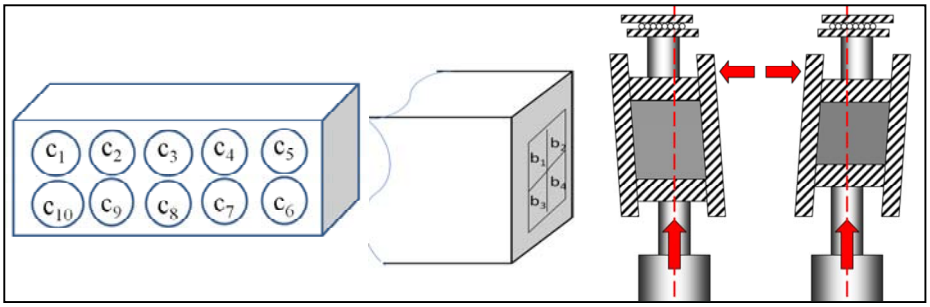

Figure 3.12 Specimen location and identification with respect to the compacting direction in the shear box compactor.

In order to study homogeneity of cylindrical samples, they are categorized in two groups called "outer" and "middle" cylinders. They are shown in Figure 3.13. In order to compare the homogeneity of compaction in the length of the compacted block, an equality line for air voids content between outer cylinders and middle cylinders is given in Figure 3.13. In this chart the horizontal axis shows the average of the air voids content of the middle cylinders being C_2, C_3, C_4, C_7, C_8 , and C_9 and the vertical axis shows the average air voids content of the outer cylinders being; C_1, C_{10}, C_5, and C_6.

Each point in the chart relates to air voids data from one compacted block. In this figure any point below the equality line shows higher average air voids content of middle samples compared to the average air voids content of outer samples.

It is observed that the air voids content in the middle of the blocks is higher compared to at the sides. In other words the middle part of the block is compacted slightly less than the outer sides of the block. The lower air void content of the mixture on the outer sides of the block might be because of manual treatment of the mixture in the mold prior to compaction. In order to get better edges in the block corners, a rod was used to help the compaction in the corners right after filling the mould with hot mixture. That may have caused more compaction at the two ends of the compacted block.

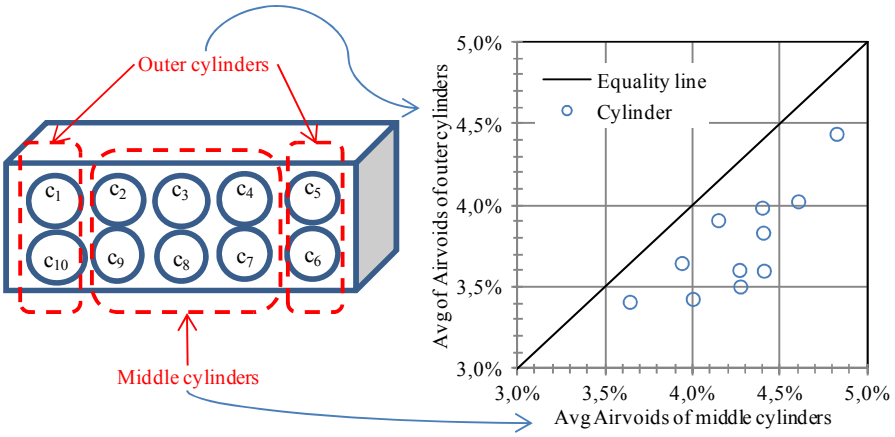

Figure 3.13 Comparison of lateral cylinder air voids with those in the middle (each point relates to a compacted block)

Another comparison is made between average value of the air voids of the top of the compacted block and that of the bottom of the block. This comparison is plotted in Figure 3.14 for beams and cylinders. Each point in this figure belongs to one block which is either being cut into the cylinders or the beams. The results show that the upper sides of the blocks are compacted less than the bottom parts. The air voids content of the upper cylinder corresponds to the average air voids content of C_2, C_3, and C_4. The air voids content of the bottom cylinders corresponds to the average air voids content of C_7, C_8, and C_9.

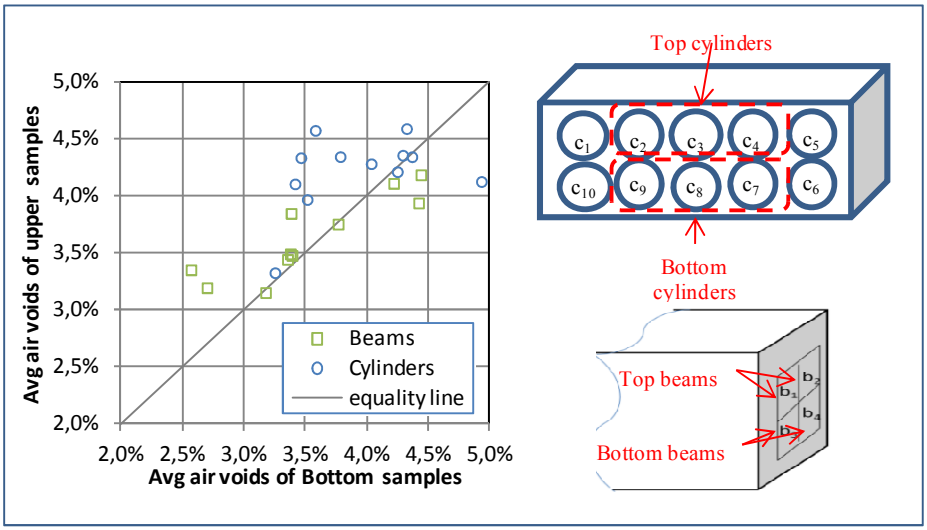

Figure 3.14 Comparison of average air void between top and bottom of block

The results of these comparisons reveal that density variations occur in the height and the length of slabs. The variation in air voids content seems to be less in 4PB beams from each block when comparing the top and bottom beams.

CHAPTER 4

INFRARED THERMOGRAPHY

4.1. Introduction

Thermography analysis has been used over the last decades in some research and projects to monitor the heat differences and temperature segregation on pavement mats [51] [52] [53] [54]. Given the fact that the viscosity of the asphalt binder is temperature dependent, the workability of asphalt mixtures is significantly influenced by temperature. Assuming that the compaction energy is equally applied on the surface of the asphalt mat during construction, one can conclude that the heat differences between different parts of the mat cause inhomogeneity in air void distribution and might cause unevenness due to compaction by the roller (or later through traffic). Consequently the quality of the pavement will be reduced if the temperature distribution of the mat is not homogeneous. Therefore, mapping the surface temperature of asphalt pavements in contour plots in real time can be of great help in HMA quality control systems. The combination of the infrared thermography mapping data with real-time GPS information provides a good quality control system [54]. An example of temperature mapping on an asphalt pavement is shown in Figure 4.1.

Furthermore, the efficiency of heat transfer between superheated virgin aggregates and cold reclaimed asphalt when mixing cold RA with superheated material in the double barrel drum mixer determines the extent of blending of RA binder and virgin bitumen. The amount of blending between aged RA binder and soft virgin bitumen will influence the properties of the recycled mixture.

The amount of blending in the large mass of an HMA mixture is being influenced by two factors being:

(a) exposure of cold RA to superheated virgin material by mechanical mixing (at macro level) and

(b) diffusion between the two binders (at micro level).

Since RA is being mixed with virgin aggregate at different preheating temperatures and moisture conditions (dependent on the type of the plant) thermographic analysis will provide helpful information about the mixing efficiency.

The mixing efficiency of recycled mixtures is characterized by:

- the thermal homogeneity of the mixture after mixing;
- the homogeneity in gradation and bitumen content.

Obviously the first factor could be explicitly studied by infrared thermography analysis. The second factor is attributed, to some extent, with the distribution of RA aggregate in the whole mixture. Temperature Mapping with Infrared Thermography (TMIT) would be helpful in analyzing the second factor, given the fact that the RA temperature is different from that of virgin aggregates. This is important because there is no other possibility to visually distinguish RA from virgin aggregates because all aggregates are coated with black material. Visual distinction of RA from virgin aggregates is possible with TMIT on the images made during showering of the recycled HMA mixture at the discharge point of the double drum mixer. In such figures superheated aggregates could be marked with their high temperature.

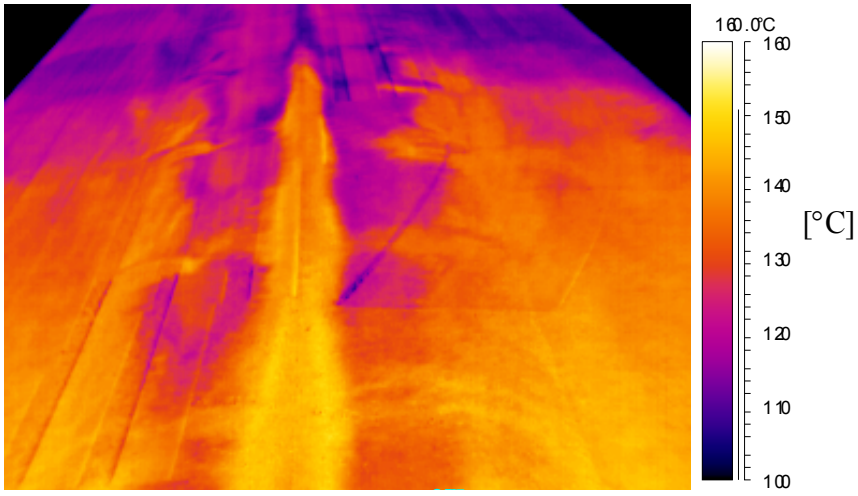

Figure 4.1 An example of thermo graphic images to evaluate final temperature homogeneity on the compacted pavement.

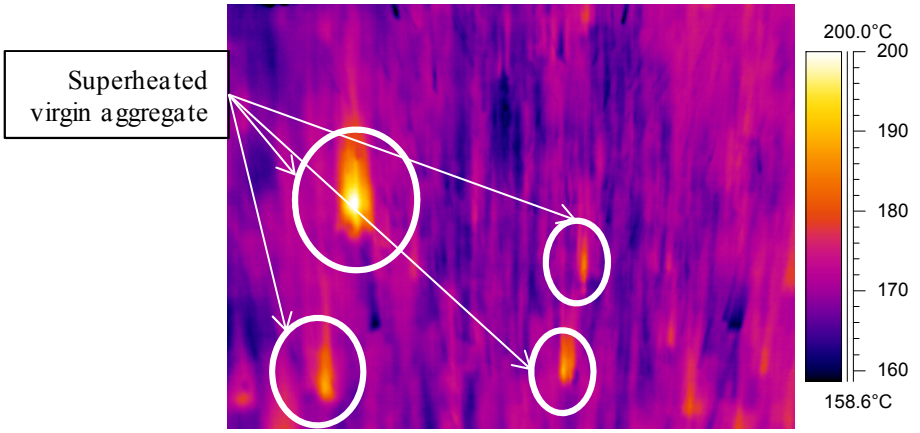

Figure 4.2 A thermo graphic image of material falling from the end of the mixer on the conveyor

4.2. Experimental design

In this chapter it is shown how TMIT is used in studying;

- the efficiency of mixing and blending of recycled HMA in laboratory and double drum mixes and,
- temperature segregation during pavement construction.

The efficiency of mixing is determined by means of TMIT measurements used on the laboratory mixing methods SM, UPG and PW, which were described in section 2.1.1 of this thesis. These mixtures contained 60% RA, preheated to different temperature levels and with different amounts of moisture. Details of the corresponding mix design and mixing procedures as well as the mechanical properties of the materials were reported earlier in section 3.2.5.1.

Also the efficiency of mixing and blending of a double drum mixer was studied through TMIT. Two temperature contour maps were produced while the double drum was producing an HMA mixture with 50% RA and 4% moisture. This mixture is tested in section 5.3 and is known in this report as mixture “A”.

Material produced in the double drum was then used for pavement construction. The temperature segregation of the product as laid was measured during compaction by means of TMIT.

The general layout of this chapter is presented in Figure 4.3.

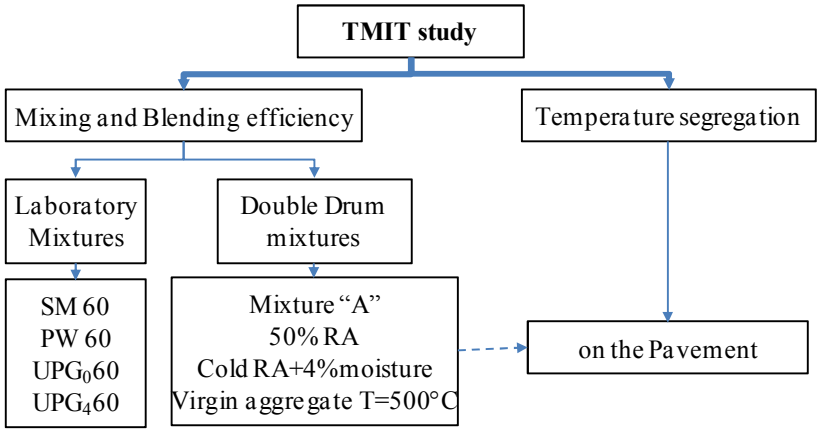

Figure 4.3 Flowchart layout of the TMIT study on mixing efficiency and temperature segregation.

4.2.1. Material and TMIT instrumentations

In this study a FLIR A320 infrared camera was used to continuously capture thermo graphic images. It is coupled with a real-time digital storage, measurement, and analysis software (Research Cam). It has the capability of capturing images at a maximum frequency of 5Hz. This frequency is good enough for TMIT with respect to the speed of mixer rotation in the laboratory or showering speed of hot mixtures in the double drum.

During mixing in the laboratory, the camera was mounted with a tripod on top of the 10 liter Hobart mixer (see Figure 4.4) to make images



Figure 4.4 Infrared setup used in laboratory TMIT.

4.2.1.1. TMIT setup in the double drum mixer

In the double drum mixer aggregates are superheated in the inner drum and are mixed with cold and moist RA in the outer shell. The HMA mixture is discharged at the end of the mixing chamber to a conveyer. The discharging shute is a rectangular shape opening with a width of 40 cm. The final hot mixture drops on the conveyor in a continuous showering manner with a falling height of 50 cm. The camera was installed in such a position that a full view over the width of the showering particles could be obtained. The TMIT setup used for measurements on the double drum is illustrated in Figure 4.5. An example of a full width thermography image is shown in Figure 4.2.

Image capturing started half an hour after running the mixer at full capacity at a production rate of 500 tons per hour. The mixture contained 50% RA. The final temperature of the mixture was targeted to be at 180°C.

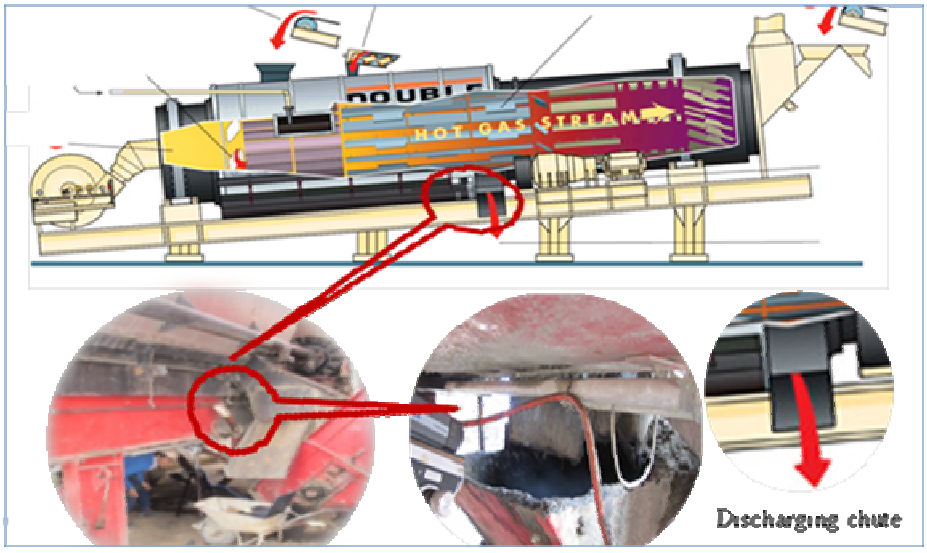

Figure 4.5 Details of the location of the infrared camera at the end of the double drum mixing process.

4.2.1.2. TMIT setup during pavement compaction

TMIT measurements were conducted for two days during construction of a main road in the Province of Groningen. On the first day measurements were

done during the construction of a 60 mm thick base course. The base course was paved at a speed of 3 m/min at an ambient temperature of 10°C.

The next day a 45 mm thick binder course was laid on top of it at the speed of 3.5 m/min. The ambient temperature was 4°C at this day. The weather was dry in both days.

The infrared camera was mounted on the paver providing TMIT images of an area behind the paver as it was running forward. The TMIT setup is shown together with the paving train in Figure 4.6. As it is shown in the figure, first the mixture is unloaded from the truck into a feeder. Then the feeder transfers the mixture to the paver. The feeder is used between truck and paver to ensure constant asphalt feeding and temperature homogeneity of the mixture. It was also expected to prevent aggregate segregation in this way prior to compaction. Furthermore, by using the feeder contact between the discharging trucks and the paver was prevented.

In the paver the mixture is distributed with the augers from the center to either sides. The infrared camera could only view a limited width while zooming in. Therefore the TMIT measurement was done at different locations on the pavement. The coverage of the infrared lens will be shown in relation to the paver position and pavement.

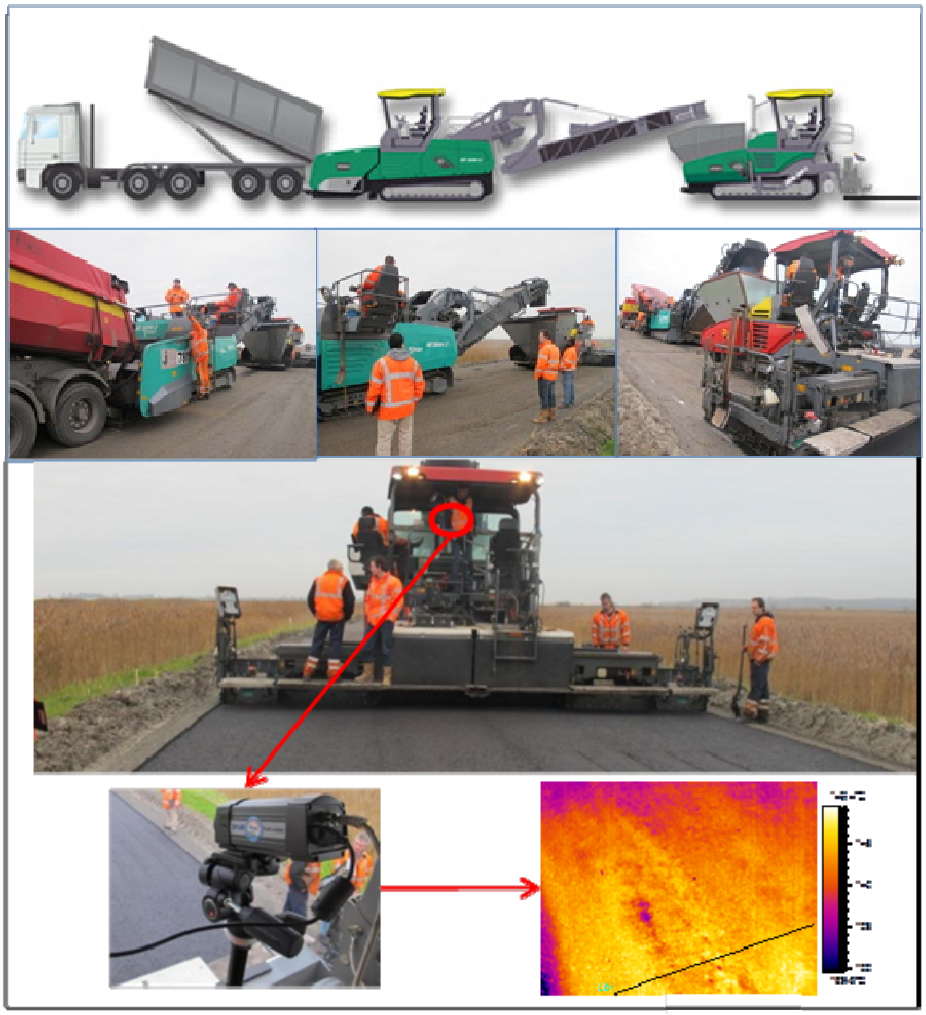

Figure 4.6 TMIT setup on the paver

4.2.2. Results and discussion

4.2.2.1. TMIT on laboratory mixtures

As is noted in section 3.2.5.1, different mixing methods (SM, PW and UPG) using a laboratory mixer were used to study the effect of the RA moisture content and preheating temperature on the quality of the mixture. The following table 4.1 presents a brief summary of the four mixtures on which TMIT measurements were done during mixing.

Table 4.1 Overview of laboratory mixing conditions

	RA content [%]	***Moisture Content of RA [%]***	***Preheating Temperatures [°C]***	
			RA	Virgin aggregate
SM60	60	0	170	170
PW60	60	0	130	330
UPG060	60	0	25	430
UPG460	60	4	25	515

It has to be noted that the mixing time was 3 minutes for every mixture and TMIT was continued after 3 minutes of mixing up to 7 minutes after mixing was finished. The homogeneity of each mixture is studied by comparing the temperature distribution histograms obtained at certain moments in time. They are presented in Figure 4.7, Figure 4.8, and Figure 4.9 for respectively SM60, PW60 and UPG460. Unfortunately the temperature distribution of UPG060 was not available (due to some technical problems) to be included in this chapter; however, the temperature profile of this mixture is included next to other three mixtures in Figure 4.10. This figure is showing the maximum temperature at each moment in time indicating the temperature loss of the virgin aggregates during mixing.

It is obvious that the SM60 mixture is homogeneous (in terms of temperature) from the beginning. It only loses temperature with time. The PW mixture shows relatively larger temperature differentials compared to those of SM60, however, it reaches a homogeneous temperature after 1:30 minutes of mixing.

The infrared camera was capable of measuring up to 1000°C. However, only one range of temperatures could be selected. The range of 0-350°C was chosen. Consequently, all particles above the maximum limit are considered to have a temperature of 350°C. However, this only affects the TMIT measurements made during the very early stages of UPG460 mixing.

UPG460 has the highest temperature differences since the virgin aggregates are initially at 515°C before they are added to the cold RA. Nevertheless the whole mixture became thermally homogeneous in less than 2:30min.

As can be seen in Figure 4.10 , the slope of each curve is indicating the speed of temperature loss of the virgin aggregates given the fact that the temperature of virgin material was higher in all mixtures (except in SM60).

When the slope of the curve is very small, a balance in temperature is reached. The mixing times needed for mixture homogeneity are varying with respect to each mixing method; however, all of them become homogeneous within 3 minutes of mixing. It has to be noted however that this mixing time is much longer than in real plants.

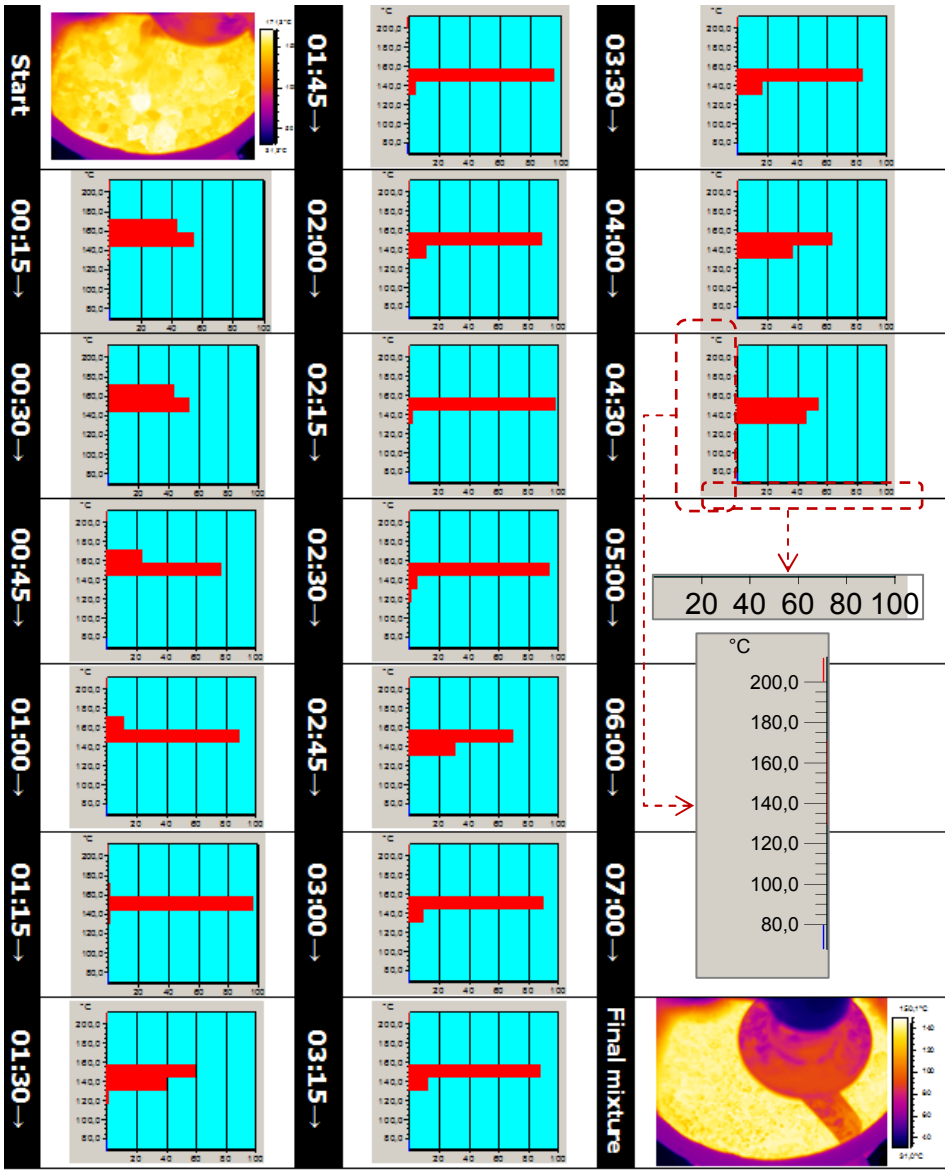

Figure 4.7 Temperature distribution during mixing of SM60

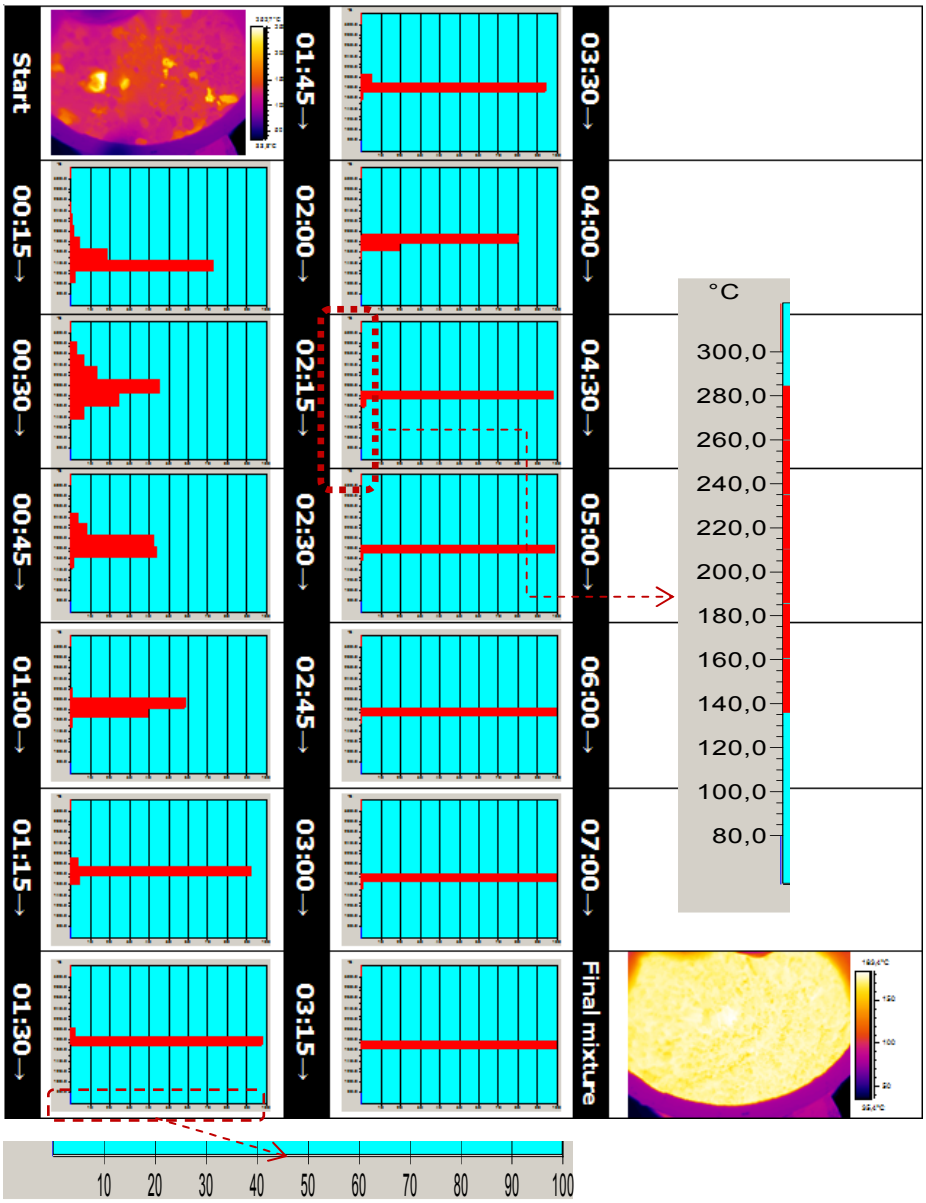

Figure 4.8 Temperature distribution during mixing of PW30

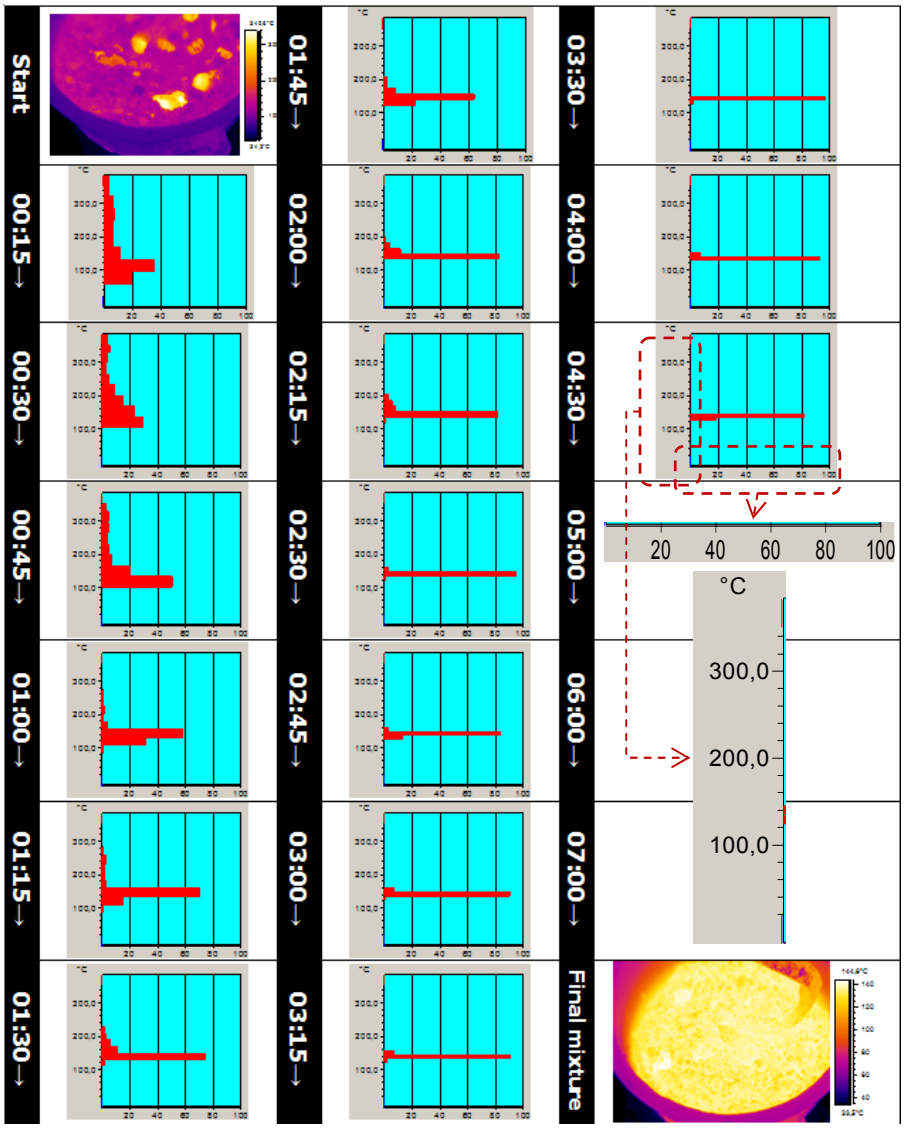

Figure 4.9 Temperature distribution during mixing of UPG460

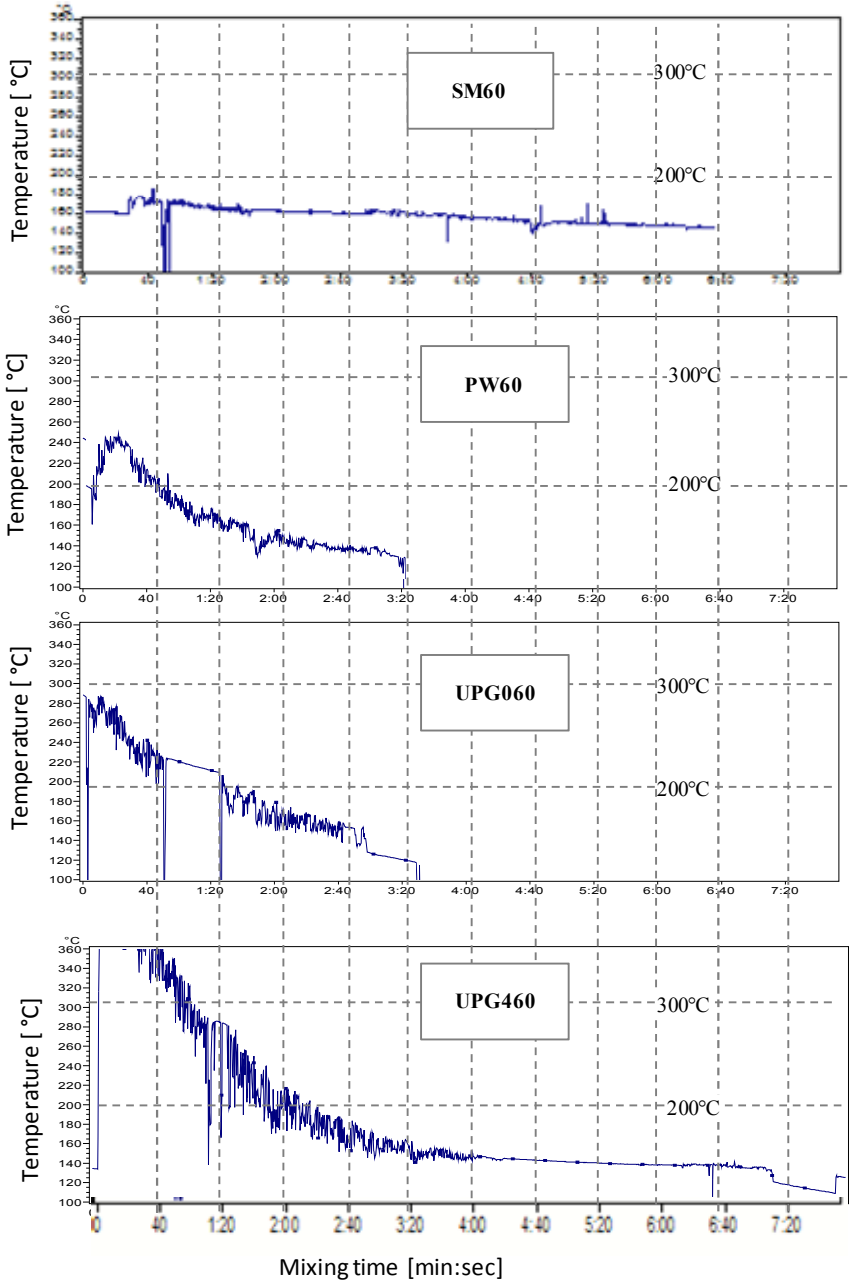

Figure 4.10 Temperature profile of all laboratory mixtures (graphs are showing the max temperature at each moment)

4.2.2.2. TMIT on double drum mixtures

TMIT measurements were done during two different days when the double drum was producing an AC22 mixture containing 50% RA with 4% moisture. They are identified here as TMIT-A1 and TMIT-A2. The mixture compositions were identical during both measurements.

Infrared images are captured at the rate of 5Hz. Each image consists of 76×10^3 pixels (320×240mm) and the size of each pixel is about 1 mm^2. Each falling particle therefore consists of a number of pixels. The results of TMIT-A1 and TMIT-A2 measurements are shown in Figure 4.11 and Figure 4.12, respectively. A temperature contour map is created for the length (duration) of production. The duration of the production is divided into three distinctive periods. Three temperature distribution histograms (TDH) are created for each period. Period 1 is the most unstable period during which the average temperature soars to 220°C and drops to 190°C while the target temperature is 180°C. In period 2, the temperature continues to decrease until it reaches 180°C. During the third period, the temperature stays rather constant. The homogeneity of the mixture could be derived from the TDH of each period. The increase and decrease of the temperature is partly controlled by the operator who may have made a wrong decision about the preheating temperature of the virgin aggregates. However the consistency of the moisture content of RA may also be partly the reason. It seems that a stable target temperature is eventually achieved after 15 minutes.

Nevertheless, in the TDH graphs, two peaks are always observed which is most likely caused by the two groups of aggregates, the RA and virgin aggregates. The closer the peaks are to each other, the more homogenous the mixture is in terms of temperature.

TMIT-A2 shows a rather stable temperature profile and is therefore more homogeneous than TMIT-A1, therefore the two peaks in the TDH are closer to each other; hence the mixture temperature is more homogeneous. Looking at the width of the contour map, a temperature difference at each moment could be observed. This is due to local small segregation of RA from virgin aggregates.

Nevertheless, all these batches are stored in the storage silos prior to transportation and construction and they have enough time to exchange more heat and become more homogeneous in temperature.

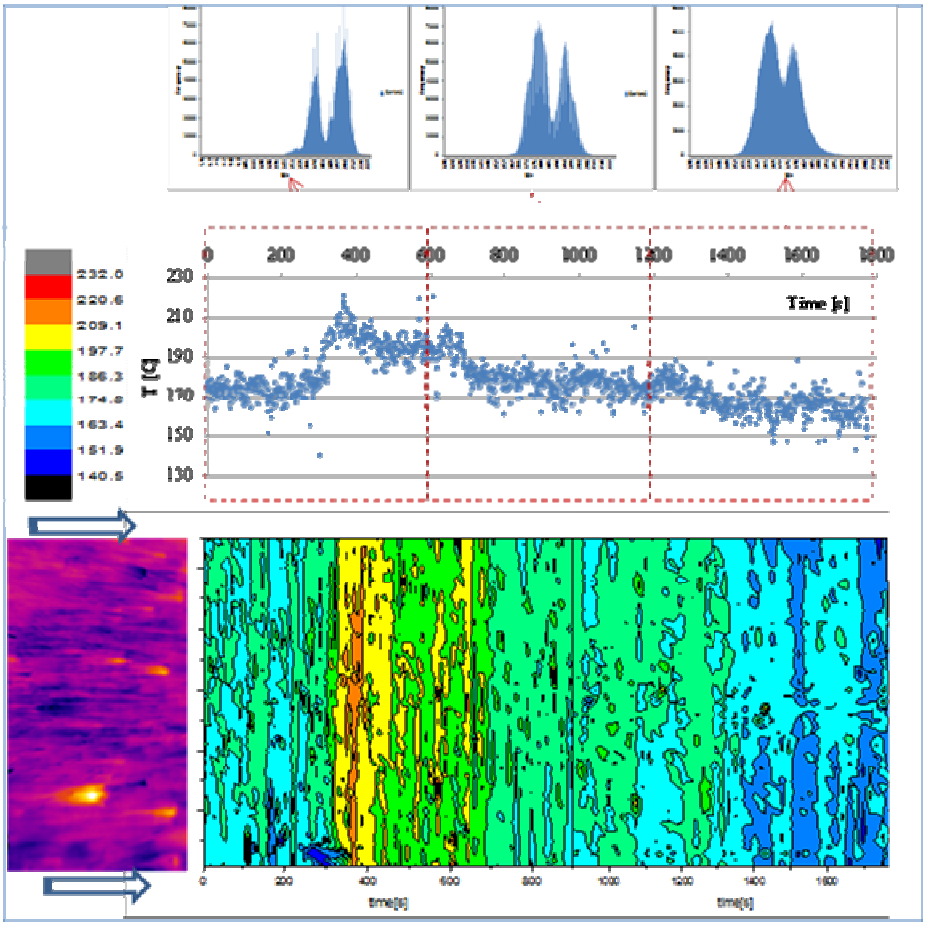

Figure 4.11 TMIT-A1 results

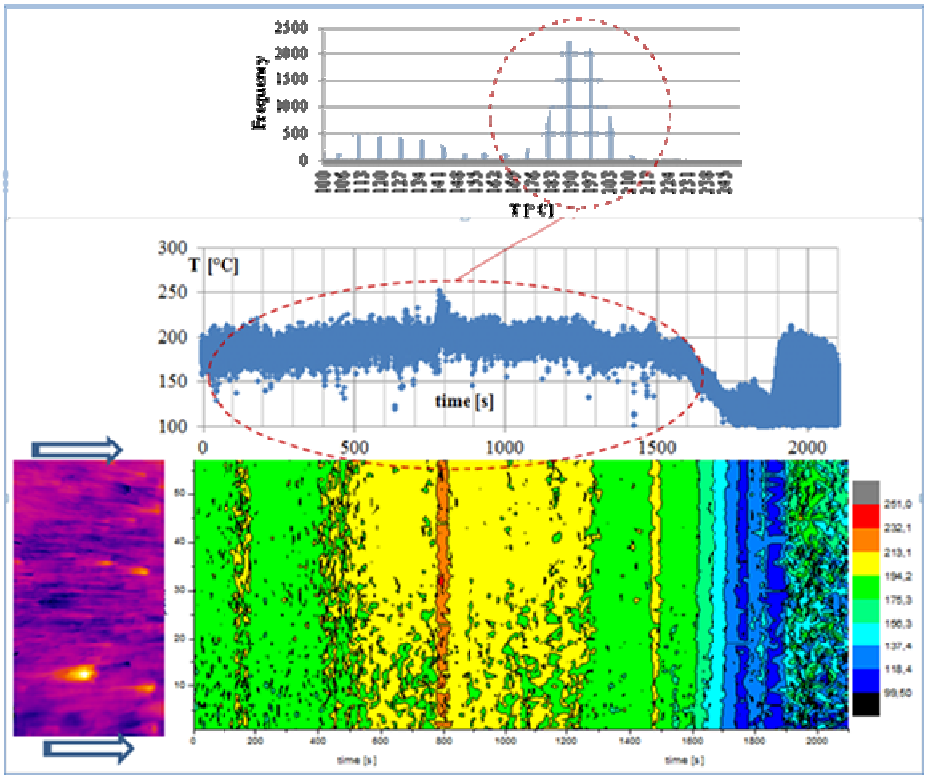

Figure 4.12 TMIT-A2 results

The quality control process (in HMA plants) partly depends on the temperature control of the final mixture and is usually done by measuring the temperature of only a small part of the mixture with a thermometer or by measuring the surface temperature of only a small area by means of an infrared tool. These measurements may mislead the operator and might make him decide to preheat virgin aggregate far less or far more than required because of the limited amount of information he has available (only a (very) small part of the produced mixture is measured). Therefore using real-time continuous infrared measurements with an image capturing frequency between 1 to 5 image/minutes could greatly assist operators in preheating virgin aggregate to the correct temperature.

4.2.2.3. TMIT on the pavement

A number of TMIT measurements and analyses have been made during the two days that were available. Four TMIT measurements were done on the base course during the first day and three measurements are done on the

binder course which was placed the following day on top of the base course. Both base and binder layers contained 50% RA. The maximum aggregate sizes of mixtures were 22 and 16 mm for base and binder courses respectively. The minimum allowed compaction temperature of the base course was 150°C while in the binder course it was slightly lower (140°C).

The TMIT results as well as temperature profile and temperature distribution curves are presented in Figure 4.13 to Figure 4.19. TMIT-BASE and TMIT-BIND are representing the thermal analyses on the base course and binder courses respectively. The location of the paver and infrared camera with respect to the paver is illustrated in the top right side of each figure. The scanning line on the pavements is also shown on each figure. Temperature mappings are shown on the bottom of each figure; the vertical axis shows the width of the scanning line and the horizontal axis shows the time. The horizontal axis could be converted to the length of the pavement according to the speed of the paver. The speed of the paver for the base course was 3m/min and 3,5m/min for the binder course.

The corresponding temperature profile is also shown in the middle part of each figure. On the top left side of each figure, a histogram chart is plotted to show the temperature distribution over the width and length of the scanned area.

The mapping charts show that the temperature distribution over the width and length is different. In each direction, specific patterns could be detected.

As one can see, the measured temperatures show approximately a normal distribution but when the distribution along the longitudinal direction is observed a cyclic increase and decrease in temperature is occurring over the length of the pavement. Analysis of the temperature data together with the time of arrival of the different trucks showed that this could be related to the different truck loads. The mixture of a single truck is used in 10 to 15 minutes by the paver. The mixture remains in the feeder and paver during this period which results in a temperature loss in the mixture and a decrease in the temperature of the pavement mat surface. From this it can be concluded that the feeder was not very helpful in homogenizing the temperature of the mixture.

Next to the temperature difference over the length of the pavement, a temperature difference over the width of the pavement can be observed. This might be caused by the spreading of the mixture in the horizontal direction by means of the augers. All in all the temperature of the asphalt mat as laid was not very homogeneous. At some point of the pavement mat, the temperature is as low as 120°C while there are also areas with a temperature of 160°C, so this may cause compaction differences on the surface. It has to be noted that

measured temperature with infrared camera is only the temperature of the surface of the mixture. The real temperature would have been higher if measured with real thermometer. Infrared measurements, here, is done only to make comparison between temperatures of different points.

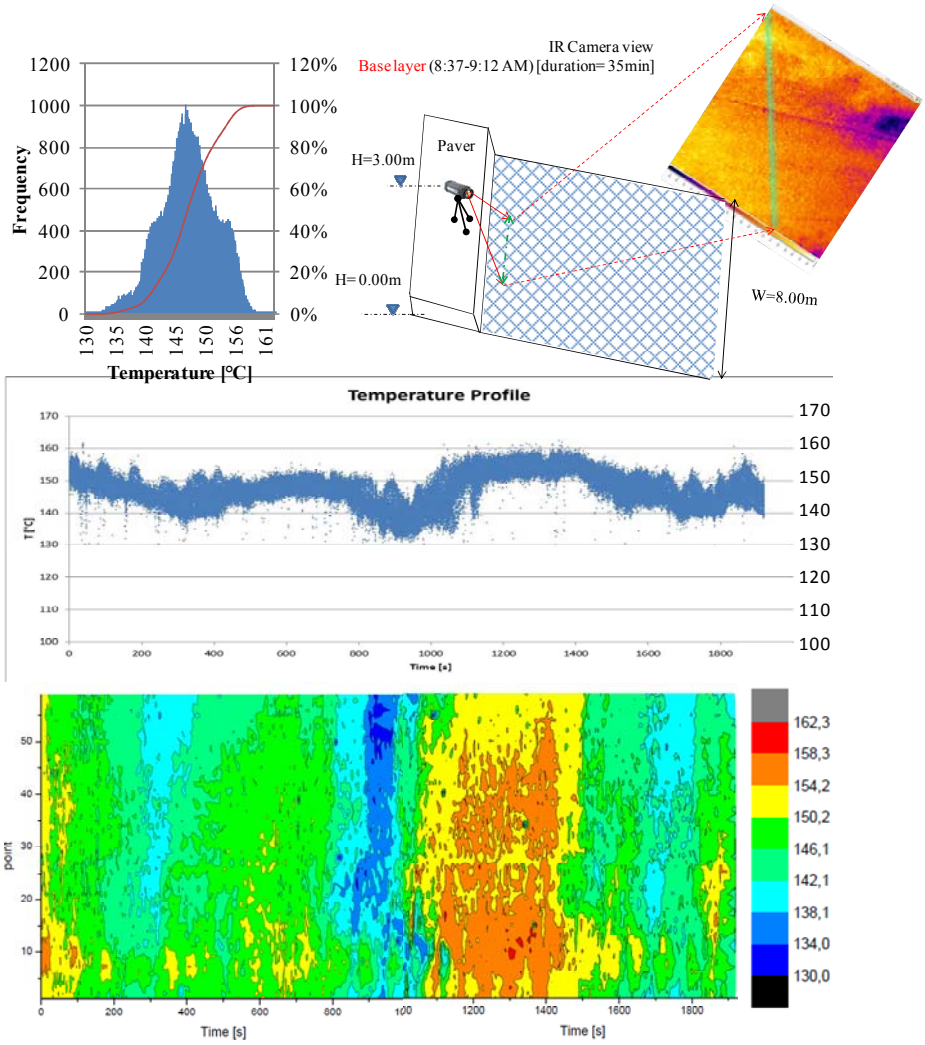

Figure 4.13 TMIT-BASE1 results [Note: top left shows histogram of measured temperatures; top right shows scanned area; the middle figure shows temperature variation in the longitudinal direction in the centre of the paver; the bottom figure shows the temperature variation in the longitudinal and transversal direction (paver speed=3m/min.]

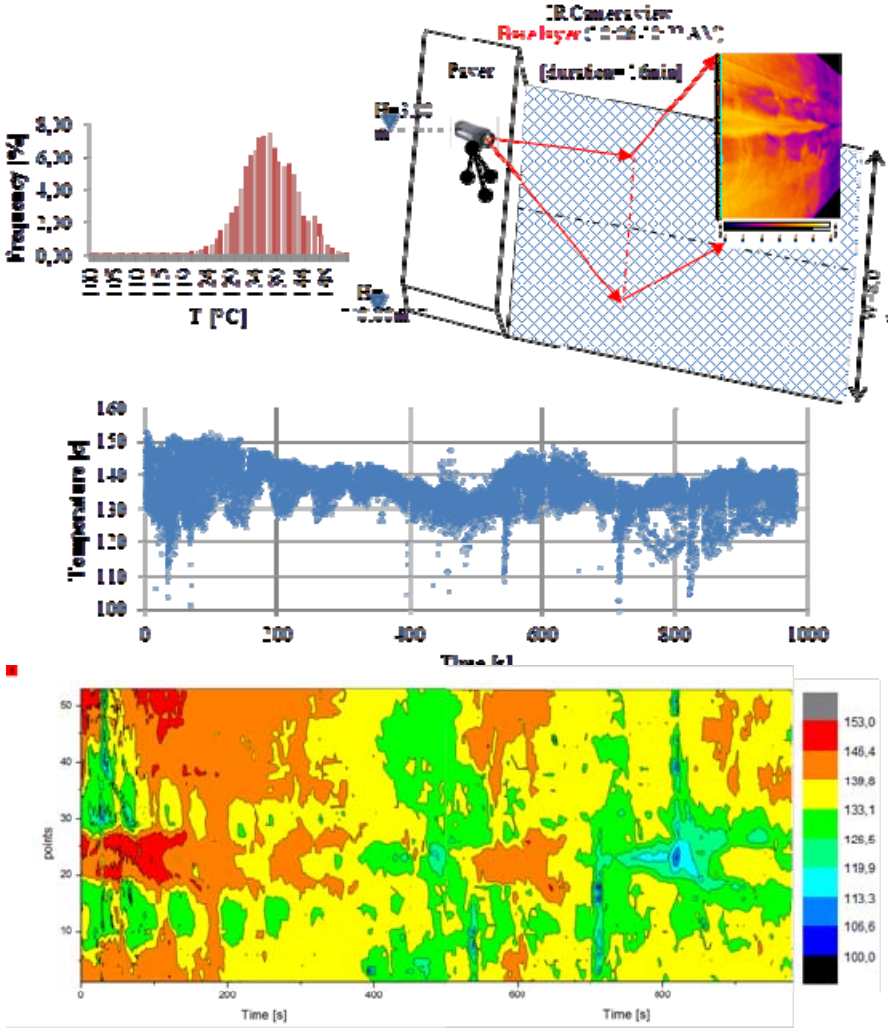

Figure 4.14 TMIT-BASE2 results [Note: top left shows histogram of measured temperatures; top right shows scanned area; the middle figure shows temperature variation in the longitudinal direction in the centre of the paver; the bottom figure shows the temperature variation in the longitudinal and transversal direction (paver speed=3m/min.]

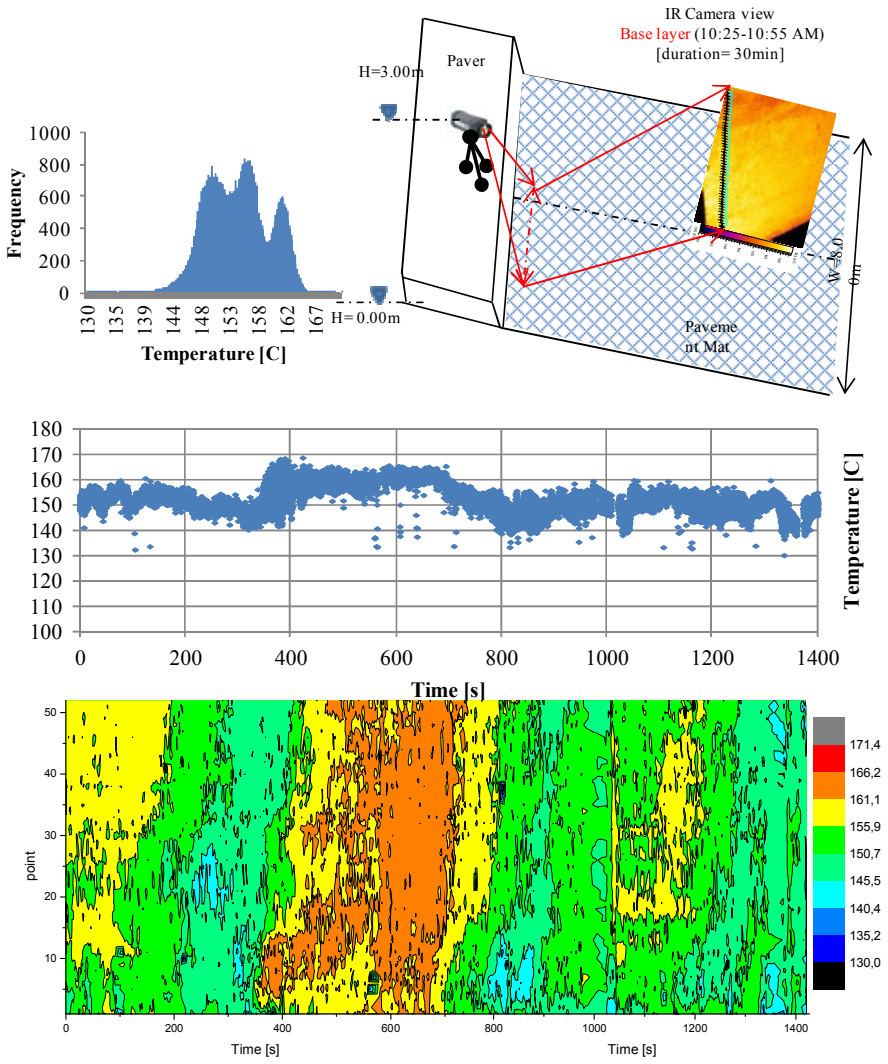

Figure 4.15 TMIT-BASE3 results [Note: top left shows histogram of measured temperatures; top right shows scanned area; the middle figure shows temperature variation in the longitudinal direction in the centre of the paver; the bottom figure shows the temperature variation in the longitudinal and transversal direction (paver speed=3m/min.]

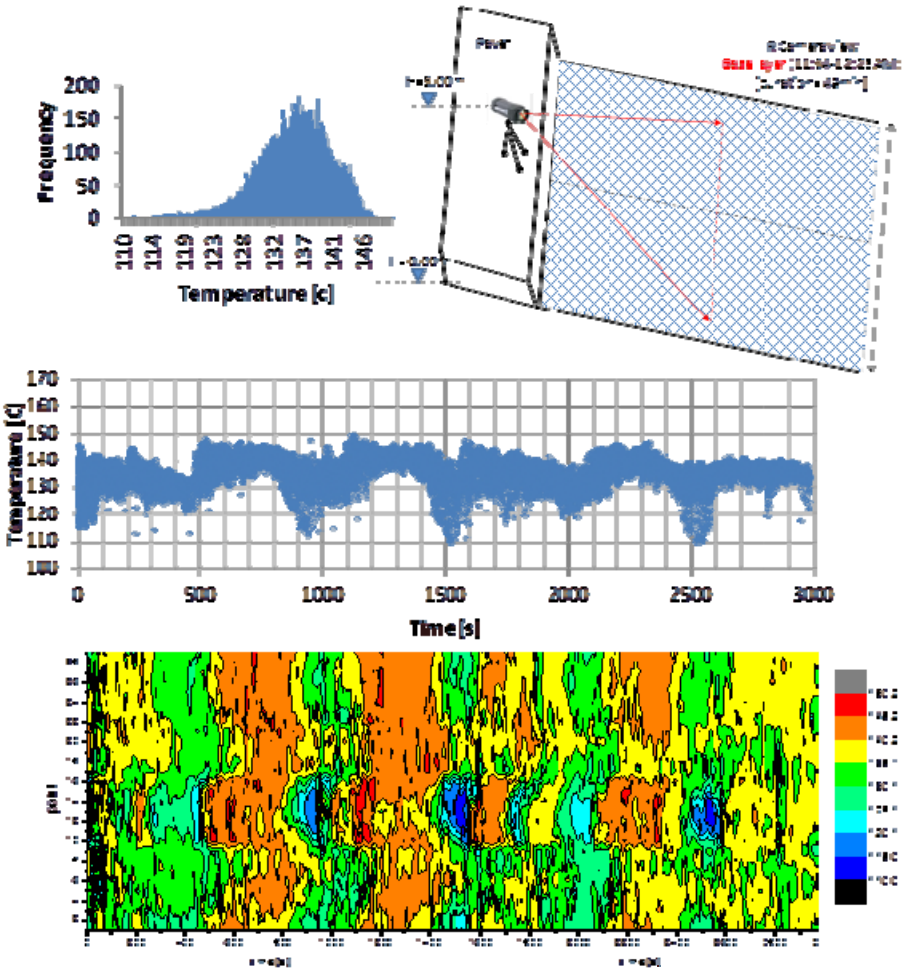

Figure 4.16 TMIT-BASE4 results [Note: top left shows histogram of measured temperatures; top right shows scanned area; the middle figure shows temperature variation in the longitudinal direction in the centre of the paver; the bottom figure shows the temperature variation in the longitudinal and transversal direction (paver speed=3m/min.]

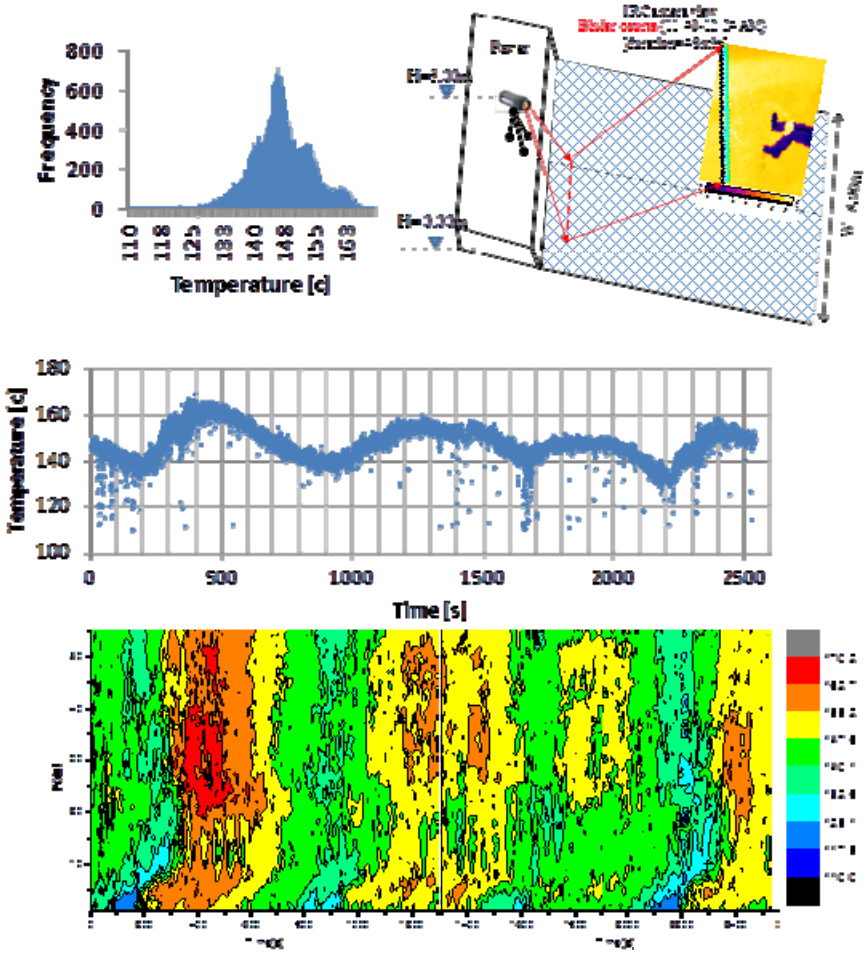

Figure 4.17 TMIT-BIND1 results [Note: top left shows histogram of measured temperatures; top right shows scanned area; the middle figure shows temperature variation in the longitudinal direction in the centre of the paver; the bottom figure shows the temperature variation in the longitudinal and transversal direction (paver speed=3.5m/min.]

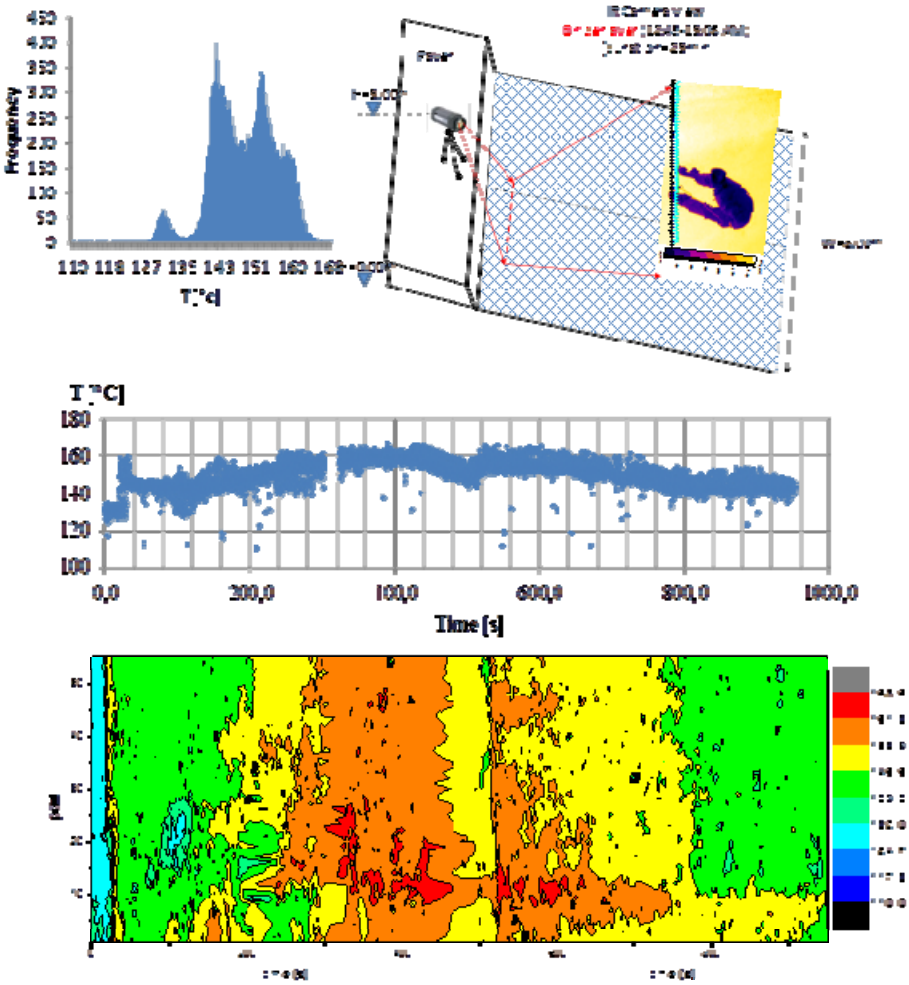

Figure 4.18 TMIT-B1ND2 results [Note: top left shows histogram of measured temperatures; top right shows scanned area; the middle figure shows temperature variation in the longitudinal direction in the centre of the paver; the bottom figure shows the temperature variation in the longitudinal and transversal direction (paver speed=3,5m/min.]

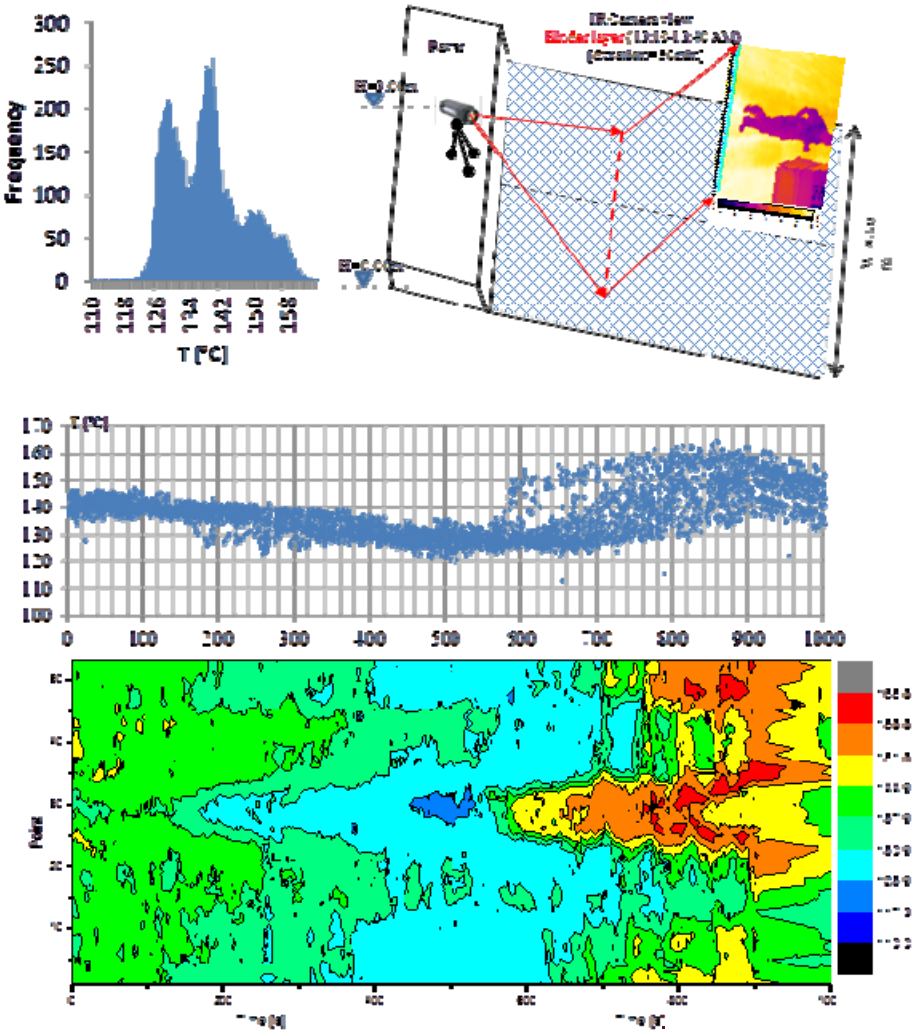

Figure 4.19 TMIT-BIND3 results [Note: top left shows histogram of measured temperatures; top right shows scanned area; the middle figure shows temperature variation in the longitudinal direction in the centre of the paver; the bottom figure shows the temperature variation in the longitudinal and transversal direction (paver speed=3,5m/min.]

4.2.3. Conclusions

1. TMIT was successfully applied for the analysis of mixing efficiency and temperature blending in the laboratory and at a double drum mixer.
2. When mixing is done in the laboratory according to the SM, PW and UPG methods, a mixing period of three minutes showed to be enough to achieve a thermally homogeneous mixture when RA is fed cold and moist. This mixing time is much longer than at actual plants so the temperature homogeneity of plant produced mixtures can be questioned.
3. Measurements of the temperature homogeneity of mixtures produced with the double barrel drum (using 50% moist RA at ambient temperature) however showed that the temperature homogeneity was much better than was expected from the laboratory tests. This in spite of the fact that the plant mixing time is much shorter.
4. The process quality control (in HMA plants) partly depends on the temperature control of the final mixture and is usually done by measuring the temperature of only a small part of the mixture by means of a thermometer or by measuring the surface temperature of only a small area by means of an infrared tool. This type of measurement control may mislead the operators in preheating the virgin aggregate far less or far more than required. Therefore using real-time continuous infrared measurements with a frequency of between 1 to 5 image/minutes could assist operators preheating virgin aggregate to the correct temperature.
5. The temperature measurements (in hot mix asphalt production) showed two normally distributed temperature groups. One is most probably related to the cooler RA part and the other to the hot virgin part. Thorough mixing is merging both groups. This phenomenon is clearly shown in DTH.
6. IR thermography is a helpful tool in studying temperature segregation during pavement construction.
7. The average temperature on the pavement surface increases and decreases periodically by each truck unloading.
8. With a normal feeder, the average temperature fluctuation (on the pavement) was up to 20°C for the base layer and 25°C for the binder layers.
9. Temperature variation over the width of the pavement due to horizontal transport via the paver auger is about 10°C.

10. From the results it seems that the homogeneity of the final mixture and the variation in the pavement is mainly controlled by the laying and compaction conditions and hardly by the mixing process provided the mixture is produced at the right temperature in the plant and operated by skilled personnel and the mixture is transported in insulated trucks (which was the case during the project studied).
11. This in turn leads to the conclusion that improvements in laying equipment as well as laying procedures are necessary to obtain pavement mats with a homogeneous temperature which most likely will be less prone to surface damage (mainly cracking and raveling).

CHAPTER 5



ANALYSIS OF THE MECHANICAL CHARACTERIZATION TEST RESULTS

5.1. Introduction

The test results, analyses and final conclusions made in both phases of the laboratory test program are presented in this chapter. The test methods and sample preparation procedures are explained in Chapters 2 and 3. Further description of testing methods or sample preparation is provided in this chapter where necessary. After the presentation of the test results they are further analyzed and the effect of the research variables on the test results for each phase of the study are discussed. A summary of the sample codes used in both phases of the study is presented in Table 5.1. These codes are used to compare the results of each phase.

5.2. Test results of Phase I

In this section, the results and analysis of data obtained during the laboratory study (phase I) are discussed. The performance and mechanical properties of mixtures produced by means of three mixing methods (SM, PW, and UPG) with 30% and 60% RA are compared by means of results from the following tests:

- Indirect Tensile Stiffness Modulus test (ITSM)
- Indirect Tensile Strength (ITS)
- Indirect Tensile Fatigue (ITF)

Table 5.1 Abbreviations and identification codes of samples used in Phase I and Phase II

	Description of mixing methods	*RA [%]*	*abbreviation*
Phase I	Mixing RA and virgin aggregate at same temperature of 170°C (Standard Method)	0	SM0
		30	SM30
		60	SM60
	Mixing preheated RA (130°C) with extra hot virgin aggregate (Partial warming)	30	PW30
		60	PW60
	Mixing cold RA in dry and moist (4%) condition with superheated virgin aggregate. The index after UPG indicates the moisture content of 0 and 4%.	30	UPG030
		60	UPG060
		30	UPG430
		60	UPG460
Phase II	Cold and moist RA is mixed to superheated aggregate in an Astec Double Drum mixer	50	A
	Preheated RA (50% base RA) at 130°C in parallel drum are mix with hot virgin aggregate in batch plant pug mill mixer (Batch Plant)	50	BB
	Preheated RA (25% base RA+25% Reclaimed porous asphalt) at 130°C in the parallel drum is mixed with hot virgin aggregate in batch plant pug mill mixer (Batch Plant)	50	B
	Mixing RA and virgin aggregate at the same temperature in a laboratory pug mill mixer	50	L

5.2.1. Indirect tensile stiffness modulus test (ITSM)

The test is carried out according to EN 12697-26: "Test Methods for hot mix asphalt-part26: Stiffness". Gyratory compacted cylinders, 100mm in diameter, were used in this test. They were compacted to a height of 77mm. Then they were cut to a height of 50 mm. Three specimens were tested for each mix design. The stiffness modulus was determined by performing a frequency sweep at 5 temperatures (5, 10, 15, 23 and 35°C); the frequencies used were (1, 2, 4, 8, and 12 Hz).

In this test, 5 loads with a haversine shape are applied at 3000 ms pulse repetition; this implies a rest period between the load pulses. Hence, the

stiffness modulus was calculated for each pulse from the peak load and the total recoverable horizontal deformation (equation 5.1).

A maximum horizontal deformation was set as target criterion at the different test temperatures in order to prevent potential damage to the specimen because of high peak load values. The maximum horizontal deformation was set based on experience to 2µm at 5°C and 10°C, 3µm at 15°C, 4µm at 23°C and 5µm at 35°C. The relation between peak load (F) and the amplitude of the resulting horizontal deformation (z) at different temperatures for a given mixture (PW30) are illustrated in Figure 5.1. It is obvious that the mixture stiffness S_m is related to the slope of each line ($\frac{F}{z}$). It implies that the higher the slope is, the higher the modulus.

The S_m value for each specimen at a certain temperature and frequency is determined by averaging the values from 5 pulses. An example of the loading pulses is shown in Figure 5.2. Prior to each measurement, a preconditioning loading is also applied to make sure that the loading strips are properly connected to the specimen.

$$S_m = \frac{F \times (\vartheta - 0.27)}{z \times h} \qquad (5.1)$$

Where:

S_m = measured stiffness modulus [MPa]

F = value of the applied vertical load [N]

z = is the amplitude of the horizontal deformation obtained during the load cycle [mm]

h = mean thickness of the specimen, [mm]

v = Poisson's ratio.

The measured stiffness values are also adjusted due to the load area factor (k) by using equation (5.2)[15]. The load area factor is the ratio of the shaded area (A_2) in Figure 5.3 to the product of the rise area (A_1). When this factor deviates from 0.60, the measured stiffness modulus has to be corrected using equation (5.2). The magnitudes of k values at different loading frequencies are illustrated in Figure 5.4.

$$S'_m = S_m * (1 - 0.322\ (\log S_m - 1.82) * (0.6 - k)) \qquad (5.2)$$

[15] EN2967-26 -2000

Where:

S'_m = stiffness modulus adjusted to a load area factor of 0.60 [MPa],

k = the measured load area factor

S_m = measured stiffness modulus at a load factor k [MPa]

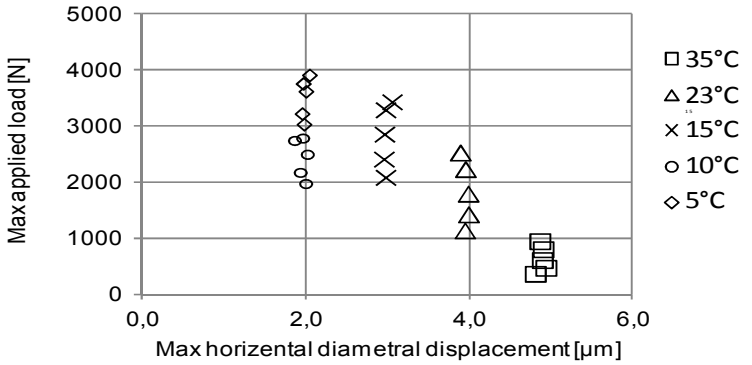

Figure 5.1 Peak load vs. horizontal displacement at different temperatures (legend unit [°C])

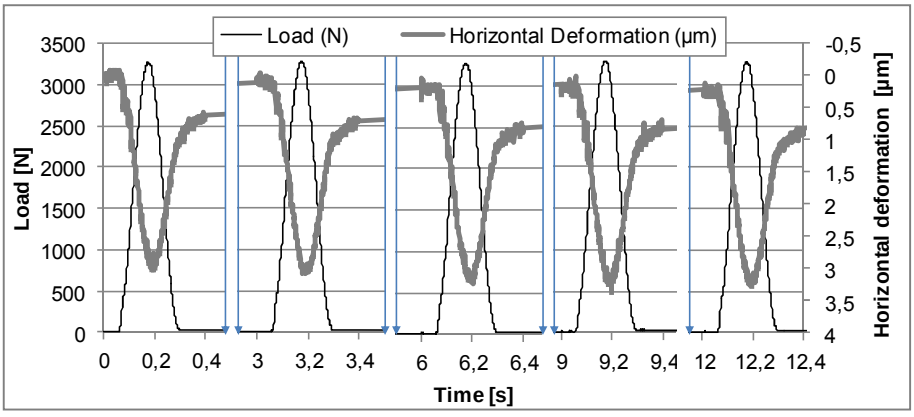

Figure 5.2 Example of the 5 pulse loading at 15°C, 2 Hz (500ms) and target horizontal deformation of 3µm.

The stiffness value for each mixing method is the mean value of three specimens. The mean stiffness modulus as well as the mean value of peak loads and horizontal deformation is presented in Appendix B together with related measurement details. These data were used further in the construction

of stiffness master-curves. A summary of the stiffness modulus (S_m) at different frequencies and temperatures is presented in Appendix B.

Stiffness modulus values at the frequency of 8Hz are also illustrated in column bar charts in Figure 5.5, for the purpose of modulus comparison between mixing methods.

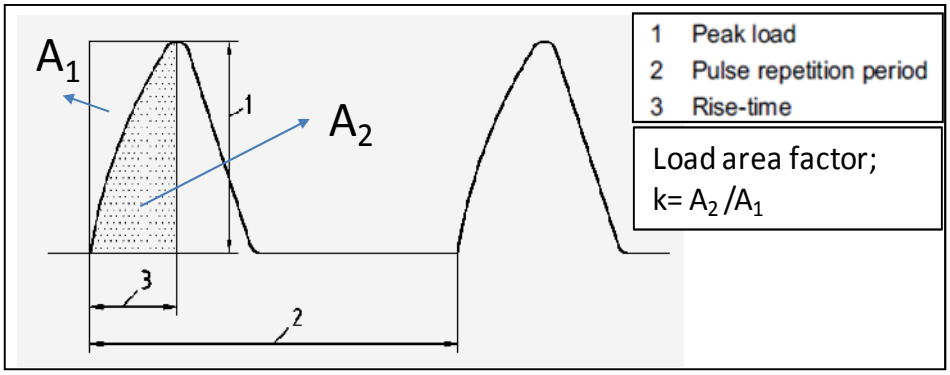

Figure 5.3 Determination of load area factor (k) from load signals according to EN 12697-26

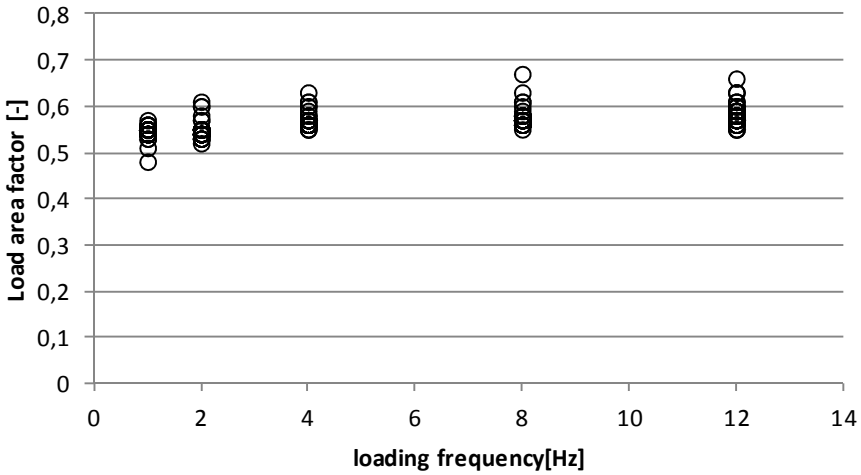

Figure 5.4 Magnitude of load area factor (k) values at different loading frequency

To facilitate the comparison of relative differences in stiffness values at different temperatures, all values are compared to SM0 as the reference mixture. The differences are expressed in percentage in Figure 5.6. The difference ratio (R) is calculated according to equation (5.3) and expressed as a percentage value.

$$R = \frac{S_m - S_{ref}}{S_{ref}} * 100 \qquad (5.3)$$

Where:

S_m = Stiffness modulus of each mixture type [MPa]

S_{ref} = Stiffness modulus of reference mixture SM0 [MPa]

Figure 5.5 shows that the mixtures with higher percentages RA (60%) are stiffer than those with lower RA contents (30%). This was expected because of the influence of higher percentages of RA binder according to the log-pen rule. In the next sections the log-pen rule will be discussed by comparing the penetration of extracted binders from the mixtures. The increase of stiffness at higher temperatures in comparison to the reference mixture is also remarkable (see Figure 5.6). At 35°C the stiffness has increased 30%-70% for mixtures containing 30%RAP. The mixtures with 60% RA have an 80%-90% higher stiffness than the reference mixture at 35°C. The UPG460 mixture is an exception. It is softer than the other mixtures, while it has 60% RA. The presence of 4% moisture in cold RA in the laboratory mixing procedures may have hindered the blending of RA with virgin bitumen during the mixing process.

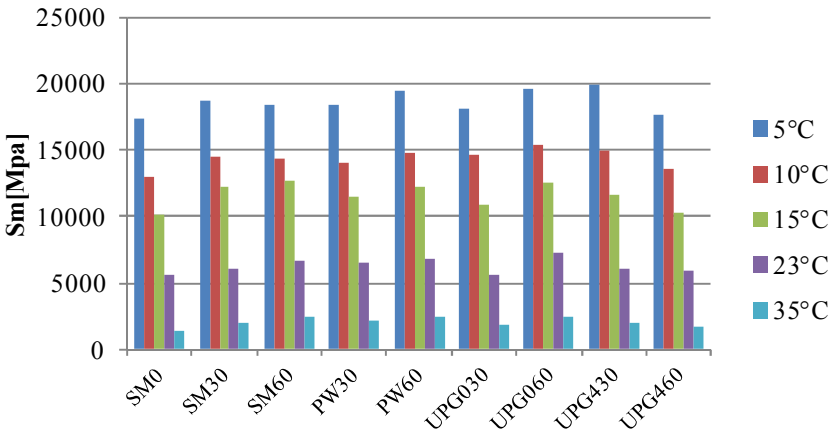

Figure 5.5 Comparison of the stiffness modulus at 8Hz

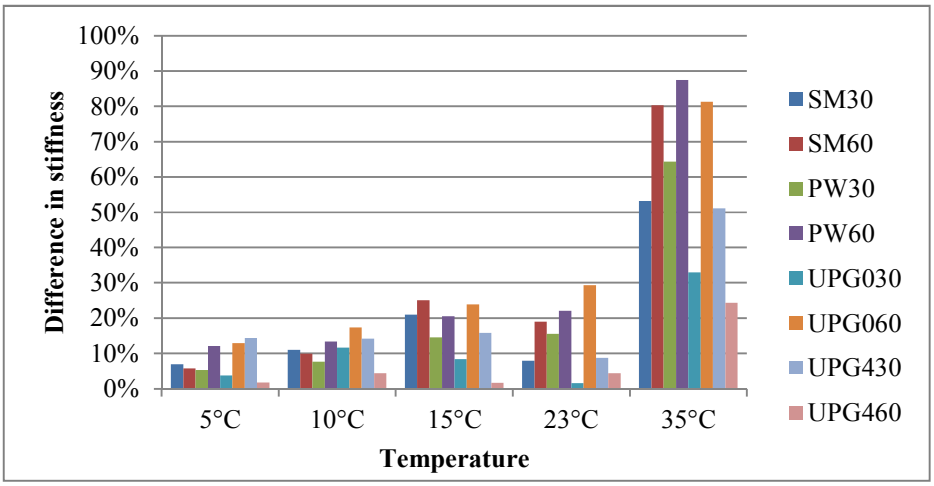

Figure 5.6 Differences in stiffness values at 8Hz and different temperatures compared to reference mix (SM0).

5.2.1.1. Stiffness master-curves

According to the time-temperature superposition principle, which is also applicable to bituminous materials, frequency and temperature are exchangeable. This principle is therefore used to create master-curves of material properties at a reference temperature.

A master-curve of a bituminous mixture at any reference temperature (T_{ref}) is defined as the relation between the mixture stiffness and the reduced frequency. Shifting factors are required to exchange temperature to time or frequency. The Arrhenius equation was used to perform the time-temperature super positioning method. Shifted values are fitted to an "S" shape sigmoidal curve to model the mixture stiffness values at high, intermediate and low loading frequencies with one single equation.

The sigmoidal fitting model (equation (5.4)) based on Medani's work [46] was used to plot the master-curves.

$$S_m = S_h + (S_h - S_l) * e^{-[\frac{f_r}{f_0}]^{\gamma}} \qquad (5.4)$$

$$f_r = f.\beta_T \qquad (5.5)$$

$$\beta_T = e^{\frac{\Delta H}{R}[\frac{1}{T}-\frac{1}{T_r}]} \qquad (5.6)$$

Where:

S = mixture stiffness [MPa]

S_h = high stiffness value when $f \rightarrow \infty$

$S_{l=0}$ = low stiffness value when $f \rightarrow 0$

f_r = reduced frequency [Hz]

f = loading frequency obtained from test at different temperatures [Hz]

f_0 = an initial frequency value [Hz]

β_T = shift factor [-]

ΔH = activation energy [J/mol]

R = ideal gas constant [8.314 J/mol.K]

T = considered temperature in Kelvin [K]

T_r = reference temperature in Kelvin [K]

γ = model parameter [-]

In this model, it is assumed that $S_l \rightarrow 0$ at low frequencies and high temperatures. The average stiffness values obtained from ITSM at different temperatures and frequencies were firstly shifted to the reference temperature. The four model parameters were obtained by minimizing the mean squared error between the log values of measured stiffness and the model value at the reference temperature of 20°. The model parameters, S_h , f_0, ΔH and γ, at a reference temperature of 20°C are presented in Table 5.2.

Table 5.2 Shift factors and model parameters at 20°C

Mix design	***ΔH***	***f_0***	***γ***	***S_h***	***Shift factor log α***				
					5ºC	**10ºC**	**15ºC**	**23ºC**	**35ºC**
SM0	210,9	36,06	0,422	16259	2,03	1,33	0,65	-0,38	-1,83
SM30	206,6	27,20	0,391	17509	1,99	1,30	0,64	-0,37	-1,79
SM60	200,2	19,59	0,390	17354	1,93	1,26	0,62	-0,36	-1,74
PW30	207,1	35,02	0,365	18263	1,99	1,30	0,64	-0,37	-1,80
PW60	199,9	25,41	0,373	18263	1,92	1,26	0,62	-0,36	-1,74
UPG030	213,3	37,13	0,389	17728	2,05	1,34	0,66	-0,39	-1,85
UPG060	205,2	25,07	0,382	18897	1,97	1,29	0,63	-0,37	-1,78
UPG430	205,7	50,65	0,383	20175	1,98	1,30	0,64	-0,37	-1,79
UPG460	200,1	25,65	0,420	15611	1,93	1,26	0,62	-0,36	-1,74

From Table 5.2 one can observe that the shift factors are independent of the type of the mixture types. The logarithmic values of the shift factors are plotted vs. temperature in Figure 5.7. A linear regression could be made and this line provides an indication of the temperature susceptibility of the mixtures. It seems that all mixtures have almost the same slope. The shift factors for other temperatures can be calculated by extrapolation.

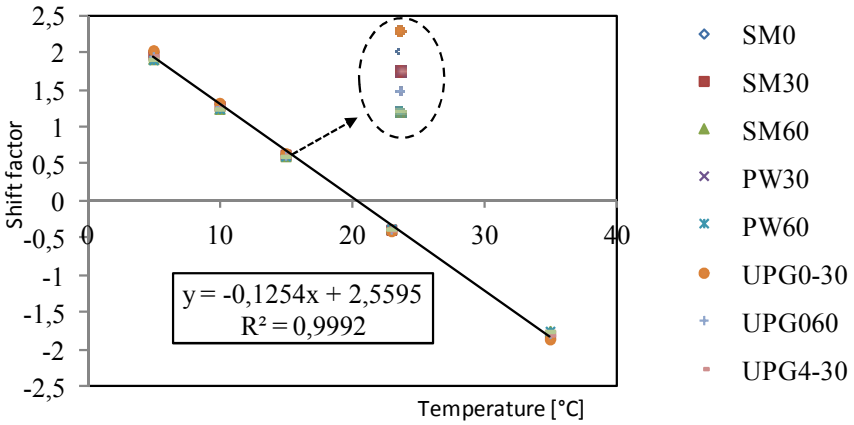

Figure 5.7 Shift factors vs. temperature (°C)

An example of the creation of a master-curve at 20°C is illustrated in Figure 5.8. The master curves for all mix designs are shown in Figure 5.9.

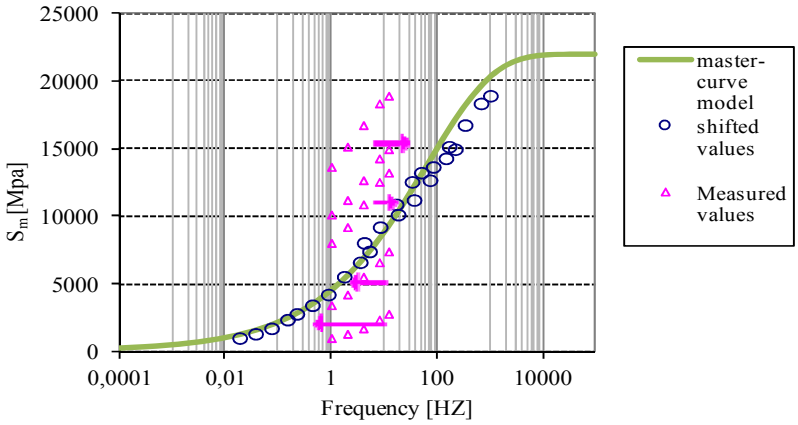

Figure 5.8 Example of a stiffness master-curve (SM60) derivation at 20°C

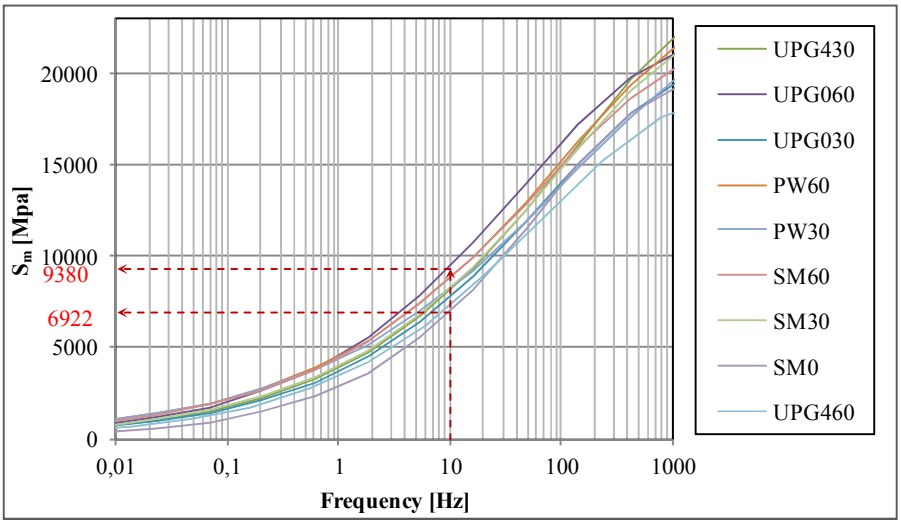

Figure 5.9 Stiffness master curves of all mix design sat 20°C

Since the master curves in Figure 5.9 are close to each other, it is difficult to analyze them visually using this figure. Therefore they are also given per mix design type in the following three plots.

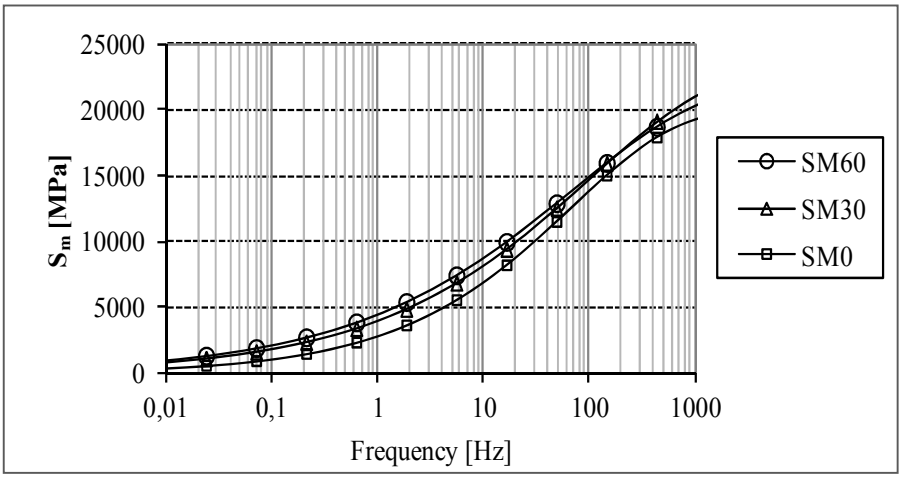

Figure 5.10 Stiffness master-curves of SM mixtures at 20°C

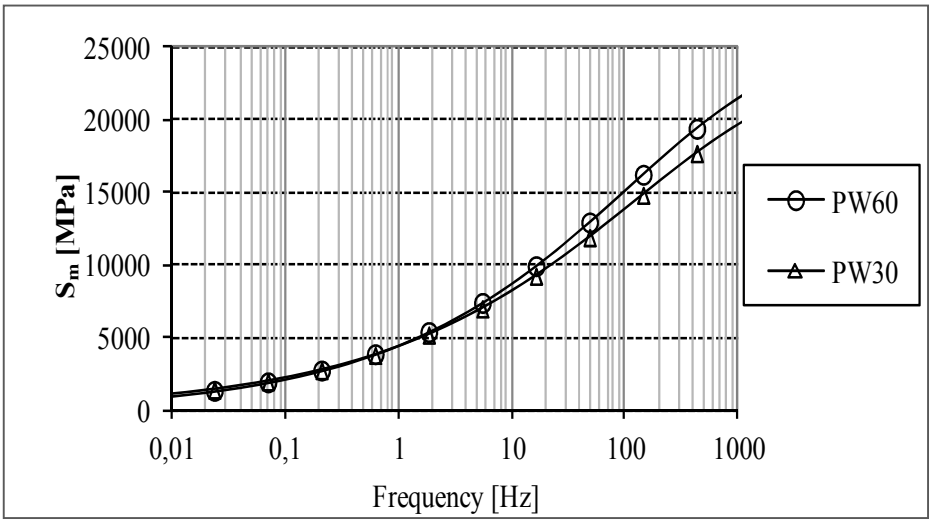

Figure 5.11 Stiffness master-curves of Partial Warming mixtures at 20°C

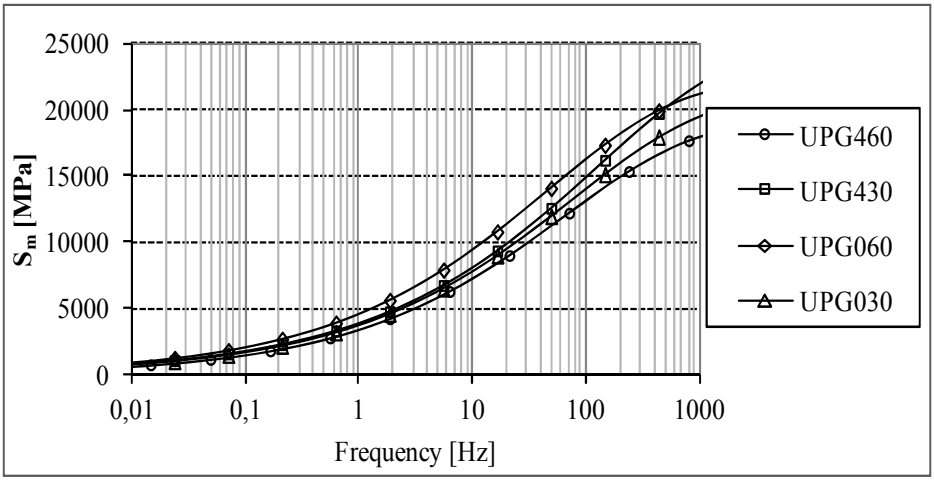

Figure 5.12 Stiffness master-curves of UPG mixtures at 20°C

5.2.1.2. Comparison of stiffness modulus results

RA content and type of mixing method are considered in analyzing and comparing the results of the stiffness modulus tests.

5.2.1.2.1. Effect of RA content on stiffness

Comparison of the stiffness values of mixtures containing 30% and 60% RA (see Figure 5.10, Figure 5.11 and Figure 5.12) shows that the stiffness increases with increasing RA content. That was expected due to the higher stiffness of the RA binder which contributes to the stiffness of the whole mixture. As it was mentioned earlier, stiffness values were compared relatively in Figure 5.6. This figure shows increments of 11%, 8%, and 27% in stiffness values (at 23°C and 8Hz) respectively in SM, PW and UPG0 due to the increase in RA content.

In the UPG4 mixtures, increase of the RA content from 30% to 60% didn't increase the stiffness modulus. Since the UPG4 method comprises of superheating virgin aggregates and 4% moisture in cold RA, it appears that the presence of moisture may have influenced the blending between the old and new binders, otherwise, according to the log-pen rule, the stiffness of the UPG460 would have been higher than UPG430.

To explore the validity of the log-pen rule, the binder of all mixtures containing 30%RA and 60%RA were extracted using the method described in 2.2.2. Extracted binder of 30% is a combination of SM30, PW30, UPG030 and UPG430. Extracted binder of 60% is a combination of SM60, PW60, UPG060 and UPG460.

The complex modulus of each (combined) binder was determined with the DSR (see 2.2.3). Then the master curves of G* values as well as phase angles were constructed with the model shown in 2.2.3. The master curves of the RA binder and Virgin 70/100 and 40/60 are also determined at 25°C. All master curves are shown in Figure 5.13. These master curves are also used to determine G* at 0.4Hz. Then equation 5.7, which was derived in 1958 by Saal and Labout [55] is used to calculate the equivalent needle penetration at 25°C.

Van den Bergh shows in his research [37] a good correlation between the G* values at 25°C and 4Hz by using equation (5.7).

$$log\ (G^*_{0.4\ Hz;25°C;[MPa]}) = 2.923 - 1.9\ log\ (pen_{25°C:[dmm]}) \qquad (5.7)$$

The calculation of the penetration according to this equation is presented in Table 5.3. At the last row of this table the penetration of the blended binder of the 30% and 60% RA mixtures is also determined according to the log-pen rule which was already explained in 1.2.9. It has to be mentioned that the effect of hardening of the extracted binder due to short term aging is not taken into account. The difference between the two predicted penetration values is also shown in this table. In many standards up to 40% decrease in penetration of the original binder is taken into account. Mixtures with higher RA contents

would be less sensitive to short term aging since the RA binder was already aged before mixing.

According to the predicted values in Table 5.3, the UPG460 should be much harder than the reference mixture which contains only 40/60 pen bitumen but according to Figure 5.5 and Figure 5.6 this mixture has only a slightly higher stiffness than the reference mixture.

Table 5.3 Determination of penetration with G master curves*

	RAP		***40/60***		***RAP30%***		***RAP60%***		***virgin 70/100***	
	G* [Mpa]	δ [°]	G* [Mpa]	δ [°]	G* [Mpa]	δ [°]	G* [Mpa]	δ [°]	G* [Mpa]	δ [°]
at 0,4 Hz	2,363	59,8	0,530	74,0	0,810	66,3	2,020	62,5	0,181	78,5
Predicted penetration [dmm]	22		48		39		24		85	
Predicted penetration with log-pen					**53**		**32**			
Difference between two predicted values					$\frac{(53-39)*100}{53}$ **=27%**		**25%**			

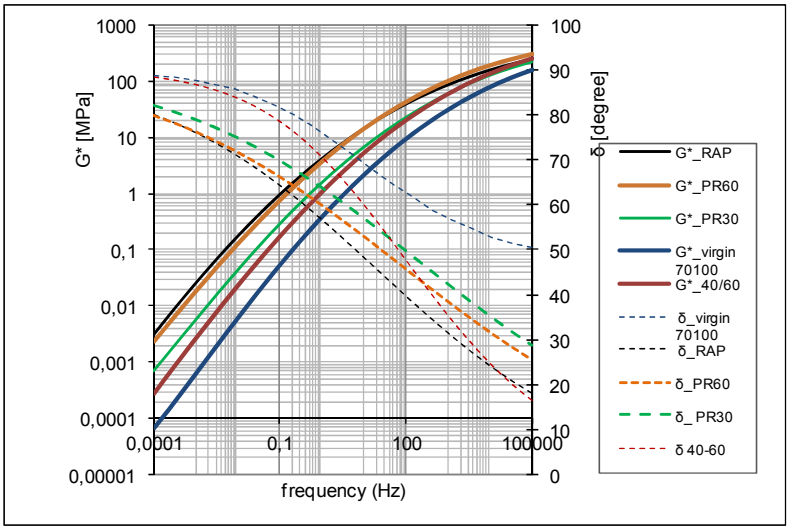

Figure 5.13 Master curves of extracted binders in comparison with RA binders, 70/100 pen and 40/60 pen bitumen (NB: 40/60 was used in reference mixture SM0)

Although bitumen of PR30 and PR60 are mixtures of SM, PW and UPG, the results indicate that the log-pen rule was not successful in predicting the penetration of the recovered bitumen

5.2.1.2.2. Effect of mixing method on stiffness

Figure *5.14* and Figure 5.15 show the effect of the mixing method on the stiffness modulus. The RA content is kept constant to facilitate the comparison.

Figure *5.14* shows that a difference in mixing method doesn't affect the stiffness of the mixture at a low RA content. Only minor differences are notable at high and low frequencies. These differences can be seen in the slope of the master curve which could be interpreted as the sensitivity of the mixture to the loading frequency and temperature.

Figure 5.15 demonstrates larger differences in stiffness between mixtures containing 60% RA and prepared using different methods. The figure shows that UPG4 with 60% RA has a significantly lower stiffness than the mixtures produced with the other mixing methods. Two possible reasons for this effect are given here. Firstly, the RA is not aged during the preheating period because it was added at ambient temperature. Secondly, it appears that the mixing conditions might not allow the virgin bitumen to blend efficiently with the hard RA binder and it causes the soft virgin bitumen to be the dominant binder in the mechanical properties of the mixture.

The PW and SM master curves with 60% RA have an identical stiffness modulus which accounts for the fact that RA is preheated at temperatures of 130°C and 170°C.

Comparison of the stiffness modulus between UPG060 and UPG460 shows that the presence of moisture (4% in UPG4) may have prevented extra aging during mixing. It should be noted that 60% cold RA was added in both mixtures. However, in the UPG060 mixture the RA binder was exposed directly to superheated virgin aggregate in dry conditions. It seems that moisture protects the RA binder from a rather large temperature shock during the very first exposure moments. It should be mentioned that the binder of UPG460 was stiffer than the binder of SM0, however, the stiffness of the UPG460 mixture is lower than that of SM0 mixture. Presence of moisture could have caused some kind of foaming or emulsifying effect which also may result in lowering the stiffness of the UPG460 mixture.

However, it is still unknown how the RA binder and virgin bitumen blend in both mixtures. This immediately shows the importance of studying blending of RA and virgin bitumen and the effects of preheating and moisture conditions in the mixture containing high amounts of RA.

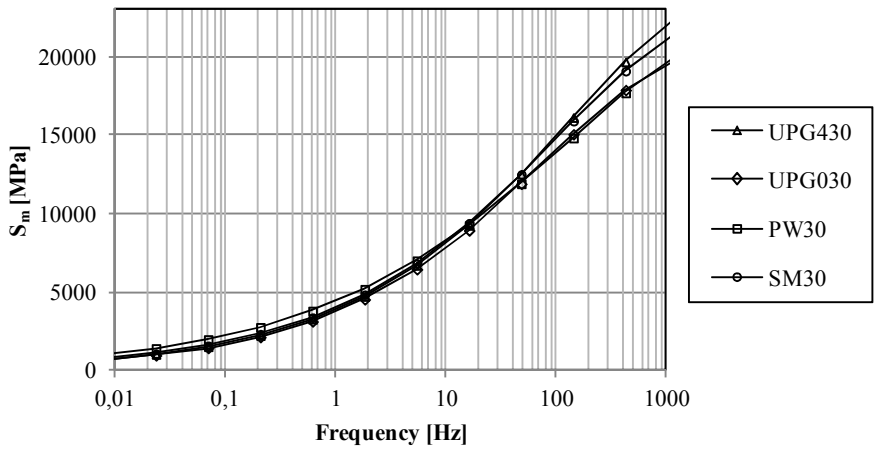

Figure 5.14 Comparison of the effect of mix design on the master curve of the stiffness modulus of mixtures with 30% RA at 20°C

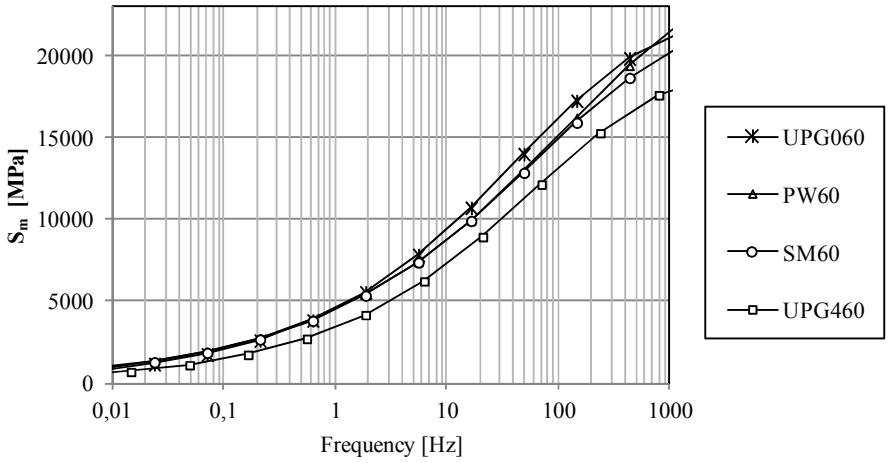

Figure 5.15 Comparing the effect of mix design on the stiffness modulus of mixtures with 60% RA at 20°C

5.2.2. Indirect tensile strength (ITS)

This test was done to evaluate the tensile strength of the mixtures at a low temperature at a displacement rate of 0.85mm/s (=51mm/min). The tests were done according to EN 12697-23, bituminous mixtures - Test methods for hot

mix asphalt - Part 23: Determination of the indirect tensile strength of bituminous specimens". The concept of the ITS determination is discussed in Chapter 3. Figure 5.16 shows the test setup as well as the stress distribution due to the vertical loading from the top steel strip.

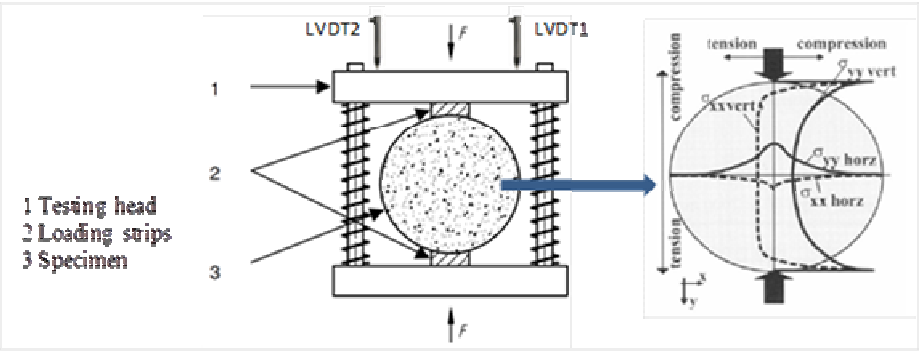

Figure 5.16 ITS test setup and stress distribution inside the loaded specimen

One specimen per mixing method is tested because only a limited number of samples were prepared. They were stored in a temperature cabinet for at least 6 hours at 5°C. Specimens of 100mm diameter and 50mm height are used in the ITS measurements.

The resulting forces are plotted against displacement and time in Figure 5.17 and Figure 5.18. The peak force value is used to calculate the ITS.

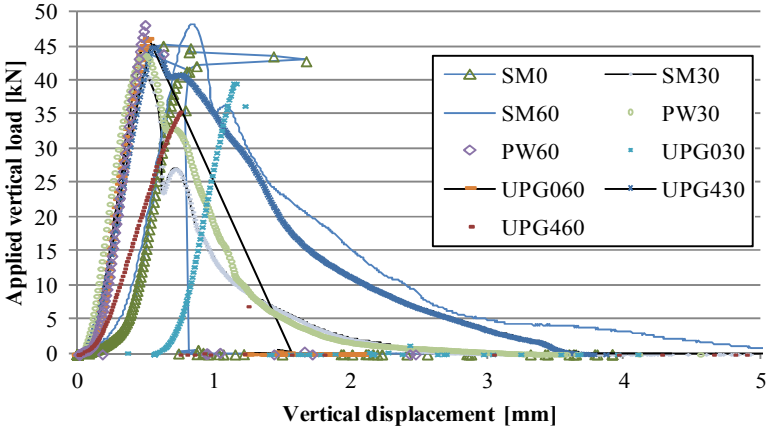

Figure 5.17 ITS test at 5°C and a displacement rate of 50mm/min (load vs. Displacement)

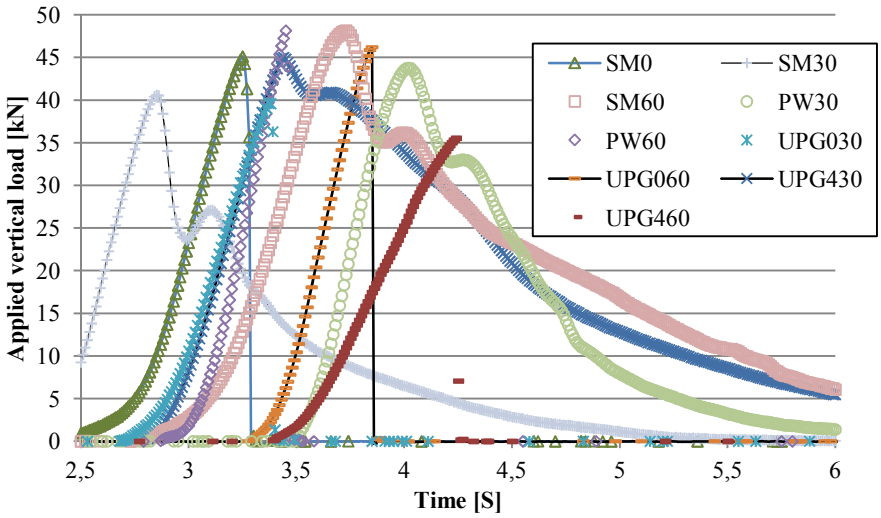

Figure 5.18 ITS test at 5°C and a displacement rate of 50mm/min (load vs. time)

Table 5.4 ITS values (5°C)

Sample	***Air void***	***P***	***D***	***H***	***ITS***
ID	[%]	[kN]	[mm]	[mm]	[Mpa]
SM0	3,60	45,1	100,0	52,3	5,5
SM30	2,90	40,6	99,9	49,9	5,2
SM60	2,76	48,1	99,9	50,5	6,1
PW30	3,06	43,8	99,9	48,2	5,8
PW60	1,97	48,2	99,8	50,8	6,1
UPG030	2,97	39,6	99,8	51,9	4,9
UPG060	2,15	46,2	99,7	52,3	5,7
UPG430	2,30	45,0	99,8	50,9	5,6
UPB460	2,15	40,6	99,7	57,1	4,5

The ITS values of all samples prepared with the different mixing methods are presented in Table 5.4. ITS values are compared according to the air void contents in Figure 5.19. The results are also summarized in Figure 5.20. This figure clearly shows that the tensile strength increases with the increase of RA content except in UPG430 and UPG460. This is similar to the results of the stiffness values. As it was discussed earlier this might be because of less blending and less aging in UPG with 4% moisture and 60% RA.

PW and SM mixtures give a relatively higher tensile strength compared with the UPG mixtures.

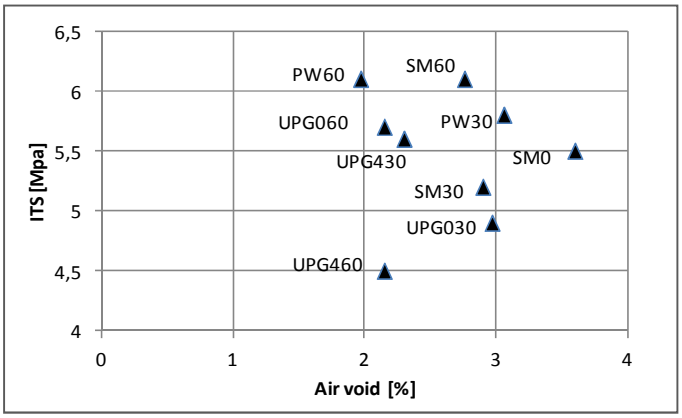

Figure 5.19 Indirect tensile strength values (at 5°) vs. air void content

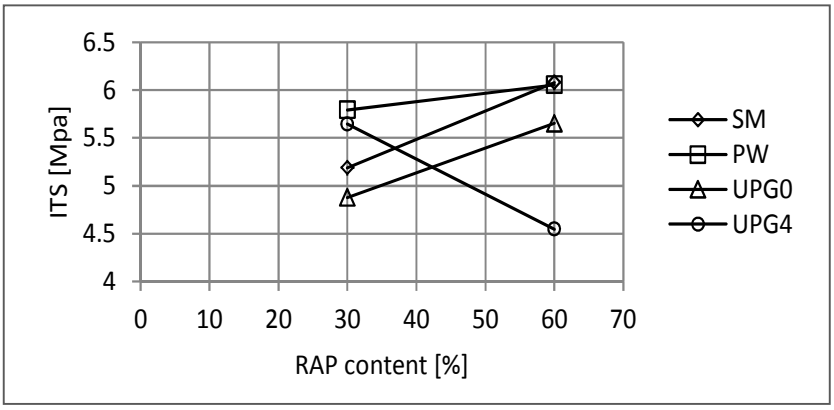

Figure 5.20 Comparison of ITS results with respect to RA content and mixing method at 5°C

5.2.3. Fatigue life evaluation

Cylindrical samples of 100mm diameter were used for indirect tension fatigue tests under controlled load conditions. This test is conducted according to NEN-EN 12697: "Test methods for hot mix asphalt – Part 24: Resistance to fatigue". A loading frame, similar to the ITS test, was used with identically curved steel strips. The vertical displacement was measured and controlled with two LVDTs. It was decided not to measure the horizontal radial deformation because of possible damage to the LVDTs.

A continuous haversine loading signal was programmed for the test. No rest period was considered; the tests were done at only one temperature of 20°C and a stress level of 220kPa. An IPC Universal Testing Machine (UTM-25) was selected to run the test. Repetitive vertical loading was applied until the failure of the specimen occurred. This is in accordance with EN 1697-24.

The fatigue test at identical loading, temperature and stress levels were conducted in two conditions; firstly, in the standard and dry condition and, secondly, in saturated condition. With this non-standard fatigue test, the effect of saturation on the fatigue life was investigated. It was performed because it was hypothesized that the mixing of the super-heated aggregates with the moist and cool RA could have an effect on the adhesion of the binder to the aggregates because of excessive hardening.

for this type of fatigue test, cylindrical samples were firstly placed on the perforated shelf in a vacuum container filled with distilled water at room temperature (20 ± 5°C) to a level at least 20 mm above the upper surface of the test specimen. Saturation of pores in the mixture is obtained by applying a vacuum at an absolute (residual) pressure of (6,7 ± 0,3) kPa within (10 ± 1) min. Once the vacuum pressure became stable, the pressure was maintained for (30 ± 5) min. After saturation conditioning, the specimen was brought to a container filled with water, by means of which wet conditioning at atmospheric pressure was maintained during fatigue testing.

The loading setup was located in the water container and the water temperature was maintained at 20°C by water circulation to a water bath as it is shown in Figure 5.21.

Test setups at dry and saturated conditions along with images of fractured specimen due to ITS cyclic fatigue loading are illustrated in Figure 5.22 and Figure 5.23.

Graphs showing the vertical displacement vs. number of load cycles related to both dry and saturated conditions are illustrated in Figure *5.24* and Figure 5.25. In these charts, data are plotted on a logarithmic scale, at the top, and a

normal scale at the bottom. The cyclic loading was stopped when the vertical accumulated deformation exceeded 6mm.

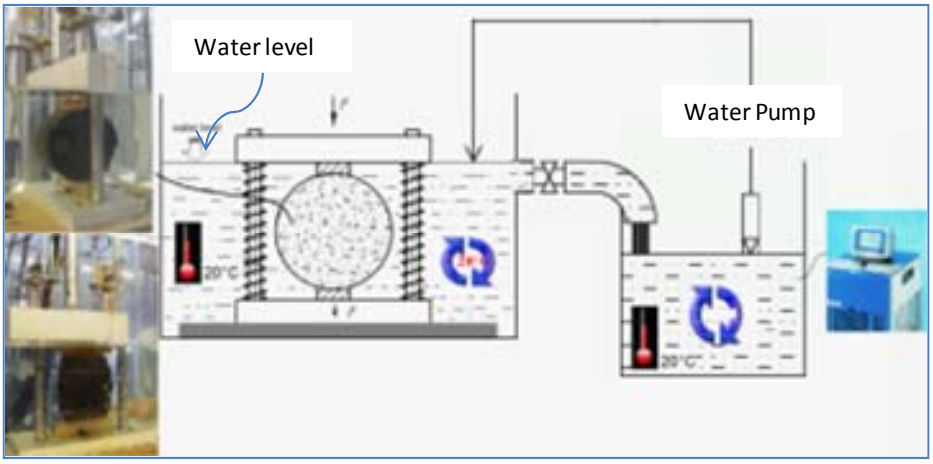

Figure 5.21 Saturated IT fatigue setup

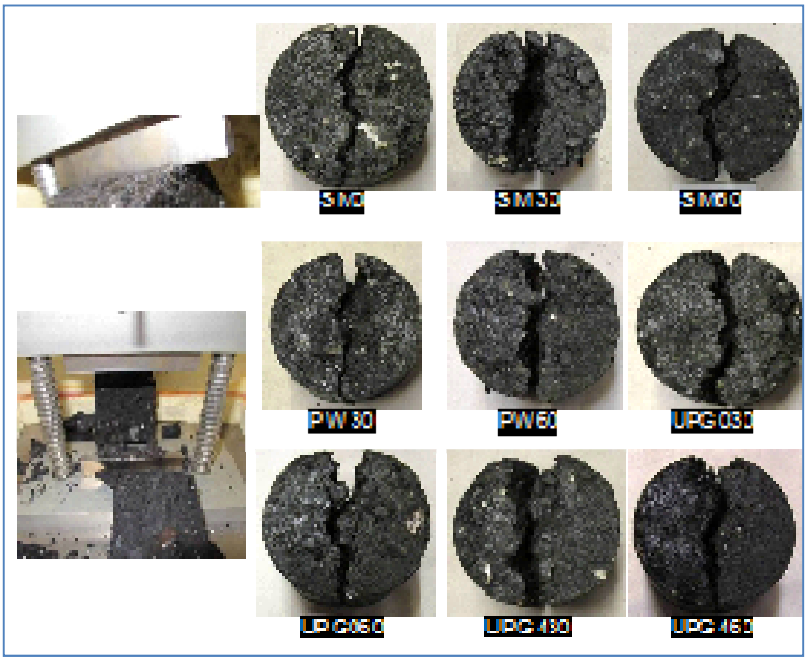

Figure 5.22 Specimen fractures and failure modes in dry condition

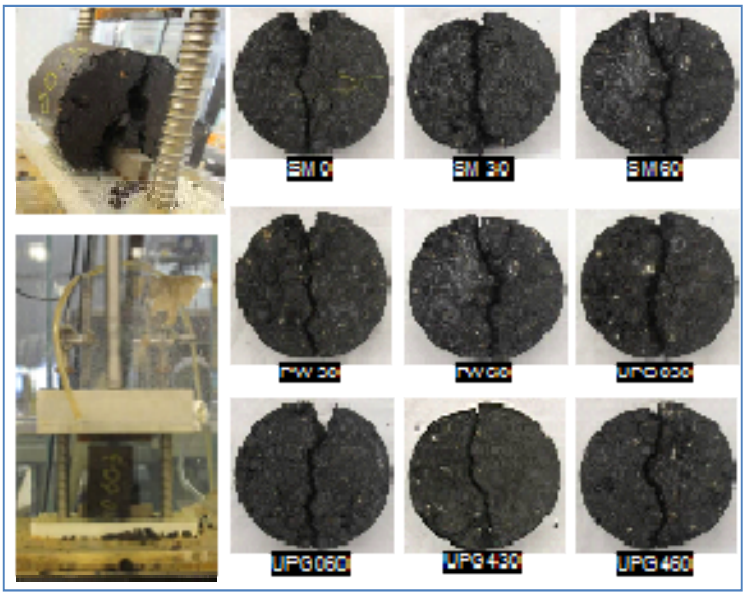

Figure 5.23 Specimen fractures and failure modes in saturated condition

It is often debated whether specimens fail in creep in a load controlled fatigue test or whether the failure is really due to fatigue. This is a valid discussion especially when specimens are loaded in only one direction as is the case in the indirect tension fatigue test. From the *log N* vs. vertical displacement relationship Figure *5.24* and Figure 5.25, (top part) one might conclude that failure occurs when the cumulative vertical deformation is approximately 1.3 mm. From the right hand part of the same figures however a somewhat higher cumulative vertical strain at failure is estimated but also in these figures it seems that the vertical displacement at failure is approximately the same for all mixtures.

It is believed that failure in the indirect tension fatigue test can be considered as a mix of creep and fatigue failure. It should be noted however that the cumulative deformation not only consists of creep (permanent deformation) but also of non-recovered delayed elastic deformation. Since the load signal was a continuous haversine signal without rest periods, the delayed elastic recovery which should occur after each loading cycle could not develop, implying a gradual increase of this deformation in time. It was not possible to determine which part of the accumulated deformation is permanent and which part is due to accumulation of the non-recovered delayed elastic displacement.

The results of the fatigue tests under dry and saturated conditions are shown in Figure 5.26. The figure shows that the reference mixture had the lowest fatigue resistance. The effect of RA content on the fatigue life is shown in Figure 5.27, in which each line belongs to a particular mixing method while the reference mixture is represented by one point. This figure shows that increasing the RA content has improved fatigue lives in both dry and saturated conditions. However, this relation is not consistent because SM60 shows less resistance in comparison to SM30. The same inconsistency was already observed in the stiffness values. It seems that indirect tensile fatigue life is related to the mixture stiffness since the same pattern was observed in stiffness relations. The stiffness of SM60 was relatively less than SM30 while the increase in RA content also seemed to increase the stiffness of mixtures made using other mixing methods (see Figure 5.20).

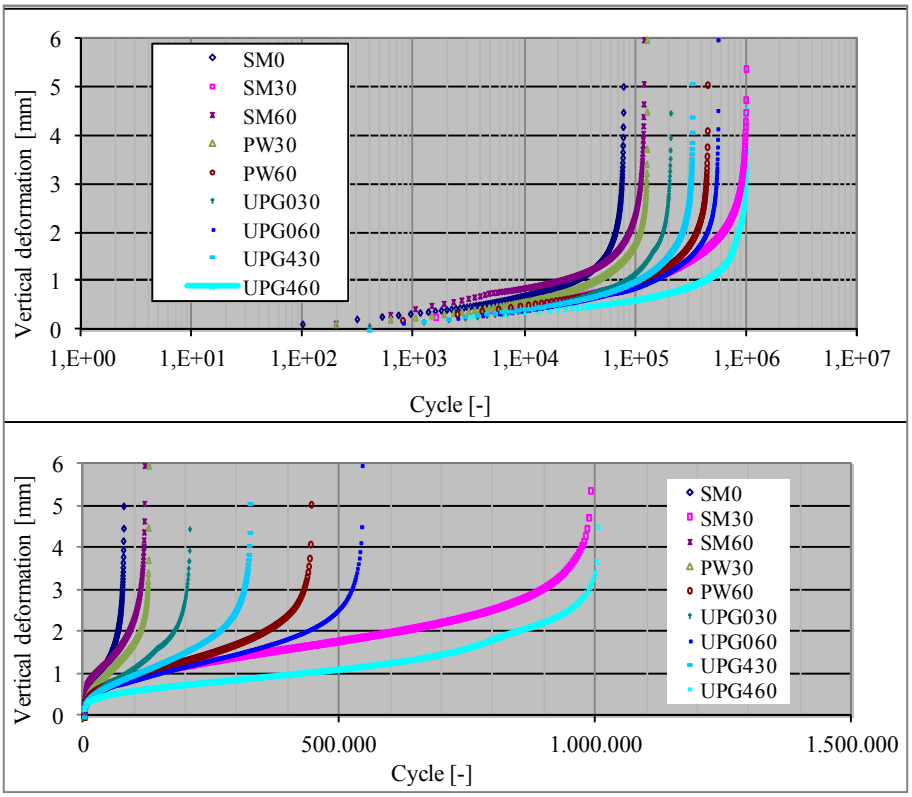

Figure 5.24 *Permanent vertical deformation vs. loading cycles in dry condition (top; logarithmic scale for cycles and bottom: normal scale for cycles)*

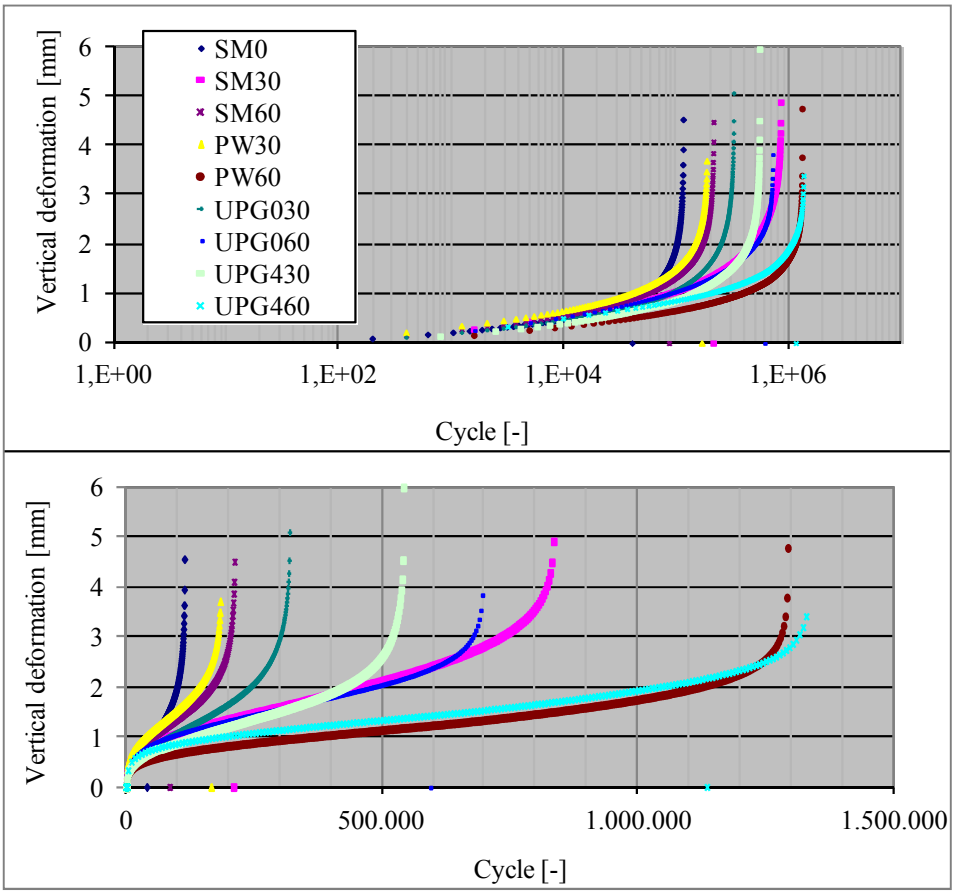

*Figure 5.25 Permanent vertical deformation vs. loading cycles in **Saturated** condition (top; logarithmic for cycles and bottom: normal scale for cycles)*

Furthermore it can be observed that the fatigue results obtained for the UPG prepared samples (UPG0 and UPG4) are certainly not less than those obtained on the samples prepared in a different way in spite of the (very) high temperature levels to which the virgin aggregates were heated and to which the RA was exposed. It is also notable that the fatigue lives of UPG430 and UPG460 are slightly higher than those of the other mixtures while their stiffness was relatively less than the others.

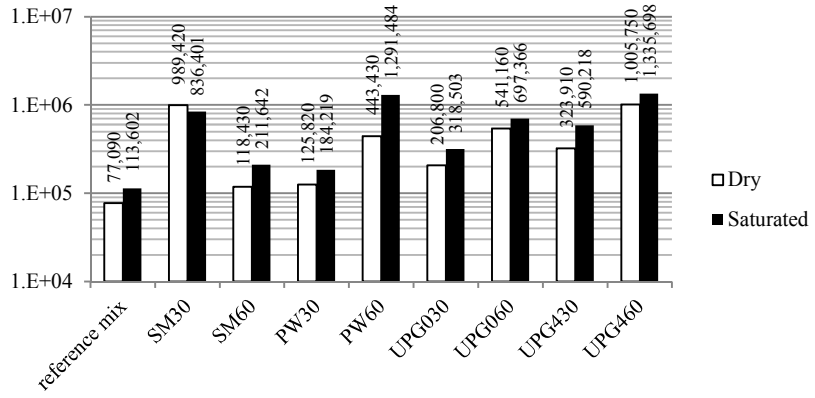

Figure 5.26 Fatigue life of samples in dry and saturated conditions at 20°C, 10Hz, and 220kPa (stress controlled)

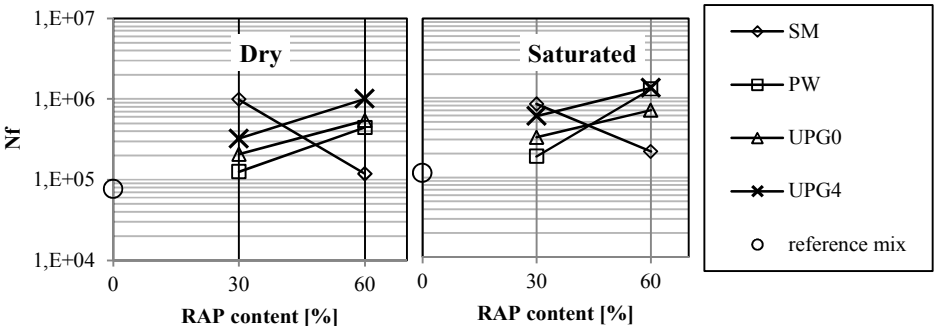

Figure 5.27 Effect of RA content on the indirect tensile fatigue life in dry and saturated conditions.

In Figure 5.28, a comparison is made between fatigue lives in dry and saturated conditions. Almost all points are above the equality line. This implies that saturation has not reduced the fatigue lives in comparison with dry conditions. This is probably caused by the fact that the void content of the mixtures was around 3%, implying that water could not enter the specimens because of absence of interconnected voids.

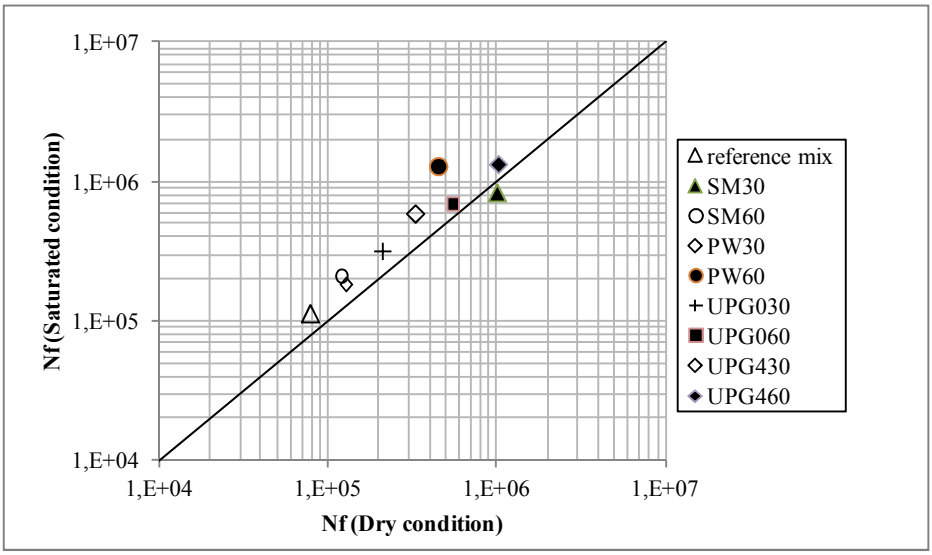

Figure 5.28 Comparison between fatigue life at dry and saturated conditions

5.2.4. The effect of mixing time and air voids content

As it was noted in chapter 3, a similar research on the SM, PW and UPG mixing methods was done by Chacho (2012). This additional work was thought to be of importance since in the work conducted so far, the low air voids of specimens and the extended mixing period (of 3 minutes) could have had significant effects on the stiffness and fatigue properties (at both dry and saturated conditions). Therefore a similar set of specimens but with a higher air voids content (5%) was produced at similar preheating conditions but at a shorter mixing time (of 1 min). The higher air voids of samples were achieved through a lower compaction effort. The volumetric properties of these specimens were presented earlier in chapter 3. The mixtures of this later work are identified as SM60*, PW60*and UPG460*.

The stiffness master curves of these mixtures are presented in Figure 5.30. The stiffness values at different temperature are presented also in Figure 5.29. They are also compared with the corresponding mixtures of the previous study in three separate charts as shown in Figure 5.31. This figure shows that stiffness values of SM and PW at 10Hz are almost equal between the two sets of mixtures, however, the slopes vary slightly. The UPG mixture in the complementary study has a higher stiffness than that from the initial study.

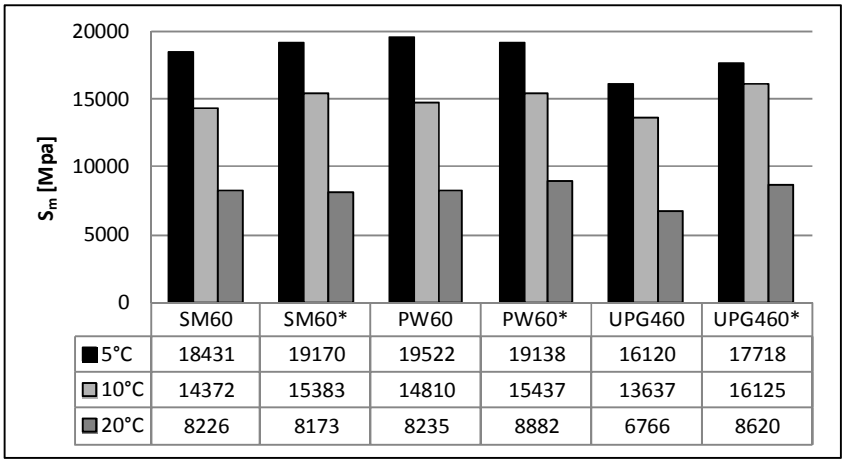

	SM60	SM60*	PW60	PW60*	UPG460	UPG460*
5°C	18431	19170	19522	19138	16120	17718
10°C	14372	15383	14810	15437	13637	16125
20°C	8226	8173	8235	8882	6766	8620

Figure 5.29 Comparison of stiffness values at 8Hz.

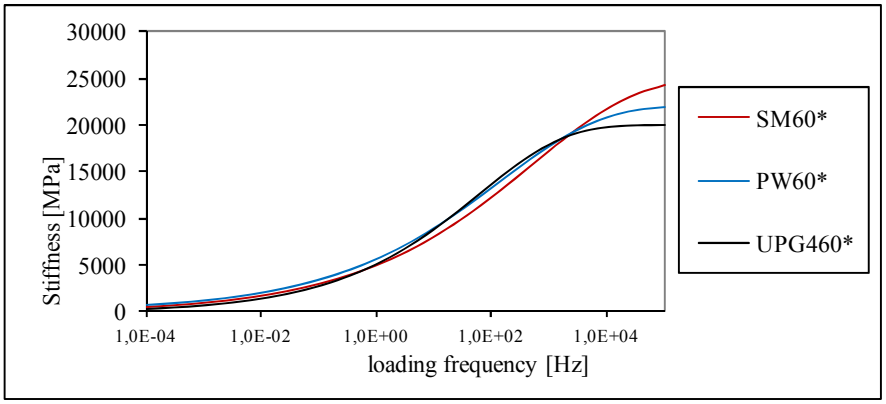

Figure 5.30 Indirect tensile modulus master curves at 20°C obtained in the extended research (Chacho2012)

Similar IT fatigue tests (load controlled) at both dry and saturated conditions were conducted at three tensile stress levels during the complementary study. Fatigue lines are created for each mixture according to the Wohler equation. The fatigue lines and corresponding Wohler equations are presented in Figure 5.32 and Figure 5.33.

The effect of saturation on the fatigue life is studied per each mix design in Figure 5.32 separately. It appears that the fatigue relation for saturated conditions gives higher slopes and lower fatigue values in comparison with those obtained in dry conditions. The fatigue results obtained on mixtures with low air voids showed that saturation didn't have any negative effect on

the fatigue life while the set of experiments on the mixtures with a higher air void content revealed the negative impact of saturation conditions. Figure 5.33 illustrates the effect of mix design on fatigue lines at dry and saturated conditions separately. It turns out that UPG460* is less resistant to IT fatigue loading in comparison to SM60* and PW60*.

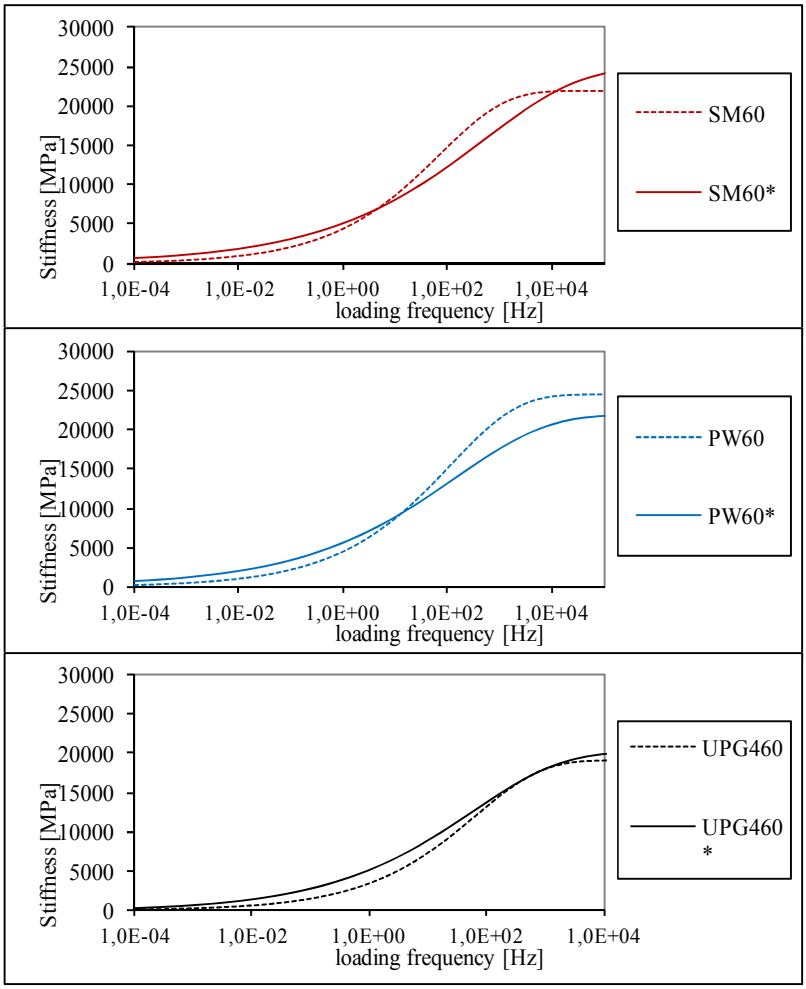

Figure 5.31 Comparison of stiffness master curves at 20°C .

The Cumulative vertical deformation vs. loading cycles at dry and saturated conditions of SM60*, PW60* and UPG460* at each stress level are presented in Figure 5.35. The effect of mixing time and air void content is studied in Figure 5.34 in which fatigue lives at a single stress level of 220kPa are

compared. It shows that the mixtures produced with a shorter mixing period and higher air voids content generally have a lower fatigue life.

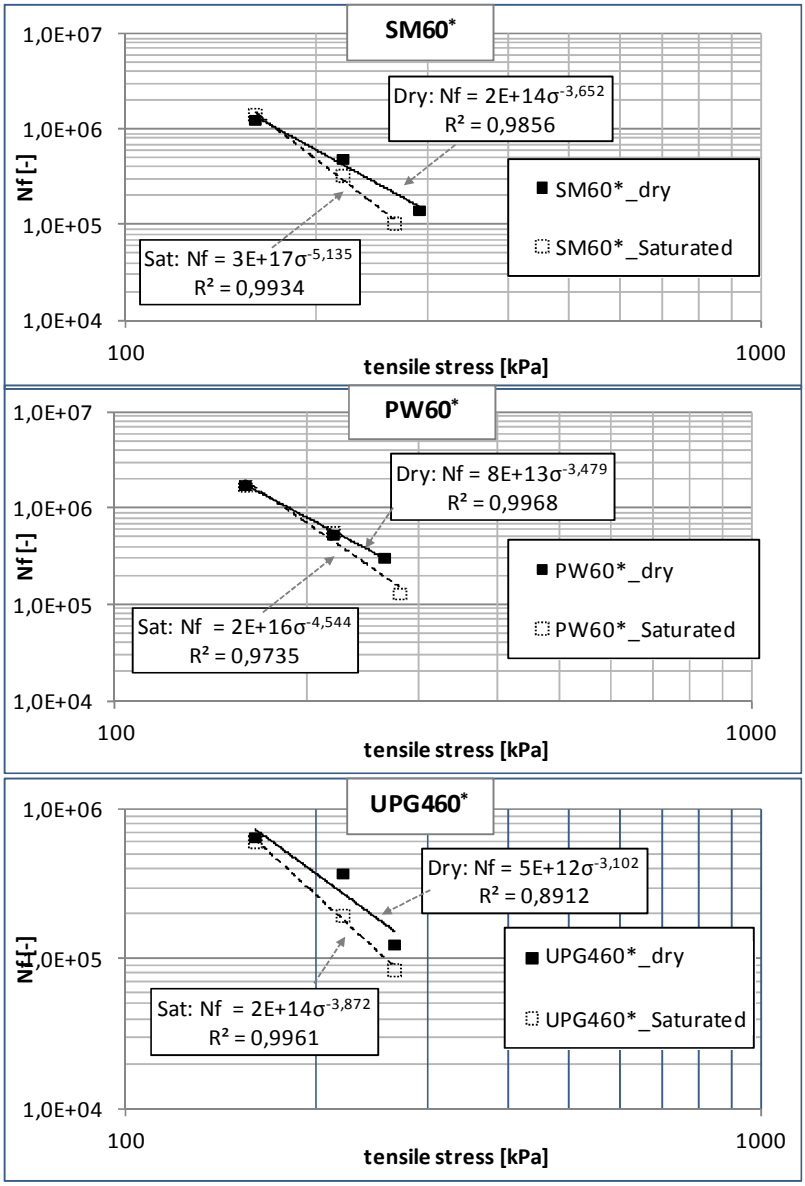

Figure 5.32 Comparison of fatigue lines between dry and saturated condition in IT fatigue [temp, stress]

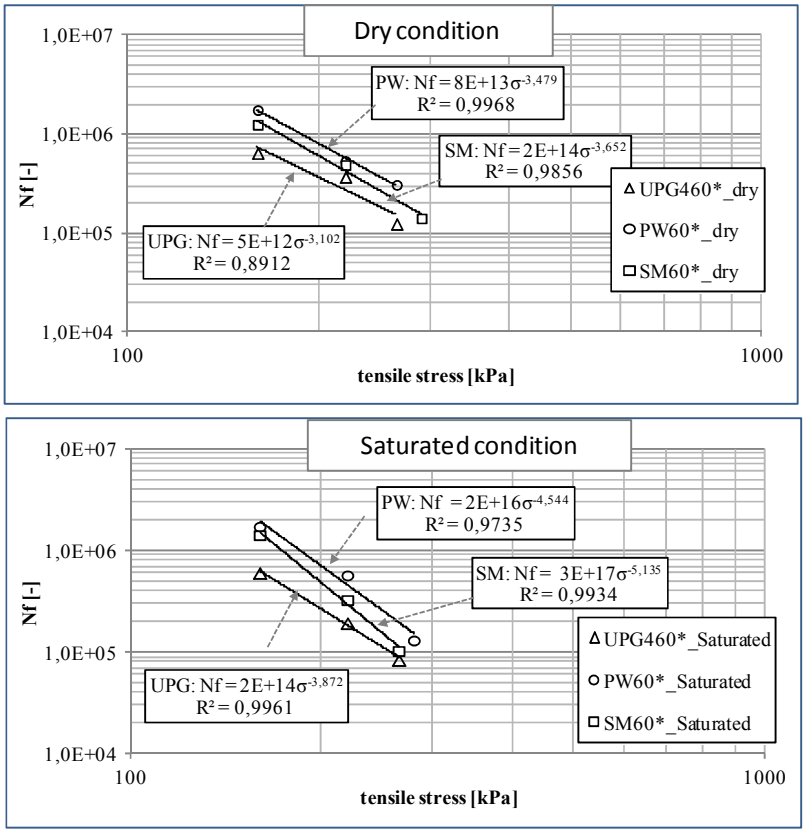

Figure 5.33 Comparison of fatigue lines between different type of mixtures in dry condition (top) and saturated condition (bottom) with IT fatigue [temp, stress]

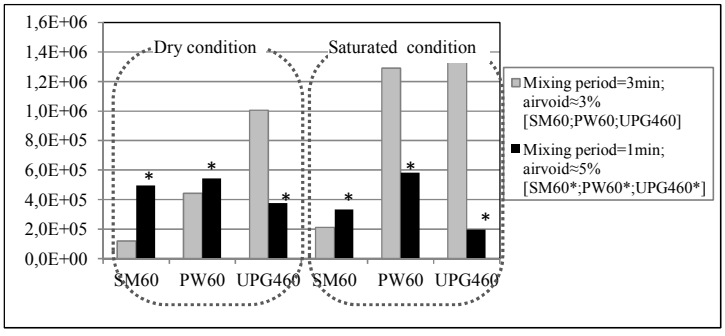

Figure 5.34 Effect of mixing period and air void content on the IT fatigue life [20°C, 220kPa] in the conditions; dry and saturated

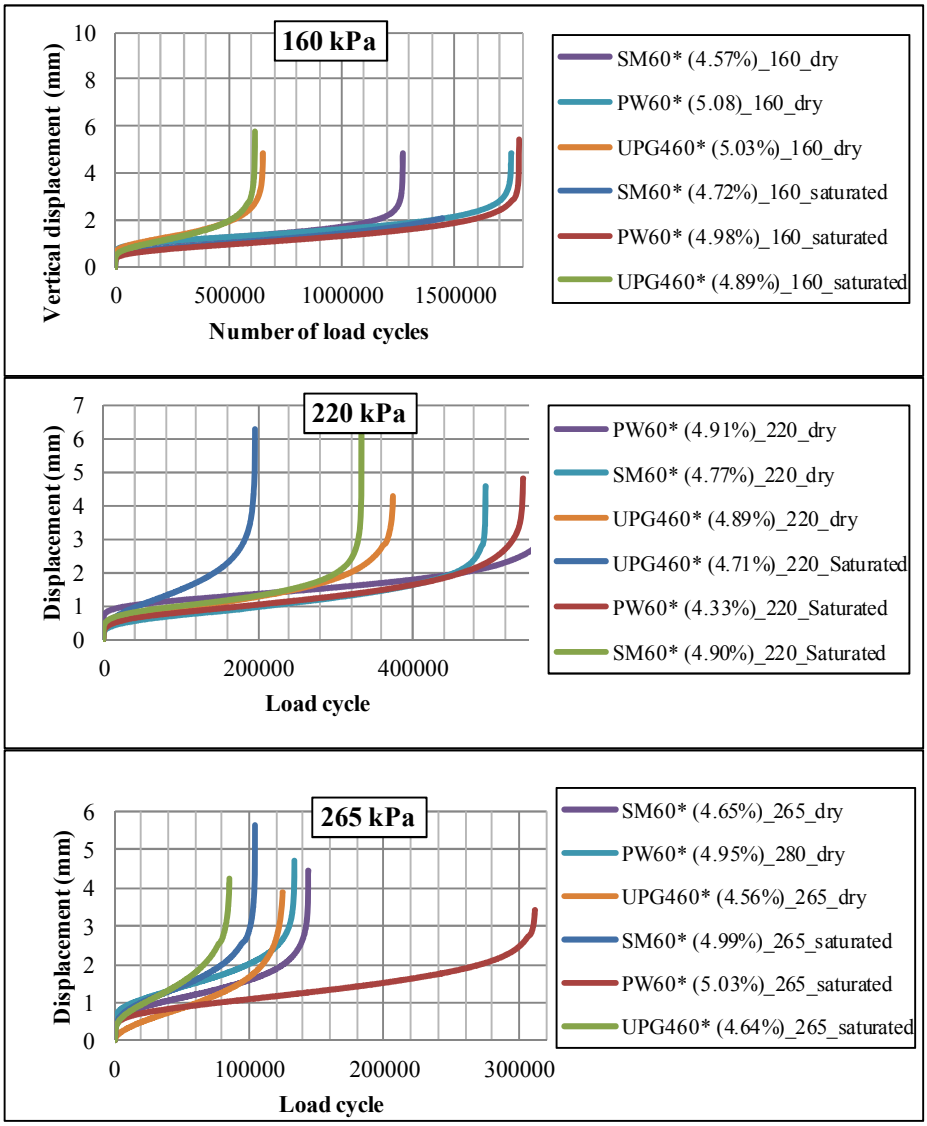

Figure 5.35 Cumulative vertical deformation vs. loading cycles in dry and saturated conditions during IT fatigue test (air voids of tested specimens are shown in parentheses in the legends at each plots)

5.2.5. Conclusions of Phase I

The main objectives of this phase of the study were; firstly to determine the effect of the amount of RA and its moisture and preheating conditions on the mechanical properties. Secondly to derive a laboratory mixture design method that simulates mixing procedures as used in practice.

1. Based on the results of Phase 1, it was shown that the amount of RA as well as the moisture content of the RA did not have negative effects on the mechanical properties of the investigated recycled mixtures when compared to those of a reference mixture made of virgin materials. The presence of a high amount of moisture in laboratory mixing conditions seems to reduce the stiffness of the mixture with 60% RA. At the same time the fatigue life increased, even with its lower stiffness values. Of course the effect of mixing conditions should also be studied using real plants, because laboratory simulations probably do not perfectly simulate plant mixing conditions.
2. The first set of the experiment was done on low air voids samples and they were also mixed at an extended mixing time (3minutes). Because of the low air voids content the fatigue test results in saturated conditions (underwater) were not influenced because of the low porosity. Then the question was what the mechanical characteristics of recycled mixtures would be when the mixing time is reduced and the samples air void content is increased. It should be noted that in reality the mixing time is much shorter than in laboratory conditions. Therefore a second set of samples was produced with similar mixing protocols but at a shorter mixing time and higher air voids content.
3. The stiffness values of SM* and PW* mixtures are almost similar to the values of SM and PW, however the slopes of the master curves vary slightly. The UPG* mixture in the complementary study has a higher stiffness than that from the initial study.
4. The experiments on the mixtures with a higher air void content revealed the negative impact of saturation conditions.
5. Generally mixtures produced with a shorter mixing time (in laboratory conditions) and a higher air voids content have a lower fatigue life.

5.3. Test results of Phase II

In this section the results of the second phase of the mixture experiments are presented and analyzed. The influence of two HMA mixing plants (batch plant and Astec double drum) on the mixture properties are investigated and compared with the laboratory produced mixtures.

Earlier, in Chapters 2 and 3, the sample preparation procedure and the test procedures were described. The sample coding system was presented in Chapter 3. Three identical mixtures (same gradation, RA content and bitumen content) were produced with an Astec (A), a batch plant (BB) and a laboratory mixer (L). An extra mixture was also produced in the batch plant with the same mix design. The only difference in this mix design was the type of RA. This mix is identified with (B). It contains 25% RA from base layers and 25% of RA obtained from porous asphalt.

All mixtures (A, BB, L and B) were compacted in a shear box compactor to produce blocks of 150×180×450mm (8 blocks per each mix type). From each mix type three blocks were used to cut 12 beams of 5×5×450 mm. They are used in 4PB stiffness and fatigue tests. Three other blocks were used to core 30 cylinders of 65×138mm to be used in monotonic direct tension and compression tests.

5.3.1. Four point bending (4PB) flexural stiffness

This test is carried out to evaluate the effect of the mixing process on the mixture stiffness properties. The stiffness results were then used for creating stiffness master curves using the temperature–loading time superposition principle. The test procedures and conditions were explained already in chapter 3. A number of test conditions are listed below:

- The test was done according to EN 12697-26
- Strain level was controlled at 100 μm/m
- Frequencies: 1, 2, 4 and 8 Hz
- Temperatures: 5°C, 10°C, 15°C, 20°C and 35°C.

In this test the specimens are subjected to a sinusoidal force in order to obtain the desired displacement amplitude. The deflection amplitude stays within 2% of the desired value. During the test the maximum applied force, the deflection and phase angle are recorded. According to EN 12697-26 it is recommended to determine the initial stiffness modulus from a load cycle between the 45th and the 100^{th}load cycle and not from the first few load cycles. This is done to avoid start-up phenomena which would affect the

stiffness determination. The initial stiffness is typically determined at the 100th cycle in most 4PB tests. The fluctuations of stiffness values during the first 100 load cycles at different temperatures and frequencies are shown in Figure 5.36.

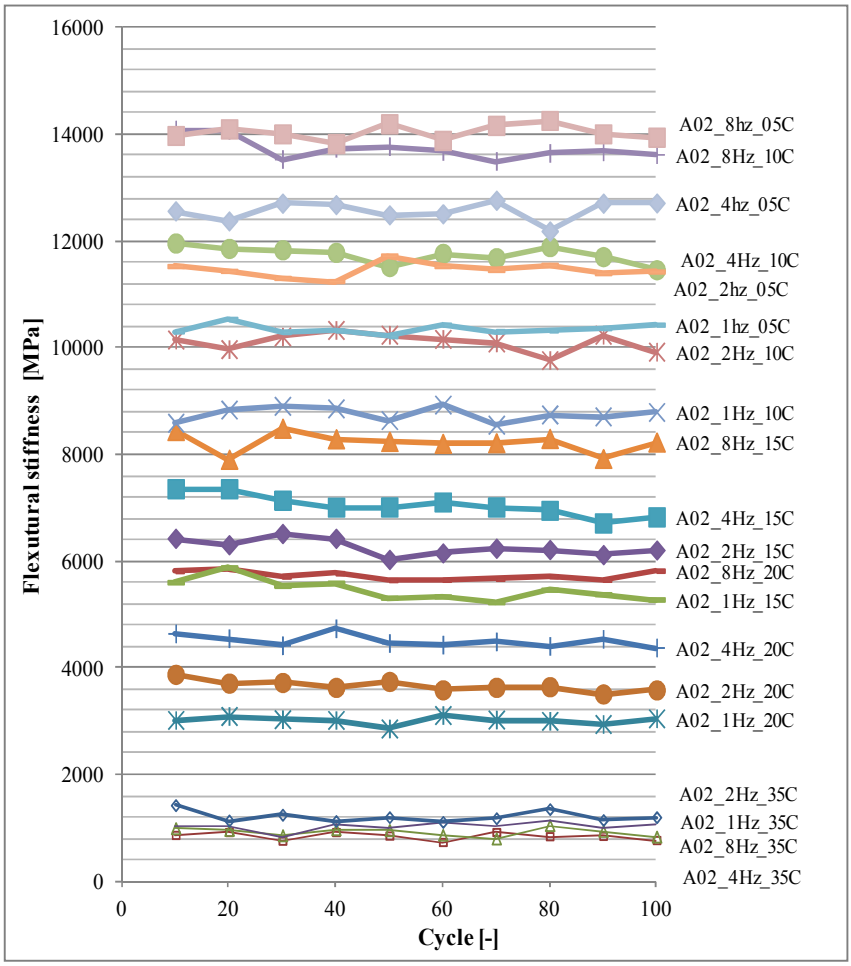

Figure 5.36 Fluctuation of the flexural stiffness values during the first 100 load cycles in a 4PB stiffness test

To get an indication of the uncertainty of taking the 100th cycle stiffness value versus other initial stiffness values, a comparison between the 100th cycle value and the average value of the first 100 stiffness values was made. The difference between the two values is calculated according to equation (5.8) for each sample, temperature and frequency.

$$d_s = [\frac{S_{avg(50,100)} - S_{100}}{S_{100}}] * 100 \qquad (5.8)$$

Where:

d_s = difference between average stiffness value and stiffness after 100th cycle [%]

$S_{avg(50,100)}$ = initial stiffness determined based on average stiffness of cycles of 50th and 100th [MPa]

S_{100} = initial stiffness value at 100th load cycle

For each test condition (specimen, temperature and frequency), d_s was calculated. The distribution of d_s is shown in Figure 5.37 and is based on 960 data (12 specimens from 4 mixture types at 4 temperatures and 4 frequencies were tested). The distribution of d_s is also shown at each loading frequency.

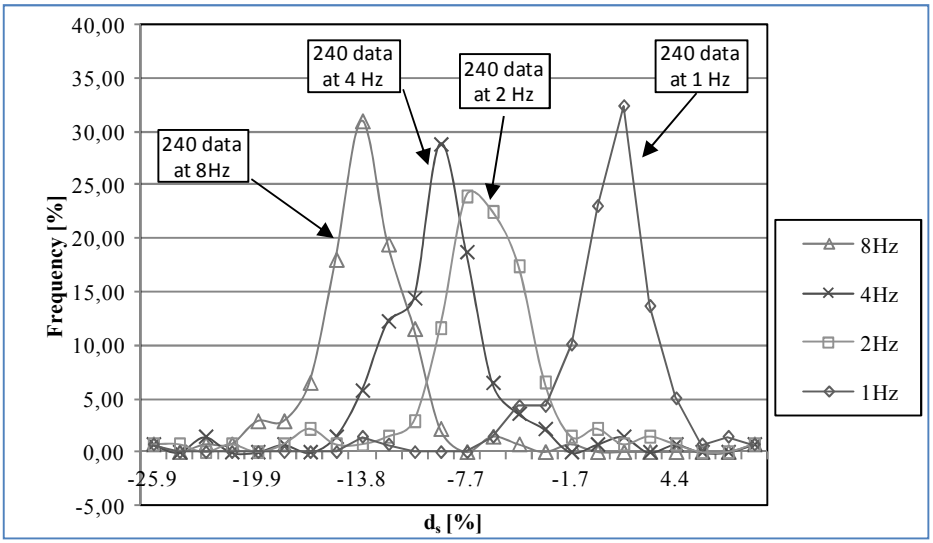

Figure 5.37 Histograms of d_s

Negative values of d_s denote that $S_{avg(50,100)}$ are smaller than S_{100}. The effect of loading frequency on d_s is remarkable. The difference between $S_{avg(50,100)}$ and S_{100} is larger at higher loading frequencies. Thus, one has to be careful in determining the initial stiffness based on S_{100}. It should be noted that the d_s distributions might be influenced by the characteristics of the test setup used.

It is concluded that $S_{avg(50,100)}$ is a more reliable and stable value to be considered as stiffness value in a 4PB test. Therefore the stiffness master

curves constructed in this study are based on this value. The stiffness values of each tested specimen are listed in details in Appendix C.

5.3.1.1. Stiffness master curve construction

Equation (5.7) was used to fit the shifted stiffness values by means of a sigmoidal curve. Frequencies are reduced in accordance with the superposition principle for bituminous materials. The Arrhenius equation (5.9) is used for exchanging temperature with frequencies.

$$S_m = S_h + (S_h - S_l) * e^{-[\frac{f_r}{f_0}]^{\gamma}} \quad (5.9)$$

$$f_r = f.\beta_T \quad (5.10)$$

$$\beta_T = e^{\frac{\Delta H}{R}[\frac{1}{T} - \frac{1}{T_r}]} \quad (5.11)$$

Where:

S = mixture stiffness [MPa]

S_h = high stiffness value when $f \rightarrow \infty$

$S_{l=0}$ = low stiffness value when $f \rightarrow 0$

f_r = reduced frequency [Hz]

f = loading frequency obtained from test at different temperatures [Hz]

f_0 = an initial frequency value [Hz]

β_T = shift factor [-]

ΔH = activation energy [J/mol]

R = ideal gas Constant [8.314 J/mol.K]

T = considered temperature in Kelvin [K]

T_r = reference temperature in Kelvin [K]

γ = model parameter [-]

Given the fact that 12 beams were tested per each mix type, each point in the master curve represents an average of test data obtained on 12 beams. Figure 5.38 shows an example of the master curves of each of the 12 beams as well as the average master curve for mixture A.

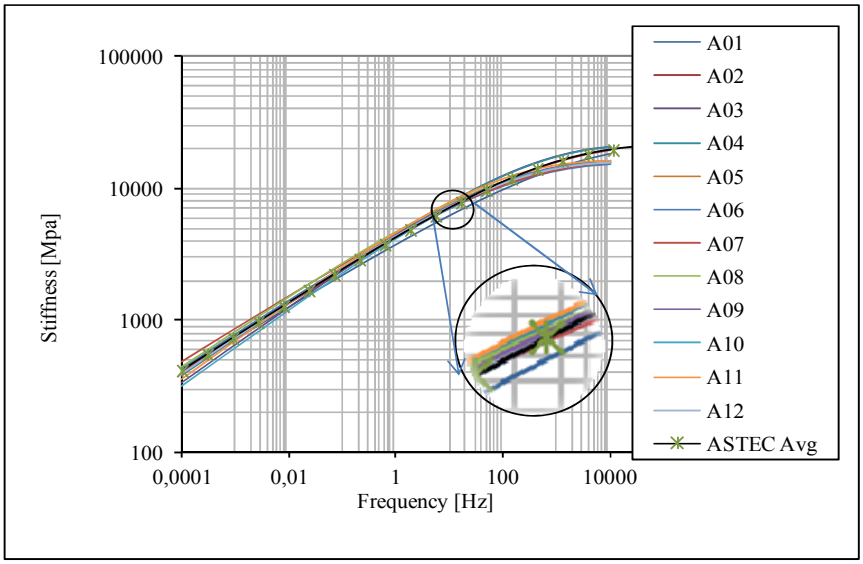

Figure 5.38. Master curve at 20°C of each of the 12 tested beams of mixture A and the average master curve.

The average stiffness master curves of all four mixture types are plotted in Figure 5.39. The model parameters are determined by solving the equations in the "MS office solver option". They are listed in Table 5.5 for each mixture type. Another comparison (Figure 5.40) is made to clearly show the difference between the average stiffness values of each mix type at 20°C and a frequency of 8Hz.

Table 5.5.Stiffness master curve model parameters of mixtures in 4PB test

Mixture	Δh	f_0	Γ	S_h
A	280	726	0.26	19960
B	305	37.9	0.29	16352
BB	278	126.3	0.29	16347
L	264	44.5	0.31	16350

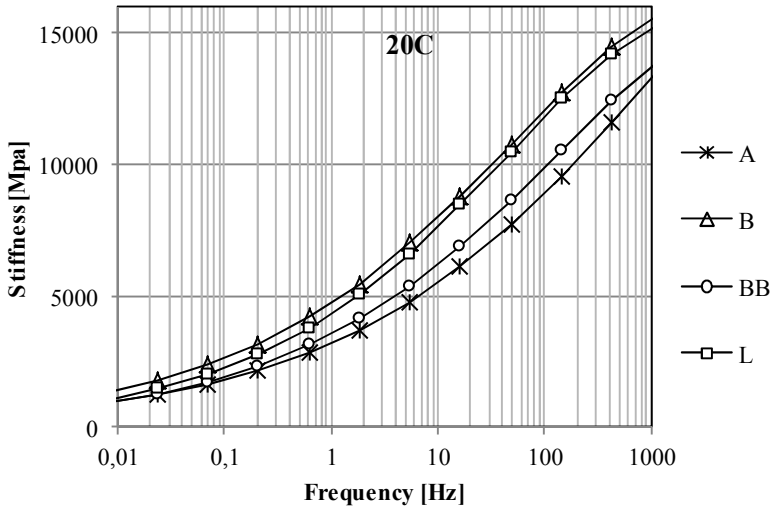

Figure 5.39. Stiffness master curves at 20°C.

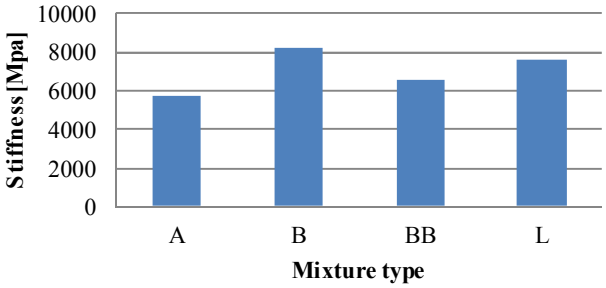

Figure 5.40 Comparison of average stiffness values at 20°C and 8Hz

When comparing the stiffness values of mixtures A, BB and L, it seems that mixture L (laboratory mixture) has a higher stiffness than A and BB over the whole testing range. Mixture BB is slightly stiffer than A, although this difference is not significant compared to L. Given the fact that A, BB, and L contain similar materials (binder, RA and aggregates) and volumetric properties, the short term aging of RA binder and virgin bitumen in mixture L may be the principal cause of the observed difference. The significant different stiffness of the L mixture indicates extra aging because of a too long RA preheating time in the oven at 170°C.

RA was preheated for 3hrs prior to mixing the L mixture. Then this preheated RA was mixed with virgin aggregates. After 1 minute of mixing, the virgin bitumen and fillers were added to the mix. Laboratory mixtures were prepared in separate batches of 30 kg. They were stored, afterwards, in the oven as loose mix (at 170°C) for a period of 1.5 hours prior to compaction.

The RA in the batch plant mixtures is preheated in a much shorter period (30 seconds) in a parallel drum dryer to 130°C, and it also takes less than one minute to be transferred to the batch pugmil mixer. Thus the total preheating time is less than 2 minutes. Immediately after mixing samples were stored in the laboratory oven for compaction. Since 8 blocks were supposed to be compacted, the storage time of the samples varied between 30 minutes and 5 hours, because every 45 minutes only one block could be compacted.

Mixture "A" which was mixed in the double drum mixer has the lowest stiffness, most probably because cold and moist RA at ambient temperature were fed in the double drum system without any preheating period. As was mentioned before, mixing of RA and virgin material takes place within less than 40 seconds. Immediately after production in the double drum mixer, the required mixture was brought to the lab for compaction. The storage time varied for the different blocks between 30 min and 5 hours in the oven (at 170°C).

Next to aging issues, blending might be a potential cause for the difference in stiffness values. A better blending between RA binder and virgin bitumen may result in a mixture with a higher stiffness. The RA binder in mixture L, is sufficiently preheated to a certain temperature (170°C) prior to mixing. Once it is brought in the mixer with the virgin aggregates and virgin bitumen which are preheated to the same temperature, a better mixing of the materials might be expected. In addition, the mixing time of three minutes that was used to prepare the L mixtures certainly has contributed to the blending process.

However, it is likely that mixing and diffusion between the RA and virgin bitumen may also occur during storage time and mixture handling prior to compaction. Therefore it is difficult to allegedly confirm the better blending and mixing of the laboratory mixture in comparison with the batch plant and double drum mixtures.

A comparison between mixture "B" and "BB" clearly indicates the effect of RA properties on the stiffness. Mixture B contains 25% reclaimed porous asphalt (RPAP) besides 25% normal RA while mixture BB contains 50% normal RA. The binder combination in B is significantly stiffer than the binder in BB because of the extremely hard binder of the reclaimed porous asphalt used in B. It can be argued that, in-plant mixing processes such as the batch plant are capable of providing sufficient blending between all recycled

materials. However it is still not clear to what extends blending is really occurring given the short mixing times used in the batch plant.

5.3.2. 4PB fatigue life

The resistance to fatigue is measured using displacement controlled four-point bending (4PB) tests. According to "RAW[16] (2005)" and "NEN-EN 13108-20: Bituminous mixtures- Type test", fatigue tests in the 4PB setup have to be done at a frequency of 30Hz and a temperature of 20°C. The current 4PB setup was not capable of applying loading frequencies above 8Hz. Since one of the goals of this research was to compare the material properties based on type test requirements specified in NEN-EN 13108-20 and RAW 2008 and given the fact that the maximum frequency at which the tests could be performed was 8Hz instead of 30Hz, the testing temperature of 20°C was changed in order to achieve similar initial stiffness values in the fatigue test. The equivalent temperature to be used when testing at 8 Hz was determined based on the time-temperature superposition principle for bituminous mixtures. The procedure of determining the equivalent temperature at 8 Hz for mixture A is illustrated in Figure 5.41. It indicates that at 30Hz and 20°C the stiffness is equal to the stiffness at 8Hz and 16.9°C. This equality of stiffness is also shown in Figure 5.42 till Figure 5.44 for other mixtures (B, BB and L). Therefore all fatigue tests were performed at a temperature of 16.9 ^{0}C and a frequency of 8 Hz.

[16] RAW Standard Conditions of Contract for Works of Civil Engineering Construction 2005.

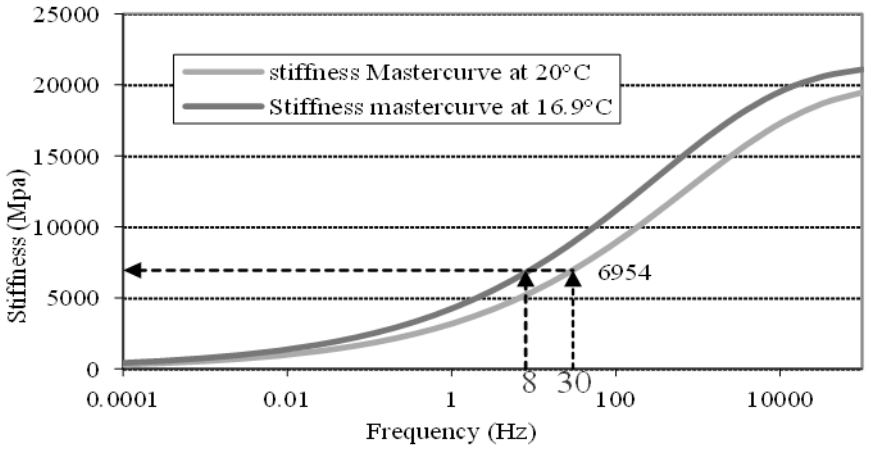

Figure 5.41 Temperature determination for fatigue tests at 8 Hz instead of at 30 Hz and 20 °C, based on initial stiffness (mixture A)

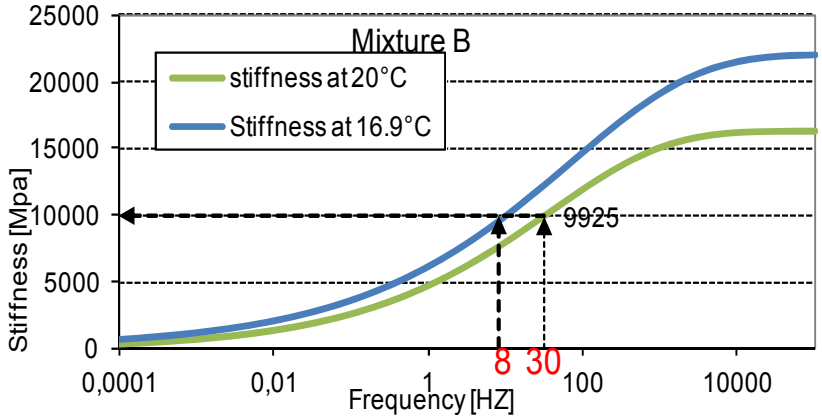

Figure 5.42 Temperature determination for fatigue tests at 8 Hz instead of 30 Hz and 20 °C , based on initial stiffness(mixture B)

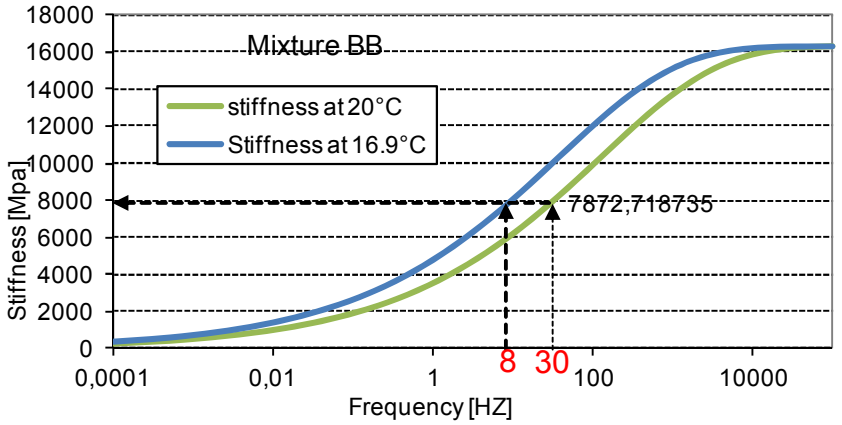

Figure 5.43 Temperature determination for fatigue tests at 8 Hz instead of 30 Hz and 20 °C (mixture BB)

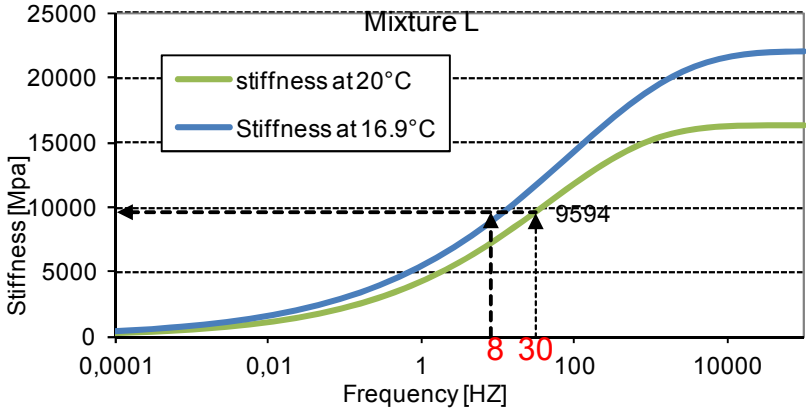

Figure 5.44 Temperature determination for fatigue tests at 8 Hz instead of 30 Hz and 20 °C (mixture L)

The number of load cycles to reach a specimen stiffness of half the initial stiffness was considered to be the fatigue life (N_f). This is in line with NEN-EN 12697-24. Other parameters such as the deflection and the phase lag between the load and displacement signal were also measured as a function of time. The initial stiffness is determined automatically by the embedded software at the 100th cycle.

The following figures are illustrating the change of the stiffness versus the number of load cycles for each mixture type. Strain (deflection) levels between 80-300 µm/m were used.

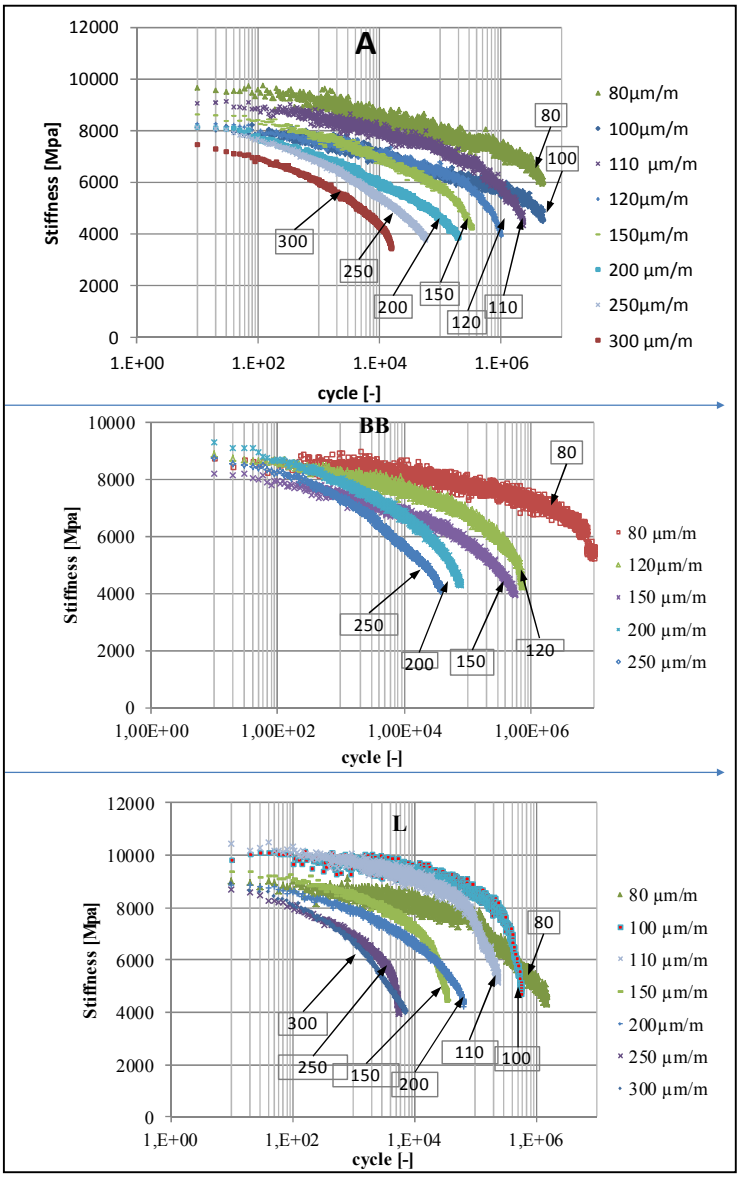

Figure 5.45 Fatigue test results of mixtures A, BB and L from top to bottom (at 16.9°C and 8Hz)

5.3.2.1. Fatigue equation

Fatigue equations relating N_f to the maximum tensile strain (at the bottom of the beam) were developed using the Wohler relation equation (5.12).

$$N_f = k\,(\frac{1}{\varepsilon})^n \qquad (5.12)$$

Where:

N_f = number of load or displacement applications to failure

ε = strain at the bottom of the AC layer [m/m]

k, n = mixture parameters depending on stiffness modulus, volumetric properties and loading type

Linear regressions between *log* N_f and *log* ε for all mixtures (A, BB and L) are made and the results are shown in *Figure 5.46*.

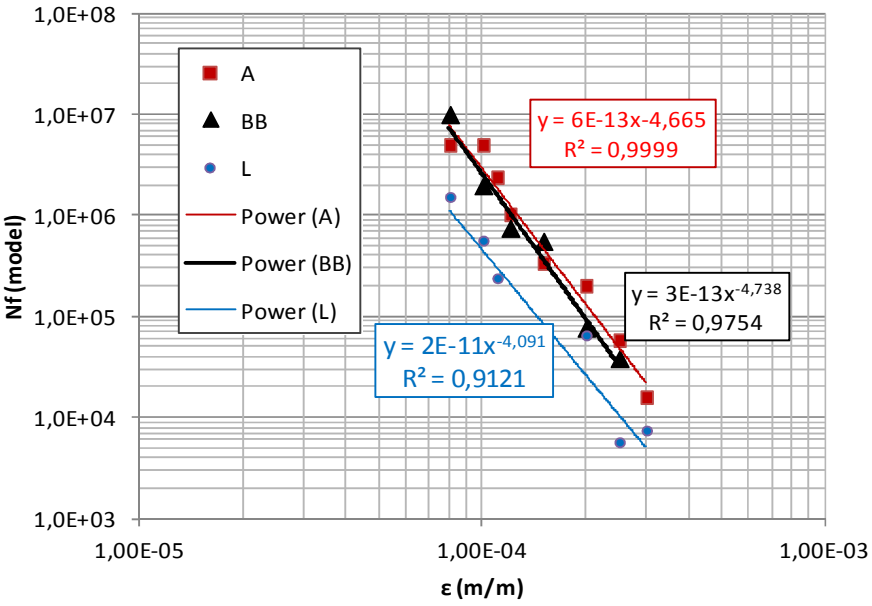

Figure 5.46. Fatigue lines at log-log scale (obtained from experiment) of mixtures A (Astec), BB (batch plant) and L (lab)

Different regression models have been developed to determine the Wohler parameters for displacement or force controlled fatigue tests. They primarily use stiffness and volumetric properties of the mixtures. They were developed

by SPDM [56], Bonnaure [57], Francken and Medani-Molenaar [58], Asphalt Institute, etc. The model developed by Medani-Molenaar [58] is used here to compare the fatigue life estimated with the results obtained from the 4PB fatigue test. This model is used here because it is suitable for predicting strain controlled 4PB fatigue life. In this model, the Wohler parameters are determined based on volumetric properties of the mixtures and the slope of the stiffness curve while the x axis reflects time instead of frequency.

$$logk = 6.589 - 3.762n + \frac{3209}{S_m} + 2.332 * \log V_b + 0.149\,\frac{V_b}{V_a} + 0.928\,PI - 0.0721\,T_{R\&B} \quad (5.13)$$

$$n = \frac{n_{mas}}{CF} \quad (5.14)$$

$$n_{mas} = \frac{2}{m} \quad (5.15)$$

$$m = \frac{d(\log S_m)}{d(\log t)} \quad (5.16)$$

$$CF = 0.541 + 0.173 n_{mas} - 0.03524 V_a \quad (5.17)$$

Where:

V_b = volume percentage of bitumen

V_a = volume percentage of voids

$T_{R\&B}$ = ring and ball temperature (°C) of bitumen

PI = penetration index

S_m = mixture stiffness (MPa)

CF = correction factor

Firstly, the stiffness master curve (at 16.9°C as fatigue temperature) is plotted as log mixture stiffness - log loading time. Then, the tangential slope "m" of each curve is determined at t=0.125s (8Hz) which corresponds to the frequency of the 4PB flexural bending fatigue tests (see Figure 5.47).

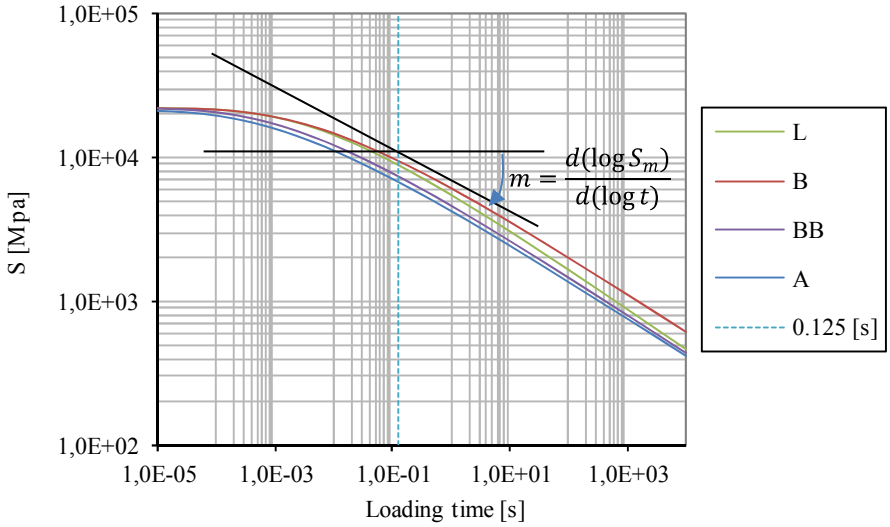

Figure 5.47 Determination of the log-log slope of the time-stiffness master curve at 0.125s (8Hz)

Predicted Wohler fatigue lines determined with the Medani/Molenaar equation are presented in Table 5.6 for every mixture together with computational details. They are compared with the experimentally determined fatigue lines. The Wohler parameters are also presented and compared in Table 5.7. The Medani/Molenaar model parameters are also calculated for each sample separately according to their unique stiffness values and volumetric properties. The predicted fatigue life of each specimen using the model is compared to the fatigue life obtained from the experiment. They are shown in Figure 5.48. It shows that this model has an acceptable precision to predict the 4PB fatigue life at the test conditions in this research.

Table 5.6 Computation details of the Medani/Molenaar prediction model

Mix Design	***S(Mpa) T=16,9°C; f=8Hz***	***at m [-]***	***Pen [dmm]***	***Tr&b [°C]***	***P.I [-]***	***Va [%]***	***Vb [%]***	***n(mas)= 2/m***	***C.F***	***n***	***log k***
A	6770	0,21	35	54,1	-1	4,2	14,6	9,39	2,02	4,65	-12,03
BB	7403	0,21	35	54,1	-1	3,3	13,8	9,39	2,05	4,58	-11,76
L	8863	0,21	35	54,1	-1	2,9	13,5	9,43	2,07	4,56	-11,68

Table 5.7 Wohler parameters obtained from experiments in comparison with those obtained with the Molenaar/Medani prediction model

Mixture type	***Experiment***			***Model (Medani/Molenaar)***		
	k	*log k*	*n*	*k*	*log k*	*n*
A	6,0E-13	-12,22	4.665	9,1E-13	-12,03	4.65
BB	3,0E-13	-12,52	4.738	1,7E-12	-11,76	4.58
L	2,0E-11	-10,70	4.091	2,1E-12	-11,68	4.56

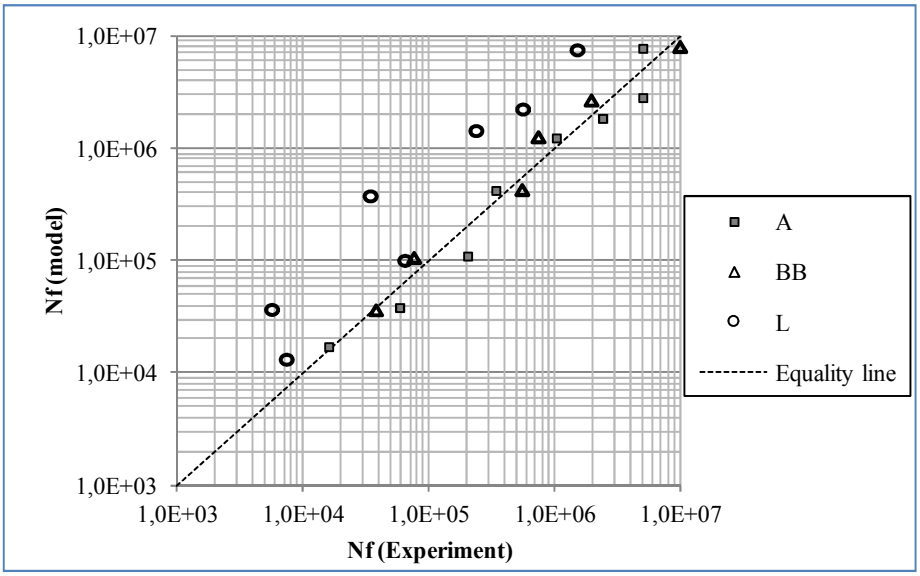

Figure 5.48 Verification of Medani/Molenaar model with real results

5.3.3. Conclusions of fatigue life results

When comparing the fatigue lines of the three mixtures, the following conclusions can be drawn:

- The 4PB fatigue life in the strain controlled mode is significantly influenced by the initial stiffness of the mixture.
- Mixture L has lower resistance to strain control fatigue life due to its higher stiffness.
- Mixture BB and A have almost the same resistance to 4PB fatigue. However, the fatigue resistance of A was slightly higher. This is because this mixture has a little lower stiffness compared to BB.
- All fatigue lines had the almost the same slope.

5.3.4. Uniaxial monotonic direct compression Test (UMDC)

Cylindrical specimens were used in the uniaxial monotonic compression tests. The specimen fabrication procedure is explained in detail in chapter 3. Specimens were prepared with a diameter of 65mm and a height of 138 mm.

The specimens were produced by taking horizontal cores (perpendicular to the compaction direction) from the blocks that were compacted by means of the Shear PressBox. After coring and trimming, both sides of the cylinders were polished to minimize any surface roughness and making them parallel. Prior to testing, the specimen properties (dimensions, density and air voids) were precisely measured by means of the methods described in chapter 2 on methodology description and in chapter 3 on sample preparation.

5.3.4.1. Instrumentation

Similar sets of test conditions were applied to all mixture types. In order to cover all loading and temperature conditions, a factorial experimental design was used to determine the strain rate and temperature conditions. Three temperatures of 1°C, 17°C and 33°C and a range of strain rates of 0.01, 0.1, 1 and 5[%/s] were chosen. Strain rates are expressed in [%/s] representing the ratio of axial deflection of the cylinders to their initial heights. Given the fact that the height of a sample is 130 mm, a strain rate of 0.1%/s means that the loading speed has to be set in such a way that the displacement rate is 0.13 mm/s. The equipment was controlled by an electronic system controller. Displacements were measured by three long range LVDTs (10mm) for large deformations and three short range (1mm) LVDTs for initial deformations. The system controller was adjusting the load according to the feedbacks of the LVDTs to achieve the desired displacement speed. This showed to be an issue at higher strain rates which are associated with higher applied loads. It implied that the system controller had to increase and decrease the applied load to achieve a specific displacement rate in a very short period of time; this showed to be problematic in some cases. Therefore it is very important to

have a slight preloading on the specimen to avoid initial fluctuation in strain rate signals. Strain rate signals for each set of test were therefore plotted to determine if extra displacement beyond the intended strain rates occurred.

Radial deformations were also measured. For the short range displacements this was done by means of extensometers while two extra potentiometers and a string were used to measure the larger radial deformations when the extensometer was out of range. Figure 5.49 shows the axial and radial measurements during the compression test. This figure is showing a failed specimen after the test is conducted. The extensometer had gone out of its range and dropped down. Initially the extensometer and the string (which is attached to lateral potentiometers) are installed at mid height of the cylinder.

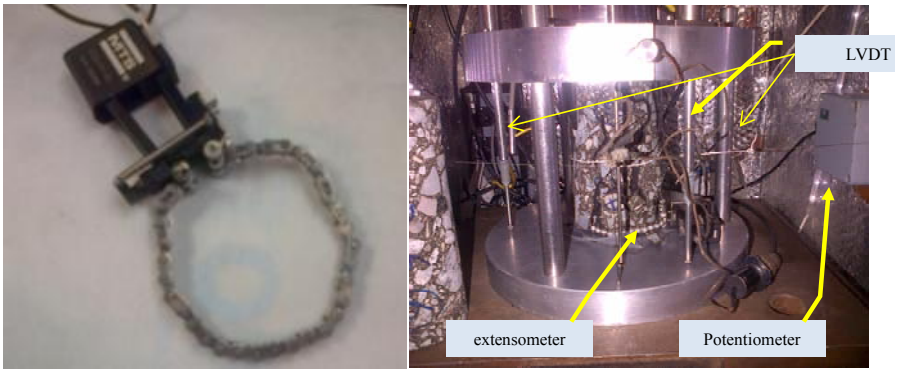

Figure 5.49 Axial and radial measurement setup in the compression test (left: extensometer chain, right: setup

In order to get a sufficient amount of data allowing analysis of the results, the data acquisition frequency was determined with respect to the applied strain rates. The data collected by means of the acquisition system were saved in a text file. The following equations were used for analyzing the data.

$$\sigma = \frac{f}{A_0} \qquad (5.18)$$

$$\varepsilon_a = \frac{\Delta h}{h_0} \qquad (5.19)$$

$$\varepsilon_r = \frac{\Delta r}{r_0} \qquad (5.20)$$

$$\varepsilon_v = 2\varepsilon_r + \varepsilon_a \qquad (5.21)$$

Where:

σ = Vertical stress

$\varepsilon_a, \varepsilon_r, \varepsilon_v$ = Axial, radial and volumetric strains

h_0, r_0 = Initial height and diameter of the specimen

$\Delta h, \Delta r$ = Vertical and radial deformation

f = Applied load

A_0 = Initial cross section area

According to the MTS extensometer manual, the radial deformation (Δr) is measured based on following equations:

$$\Delta r = \frac{l - l_i}{2\left[\sin\left(\frac{\theta_i}{2}\right) + \left(\frac{2\pi - \theta_i}{2}\right)\cos\left(\frac{\theta_i}{2}\right)\right]} \qquad (5.22)$$

$$\theta_i = 2\pi - \frac{l_c}{(r_o + r_r)} \qquad (5.23)$$

Figure 5.50 shows the details of the extensometer used in tension and compression tests.

The radial deformation was also measured through the potentiometers. Erkens [47] has suggested equation 5.19 for analyzing the radial deformation measured by means of potentiometers. Details of the potentiometer measurements are illustrated in Figure 5.51

$$\Delta r = \frac{P - \sqrt{(L_i^1)^2 + (\frac{\Delta h}{2})^2 + \Delta r^2} + L_i^1 - \sqrt{(L_i^2)^2 + (\frac{\Delta h}{2})^2 + \Delta r^2} + L_i^1}{2\pi} \qquad (5.24)$$

Where P is the change in the length of the string which is measured by two potentiometers.

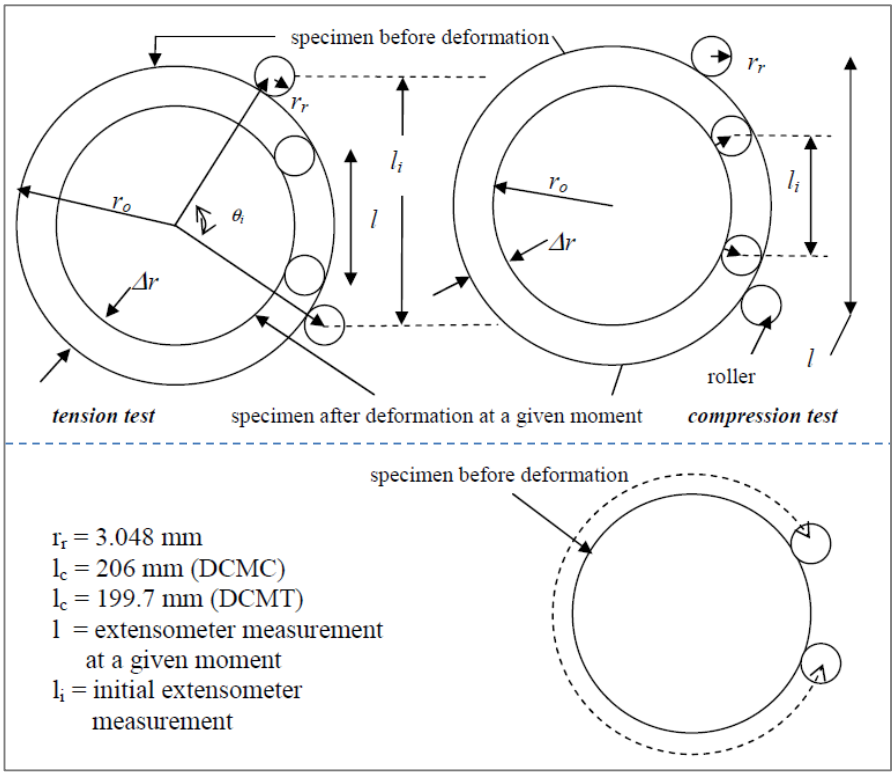

Figure 5.50 Details of radial measurements by means of an extensometer [59]. Top-left: tension test. Top-right:compression test

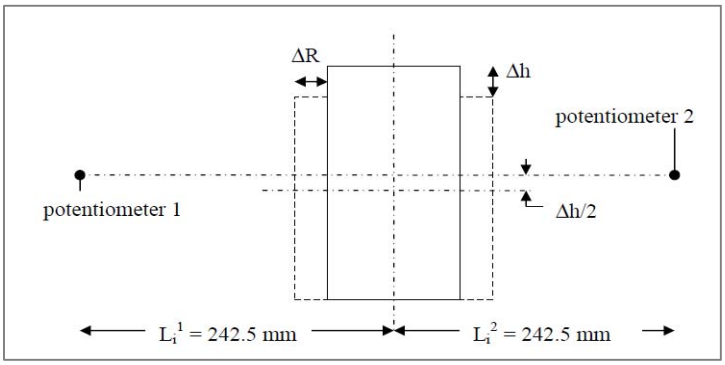

Figure 5.51 Determination of radial deformation in the compression test using two potentiometers [47].

To avoid friction between sample and steel plates in the compression test, a special plastic foil which is covered with grease is employed on both sides of the cylinder. This friction reduction system is used to improve the uniformity in the stress distribution of the sample.

5.3.4.2. Factorial design

Test conditions per mix type were planned based on a factorial design . The varying factors are; temperature and strain rate. The factorial design is shown in Figure 5.52.

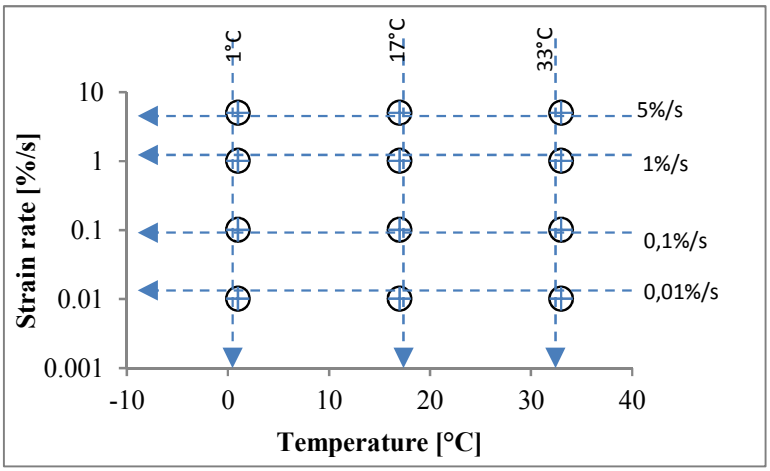

Figure 5.52 Factorial design for the compression tests

5.3.4.3. Temperature control

A temperature cabinet was installed around the compression setup to maintain the temperature of the specimen during the test at the desired level. Every specimen has to remain in the cabinet (after installation of the extensometer, radial string, and LVDTs) for at least one hour prior to loading for stabilizing the temperature at the intended level. The temperature is controlled by blowing either cold or warm air through long pipes. Therefore the temperature was fluctuating during storage time. Nonetheless, the intended temperature was maintained by adjusting the average value. Figure 5.53 is demonstrating the quality of temperature control in the compression setup cabinet at the intended temperatures. It shows that the accuracy of the temperature control in the compression cabinet reduced at low testing target temperatures compared to high testing target temperatures. This has to be taken into account when conducting compression tests at low temperatures in this setup.

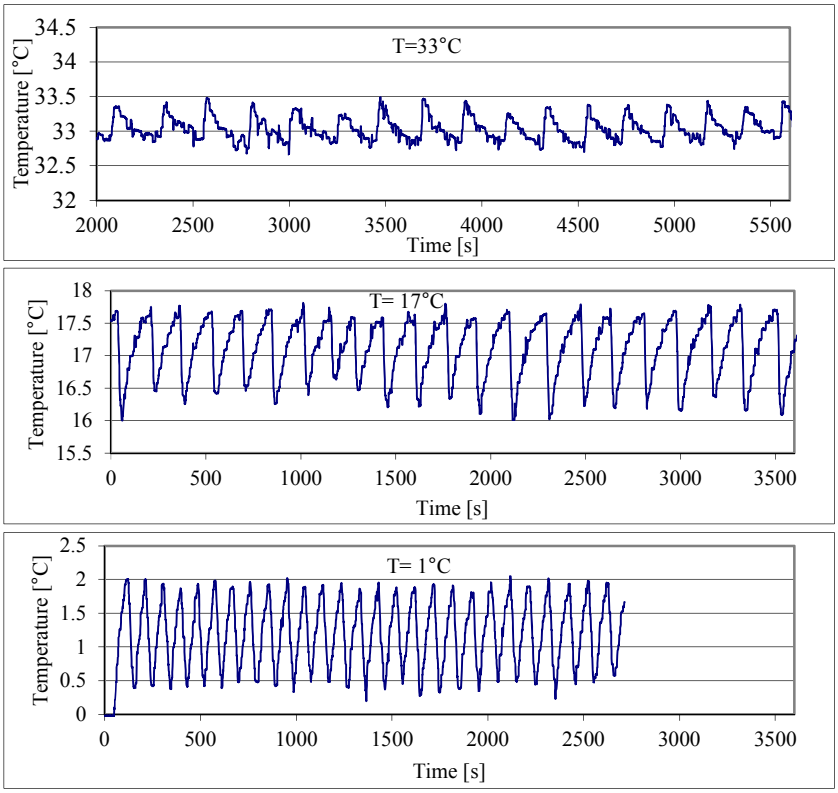

Figure 5.53 Temperature control in the compression cabinet at target testing temperatures of 1, 17, 33°C

5.3.4.4. Strain rate control

The other experimental factor is the strain rate which had to remain constant during the loading time. However, strain rates may fluctuate at different stages of loading. This fluctuation is high in the early stages of loading. The system controller attempts to adjust the displacement rate by increasing and decreasing the applied load continuously according to the system feedback. Examples of strain rate fluctuation due to temperature and initial intended strain rate are shown in Figure 5.54. Four charts are presented in this figure. Each chart shows the effect of temperature on the strain rate signals. The target strain rate is mentioned on top of the chart legends. The conclusion is that strain rate control becomes more difficult at higher displacement rates and at lower temperatures, because the equipment has to apply and regulate higher loads in shorter periods of time.

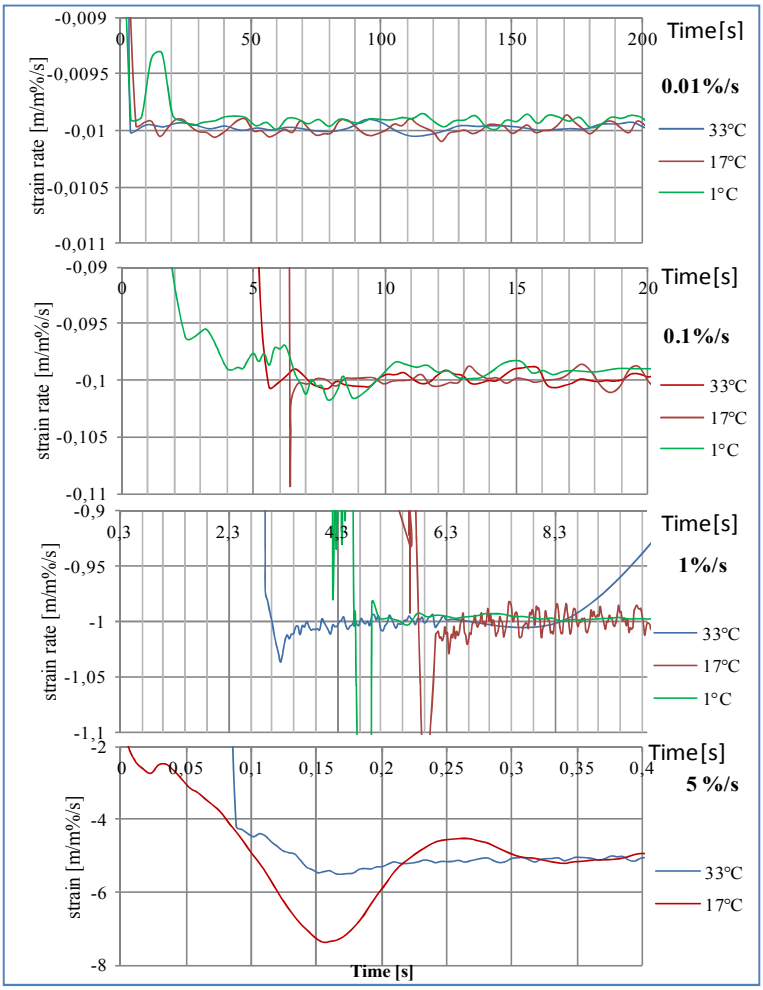

Figure 5.54 The effect of intended test conditions (temperature and strain rate) on strain rate control during compression tests

5.3.4.5. Analysis of the compression test results

Examples of the charts that have been made using the test results are given in the following figures. In the compression test, the axial stress and strain are shown with negative values (compression) while the radial strain is shown with positive values (extension)

The vertical compressive stress is determined by dividing the applied force by the area of the middle cross section (eq. 5.18).

Figure 5.55 is showing an example of a stress versus time plot as well as the fluctuation of the strain rate corresponding to the stress condition in the sample. The strain rate curve is obtained by taking the first derivative of the strain-time curve [see eq.(5.25)]. The average value of this curve represents the actual strain rate. Stress-strain curves are plotted in Figure 5.56 in which the negative x axis direction represents the axial strain (ε_a) and positive values represent radial strains (ε_r). The two ε_a curves in this chart, represent data obtained from low range and high range LVDTs and the two curves of ε_r are showing results from the extensometers (for low ranges) and potentiometer strings (for higher ranges).

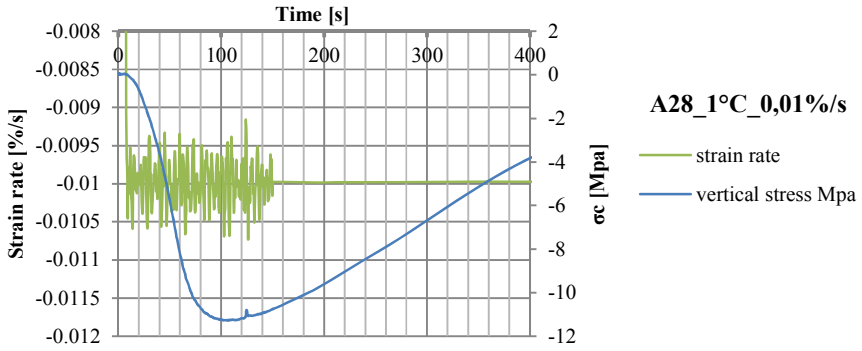

Figure 5.55 Vertical compressive stress and strain rate vs. time signal (sample A28 from mix type A at 1°C and 0.01%/s)

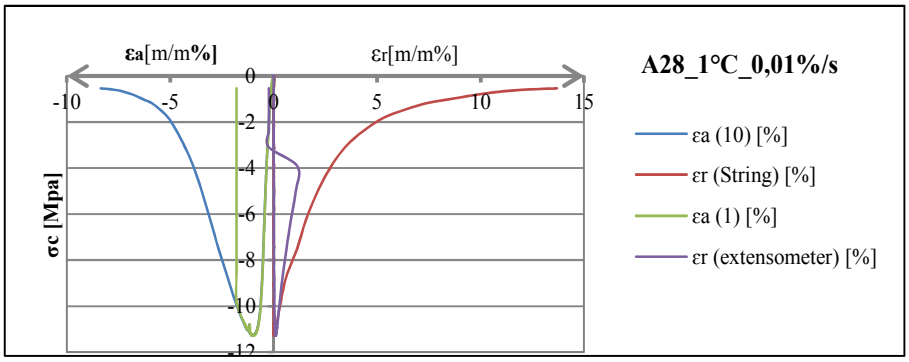

Figure 5.56 A*xial and radial strain (sample A28t from mix type A at 1°C and 0.01%/s).*

The tangential modulus was determined by taking the first derivative of the stress-strain curve [eq.(5.25)]. An example of the tangential modulus curve is shown in Figure 5.57. The peak value of this curve is considered as E_{tan}.

$$\varepsilon\cdot(t) = \frac{d\varepsilon(t)}{\partial t} \qquad (5.25)$$

$$E_{tan} = \frac{d\,(\sigma)}{d(\varepsilon)} \qquad (5.26)$$

Where:

$\varepsilon\cdot(t)$ = Strain rate as a function of time

E_{tan} = Tangential modulus (slope of stress strain curve)

An example of a failed compression test specimen (A36 at 1°C and a strain rate of 0.01%/s) is shown in Figure 5.58. Some clean aggregate surfaces were observed in the failed samples. They were mostly the surfaces of round gravel stones from RA aggregates, showing weak adhesion with the bitumen.

The type of failure during uniaxial compression at different temperatures and strain rates is different. At a high temperature (33°C) which is above the laboratory temperature, specimens often tend to fail from the top side at which the actuator is connected.

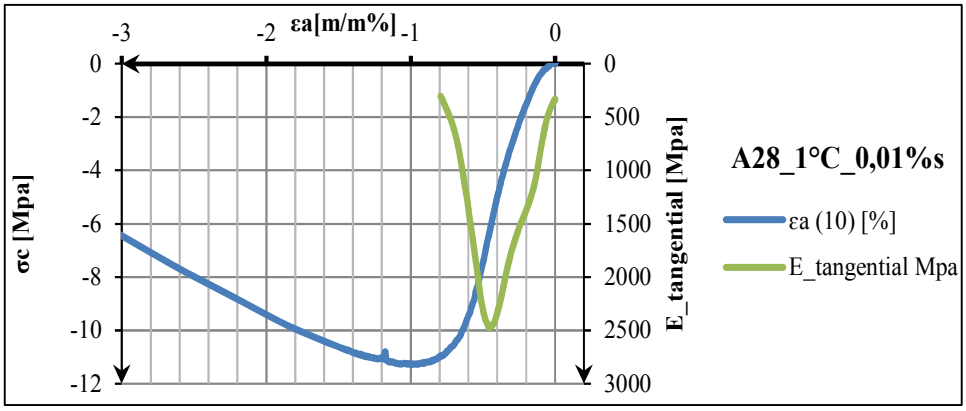

Figure 5.57 Evolution of the tangential modulus during a compression test



Figure 5.58 Example of a failed compression test specimen (A36 at 1°C and a strain rate of 0.01%/s)

5.3.4.6. The effect of test conditions on compression

Some examples of the compression test results are shown in the following figures. The effect of the strain rate on the stress-strain curves obtained at 17°C is illustrated in Figure 5.59 .The figure shows that the peak stress at failure increases with increasing strain rates. Figure 5.60 shows the effect of temperature; at lower temperatures a higher compressive strength (f_c) is obtained.

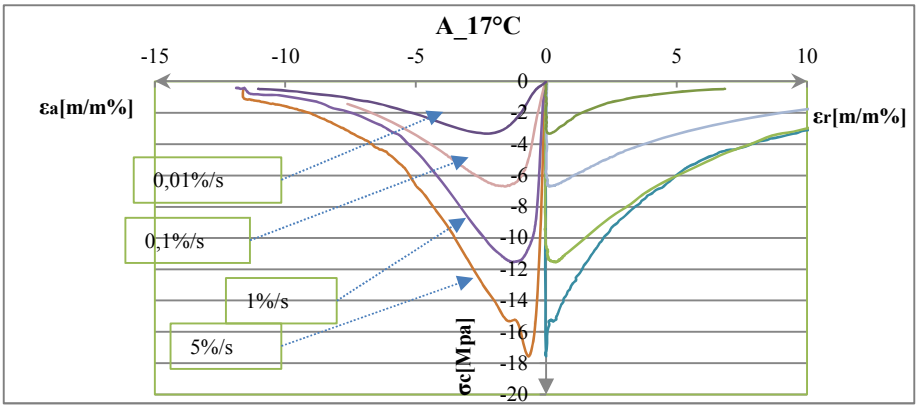

Figure 5.59 Compressive stress-strain curves for mix type A at 17°C and different strain rates

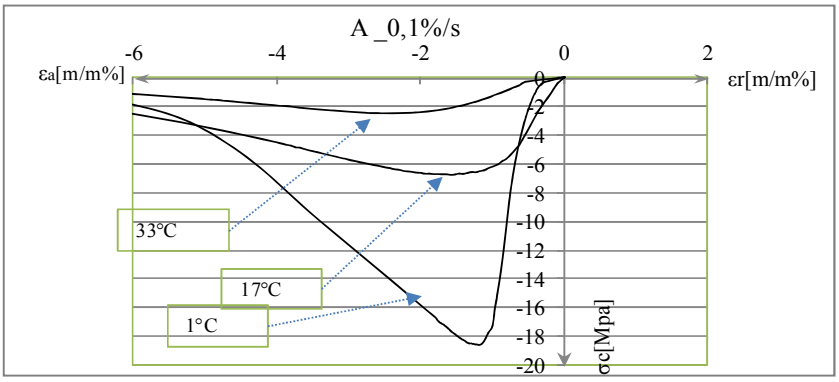

Figure 5.60 Effect of temperature on compressive stress-strain curve for mix type A at a constant strain rate of 0.1%/s

5.3.4.7. Overview of compression test results

An overview of the test results per mixture type is given in Tables 5.9 to 5.12. In these tables; "f_c" represent peak stress or compressive strength, "$\varepsilon_{a,max}$" stands for axial strain at peak stress, "$\varepsilon_{r,max}$" indicates radial strain at peak stress and "E_{tan}" stands for tangential modulus.

Table 5.8 Compression test results of mixture A

Code	*Temperature [°C]*	*Target strain rate [m/m%/s]*	*Actual strain rate [m/m%/s]*	f_c *[MPa]*	E_{tan} *[Mpa]*	$\varepsilon_{a,max}$ *[m/m%]*	$\varepsilon_{r,max}$ *[m/m%]*
A28	1°C	0.01	0.0100	11.27	1132	0.995	0.090
A21	1°C	0.10	0.1002	18.60	3890	1.180	0.062
A2	1°C	1	1.2675	29.74	7260	0.805	0.052
A19	17°C	0.01	0.0100	3.33	297	2.360	-
A21	17°C	0.10	0.0998	6.72	889	1.586	0.252
A12	17°C	1	1.0113	11.54	3060	1.289	0.217
A25	17°C	5	6.7889	17.55	7875	0.656	0.082
A24	33°C	0.01	0.0100	1.50	118	2.201	0.401
A23	33°C	0.10	0.0998	2.42	216	2.382	0.367
A11	33°C	1	1.0035	4.27	705	1.972	0.420
A20	33°C	5	5.1768	6.55	1354	1.804	0.237

Table 5.9 Compression test results of mixture B

Code	*Temperature [°C]*	*Target strain rate [m/m%/s]*	*Actual strain rate [m/m%/s]*	f_c *[MPa]*	E_{tan} *[MPa]*	$\varepsilon_{a,max}$ *[m/m%]*	$\varepsilon_{r,max}$ *[m/m%]*
B30	1°C	0.01	0.0098	12.13	2139	1.249	-
B23	1°C	0.10	0.0979	21.53	6013	0.888	-
B27	1°C	1	1.0809	30.21	7407	0.854	-
B25	17°C_	0.01	0.0100	3.99	551	1.971	-
B17	17°C	0.10	0.0922	8.51	1601	1.247	-
B15	17°C	1	0.9255	14.93	5126	0.794	-
B16	17°C	5	5.7279	24.35	5606	0.800	-
B28	33°C	0.01	0.0099	1.15	111	1.914	-
B26	33°C	0.10	0.0990	2.42	243	1.836	-
B29	33°C	1	0.9971	4.60	664	2.235	-
B21	33°C	5	5.0587	7.19	827	1.728	-

Table 5.10 Compression test results of mixture BB

Code	*Temperature [°C]*	*Target strain rate [m/m%/s]*	*Actual strain rate [m/m%/s]*	f_c *[MPa]*	E_{tan} *[MPa]*	$\varepsilon_{a,max}$ *[m/m%]*	$\varepsilon_{r,max}$ *[m/m%]*
BB24	1°C	0.01	0.0100	11.65	3426	0.830	0.085
BB29	1°C	0.10	0.1001	16.40	2060	1.706	0.086
BB22	1°C	1	1.1308	30.15	7089	0.719	0.047
BB27	17°C	0.01	0.0100	3.36	347	2.114	-
BB30	17°C	0.10	0.0967	6.28	1006	1.663	0.246
BB06	17°C	1	1.0053	11.47	3439	1.127	0.171
BB20	33°C	0.01	0.0098	1.08	88	2.044	0.410
BB28	33°C	0.10	0.0995	1.82	146	2.162	0.416
BB23	33°C	1	1.0025	3.72	471	2.040	0.318
BB12	33°C	5	5.1146	6.23	990	1.799	0.258

Table 5.11 Compression test results of mixture L

Code	*Temperature [°C]*	*Target strain rate [m/m%/s]*	*Actual strain rate [m/m%/s]*	f_c *[MPa]*	E_{tan} *[MPa]*	$\varepsilon_{a,max}$ *[m/m%]*	$\varepsilon_{r,max}$ *[m/m%]*
L29	1°C	0.01	0.0100	11.09	3388	0.826	0.095
L23	1°C	0.10	0.1013	18.30	6941	0.900	0.046
L24	1°C	1	1.0093	27.74	6277	0.855	0.059
L12	17°C	0.01	0.0098	4.03	587	1.738	-
L25	17°C	0.10	0.0974	7.52	1757	1.337	0.267
L14	17°C	1	1.0241	12.42	3614	1.019	0.111
L11	17°C	5	6.9591	16.38	4669	0.715	0.055
L30	33°C	0.01	0.0100	0.94	81	2.442	0.416
L27	33°C	0.10	0.0999	2.00	385	1.332	0.327
L28	33°C	1	1.0037	3.63	465	1.991	0.342
L10	33°C	5	5.3567	7.18	1012	1.436	0.191

5.3.4.8. Effect of mixture types on compressive strength

Since different types of mixtures were used a comparison between the strength values of each mixture at the same test conditions is given in Figure 5.61. In this chart each group of columns indicates f_c in *[MPa]* at different strain rates. In Figure 5.62 a similar comparison is given for E_{tan}.

At almost all temperatures and strain rates the compressive strength of Mixture B seems to be higher than the compressive strength of the other three mixtures. Mixture A, BB and L show almost the same compressive strength. The reason may lie in the composition of the mixtures. It is recalled that mixtures A, BB and L were produced with the same materials, whereas Mixture B included 25% reclaimed porous asphalt (RPA) besides 25% normal RA.

With respect to E_{tan} , mixtures L and B show a higher tangent modulus than mixtures A and BB; this is almost in line with the 4PB stiffness results. The

reasons for the higher stiffness values are more aging in mixture L and an initial stiffer binder in mixture B.

However, it is difficult to maintain these conclusions based on a point to point comparison of data. It is more practical to translate a group of data in a single line or plane by fitting them to a suitable model. It facilitates the comparison of f_c and E_{tan} .

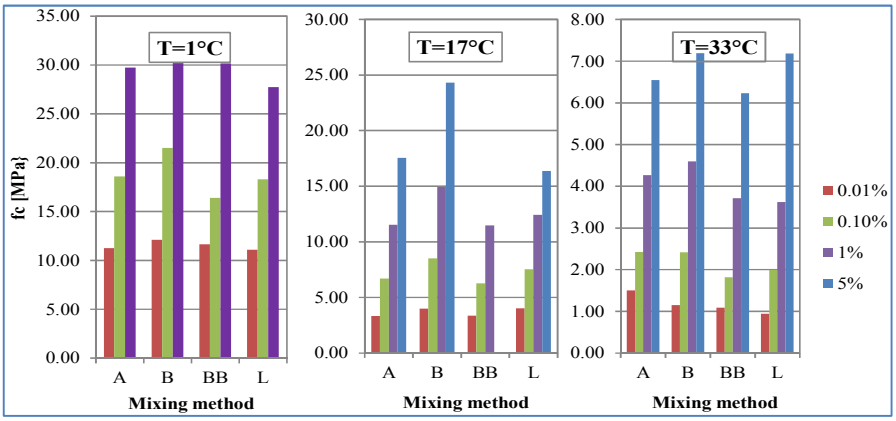

Figure 5.61 Comparison between f_c with respect to temperatures and strain rates

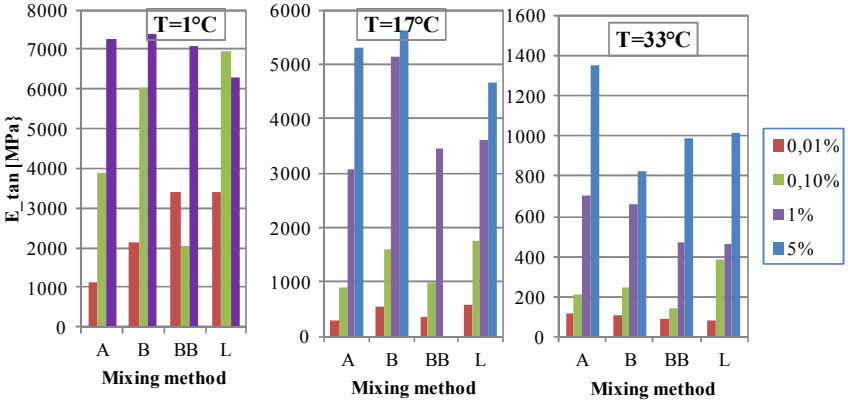

Figure 5.62 Comparison between E_{tan} in compression with respect to temperatures and strain rates

5.3.4.9. Master curves in compression

The compression test results showed that material properties such as f_c and E_{tan} are sensitive to temperature and strain rate. Higher temperatures and lower strain rates result in lower f_c and E_{tan} values, whereas the opposite is valid at lower temperature and higher strain rates. Temperature and loading time are exchangeable in characterizing bituminous material properties. This characterization is already used in creating a generalized line for the 4PB stiffness being the "stiffness master curve". In the literature, different shift factors are used for creating master curves; they are listed below. Equation (5.27) and (5.28) are known as the Arrhenius and WLF[17] equation. The effect of using either of these equations has been compared in Figure 5.63. In the legend of this chart, EXP corresponds with equation (5.29). Shifted values relating to all of these equations seem to be in good agreement which make them equally suitable for application in our model.

$$\beta_T = e^{\frac{\Delta H}{R}\left[\frac{1}{T}-\frac{1}{T_r}\right]} \qquad (5.27)$$

$$\beta_T = e^{\frac{-C_1(T-T_r)}{C_2+(T-T_r)}} \qquad (5.28)$$

$$\beta_T = e^{-T_s(T-Tr)} \qquad (5.29)$$

Where:

β_t = shift factor [-]

ΔH = activation energy [J/mol]

R = ideal gas Constant [8.314 J/mol.K]

T_r = Reference temperature

17 Williams-Landel-Ferry

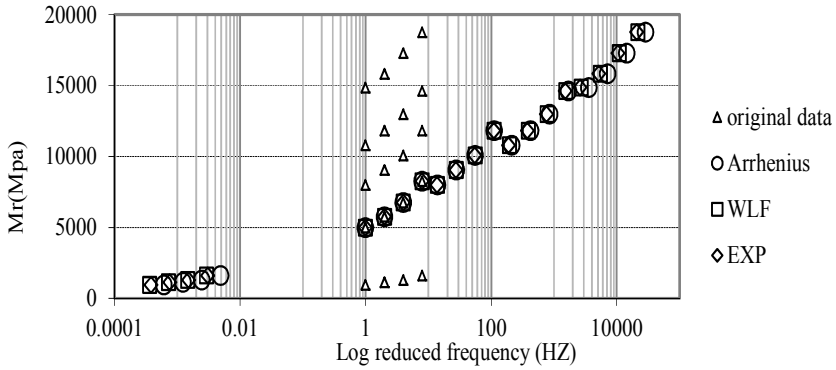

Figure 5.63 Comparison between models used with a shift factor equation (data obtained from 4PB stiffness tests).

It was decided to use the Arrhenius equation to shift the data points to the reference temperature. This shift factor is already used for the 4PB stiffness master curves by reducing the actually used loading frequency to a corresponding frequency at a reference temperature. It would be similarly applicable to any other time parameter like the strain rate in compression tests.

The final goal of constructing a master curve is to establish a relation between material properties like f_c, S_{mix} or E_{tan} and temperature and time related variables like loading time, loading frequency and strain rate.

The most convenient physical model by which data can be fitted is an S shape (sigmoidal) curve because when;

$\dot{\varepsilon} \rightarrow 0$: when strain rate (or any other time derivative variable) approaches zero, the mechanical property (P) of a material becomes zero. (P can be replaced by f_c, f_t, S_{mix}, E_{tan})

$\dot{\varepsilon} \rightarrow \infty$: the material response property (P) will approach a maximum plateau value, P_h, when the strain rate (or any other time derivative value) approaches infinity.

$T \rightarrow 0$: the lower the temperature (in Kelvin) is, the stiffer the material becomes in as much as it reaches to a glass point below which the material behaves linear elastic. At this point the stiffness of the bituminous material reaches a maximum level. At or below that temperature, sudden brittle failure occurs at a certain stress level (P_h) in tension and compression tests.

$T \rightarrow \infty$: the higher the temperature, the bituminous material becomes soft and ultimately the binder becomes a liquid and the stiffness and strength reduce to zero (P=0).

The following sigmoidal model was used in creating master curves for f_c and E_{tan} . A similar approach was used for representing the tension test results. This will be described in the next section.

$$P = P_h + (P_h - P_l) * e^{-[\frac{u_r}{u_0}]^\gamma} \quad (5.30)$$

$$u_r = u\,\beta_T \quad (5.31)$$

$$\beta_T = e^{\frac{\Delta H}{R}[\frac{1}{T}-\frac{1}{T_r}]} \quad (5.32)$$

Where:

P = mixture mechanical properties ($S_{mix,}$ f_c, f_t and E_{tan} [MPa])

u = loading frequency obtained from test at different temperatures [Hz]

P_h = high P value when $u \to \infty$

$P_{l=0}$ = low stiffness value when $f \to 0$

u_r = reduced time variable at reference temperature (being $\dot{\varepsilon}$ [m/m/%/s] or f

u_0 = an initial time variable (u) value

β_T = shift factor [-]

ΔH = activation energy [J/mol]

R = ideal gas constant [8.314 J/mol.K]

T = considered temperature in Kelvin [K]

T_r = reference temperature in Kelvin [K]

γ = model parameter [-]

In this model, it is assumed that $P_{l=}0$ when $u \to 0$.

The compressive strength and tangential modulus obtained from the uniaxial compression tests at different temperatures and strain rates were firstly shifted to the reference temperature. The remaining four model parameters were solved by minimizing the mean squared error between the log values of the measured f_c or E_{tan} and the model value at the reference temperature.

The model parameters, P_h, u_0, ΔH *and* γ, obtained in this way are listed in Table 5.12.

Master curves for the compression strength and tangential modulus derived using the model parameters are plotted in Figure 5.65 and Figure 5.66. They

are plotted at the reference temperature of 17°C (290.15K). The original data corresponding to different temperatures (before and after shifting) are plotted as well in the same chart. The master curve corresponding to each mixture type is illustrated separately. These master curves are compared in Figure 5.64. Since the curves were close to each other, it seems reasonable to combine all compression data (except mixture "B" because of the different RA material) to achieve one model which is called here as "Average mixture". It is indicated by "*Avg*" in Table 5.12 and they are plotted in Figure 5.67and Figure 5.68.

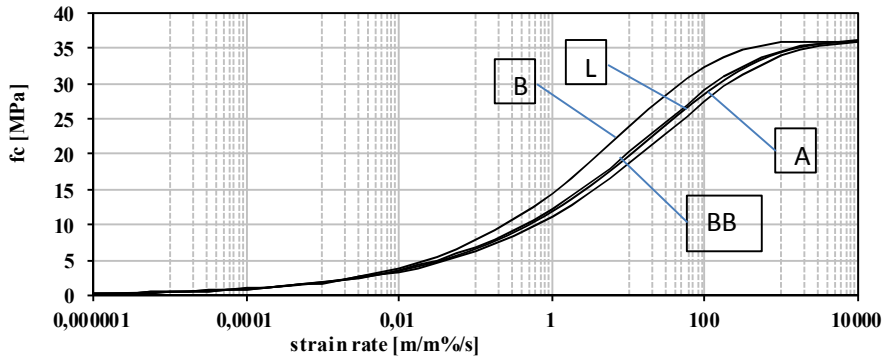

Figure 5.64 Compressive strength of all mixtures at 17°C

Table 5.12 Unified model parameter from compression test

	Mix Method	***Tr [°Kelvin]***	***ΔH [J/mol]***	***Ph [MPa]***	***u0 [m/m%/s]***	***γ [-]***
Etan	A	290.15	125.1	12000	0.298	0.483
	B	290.15	173.4	12000	0.327	0.411
	BB	290.15	173.4	12000	0.293	0.411
	L	290.15	173.4	12000	0.298	0.411
	Avg (A, BB, L)	290.15	173.4	12000	0.295	0.466
ft	A	290.15	185.0	36	19.000	0.298
	B	290.15	177.8	36	7.660	0.327
	BB	290.15	189.6	36	28.651	0.293
	L	290.15	189.7	36	21.777	0.298

Avg (A, BB, L)	290.15	189.4	36	19.360	0.301

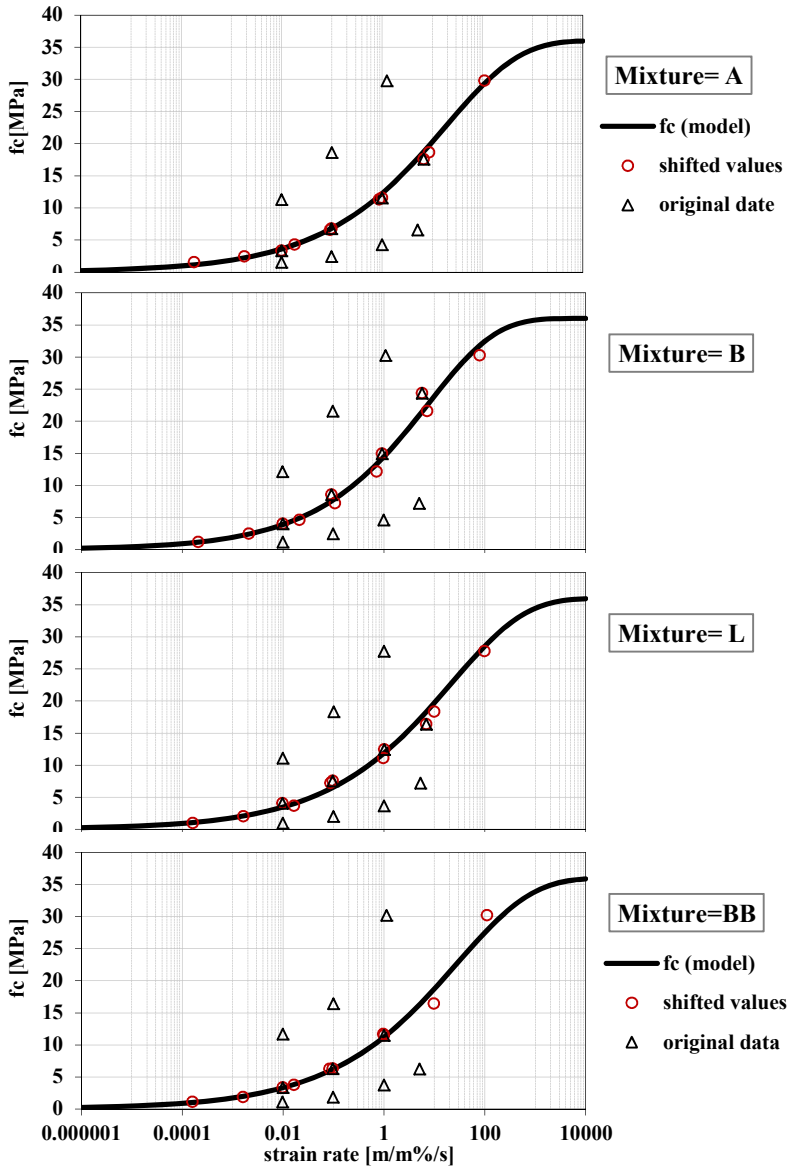

Figure 5.65 Compressive strength master curves using unified model parameters

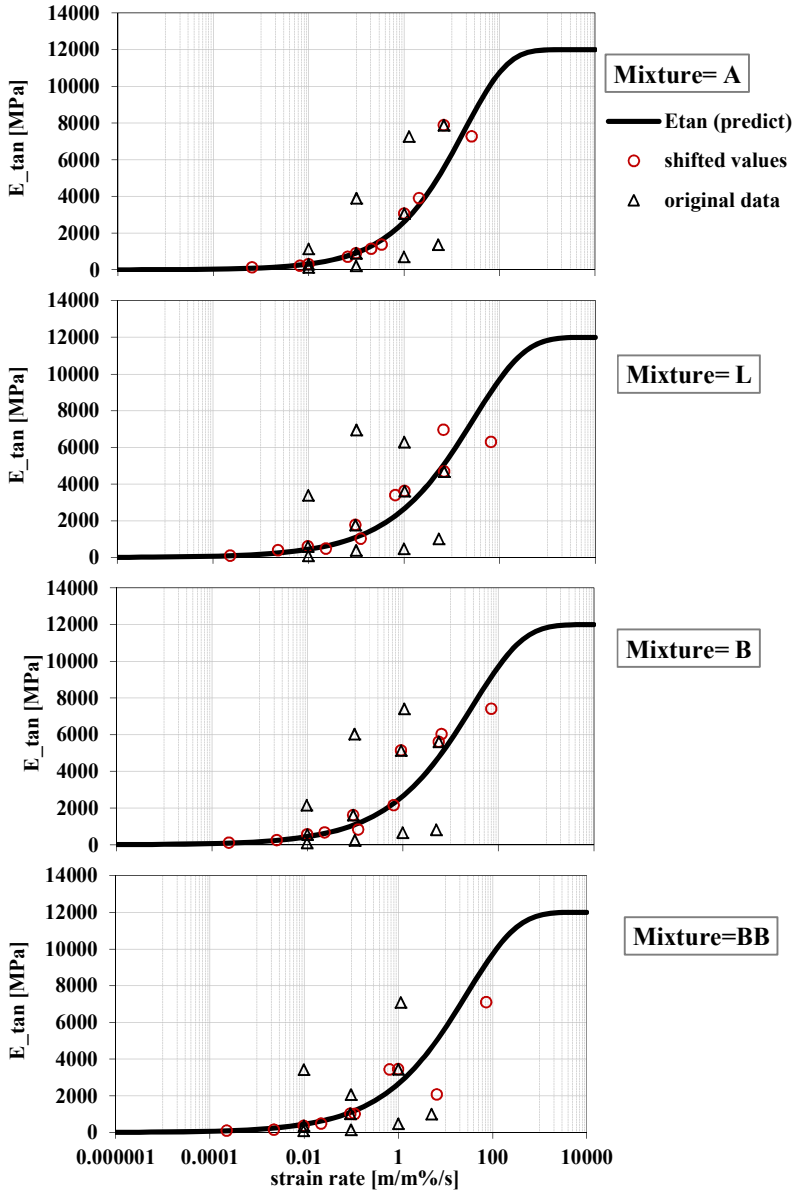

Figure 5.66 E_{tan} master curves using unified model parameters (uniaxial compression test)

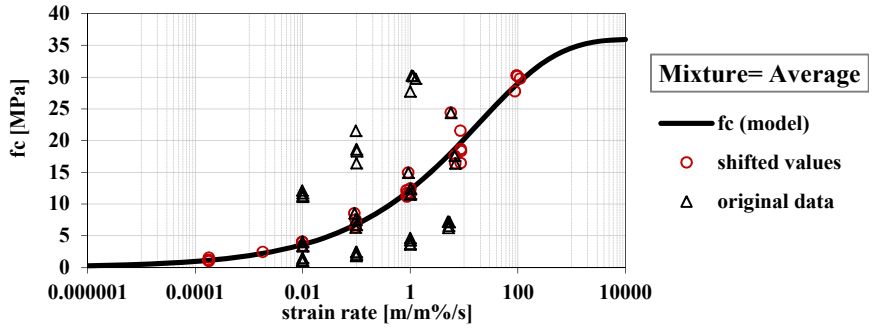

*Figure 5.67 Compressive strength master curve of the **Average** Mixture (A, BB, L)*

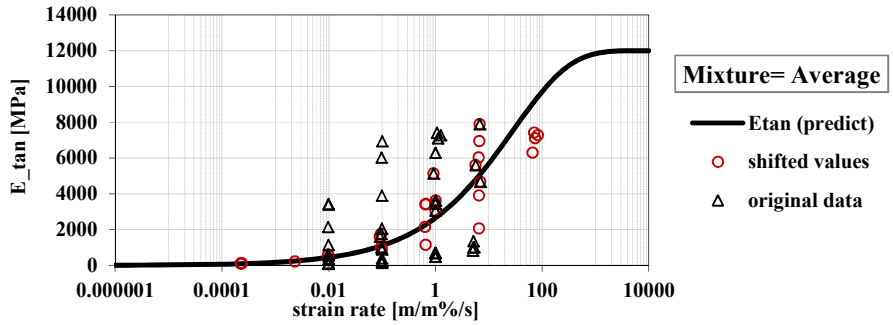

*Figure 5.68 E_{tan} master curve of the **Average** Mixture (A, BB, L)*

5.3.5. Uniaxial monotonic direct tension test (UMDT)

This section will deal with the results of the uniaxial tension tests. In UMDT tests, the specimen is subjected to a uniaxial tensile force. In this research the tests are performed in the displacement controlled mode.

The cylindrical specimen is glued to aluminum caps by means of two component epoxy glue. Then the specimen is mounted by screwing the caps to two hinges in the tension setup (see Figure 5.69). The two hinge system is designed in such a way that it allows the vertical force to be applied along the central axis of the specimen. However, imperfect alignment of the specimen was observed as a result of coring the specimen. It should be mentioned that everything was done to drill the cores as good as possible (e.g. by lowering

the speed of drilling) but some inevitable play in the machine was still causing some misalignment. It was also tried to compensate the misalignment while attaching the specimens to the caps.

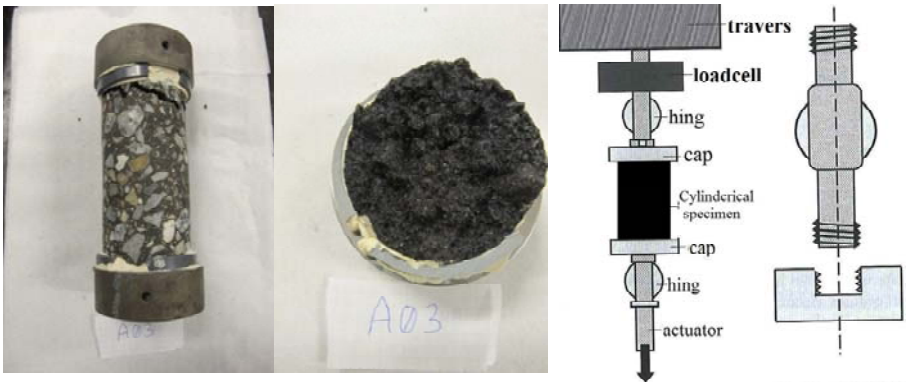

Figure 5.69 Uniaxial Tension setup

Specimen preparation and determination of their volumetric properties were presented in section 3.2.5.2. The specimens were selected in such a way, that the air voids contents were close to each other, in order to reduce influence of the voids content on the results.

In a tension test the stress distribution system in the specimen is different from that in the compression test, because the stress has to be transferred through the cap and glue system into the specimen. Therefore it is very unlikely to achieve a uniform tensile stress near the caps. Since the specimens are glued to the caps, resistance to radial deformation at the glued ends of the specimen occurs which results in stress concentrations and that can lead to cracking in the area of end caps. This phenomenon often happened during the tension tests.

This tension test setup is equipped with a temperature control cabinet (Weis-Enet) with the capability of maintaining the temperature between -40°C and 100°C with an accuracy of ±0.1°C. The 50kN hydraulic actuator of this setup is controlled by an MTS test controller (model 407) which facilitates the actuator to apply forces at high displacement rates.

Three LVDTs were installed between the two caps to measure the axial deformation. Radial deformation was measured by means of an extensometer. They are connected to a series of Peekel amplifiers in the setup with channels which are connected to a data acquisition board. The number of test scans can be changed through the data acquisition software for each test condition (strain rate). Higher strain rates require a higher frequency in data scanning.

The measurement outputs are in voltage values which have to be transformed to the required units in an MS Excel spreadsheet for further analysis.

5.3.5.1. Factorial design

Similar to the compression test, a factorial design method was adopted to determine the range of temperatures and strain rates to be used in the tension tests. Temperatures of 1, 17, and 33 ^{0}C were selected and a range of strain rates between 0.01 and1%/s was used, because these values could be applied with the available setup.

The factorial design is shown in Figure 5.70. The test conditions are the same for each mixture type (A, B, BB and L)

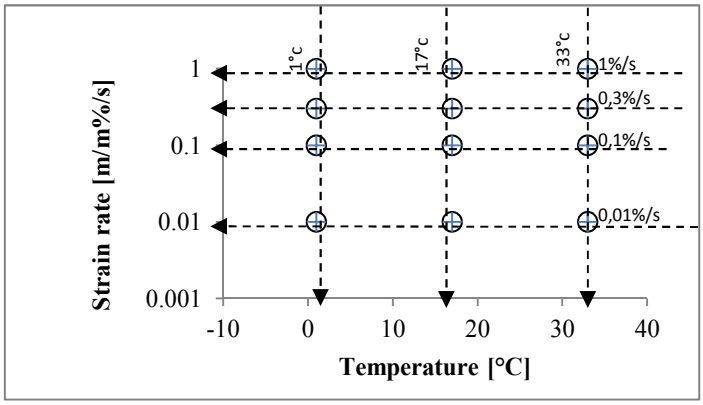

Figure 5.70 Factorial design of the tension tests

5.3.5.2. Tension test setup results

From the test results, the vertical stress, axial and radial strains were determined.

Different charts were plotted to show the stress-strain relations as well as strain rate signals. Since the tests were done in the displacement controlled mode, the strain rate signals are important because they allow to check whether the tests have been done at the intended conditions. The strain rates were determined by taking the first derivative of the axial displacement-time curve. Similar to the compression test, the strain rate is expressed as m/m%/s. The tangential modulus (apparent stiffness) and strain rates are computed by the same equations as used for analyzing the compression test results.

Although not completely true (especially near the caps) a simple homogenous stress distribution was assumed in all computations.

An example of a stress-strain curve is given in Figure 5.71. Figure 5.72 is showing the evolution of stress versus time curve as well as the strain rate signal. It shows to what extent the strain rate is instable in the starting phase of the test, when the load is applied. The strain signal instability is basically caused by the fact that the specimens are not directly connected to the actuator. This implies that other parts, like hinges, first have to get rearranged when the load is applied. Since the control system is set to control the displacement by adjusting the applied force, at some points the force increases and decreases suddenly. To minimize this effect a small preloading of the specimen before starting the actual test was enforced to compensate for possible displacements at the hinges and other moving parts of the setup.

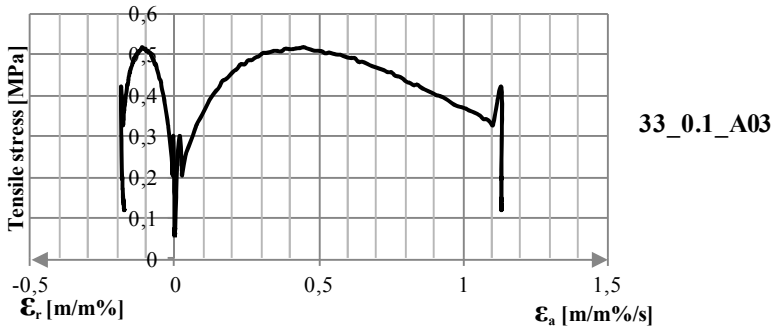

Figure 5.71 An example of the axial and radial strain curve vs. vertical tensile stress (mixture A, at 33°C and 0.1%/s)

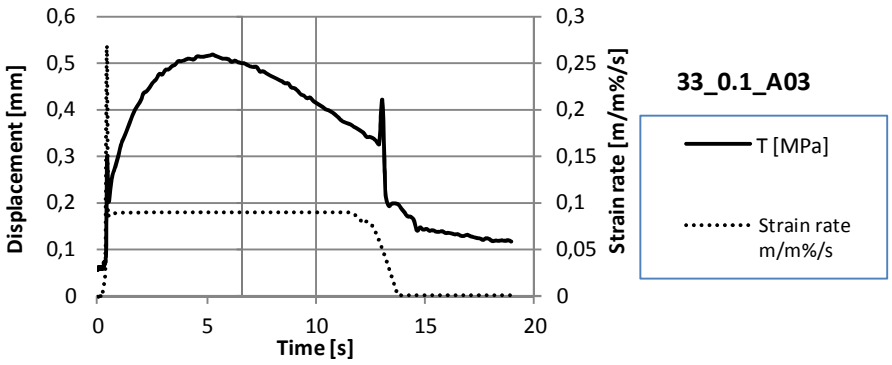

Figure 5.72 An example of the strain rate signal in time together with the stress curve

5.3.5.3. Effect of strain rate and temperature on tension properties

Because of its temperature and time dependent nature, asphalt concrete response varies with temperature and loading or strain rate. Increasing the strain rate results in an increase in stiffness and in a higher tensile strength. Figure 5.73 illustrates the effect of strain rate on the tensile response of the material at a certain temperature. The same material shows a higher tensile strength (f_t) at a higher strain rate. The figure also shows that the fracture modes are influenced by the strain rate. At $\dot{\varepsilon}$=1%/s a more brittle failure occurs, whereas at other strain rates ($\dot{\varepsilon}$<1%/s) more ductile fracture occurs.

Figure 5.74 provides a comparison between stress-strain curves at a certain strain rate and different temperatures. The figure shows that the asphalt concrete response is stiffer at lower temperatures and results in a higher f_t. Sudden failure occurs at lower temperatures. Figure 5.74 indicates a sudden failure at 1°C, whereas ductile failure is dominant at higher temperatures.

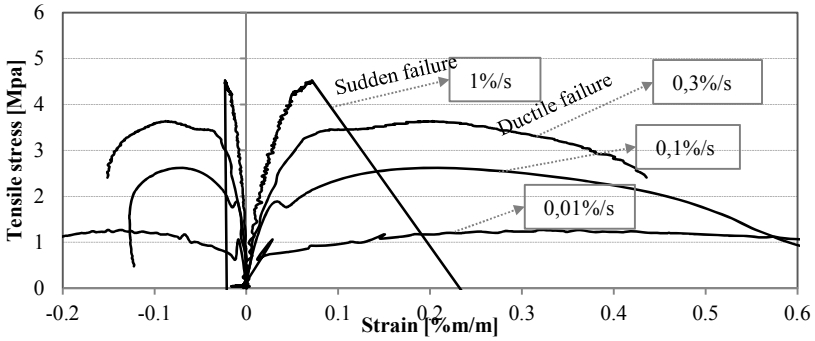

Figure 5.73 Influence of strain rate on tensile stress-strain curves

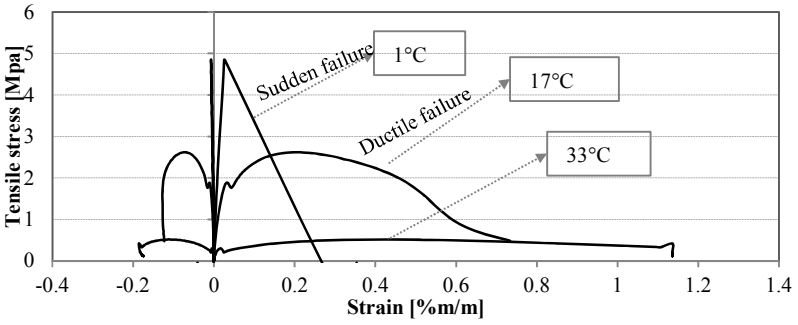

Figure 5.74 Influence of temperature on tensile stress-strain curves

5.3.5.4. Overview of tension test results

The results of the tension tests are given in Table 5.13 to Table 5.16. In these tables; "f_t" represents the tensile strength, "$\varepsilon_{a,max}$" stands for axial strain at peaks stress, "$\varepsilon_{r,max}$" indicates radial strain at peak stress and "E_{tan}" stands for tangential modulus.

Table 5.13 Tension test results of mixture A

Code	*Temperature [°C]*	*Target strain rate [m/m%/s]*	*Actual strain rate [m/m%/s]*	f_c *[MPa]*	E_{tan} *[MPa]*	$\varepsilon_{a,max}$ *[m/m%]*	$\varepsilon_{r,max}$ *[m/m%]*
A26	1	0.01	0.008	4.52	7094	0.071	0.023
A15	1	0.1	0.122	4.84	17730	0.027	0.007
A08	1	0.3	0.276	4.48	15436	0.030	0.007
A25	1	1	0.477	4.13	19990	0.023	0.007
A10	17	0.01	0.007	1.27	2706	0.318	0.136
A07	17	0.1	0.085	2.62	4240	0.193	0.068
A14	17	0.3	0.209	3.63	3988	0.203	0.088
A13	17	1	1.059	6.41	9178	0.160	0.065
A05	33	0.01	0.009	0.25	176	0.713	0.153
A03	33	0.1	0.089	0.52	272	0.447	0.112
A04	33	0.3	0.263	0.85	559	0.392	0.116
A06	33	1	0.880	1.20	1608	0.309	0.116

Table 5.14 Tension test results of mixture B

Code	*Temperature [°C]*	*Target strain rate [m/m%/s]*	*Actual strain rate [m/m%/s]*	f_c *[MPa]*	E_{tan} *[MPa]*	$\varepsilon_{a,max}$ *[m/m%]*	$\varepsilon_{r,max}$ *[m/m%]*
B11	17	0.3	0.366	4.59	8500	0.056	0.019
B12	33	0.01	0.010	0.40	150	0.696	0.214
B02	33	0.1	0.088	0.40	319	0.241	0.042
B03	33	0.3	0.263	1.24	700	0.309	0.095
B05	33	1	1.331	2.12	2783	0.102	0.038

Table 5.15 Tension test results of mixture BB

Code	*Temperature [°C]*	*Target strain rate [m/m%/s]*	*Actual strain rate [m/m%/s]*	f_c *[MPa]*	E_{tan} *[MPa]*	$\varepsilon_{a,max}$ *[m/m%]*	$\varepsilon_{r,max}$ *[m/m%]*
BB07	1	0.01	0.008	5.07	7563	0.074	0.020
BB111	1	0.1	0.115	5.37	17890	0.042	0.014
BB112	1	0.3	0.258	5.09	18653	0.025	0.007
BB25	1	1	0.421	4.17	18528	0.023	0.001
BB13	17	0.01	0.009	1.25	2535	0.402	0.160
BB02	17	0.1	0.091	2.92	4565	0.184	0.054
BB26	17	0.3	0.526	4.78	8950	0.131	0.047
BB11	17	1	0.913	5.96	9372	0.116	0.037
BB01	33	0.01	0.010	0.13	150	0.693	0.030
BB03	33	0.1	0.096	0.49	347	0.577	0.464
BB05	33	0.3	0.285	0.82	552	0.497	0.131
BB10	33	1	1.662	1.24	2041	0.092	0.036

Table 5.16 Tension test results of mixture L

Code	*Temperature [°C]*	*Target strain rate [m/m%/s]*	*Actual strain rate [m/m%/s]*	f_c *[MPa]*	E_{tan} *[MPa]*	$\varepsilon_{a,max}$ *[m/m%]*	$\varepsilon_{r,max}$ *[m/m%]*
L16	1	0.01	0.008	2.90	7428	0.033	0.008
L1	1	0.1	0.109	4.04	19171	0.021	0.005
L22	1	0.3	0.250	4.30	18111	0.024	0.006
L18	1	1	0.514	4.90	20687	0.024	0.006
L21	17	0.01	0.010	1.40	2773	0.188	0.077
L02	17	0.1	0.091	3.48	5130	0.143	0.044
L03	17	0.3	0.470	4.86	8533	0.096	0.030
L17	17	1	0.786	5.10	9178	0.085	0.026
L06	33	0.01	0.009	0.39	205	0.394	0.106
L07	33	0.1	0.096	0.65	455	0.255	0.049
L05	33	0.3	0.284	1.27	591	0.322	0.096
L04	33	1	0.962	1.44	2005	0.257	0.079

Bar charts (Figure 5.75 and Figure 5.76) show the effect of the mixture production method on tensile strength and tangential modulus at different temperatures and strain rates. A systematic pattern related to production methods could not be established by these bar charts

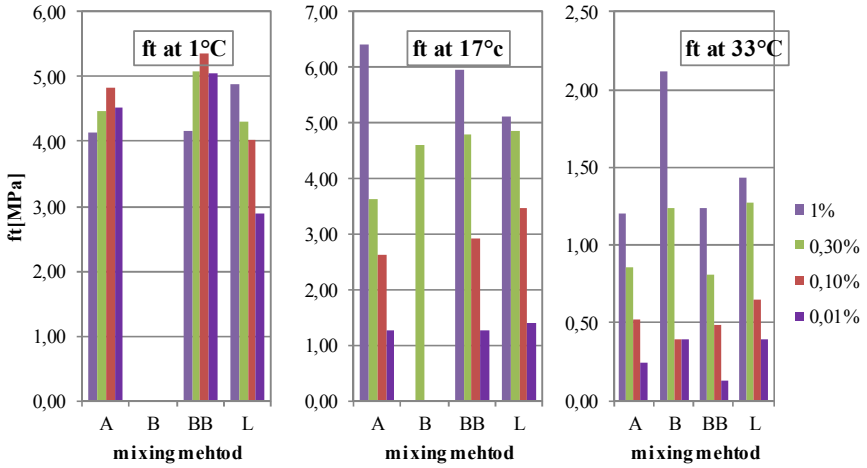

Figure 5.75 Tensile strength ft in relation to temperatures and strain rates [values in legend are target strain rates]

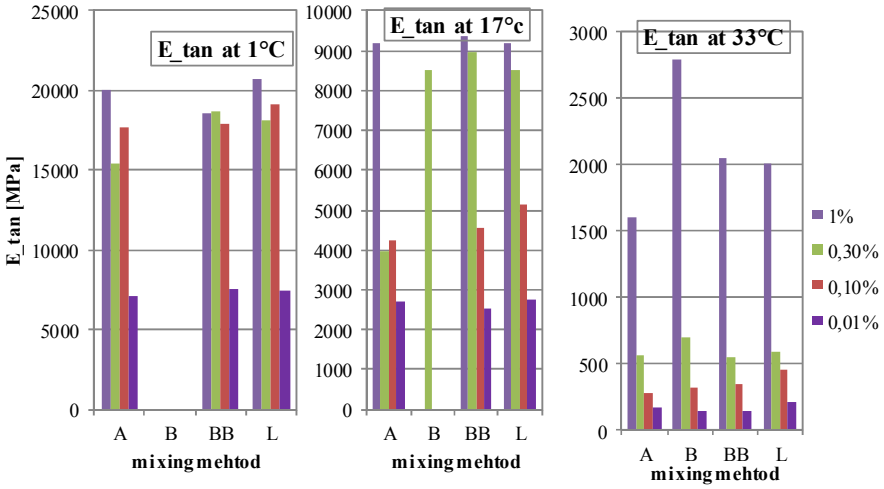

Figure 5.76 E_{tan} in tension in relation to temperatures and strain rates [values in legend are target strain rates]

5.3.5.5. Unified model for tensile strength and tangential modulus

It is useful to have a general model of material response which makes it possible to predict material properties in conditions which are beyond the capacity of test setups.

It was shown that the stiffness and strength in the compression test can be expressed by means of a sigmoidal curve and a similar approach was therefore adopted for describing the tensile strength and tangential modulus as a function of strain rate (or loading time or loading frequency) and temperature.

The Arrhenius equation was used to transform temperature to a reduced time variable (strain rate or loading frequency). The shifted points were fitted to a sigmoidal S shape curve. The used equations are shown below.

$$P = P_h + (P_h - P_l) * e^{-[\frac{u_r}{u_0}]^{\gamma}} \quad (5.33)$$

$$u_r = u\,\beta_T \quad (5.34)$$

$$\beta_T = e^{\frac{\Delta H}{R}[\frac{1}{T}-\frac{1}{T_r}]} \quad (5.35)$$

Where:

P	=	mixture mechanical properties ($S_{mix.}$ f_c, f_t and E_{tan} [MPa])
u	=	time variable at reference temperature ($\dot{\varepsilon}$ [m/m/%/s] or f [Hz])
Ph	=	high P value when $u \to \infty$
Pl=0	=	low stiffness value when $u \to 0$
ur	=	reduced time variable at reference temperature ($\dot{\varepsilon}$ [m/m/%/s] or f [Hz])
u0	=	an initial time variable (u) value
βT	=	shift factor [-]
ΔH	=	activation energy [J/mol]
R	=	ideal gas Constant [8.314 J/mol.K]
T	=	considered temperature in Kelvin [K]
Tr	=	reference temperature in Kelvin [K]
γ	=	model parameter [-]

The following conditions are important when fitting the data to a sigmoidal curve similar to the one that was used to describe the compression properties.

$\dot{\varepsilon} \to 0$: This implies the state of no loading. Since there is no load there is also no response from the material, so ft and E_{tan} can be considered to be equal to zero. Therefore, $P_l=(f_t)_{min}=0$ and $E_{tan}=0$

$\acute{\varepsilon} \rightarrow \infty$: at high strain rates, the tensile stiffness as well as the tensile strength of the material will reach a plateau value $P_{h.}$ This value has to be determined by solving the equations.

$T \rightarrow -\infty$: When the temperature (in Celcius) decreases, the material becomes stiffer till it reaches a glass point at which the material behaves linear elastic. At this point the stiffness of bituminous material reaches to a maximum level (P_h)

$T \rightarrow \infty$: At high temperatures, bituminous materials become soft and the binder liquid and the material response drops to zero (P=0).

The parameters corresponding to tensile strength and tangential modulus are presented in Table 5.17.

Master curves of tensile strength and tangential modulus are plotted in Figure 5.77 and Figure 5.78, respectively. They are plotted at the reference temperature of 17°C (290.15K). The original data corresponding to different temperatures (before and after shifting) are plotted in the same chart as well. The master curve corresponding to each mixture type is illustrated separately.

The master curves are compared in Figure 5.79. Since the curves are close to each other, it seems to be reasonable to combine all tension data (except mixture "B" because of its different RA aggregates) to achieve one model which is called here as "Average mixture". It is indicated by "Avg" in Table 5.17. Figure 5.80 and Figure 5.81 are illustrating the master curves of the Average mixture which is the combination of all data.

Table 5.17 Unified model parameters for the tension tests

	Mix Method	***T0***	***Dh***	***Ph***	***u0***	***γ***
E_{tan}	A	290.15	173.4	25000	0.396	0.411
	B	290.15	173.4	25000	0.385	0.411
	BB	290.15	173.4	25000	0.461	0.411
	L	290.15	173.4	25000	0.352	0.411
	Avg (A, BB, L)	290.15	173.4	25000	0.389	0.411
f_t	A	290.15	212.3	7.5	0.495	0.396
	B	290.15	206.2	7.5	0.422	0.385
	BB	290.15	219.0	7.5	0.397	0.461
	L	290.15	212.6	7.5	0.545	0.352
	Avg (A, BB, L)	290.15	213.3	7.5	0.435	0.399

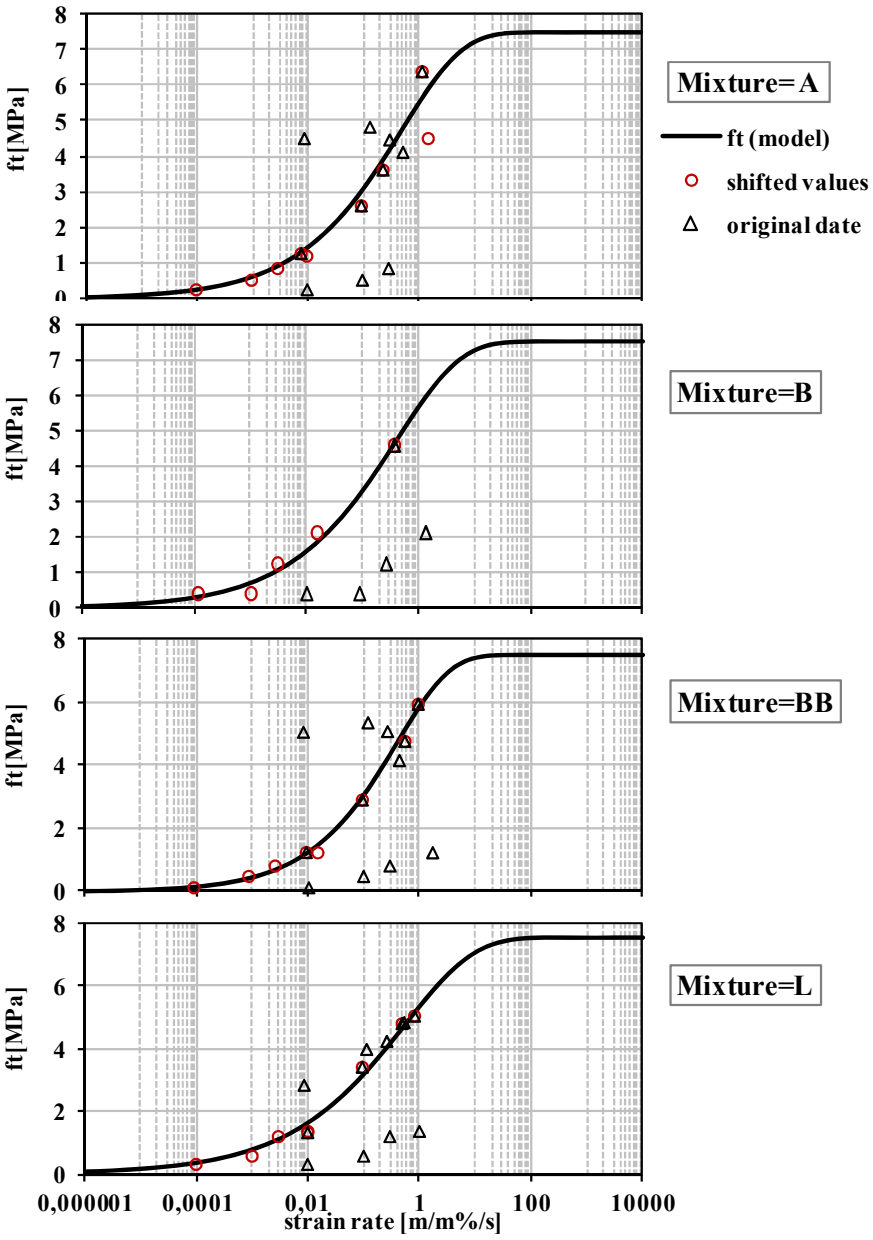

Figure 5.77 Tensile strength master curve using the unified model parameters

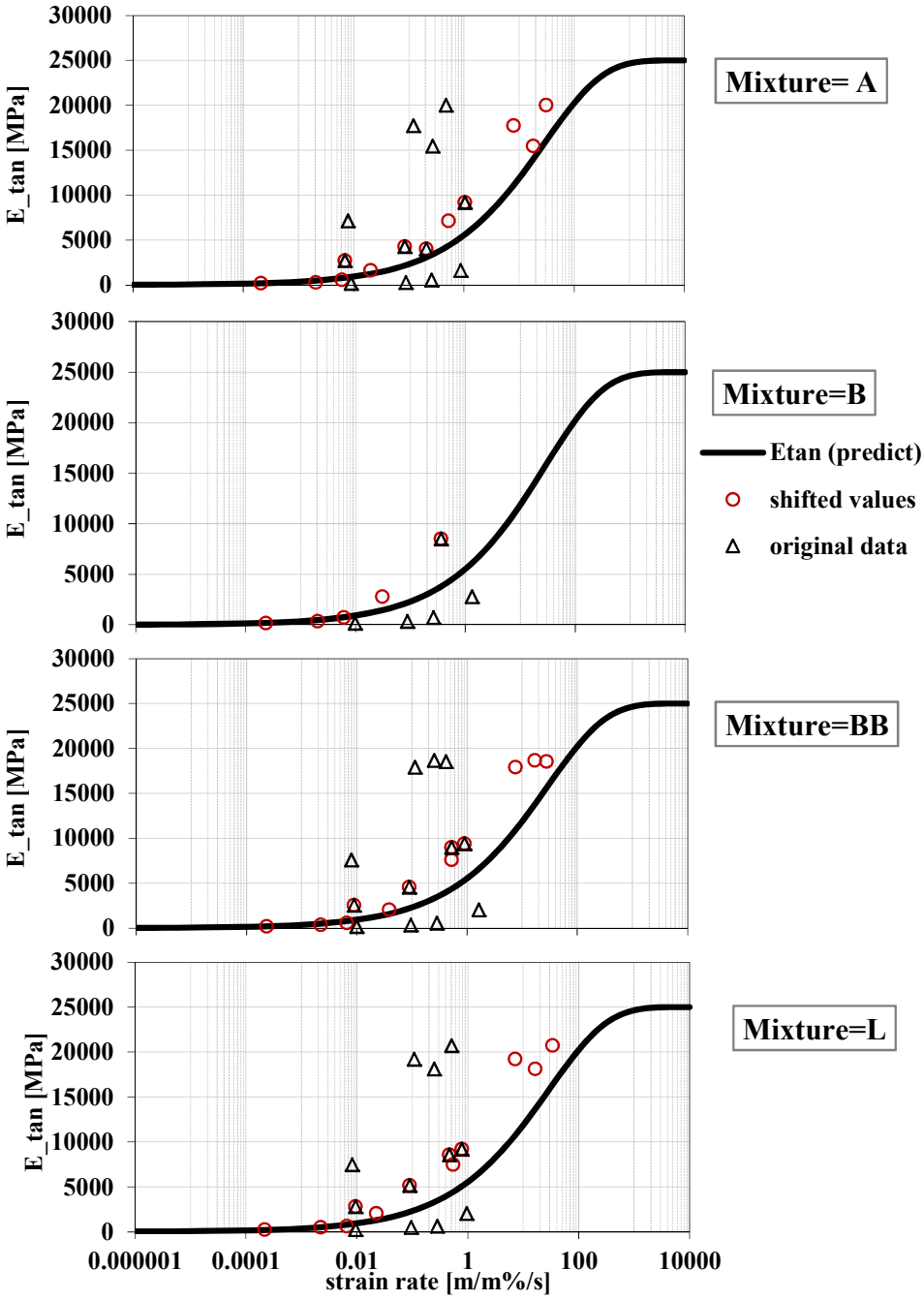

Figure 5.78 E_{tan} master curve using the unified model parameters

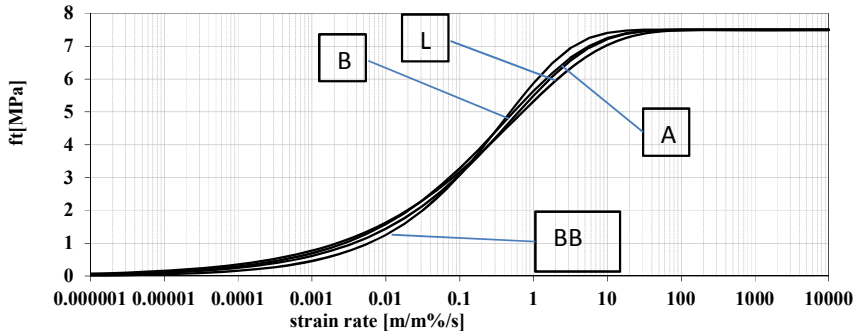

Figure 5.79 Tensile strength of all mixtures at 17°C

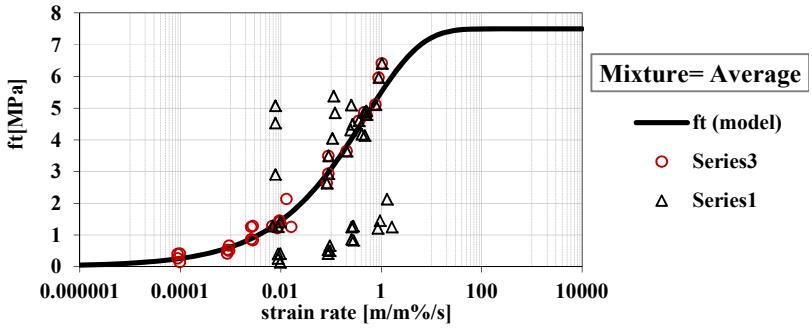

*Figure 5.80 Tensile strength master curve of **Average** Mixture*

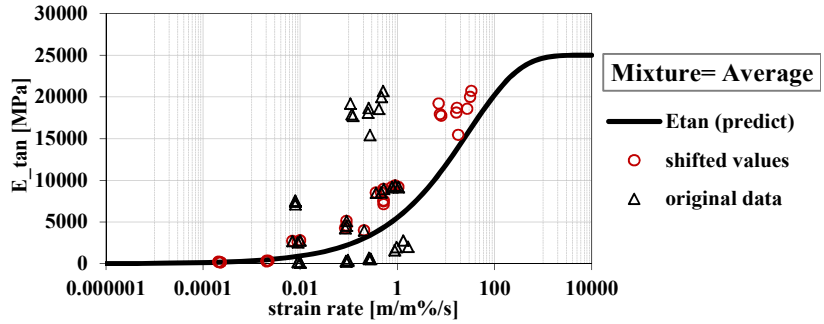

*Figure 5.81 E_{tan} master curve of **Average** Mixture*

5.3.5.6. Summary and conclusions of the uniaxial tension and compression results

Considering all test results available, it is possible to compare the material properties in tension and compression. Tension and compression results together with fatigue test results will be used in the next section to determine the fatigue endurance limit of each mixture.

Firstly, a summary of test conditions for both the tension and compression test will be presented. Then the results will be compared.

Uniaxial tension and compression tests were carried out on cylindrical specimens which were fabricated using four mixture production types being A, B, BB, and L. Both tests were run in a displacement (strain) controlled mode in a uniaxial setup.

In the tension and compression tests, two variables were taken into account being temperature and strain rate. All tests were done at 1, 17 and 33°C. Strain rates of 0.01, 0.1, 0.3 and 1[%/s] were used in the tension tests while strain rates of 0.01, 0.1, 1 and 5[%/s] were used for the compression tests. The capacity of the tension and compression setups didn't allow applying strain rates higher than 1 and 5[%/s], respectively.

The temperature in the compression setup cabinet had to be calibrated for each test. Its accuracy was ±0.5°C. The temperature control in the tension setup was more accurate (±0.1°C).

In the compression tests a system of steel plates with a greased foil was used as friction reducing system to prevent any constraint against radial deformation at the two ends of specimens. In the tension test, the specimens were glued to caps which were connected to two hinges by screwing. These hinges are meant to provide sufficient freedom to keep the force in alignment with the axis of the specimen. Since both ends of the specimen were glued to solid caps, the radial displacement was hindered at these two ends.

5.3.5.7. Strain rate control

The strain rate control was an issue at relatively high strain rates in both the tension and compression setup. Strain rate fluctuation in the beginning of the tension test was more critical compared to the compression test because the load is not directly applied to the specimen in a tension test. For this reason, the real strain rate was determined by taking the first derivative of the displacement versus time relationship. The average strain rate is calculated and considered as “real strain rate”. This value is presented in the overview of the tension and compression test results.

The efficiency of the strain rate control in tension and compression is illustrated in Figure 5.82 where the measured "real strain rate" is plotted against the intended value (target strain rate). They are shown on a logarithmic scale. It seems that the intended strain rates can be better achieved in compression tests in comparison with tension tests. Also the control of the strain rate is better at lower strain rates. Therefore it seems to be more convenient to use strain rates less than 5%/s in compression and less than 1%/s in tension tests

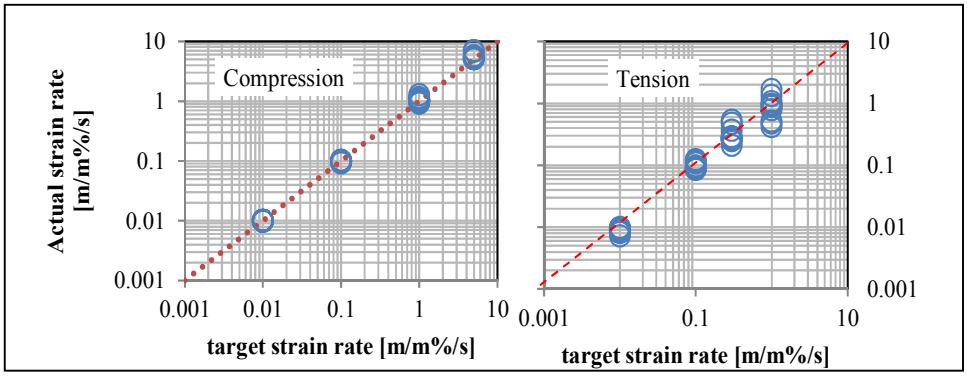

Figure 5.82 Target and actual strain rates in compression and tension tests

5.3.5.8. The effect of mixture type on tension and compression

The effect of mixture type is summarized in Figure 5.64 and Figure 5.79. It is recalled that:

- mixture A represents the mixture produced in the ASTEC double drum with 50%RAP;
- mixture B is the mixture produced in the batch plant with 25%RAP+25%PARAP;
- mixture BB is the mixture produced in batch plant with 50%RAP
- and mixture L is the mixture produced with a laboratory mixer with 50%RAP.

With respect to the tensile strength it can be concluded that there is no significant difference between the master curves (Figure 5.79). However the slope of the master curve of BB is slightly steeper than the slope of the other three mixtures.

With respect to the compressive strength it can be concluded that mixture B is showing a higher strength compared to the other three mixtures. The use of PA-RAP in mixture B makes the material stiffer (according to 4PB stiffness results).

The tension and compression master curves for mixtures A, BB, and L do not show significant differences. This is to some extent remarkable because of the quite different preheating and mixing process. Also the stiffness and fatigue resistance of mixture L is quite different. It should however be noted that all three mixtures were made of the same materials and had the same composition. Obviously the tensile and compressive strength of plant produced mixtures can be well predicted using laboratory produced mixtures!

5.4. The material model

Hot mix asphalt (HMA) is a pavement material that exhibits both visco-elastic and visco-plastic behavior and therefore shows a complicated rate-dependent behavior [60]. A number of efforts have been made to develop constitutive material models to describe the rate-dependent properties of asphalt concrete [61], [62], [63], [64], [65], [66]. The constitutive models are primarily based on strain hardening rules in metals or soil. Scarpas [65] implemented a visco-plastic model for asphalt concrete which uses a Perzyna's flow rule incorporated in the Desai yield surface relations. A material model was also developed during the ACRe project at TU Delft to describe the response of asphalt mixtures.

A material model should describe the response of a material to any state of stress. It consists of a yield surface and constitutive relations. A simple ideal elastic-plastic material behaves elastic until it reaches the yield point. Then it behaves ideally plastic. Asphalt concrete response is more complex due to its visco-elastic behavior. A complex material model with changing limit surfaces is illustrated in Figure 5.83. In this figure, the evolution of the strain in three phases is presented; elastic, hardening and softening.

5.4.1. Response surface

Historically, a number of yield surface functions have been developed; examples are the Tresca, von Mises, Mohr-Coulomb and Drucker-Prager functions. A comparison between the Drucker-Prager and Mohr-Coulomb yield surfaces is shown in Figure 5.84. They are both extensively used in the modeling of soils.

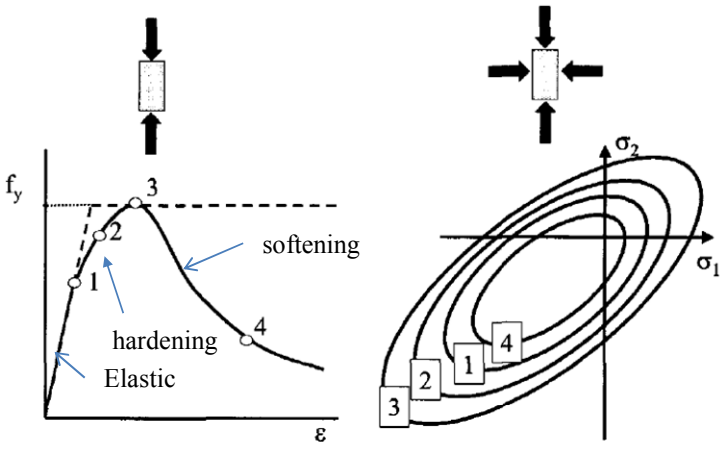

Figure 5.83 Surface limits of a complex material

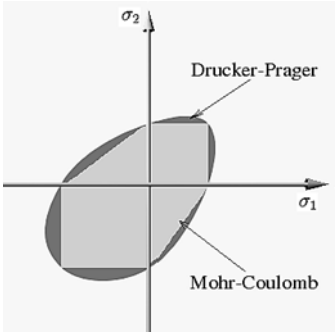

Figure 5.84Mohr-Coulomb and Drucker-Prager yield surfaces

Contrary to the Drucker-Prager and Mohr-Coulomb critera, the yield surface proposed by Desai [61] is a closed surface and allows defining stress conditions which are representative for certain conditions of the material like initiation of dilation, etc.

The yield surface is primarily expressed by means of the stress invariants I_1, J_2 and J_3 which are defined as:

$$I_1 = \sigma_{xx} + \sigma_{yy} + \sigma_{zz} \qquad (5.36)$$

$$J_2 = \frac{1}{2}(s_1^2 + s_2^2 + s_3^2)$$
$$= \frac{1}{6}\left[(\sigma_{xx} - \sigma_{yy})^2 + (\sigma_{yy} - \sigma_{zz})^2 + (\sigma_{zz} - \sigma_{xx})^2\right] + \tau_{xy}^2 + \tau_{yz}^2 + \tau_{zx}^2 \quad (5.37)$$

$$J_3 = (\sigma_{xx} - p)(\sigma_{yy} - p)(\sigma_{zz} - p) + 2\tau_{xy}\tau_{yz}\tau_{xz} - (\sigma_{xx} - p)\tau_{yz}^2 - (\sigma_{yy} - p)\tau_{xz}^2 - (\sigma_{zz} - p)\tau_{xy}^2 \quad (5.38)$$

$$p = \frac{\sigma_{xx} + \sigma_{yy} + \sigma_{zz}}{3} \quad (5.39)$$

The proposed yield surface by Desai is truncated from the single surface yield function which is presented in the following equation.

$$f = \frac{J_2}{p_a^2} - \frac{\alpha\left[\frac{I_1 - R}{P_a}\right]^n + \gamma\left[\frac{I_1 - R}{P_a}\right]^2}{\sqrt{1 - \beta\cos(3\theta)}} = 0 \quad (5.40)$$

$$\cos(3\theta) = \frac{3\sqrt{3}}{2}\frac{J_3}{\sqrt{J_2^3}} \quad (5.41)$$

Where:

S_i = i[th] principal deviator stress

P_a = atmospheric pressure (=-0.1MPa) [the negative value indicates pressure]

$\alpha, \beta, \gamma, n, R$ = model parameters, depending on the material characteristics

The Desai response surface creates a closed surface in the (I_1, $\sqrt{J_2}$ and Θ) space (see Figure 5.85).

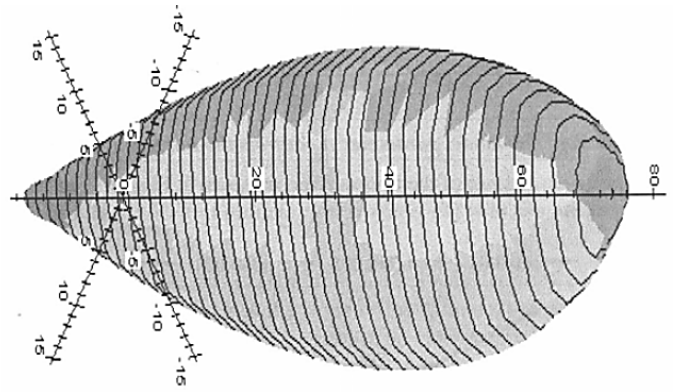

Figure 5.85 Illustration of Desai response surface in I_1, $\sqrt{J_2}$ and Θ [48]

5.4.2. Material model at uniaxial stress state

At the peak stress, the parameter α, β and γ arrive at zero and the yield surface transforms to a (straight) line in the (I_1-$\sqrt{J_2}$) space.

In case of uniaxial loading, the relation of the Desai yield surface simplifies as follows:

$$\sigma_{1=}\sigma\ , \sigma_2 = 0, \sigma_3 = 0 \qquad (5.42)$$

$$I_1 = \sigma_1 + \sigma_2 + \sigma_3 = \sigma \qquad (5.43)$$

$$J_2 = \frac{1}{2}\left[\left(\sigma_1 - \frac{I_1}{3}\right)^2 + \left(\sigma_2 - \frac{I_1}{3}\right)^2 + \left(\sigma_3 - \frac{I_1}{3}\right)^2\right] = \frac{1}{3}\sigma^2 \qquad (5.44)$$

Substituting in the equation (5.40) gives

$$\frac{J_2}{p_a^2} = \alpha\left[\frac{\sigma - R}{P_a}\right]^n + \gamma\left[\frac{\sigma - R}{P_a}\right]^2 \qquad (5.45)$$

The hardening parameter α is zero at the peak stress state, therefore:

$$\frac{J_2}{p_a^2} = \gamma\left[\frac{I_1 - R}{P_a}\right]^2 \Rightarrow J_2 = \gamma[I_1 - R]^2 \qquad (5.46)$$

Since the uniaxial tension and compression test give the tensile strength (f_t) and compressive strength (f_c), equation (5.45) can be written as:

$$\frac{1}{3}f_c = \gamma(-f_c - R)^2 \quad (5.47)$$

$$\frac{1}{3}f_t = \gamma(f_t - R)^2 \quad (5.48)$$

When f_c and f_t are known R and γ can be determined. The yield surface arrives at a straight line and $\sqrt{\gamma}$ is the slope of the line and the R is the intercept with the I axis. Dividing equation (5.47) and (5.48), provides:

$$R = \frac{2|fc|f_t}{|fc| - f_t} \quad (5.49)$$

$$\gamma = \frac{(|fc| - f_t)^2}{3(|fc| - f_t)} \quad (5.50)$$

Figure 5.86 illustrates the yield surface in the (I1-√J2) space as determined by the uni-axial tensile and compressive strength.

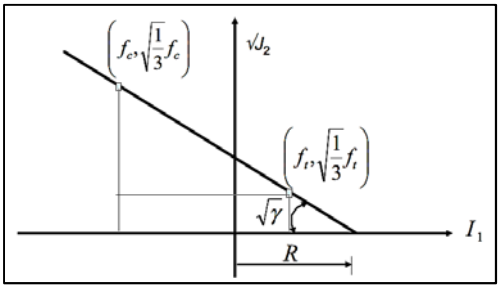

Figure 5.86 Determination of the yield surface using uniaxial tensile and compressive strength values

5.4.3. Determining yield surface for fatigue test conditions

The 4PB flexural fatigue tests carried out in this research were performed at various strain levels and a fixed frequency. As Figure 5.87 shows, this means that the fatigue tests were done at various strain rates. It should be noted that the strain rate during a fatigue test is not constant but follows a cosine relation. Nevertheless a constant strain rate was assumed which was calculated as:

$$\dot{\varepsilon} = 4f(100\varepsilon) \qquad (5.51)$$

Where:

$\dot{\varepsilon}$ = Strain rate [%m/m]

ε = Fatigue test strain rate [m/m]

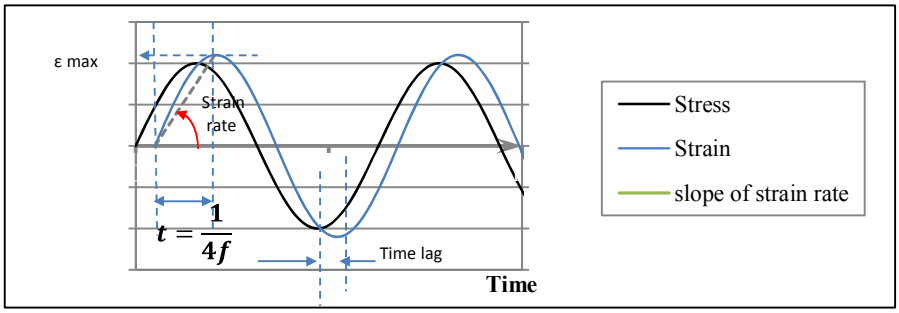

Figure 5.87 Converting applied strain and loading frequency into strain rate

On the other hand, the master curves of tensile and compressive strength give f_c and f_t as a function of strain rate.

When f_c and *ft are known*, it is possible to draw the yield surface for each fatigue test condition (see Figure 5.88).

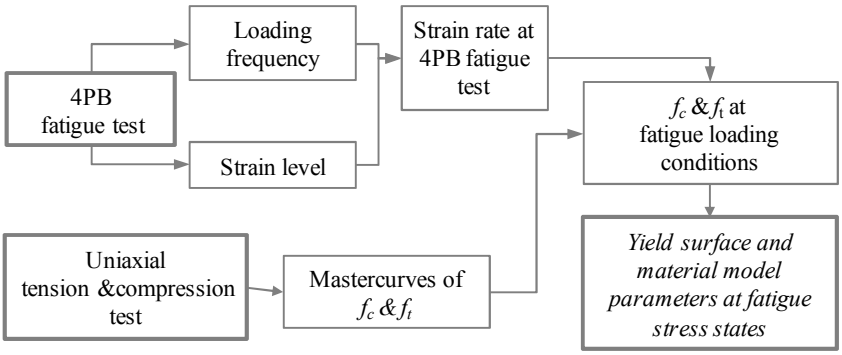

Figure 5.88 Determination of the yield surface at fatigue stress states

A summary of the 4PB fatigue test results and loading conditions is presented in Table 5.18 in which also the corresponding f_c and f_t values are given. For

the sake of completeness the master curves of f_c and f_t are illustrated again in Figure 5.89.

Table 5.18 Determination of compressive and tensile strength corresponding to each 4PB fatigue loading condition

Mixing Method	***sample***	***strain level (ε) [μm/m]***	***Initial fatigue tensile stress (σ_i) [MPa]***	***$S_{m\text{-}initial}$ [MPa]***	***Nf***	***Strain rate ($\dot{\varepsilon}$) [m/m%/s]***	***fc_Model [Mpa]***	***ft_Model [Mpa]***
A	A06	300	2.08	6938	1.6E+04	0.96	12.13	4.68
A	A09	250	1.92	7687	5.8E+04	0.8	11.61	4.49
A	A03	200	1.55	7806	2.0E+05	0.64	10.99	4.26
A	A04	150	1.25	8405	3.4E+05	0.48	10.23	3.96
A	A05	120	0.94	7914	1.0E+06	0.384	9.67	3.73
A	A07	110	0.97	8865	2.4E+06	0.352	9.46	3.64
A	A02	100	0.93	7771	6.7E+06	0.32	9.23	3.55
A	A08	80	0.97	9594	7.0E+06	0.256	8.72	3.33
BB	BB06	250	2.06	8282	3.8E+04	0.8	11.61	4.49
BB	BB05	200	1.75	8725	7.7E+04	0.64	10.99	4.26
BB	BB04	150	1.20	7959	5.6E+05	0.48	10.23	3.96
BB	BB03	120	1.04	8626	7.5E+05	0.384	9.67	3.73
BB	BB02	100	0.82	8084	2.0E+06	0.32	9.23	3.55
BB	BB01	80	0.91	8641	1.0E+07	0.256	8.72	3.33
L	L01	300	2.44	8106	7.4E+03	0.96	12.13	4.68
L	L02	250	2.00	8046	5.7E+03	0.8	11.61	4.49
L	L03	200	1.69	8575	6.5E+04	0.64	10.99	4.26
L	L04	150	1.37	9102	3.5E+04	0.48	10.23	3.96
L	L06	110	1.16	10331	2.4E+05	0.352	9.46	3.64
L	L05	100	0.98	9669	5.6E+05	0.32	9.23	3.55
L	L07	80	0.71	9027	1.5E+06	0.256	8.72	3.33

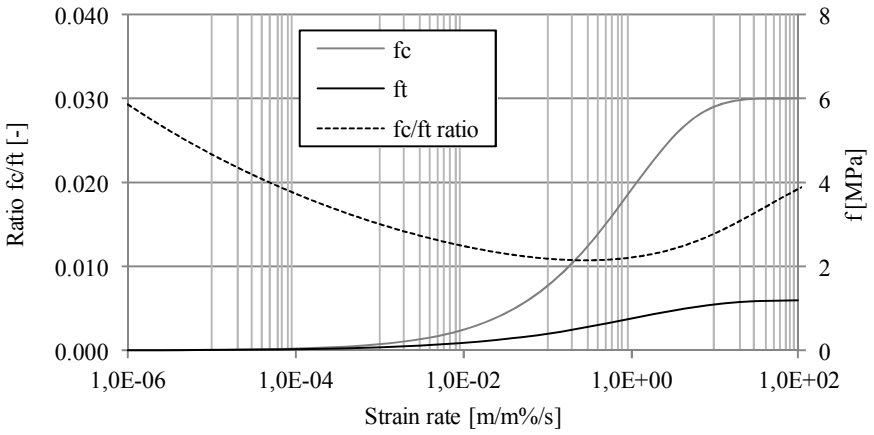

Figure 5.89 Master curves of f_c and f_t and the ratio between them (average mixture)

5.4.4. Relation between yield surface and fatigue life

Given the f_c and f_t values for each fatigue test condition, yield surfaces could be plotted and the results are shown in Figure 5.91, Figure 5.92 and Figure 5.93 per mixture type. The corresponding strain rates and fatigue strain levels are indicated for each line in the legend of the plots.

As the strain rate decreases, each data point corresponding to$(f_c, \sqrt{\frac{1}{3}}f_c)$ on the specific yield surface is moving along a straight line towards the origin of the graph.

Given the fact that each fatigue test was performed at a certain initial tensile stress, it is possible to locate this point in the $(I_1\text{-}\sqrt{J_2})$ space.

In principle, the closer this point moves to the yield surface, the more critical becomes the fatigue loading. The distance is indicated with $R_{initial}$ and called, here, "stress ratio". It is determined by equation (5.52). An example of the determination of Δ_i and Δ_{tot} by means of the maximum stress state in the 4PB fatigue test is shown in Figure 5.90.

$$R_{initial} = \frac{\Delta_i}{\Delta_{tot}} = \frac{\sigma_t}{f_t} \qquad (5.52)$$

Where;

Δ_i = distance of fatigue stress condition point from centre

Δ_{tot} = distance between a data point and yield surface along the line through original point and stress state point

σ_t = initial tensile stress in the 4PB fatigue test

If this point reaches to the yield surface ($R_{initial}=1$), it means that the mixture won't tolerate any further loading and the fatigue life ($N_{f,50}$) tends to one.

Therefore it is possible to correlate the fatigue life and R_{limit} by plotting $Nf,50$ on the y-axis and $R_{initial}$ on the x-axis; this will be shown here-after.

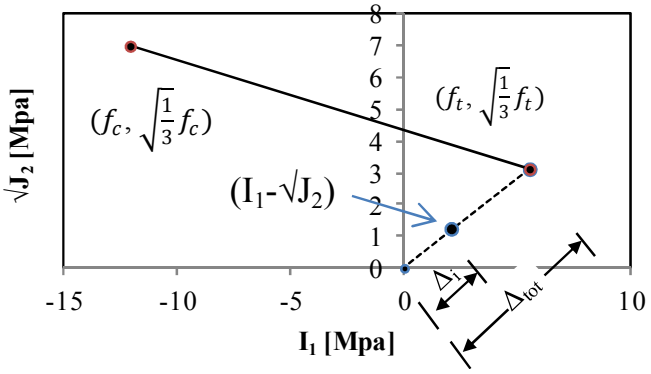

Figure 5.90 Yield surface determined by uniaxial tension and compression test results

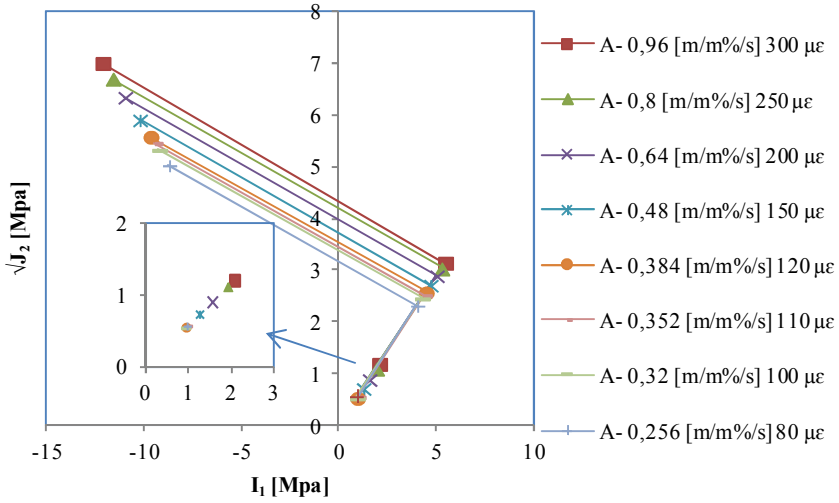

Figure 5.91 Yield surface line per strain level (mixture A)

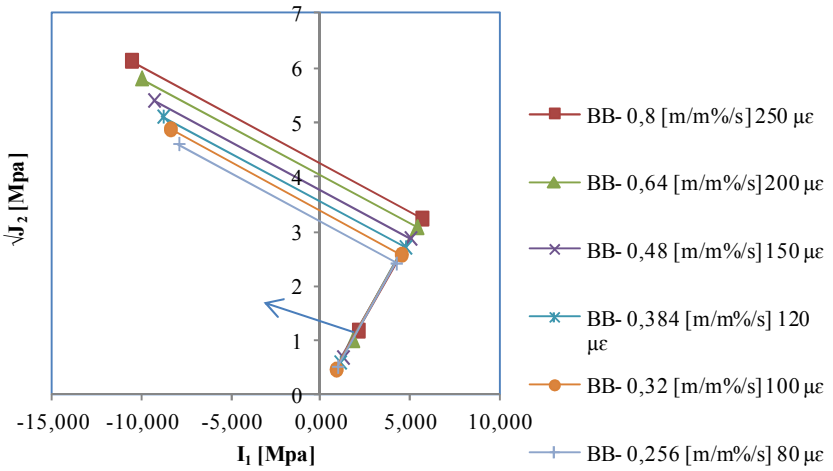

Figure 5.92 Yield surface line per strain level (mixture BB)

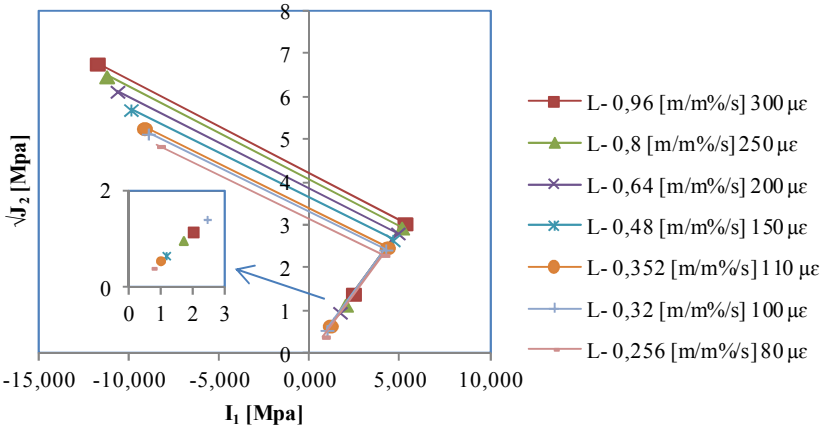

Figure 5.93 Yield surface line per strain level (mixture L)

$R_{initial}$ is determined for each fatigue test in relation to its yield surface and stress states in the 4PB fatigue test. The values are presented in Table 5.19,

Table 5.20 and Table 5.21 respectively for mixture A, BB and L. Since the fatigue data of mixture B was not available, $R_{initial}$ related to this mixture could not be determined.

Table 5.19 Determination of R $_{initial}$ (mixture A)

Specimen code	***Nf,50***	$\boldsymbol{R_{initial} = \frac{\sigma_t}{f_t}}$
A06	1.6E+04	0,380
A09	5.8E+04	0,364
A03	2.0E+05	0,310
A04	3.4E+05	0,266
A05	1.0E+06	0,210
A07	2.4E+06	0,223
A02	6.7E+06	0,217
A08	7.0E+06	0,240

Table 5.20 Determination of R $_{initial}$ (mixture BB)

Specimen code	***Nf,50***	$\boldsymbol{R_{limit} = \frac{\sigma_t}{f_t}}$
BB06	3.8E+04	0,367
BB05	7.7E+04	0,327
BB04	5.6E+05	0,241
BB03	7.5E+05	0,222
BB02	2.0E+06	0,183
BB01	1.0E+07	0,217

Table 5.21 Determination of R $_{initial}$ (mixture L)

Specimen code	***Nf,50***	$\boldsymbol{R_{limit} = \frac{\sigma_t}{f_t}}$
L01	7.4E+03	0,461
L02	5.7E+03	0,391
L03	6.5E+04	0,346
L04	3.5E+04	0,296
L06	2.4E+05	0,268
L05	5.6E+05	0,231
L07	5.6E+05	0,231

Once the $R_{initial}$ values of all fatigue test were determined, a relation between $R_{initial}$ and Nf was determined according to Li [67] by fitting the data points to equation (5.53).

$$R_{initial} = R_0 - R_1(1 - e^{-aN_f})^b \qquad (5.53)$$

Where:

R_0, R_1, a, b = regression coefficients

N_f = fatigue life

The R_0, R_1, a and b parameters for each mixture are given in Table 5.22. Figure 5.94 shows the plots of the stress ratio ($R_{initial}$) vs. fatigue life ($N_{f,50}$) for mixture A, BB and L. It shows that the fatigue life increases when the stress ratio decreases. Figure 5.94 also shows that the fatigue life tends to be infinite when the stress ratio becomes lower than certain values. The correlation coefficient (R^2) of this model for each mixture is also shown in Table 5.22.

All three predicted R-N lines are also summarized in Figure 5.95. This figure shows that the fatigue life tends to infinity if $R_{initial}$ tends to a certain value. This value is identified as R_{limit} and calculated according to the following equation in which R_0 *and* R_1 are the regression coefficients of the model.

$$R_{limit} = R_0 - R_1 \qquad (5.54)$$

Table 5.22 Model parameters of R-N line of each mixture type

Mixture type	***Regression Coefficients***				***R_{limit}***	***R^2***
	R0	*R1*	*a*	*b*		
A	0,377	0,155	5,6E-06	0,002	0,222	0,991
BB	0,405	0,205	2,3E-06	0,602	0,200	0,984
L	0,600	0,464	8,9E-07	0,147	0,136	0,935

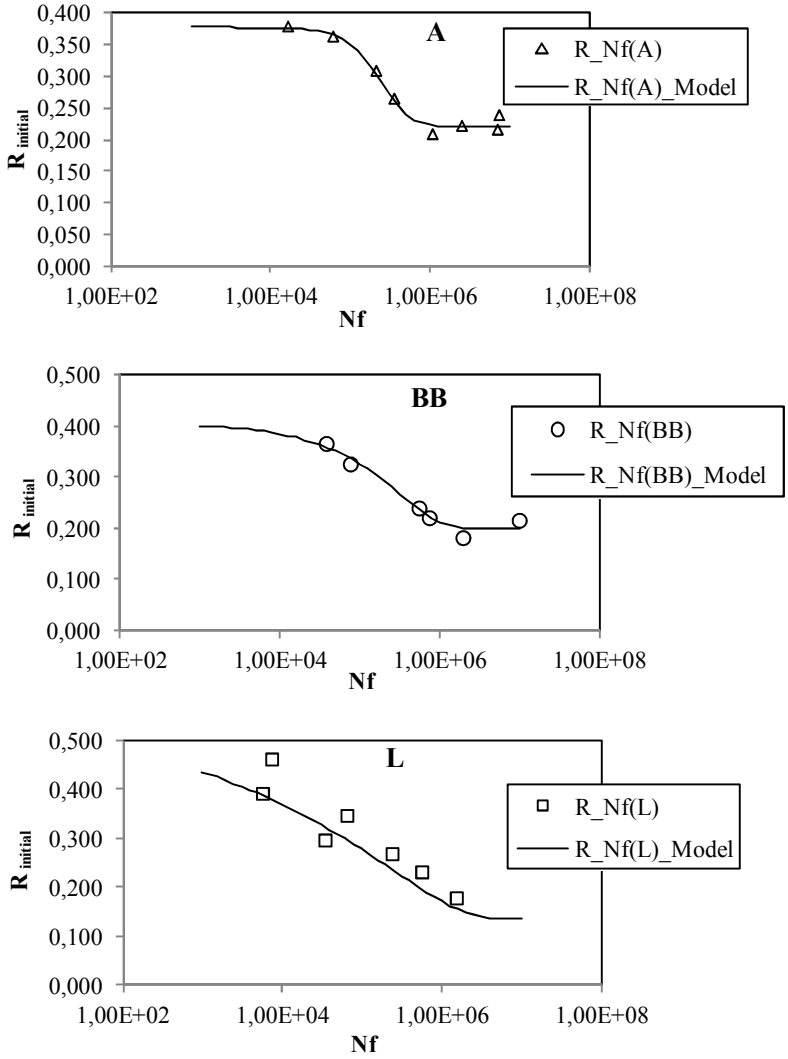

Figure 5.94 Correlation between $N_{f,50}$ (obtained from 4PB test) versus R_{Δ}

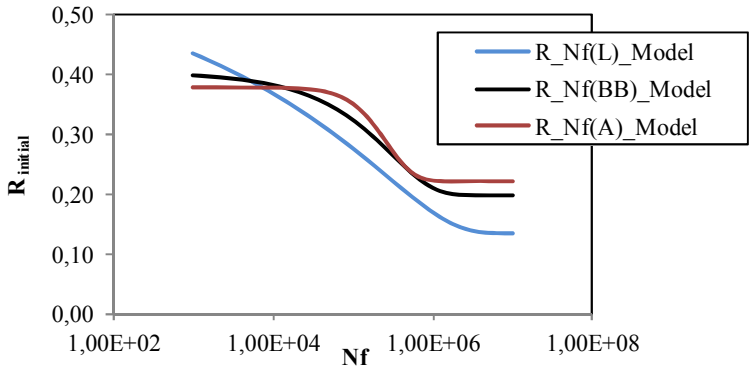

Figure 5.95 Comparison of predicted R-N lines of three mixture types

5.4.5. Fatigue endurance limit (FEL)

The fatigue endurance limit (FEL) is defined as the strain level below which fatigue damage does not occur for any number of load repetitions. Prowell et al [68] shows that an endurance limit exists for all asphalt concrete mixtures. Also Li [69] pointed out the existence of such a limit.

Hereafter the procedure which was initially developed by Li [69] is adopted to determine the FEL for mixtures A, BB and L. This procedure is based on the relation between R_{limit} and $N_{f,50}$ which was established in the previous section for mixtures A, BB and L. According to the protocol of Li [69] , the following expression can be used to relate the endurance limit (ε_{limit}) to R_{limit} when $N_{f,50} \rightarrow \infty$.

$$R_{limit} = \frac{\sigma_{limit}}{f_{t,limit}} = \frac{\varepsilon_{limit} \cdot S_{limit}}{f_{t,limit}} \Rightarrow \varepsilon_{limit} = \frac{R_{limit} \cdot f_{t,limit}}{S_{limit}} \qquad (5.55)$$

Where:

ε_{limit} = fatigue endurance limit [m/m]

$f_{t,limit}$ = tensile strength [MPa] under the strain level of ε_{limit}

σ_{limit} = initial stress [MPa] under the strain level of ε_{limit}

S_{limit} = initial stiffness [MPa] under the strain level of ε_{limit}

The relation between initial stiffness ($S_{m,initial}$) during 4PB fatigue test at different strain levels is plotted in Figure 5.96. According to this figure, there is no meaningful influence of the strain amplitude on the initial stiffness values at low and midrange strain amplitudes. Only some fluctuation around

the average value is observed. Therefore the mean value of $S_{m,initial}$ is used as a realistic approximation of the initial stiffness values at all 4PB strain levels.

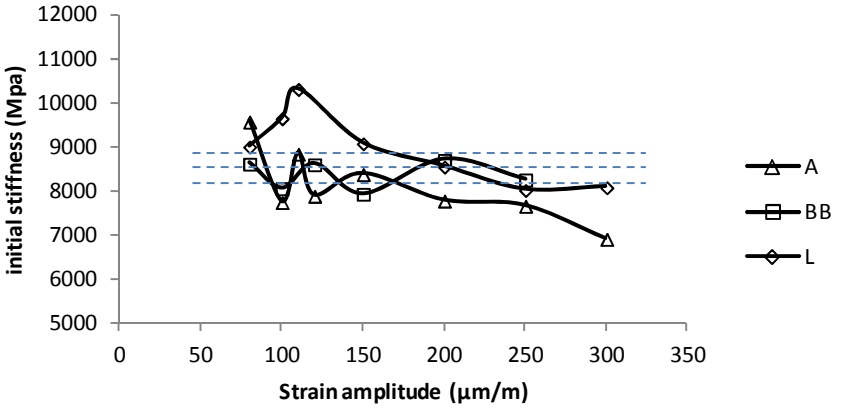

Figure 5.96 Initial stiffness values vs. Strain amplitude in the 4PB fatigue test

In section 5.3.5.5, the tensile strength of each mixture (f_t) was modelled by means of equation 5.33 and the model parameters were presented in Table 5.17. In this model P_i=0 and u_r and u_0 are the strain rates ($\dot{\varepsilon}$). Since $\dot{\varepsilon}$=4f×100ε (see equation 5.51), the tensile strength at any level of ε_{limit} can be expressed as follows:

$$f_{t,limit} = P_h + (P_h - 0) * e^{-\left[\frac{u_r}{u_0}\right]^{\gamma}} = P_h \left(1 - e^{-\left[\frac{4f(100\times\varepsilon_{limit})}{u_0}\right]^{\gamma}}\right) \qquad (5.56)$$

Where:

ε_{limit} = fatigue endurance limit [m/m]

$f_{t,limit}$ = tensile strength [MPa] (under the strain level of ε_{limit})

P_h , u_0 , γ = model parameters

f = loading frequency [Hz]

The $f_{t,limit}$ in equation 5.55 is substituted in the above mentioned expression as follows:

$$\varepsilon_{limit} = \frac{R_{limit}}{S_{limit}} * P_h \left(1 - e^{-\left[\frac{4f*100\varepsilon_{limit}}{u_0}\right]^{\gamma}}\right) \qquad (5.57)$$

The R_{limit} values determined for the three mixtures (A, BB, and L) are plotted against $S_{m,initial}$ in Figure 5.97 and a linear relationship between the two parameters was established. This linear regression is expressed in equation 5.58. Then it will be used to be substituted in equation 5.59.

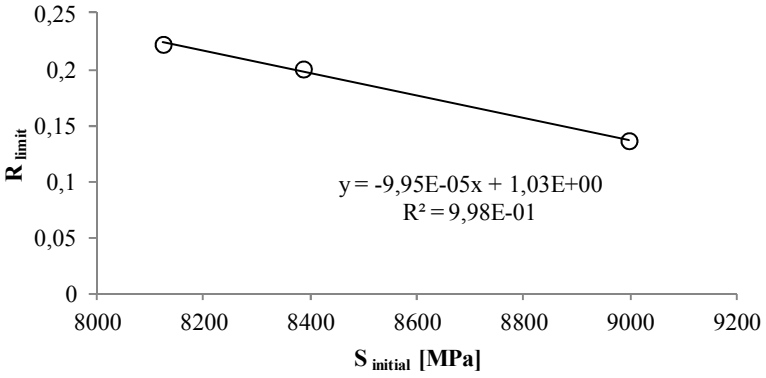

Figure 5.97 The relationship between R_{limit} and $S_{m,initial}$

The linear regression is expressed in equation 5.58.

$$\frac{R_{limit}}{S_{initial}} = \left(-9{,}95 \times 10^{-5}\right) + \frac{1{,}0321}{S_{initial}} \qquad (5.58)$$

Substitution in equation 5.57 and changing it leads to the following equation:

$$\varepsilon_{limit} = \left(-9{,}95 \times 10^{-5} + \frac{1{,}0321}{S_{initial}}\right) \times \left(P_h\left(1 - e^{-\left[\frac{4f(100\varepsilon_{limit})}{u_0}\right]^{\gamma}}\right)\right) \qquad (5.59)$$

Equation 5.59 shows that the endurance limit (ε_{limit}) can be determined if the mean values of initial stiffness of 4PB test ($S_{m,initial}$) and the model parameters of the unified model (for the monotonic tension test) are known. The parameters of each mixture which are required for solving the equation 5.59 are presented in Table 5.23. The results (per mixture) are also presented in the last column of this table.

It is found that the endurance limit for mixtures A, BB, and L is 124, 107, and 56μm/m, respectively. Mixture L has the lowest endurance limit value and mixture A has the highest value. Mixture BB has a value in between. The same trend was also found when comparing the fatigue line of the three mixtures. The formula shows that the stiffness of each mixture is also an influencing factor. As it was seen before, mixture A has lower stiffness values

in comparison to BB and L. According to this applied protocol, the type of mixing procedure has a significant influence on FEL. It is concluded here that the mixture produced in the laboratory with 50% RA at standard preheating conditions, results in a lower FEL than the plant produced mixture with similar composition but different preheating conditions..

The procedure, presented here, seems to be a practical and simple tool to express the endurance limit as a function of the tensile strength, loading frequency, temperature, and the mean value of the initial stiffness. The stiffness of each mixture can be determined by the 4PB test and the tensile strength values can be obtained with the Monotonic Uniaxial Tensile test (MUT) or even estimated following the procedure developed by Li [69].

Table 5.23 Required parameters for solving the equation of ε_{limit}

Mixture type	R_{limit}	$S_{initial}$	f_t model parameters			Calculated endurance limit
			P_h	u_0	γ	ε_{limit} [μm/m]
A	0,222	8123	7,5	0,495	0,396	**124**
BB	0,2	8386	7,5	0,397	0,461	**107**
L	0,136	8997	7,5	0,545	0,352	**56**

Note: The unit fo ε_{limit} in the equation solving was [m/m]

5.4.6. Conclusions and summary of Phase I and Phase II

The focus of this chapter was on the evaluation of the recycled mixtures which were produced in real plants. The goal was to analyze the effect of each mixing process on the final mixture properties. For this reason three mixtures of the same material and similar volumetric properties were produced in an ASTEC double drum (indicated by A), batch plant (indicated by BB) and in the Laboratory (L). Additionally, another mixture was prepared in the batch plant (B) in which the PARA (Porous Asphalt RA) was added partially (25%) to normal RA.

Mixtures were evaluated by conducting the following tests:

- 4PB flexural stiffness
- 4PB flexural fatigue resistance
- Uniaxial tension
- Uniaxial compression

The test results were used to determine fundamental behavior of each mixture by establishing master curves for the stiffness, the tensile and compressive strength. The fatigue results were analyzed by relating the applied stress conditions to the failure conditions which would occur at the same strain rate and temperature.

In this section the main findings of the testing program conducted on the four mixtures are presented.

1. In 4PB flexural stiffness tests, it seems to be more appropriate to take the average modulus value between the 50th and 60th loading cycle instead of taking the stiffness value determined at the100th cycle.
2. From the 4PB stiffness test it turns out that mixture L has a higher stiffness than A and BB. Mixture BB is slightly stiffer than A. Given the fact that A, BB, and L contain similar materials (with respect to binder, RA and aggregates) and volumetric properties, the short term aging of RA binder and virgin bitumen in the L procedure might be the primary cause of this. The significant different stiffness of L indicates extra aging because of the long RA preheating time in the oven at 170°C. For the BB mixtures, RA was preheated during a short period of time (less than 40 seconds) in a parallel drum dryer. Furthermore, mixture A has the lowest stiffness which is most probably due to the feeding of cold and moist RA in the double drum system.
3. It is very likely that mixing and diffusion between the RA binder and virgin bitumen may also occur during storage time and mixture handling prior to compaction. Therefore it is difficult to confirm the better blending and mixing of the laboratory mixture in comparison with batch plant and double drum mixtures.
4. Mixture B has the highest stiffness probably due to its initially stiffer binder.
5. Prediction of the fatigue line of each of the three mixtures (A, BB, L) was based on volumetric properties and material stiffness. It turned out that the Medani/Molenaar model could provide a reasonable prediction of fatigue properties of mixtures with high RA content which are produced in real plant.

6. The 4PB fatigue life in the displacement controlled mode (at 16.9° C and 8 Hz) is significantly influenced by the initial stiffness of the mixture.
7. Mixture L has the lowest resistance to fatigue in the 4PB test due to its higher stiffness in the displacement controlled test.
8. Mixture BB and A showed similar fatigue behavior in the 4PB displacement controlled fatigue test. However the fatigue resistance of A was slightly higher. That might be because A has a lower stiffness compared to BB.
9. Two main controlling factors during uniaxial tension and compression tests are temperature and strain rate. The strain rate control in tension was very sensitive to the level of the target strain rate. This was also true for compression testing, although to a lower degree. The strain rate control was more crucial in tension in comparison with compression tests.
10. Initially, tension and compression tests seem to be simple tests. However, they have to be done by experienced technicians because of complicated test conditions. Especially in tension tests, extra attention has to be paid to adjustment of strain rates and LVDTs because failure occurs suddenly at high forces.
11. The failure behavior in a tension test was most of the time brittle whereas in compression tests plastic failure occurred.
12. A visual inspection of the failure planes of all mixtures showed that RA material lost the bond with the new binder more easily than the virgin aggregates. Most probably this was due to the fact that the RA material contained a large amount of round, smooth shaped river gravel which has a low micro-surface texture. On the other hand the stiffer material around the RA aggregate may increase the stress concentration in its surrounding. The used virgin aggregate was of high quality and was made of crushed granite stone. Thanks to its angular shape and highly textured surface, the virgin aggregate therefore provided more surface area to increase the bond with the binder matrix at almost all temperatures and strain rates. The compressive strength of Mixture B seems to be higher than that of the other three mixtures. Mixtures A, BB and L have almost the same compressive strength. The reason may be the material composition properties of the mixtures. Mixtures A, BB and L were produced with the same material, whereas Mixture B included 25% reclaimed porous asphalt (RPA) together with 25% normal RA.
13. There was no remarkable difference between the tensile strength master curves. However, the slope of the master curve of mixture BB is slightly steeper than of the other three mixtures.

14. The method used in this thesis based on the protocol developed by Li et al [69] found to be a helpful tool to express the fatigue endurance limit (FEL) by means of some simple material properties (stiffness and tensile strength) at the right loading conditions (frequency and temperature). Using this expression would allow the prediction of the fatigue endurance limit without conducting time consuming fatigue tests.
15. The results of the FEL show that mixture A has the highest endurance limit in comparison with BB and L. the laboratory mixture (L) has the lowest FEL, probably due to its higher stiffness values.
16. In study phase I, the initial goal was to simulate the full scale process in the lab by means of the three mixing methods SM, PW, and UPG. In study Phase II, two real mixtures A and BB were studied, produced respectively with the Astec double drum and the batch plant equipped with a parallel drum to preheat the RA. The same mixture was also produced in the lab and is referred to as mixture L. Mixture SM and L were produced under similar mixing conditions. Similar preheating and moisture conditions were used for PW and BB and the same for UPG and A. However the amount of RA was not the same in the two phases. Summarizing the stiffness of the two phases shows that mixture "A" from the real plant like UPG with 4% moisture is softer than the others. Since the type of stiffness tests were different in the two phases of the study, it is not really possible to compare both values. The order of resistance to fatigue life (high to low) in phase I was UPG, PW and SM. The same trend was observed in Phase II where it was A, BB, L. Unfortunately the numerical values of the fatigue test results from the two phases are not comparable because of the different test types. The stress controlled IT fatigue test was used in Phase I and the strain controlled 4PB fatigue test was used in Phase II.
17. It is concluded that the mixing procedure and preheating conditions may have some influence on the mechanical properties of hot mix asphalt containing a high amount of recycled material. The binder properties and the amount of blending between the old and the new binder might be the reason for that. The influence of preheating conditions and the presence of moisture (in cold RA) should be studied more fundamentally. The importance of understanding the mechanism of blending and the interaction of hot aggregates and cold recycled material initiated a more fundamental study into the bitumen blending which is reported in PART 2 of this thesis.
18. It would also be interesting to check the mechanical properties of the mixture after a long period of service life.

PART 2



EXPLORATORY STUDIES ON MIXING, BLENDING AND DIFFUSION

CHAPTER 6



INTRODUCTION ON PART 2

6.1. Problem statement

Recycling of asphalt concrete is primarily the reuse of the components of old mixtures into new mixtures because its major components (mineral aggregates and bituminous binder) are still of use. During the service life of a pavement, the mineral parts of asphalt concrete remain almost unchanged. In contrast, the properties of the bituminous binder keep changing due to different types of aging during production/construction and service life.

The properties of the reclaimed asphalt (RA) can be easily evaluated and modified (with respect to gradation) by adding virgin aggregate prior to mixing into the new mixture. Other unchangeable characteristics of mineral aggregates such as mineralogy, angularity (influence of crushing) and texture have to be accepted as they are. Only the angularity is affected somehow by milling but this is hard to control.

On the other hand the bituminous part of old mixtures can be and has to be regenerated in the new mixture since it has significantly hardened due to short term and long term aging. The viscosity of the binder and other rheological properties has to be adjusted with respect to the job requirement.

The regeneration of RA binder is usually done by adding either liquid rejuvenator or softer grade binders depending on the recycling process.

If soft grade binder is added, the amount of virgin bitumen can easily be determined with respect to the percentage of RA and its bitumen content by means of blending charts which are based on the viscosity or stiffness of the new and old binder.

These issues were extensively discussed in Part1 of the thesis which basically focused on phenomenological aspects of hot mix recycling. The properties of mixtures containing different percentages of RA were investigated by simulating in the lab as good as possible the conditions in hot mix asphalt

plants. The properties of a mixture produced by two different asphalt plants, a double drum mixer and a batch plant (with parallel drum), were assessed in comparison with those of the same mixture produced with the standard laboratory mixing process. Special attention was given to the effect of the amount of RA, its moisture content and the preheating conditioning.

Since only slight differences were obtained between the mechanical properties of the mixture produced with different mixing methods, studying the fundamental aspects of blending between RA binder and virgin bitumen became important to understand the reasons for these small differences. Such a study would of course also be important and necessary if large differences between the mechanical properties were obtained.

It is evident that the mechanical properties of recycled mixtures are influenced primarily by their binder properties in cases where aggregate and volumetric properties are identical to the virgin mixture. It is very likely that the mixing process, preheating conditions and moisture content influence the blending between the RA binder and virgin bitumen. Furthermore, the interaction between the RA binder and virgin bitumen is influenced by the complex molecular structure of the virgin and RA bitumen. On the other hand, studying the interaction of two phases asks for distinguishing them from each other. This raised the issue of interface detection between two bituminous binders which are visually and physically difficult to distinguish.

The other challenge in understanding the fundamental principles of blending was studying the effect of different layers of bituminous coating around aggregates. First of all it required a technique to peel off the layers and secondly, an appropriate method of bitumen recovery from the solvent is essential since any remaining solvent (or filler) will affect the binder properties, while also the solvent itself might affect the characteristics of the binder.

6.2. Organization of Part 2

The reason to start an investigation on blending was to find answers for the questions about fundamental aspects of recycling related to blending between two binders. Answering of the fundamental questions will results in much better insight in what is happening during mixing, storage, transportation, and construction and to what extent blending between the RA and virgin binder is really occurring.

The following questions and challenges were addressed in Part 2 of the thesis:

1. How do superheated virgin aggregates influence the extent and quality of blending between the virgin and RA binder? This question

is especially of importance for the double barrel drum mixer but also for the batch plant with parallel drum at RA contents higher than 50%.

2. What is the consequence of exposing the RA binder and virgin bitumen to superheated aggregates in terms of their molecular microstructure?
3. Is it possible to characterize binders coating the aggregates layer by layer?
4. Is it possible to predict the blending and diffusion with a mechanistic approach?
5. How does the RA binder interact with virgin bitumen at their interface?
6. What are the possibilities in detecting RA, virgin and blended binders in a mixture?
7. How does diffusion happen between two binders with different grades? Is it possible to measure it?

This chapter is providing a literature survey on blending of binders in HMA recycled mixtures. Special attention is paid to the micro-structural aspect. In the literature also answers are searched for the above mentioned questions.

Chapter 7 is primarily dealing with questions 1 to 3 and a novel method is presented to distinguish and separate the RA material from virgin material by simulating each group with particular mono-sized glass beads. The essence of using artificial RA binder was to study and implement aging methods to simulate an aged binder comparable with the RA binder. Rheological analysis with the DSR is employed to evaluate the aging process. Fourier transform infrared spectroscopy (FTIR) was used to analyze the aging index of the artificially aged bitumen by measuring related absorption spectra at particular wavelengths. The results of this chemical analysis are compared to those obtained on the binder of a real RA sample taken from the stockpile at an asphalt plant.

In the literature some evidence was found for the fact that residual solvent and filler (as a result of the solvent extraction method) can influence significantly the results of the chemical and mechanical analysis. As a result of this uncertainty, a calibration method was used to study the effect of solvent extraction.

Another simulation was done by combining real RA aggregates and glass beads. Also in this case binders of separated virgin aggregates and RA aggregate after mixing were extracted and recovered to analyze the effect of superheating on the blending degree and binder properties.

In Chapter 8 (related to questions 4 and 7) a mechanistic method based on DSR analysis was used to study the possible diffusion between two binders with respect to time and temperature conditioning. A number of binder combinations in parallel and series order were tested.

Chapter 9 is devoted to questions 6 and 7 which are focused on diffusion of two bituminous binders. Sophisticated techniques such as nano-indentation and nano-computed tomography scanning were used to characterize the morphology of each binder as well as their interfaces. Optical microscopy was utilized to detect the distribution of two binders within a mixture.

6.3. Literature survey

6.3.1.1. Bitumen structure

It is necessary to have a good understanding of bitumen chemistry and bitumen morphology before starting any investigation related to the interaction of two different binders. Bitumen is a complex chemical mixture of predominantly hydrocarbons molecules with small amounts of structurally analogous heterocyclic species and functional groups containing Sulfur, Nitrogen and Oxygen atoms [10]. It consists of millions of similar but different molecules which are hydrophobic and insoluble in Glycerin, water and Methanol. More than 97% of the molecules have never been isolated, identified or characterized [70]**.** Chemically, bitumen is dominated by Carbon atoms. The composition of atoms in a typical bitumen molecule is illustrated in Figure 6.1. It consists of 78 atoms (32 Carbons, 44 Hydrogen, 1 Sulfur and 1 Oxygen).

Given the fact that various sizes of molecules are present in bitumen, it is impossible to identify every single molecule in a chemical analysis. It turns out that bitumen is characterized with functional groups. A number of separation methods have been established. The definition of the functional groups of bitumen molecules is based on the separation method used. Five major separation methods are identified in the literature being:

- Rostler-Sternberg separation
- Hoiberg separation
- SHRP Size Exclusion Chromatography (SEC)
- SHRP Ion Exchange Chromatography (IEC)
- SARA separation

Three different methods are used mostly in SARA analyses. The most popular method is Iatroscan. With this technique four fractions named Saturates, Asphaltenes (polar), Resins (polar aromatics), and Aromatics (non-polar,

cyclic) can be separated. It divides bitumen fractions due to their capability of being polarized (see Figure 6.2). Asphaltene fractions are basically the largest groups in the sense of their molecular weight which is between 10^3 and 10^4 g/mol. In contrast, Saturates have a molecular weight of 300-2000g/mol.

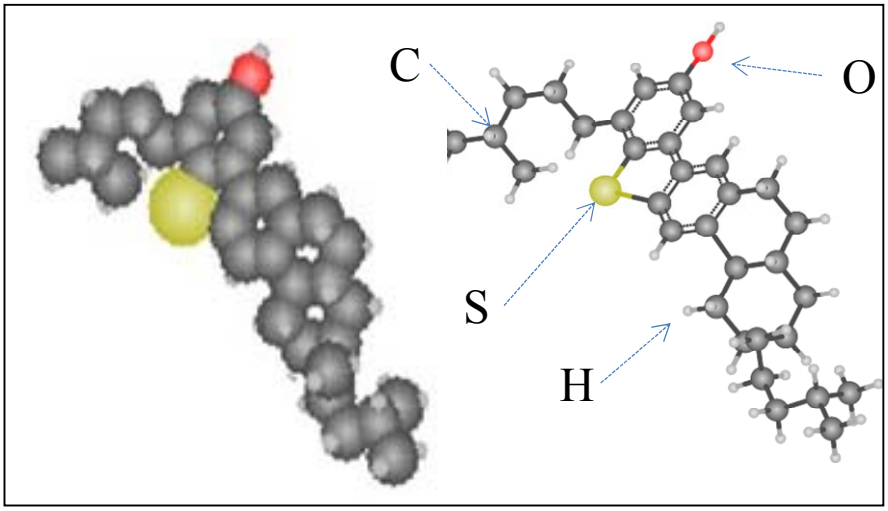

Figure 6.1 Composition of a typical bitumen molecule [70]

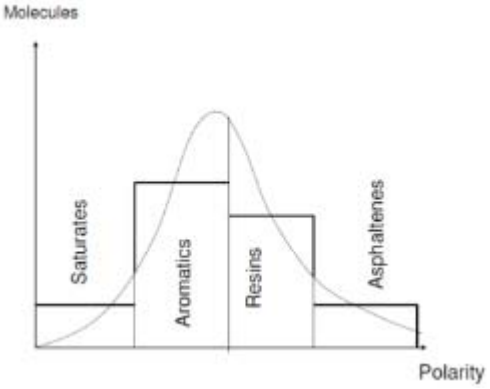

Figure 6.2 Comparing the polarity of SARA fractions [10]

The chemical structure of bitumen has been argued widely among chemists. Different models are proposed. Some of them believe in a multiple-phase

system (traditional approach) [71]. Recent studies emphasize single-phase systems [72].

Nellensteyn [71] proposed that bitumen contains micellar colloids or dispersions of asphaltene particles in a maltene phase assuming that asphaltenes are insoluble. This colloidal model of bitumen originated from a study by Mack [73]. He studied rheological properties of bitumens and concluded that bitumens are colloidal. He believed that asphaltenes as a separate phase are dispersed in a maltene phase as large agglomerations in which aromatic components stabilize them. Based on the colloidal nature of bitumen, Labout [74] suggested two types of bitumen, Sol-type and Gel-type. He proposed that the Sol-type bitumen has a highly aromatic maltene phase and that the asphaltenes are thoroughly dispersed to a degree that they don't form any associations. In contrast, gel-type bitumens have less aromatic maltene fractions and the asphaltenes are not dispersed thoroughly and consequently associate to each other to form agglomerations. These agglomerations may result in networks at higher asphaltene contents. These two types of bitumen, a Sol and Gel type bitumen are illustrated in Figure 6.3.

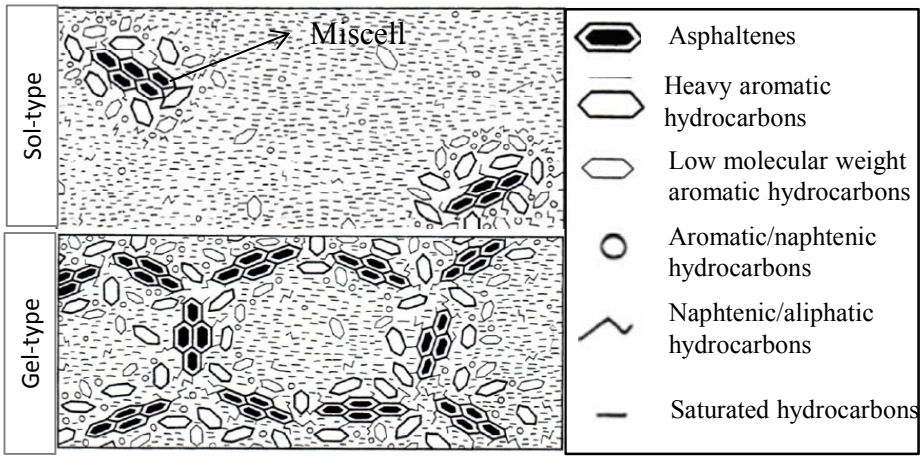

Figure 6.3 Bitumen colloidal model based on Gel and Sol-types [10]

Van der Poel [75] characterized the Sol and Gel types by means of a well-developed scheme based on their rheology. He concluded that in Sol-type bitumen a rapid transition develops from the glass point to Newtonian flow. By contrast this transition happens gradually in Gel-types.

Modifications have been made to the colloidal model by a number of scientists. Pfeiffer and Saal [76] hypothesized that the dispersed phase in bitumen colloid systems is composed of an aromatic layer, which is

surrounded by layers of less aromatic molecules. X-ray diffraction studies by Yen [77] confirmed the principles of a colloidal system.

Altgelt [78] explained bitumen rheological behavior on the basis of stacking of condensed aromatic structures.

The principle of a colloidal system has been widely used by many researchers since it could be reasonably related to the rheological properties of bitumen.

However, the colloidal model of bitumen has been criticized because of the discrepancies between the original definition of colloids and the one used for bitumen.

The model of a bitumen structure proposed by Pfeiffer and Saal, which is an elaboration of the model suggested by earlier researchers, specifically disagrees with the existence of a sharp boundary between the solvent (maltene) and dispersed (asphaltene) phases in bitumens, but proposes an aromaticity gradient instead. Therefore it may be inappropriate to describe this model as colloidal, because it allows no dispersed-phase surfaces. The term *phase* also may be inappropriate when applied to bitumen components [72].

In contrast to the colloidal system, a Single-Phase system was introduced by SHRP [72] which asserts that bitumen is a continuous, homogeneous material the flow characteristics and performance of which are based on the molecular size distribution and the polar forces holding the molecules together. According to Peterson and Harnsberger [79], bitumen is considered as a dispersion of strongly associated polar molecules in a solvating medium composed of less polar bitumen molecules. Because polar molecules associate together, polar oxidation products strongly change the state of dispersion of binder components, thus changing the mobility and, therefore, the chemical reactivity of binder molecules and its susceptibility to oxidation..

6.3.2. Physical and chemical aspects of RA binder

Given the fact that the binder in most HMA recycled mixtures is a combination of a virgin binder and the RA binder, it is essential to study the chemical and physical differences between them. The RA binder can be characterized as bitumen which is aged during production, construction and service life. Like the virgin bitumen it is also exposed again to extra aging during HMA recycling.

Understanding the difference in chemical properties of RA binders would be helpful in detecting the interface between RA binder and virgin bitumen for blending and diffusion studies. Given the fact that the chemical composition of bitumen affects the mechanical properties of asphalt concrete, knowledge

of the chemical composition of the RA binder leads to a better understanding of the properties of recycled mixtures as well.

A major consequence of aging of a binder is hardening due to chemical changes. However, hardening may also take place physically due to "steric hardening" which is reversible. Physical hardening may be related to the crystallization of waxes in bitumen.

Oxidation is the major reason for chemical changes in bitumen. The hardening because of oxidation is irreversible. Oxidation primarily affects the polarity of molecules whereas oxygen makes strong bonds with molecular groups such as sulfoxides, carboxylic acids, and ketones. The strong bonds of these molecular groups result in a higher viscosity.

Elevated temperatures during HMA mixing and construction facilitate oxidation. Aging also occurs at ambient temperature during the service-life of the pavement.

Evaporation of volatile components of bitumen is believed to be another reason for hardening. It may occur at the elevated temperatures during mixing, storage, transportation and laying of the material.

Volatile components may also be absorbed in the aggregate surface. This is known as exudative evaporation.

Important factors that determine to what extend the RA binder is aged are: the mixing temperature, service life temperature, binder film thickness, voids content of the mixture, mineralogy of the aggregates. The source of RA is also a decisive factor. RA which is milled from porous asphalt surfaces is different from RA of base courses, because the latter is hardly exposed during service life to oxygen and other environmental factors.

Comparison of the rheological properties shows that RA binder generally has a higher viscosity, lower penetration, higher softening point ($T_{R\&B}$) and higher shear modulus (G*) than the original binder.

All in all, an RA binder is an aged binder as a result of all the above mentioned aging processes. Therefore in some researche [37], artificial aged binders have been used instead of real RA, because in this case the initial properties of the artificial aged binder are known.

6.4. Aging index

For the purpose of making an artificial RA binder, a virgin binder has to be aged to a predetermined extent. The extent of aging is measured by aging

indicators. They are based on either a chemical analysis or rheological measurements.

Aging indicators are basically determined by comparing certain properties and in most cases the ratio of the property after and before aging is used.

Some rheological properties have been widely used as aging indicators [4]. Examples are retained penetration, change in Ring and Ball temperature, retained G* and retained viscosity.

Also chemical parameters are used in characterizing the amount of aging. A comparison between functional groups (SARA) is sometimes used as aging indicator. For example the Gaestel index (IC) is used [80] to show the changes in asphaltenes and saturates content compared with the aromatic and resins content as it is assumed in the colloidal model for bitumen.

$$IC = \frac{Asphaltenes + Saturates}{Aromatics + Resins} \qquad (6.1)$$

Aging indicators are also derived from FTIR spectrum analyses. The areas around certain peak values are used to calculate aging indicators. Band areas around 1700 cm^{-1} (C=O, ketones) and 1030 cm^{-1} (S=O, Sulfoxide) have been used to calculate an aging index for ketones (ICO) and an aging index for sulfoxide (ISO) as shown in formulas (6.2) and (6.3):

$$\text{ICO} = \frac{\text{Area around } 1700 \text{ cm}^{-1}}{\text{Area around } 1460 \text{ cm}^{-1} + \text{ Area around } 1375 \text{ cm}^{-1}} \qquad (6.2)$$

$$\text{ISO} = \frac{\text{Area around } 1030 \text{ cm}^{-1}}{\text{Area around } 1460 \text{ cm}^{-1} + \text{ Area around } 1375 \text{ cm}^{-1}} \qquad (6.3)$$

6.5. Microstructure of the RA binder

The RA binder as an aged bitumen could be characterized by its microstructure in comparison to virgin bitumen. It has been found that any physical changes (due to loading or temperature) and chemical changes (aging or blending) may affect the string shape of the highly aromatic asphaltenes network. Stangl e.a. [81] observed this network by means of ESEM (Environmental scanning electron microscope). Figure 6.4 shows an ESEM image of a bitumen surface observed by Stangl. The string like structure in this figure is shaped because electron beams during ESEM volatize the low molecular weight fractions whereas the higher weight fraction (consisting of

resins and asphaltenes) remains. Stangl tried to model this structure by drawing this string structure by means of lines passing through the middle of the string axis. He determined the average diameter of the ring shaped by strings at approximately 20 µm.

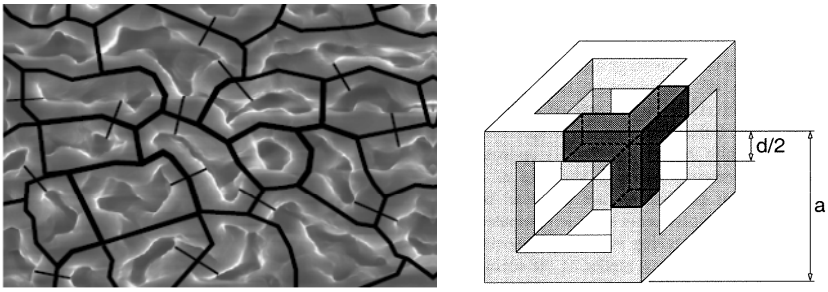

Figure 6.4: Example of quantification of properties of bitumen microstructure from ESEM images (left), creation of a string shape network of asphaltenes and resins (right). Modelling of the string network in string diameters is shown by "d" and the spacing between two adjacent strings is shown as "a" [81]

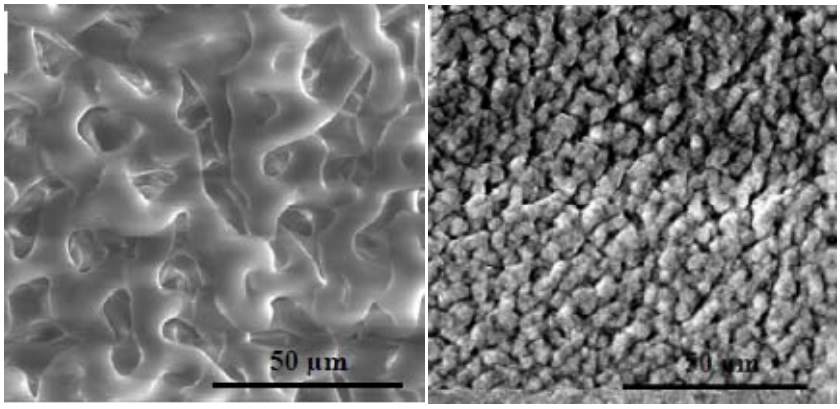

Figure 6.5: ESEM images: (left) 50/70 un-aged bitumen, (right) 50/70 aged bitumen after RTFOT+PAV [81]

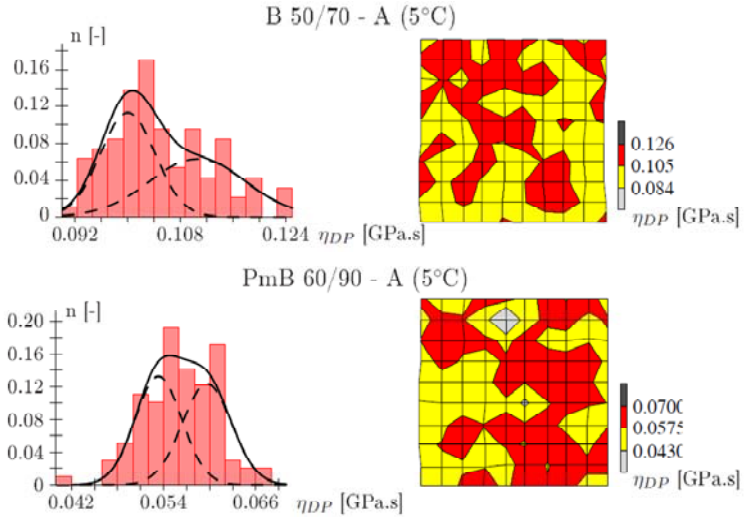

Figure 6.6 Viscosity η [GPa s] for B 50/70-A (top left) and PMB 60/90-A (bottom left)tested at 5 °C: frequency plots and corresponding grid plot (plots on the right are showing the viscosity of each point at the bitumen surface measured by nano indentation) [81]

He showed that the microstructure of bitumen may change due to aging. In Figure 6.5, the microstructure of an RTFOT+PAV aged bitumen (pen 50/70) is compared with the original one before aging [81].

The variation in stiffness and viscosity differences among different groups of molecules in bitumen could be used as a criterion to map their physical structure in the bitumen. With nano-indentation it is possible to measure stiffness and viscosity locally by indenting a diamond tip on the surface of a material. It has also been used to map the microstructure of bitumen (e.g. Jager [82]). He used a back calculation analysis with a creep compliance model to map the viscosity on the indented points at the surface of bitumen (Figure 6.6). He showed some conformity between the ESEM images and mapping results from the nano indentation.

Atomic force microscopy has also been utilized to detect the bitumen microstructure by phase detection on the surface with the so-called tapping mode (see Figure 6.7). The “bee structure” created on the surface is claimed to be related with asphaltenes or waxes in the bitumen [83]. These bee structures could vary due to the chemical composition of bitumen. However, the relation between bee structures and asphaltenes has been criticized.

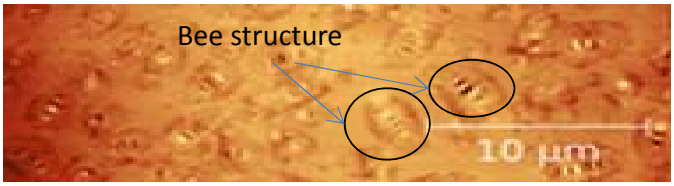

Figure 6.7 Bee structure in AFM [83]

6.6. Conclusions of the literature review

The main conclusions of the literature review are:

1. Bitumen is a complex material. To understand its behaviour different simplified imaginary models of molecular structures in bitumen have been proposed based on multiple and single phase perceptions.
2. The micro structure of bitumen could transform by any physical and chemical change such as temperature, aging, loading rate. Therefore RA binder may be distinguished by its molecular differences from the un-aged binder.
3. Various techniques are available to observe the bitumen microstructure such as nano-indentation and atomic force microscopy.
4. Simulating RA binders by means of artificial aging of virgin binders should be measured and evaluated by aging indicators. Because of the complex nature of bitumen, a single indicator is not enough for simulation of RA binders and a combination of them is recommended.
5. In the literature limited research was found in relation to the seven questions (in section 6.2), therefore exploratory studies are conducted which will be reported in chapters 7, 8, and 9.

CHAPTER 7



BLENDING OF RA AND VIRGIN BINDER AND THE EFFECT OF SUPERHEATED AGGREGATE

7.1. Introduction

In the Netherlands, hot mix asphalt containing high percentages of reclaimed asphalt (RA) is produced by either a batch plant to which a parallel drum is attached to preheat the RA to approximately 130°C, or by means of a double barrel drum. In the double barrel drum virgin aggregates are preheated in the inner drum and then mixed with moist RA of ambient temperature in an outer drum which is folded around the inner drum. In the outer drum also the virgin fines (filler) and bitumen in quantities as determined by means of the mixture design are added. Since the mixing temperature is between 160 – 180°C, the virgin aggregates have to be preheated to (very) high temperatures, especially when high RA percentages are used. In the Netherlands, using 50% RA is common practice for all base, binder and most wearing course mixtures. The only real exception is that RA is not allowed in SMA. Porous asphalt concrete mixtures are only allowed to have an RA percentage up till 25%.

It is not uncommon to preheat the virgin aggregates to 320°C and higher in the double drum mixer to obtain a temperature after mixing of 160°C. Especially when the RA is moist, moisture contents of 5% are not uncommon in the Netherlands, even higher preheating temperatures are required.

Also in a batch plant, the virgin aggregates are heated to fairly high temperatures, even when the RA is preheated in a parallel drum to 130°C. The virgin aggregates should be heated to much higher temperatures when larger amounts of RA than 50% are used.

It might very well be that the heat transfer between superheated aggregates and binders may locally damage both the RA and virgin bitumen. Therefore it is essential to study the effect of this kind of harsh heat transfer on the binder properties.

The target average temperature after mixing (160-180°C) is usually achieved by adjusting the preheating temperature of the aggregates in both the batch plant and double drum mixer. The process of interaction between RA and superheated aggregate in the double drum mixer is explained in detail in section 1.2.1.3.

In order to understand the impact of the above on the final mixture behavior two important questions should be answered:

- Will the superheating of virgin aggregates soften the RA binder enough to make the RA binder coat the virgin aggregates before the virgin bitumen is added?
- Will the RA binder and virgin binder blend such that a homogeneous binder is obtained?

These two questions initiated the research which is presented in this part of the thesis.

7.2. Experimental design

In order to be able to answer these questions it is necessary to determine the amount and characteristics of the binder that has coated the RA and virgin aggregates (VA) after mixing. However, the major difficulty in studying the interaction between RA binder and virgin bitumen is the separation of RA aggregates from VA in the recycled mixture, because they cannot be distinguished from each other since each aggregate particle is coated with black binder and the shape of the RA and VA particles is similar.

Since distinction by color differences between aggregates is not applicable, a novel method was devised in this research by using mono-size glass beads (GB) as artificial aggregates instead of real aggregates. RA could then be separated from VA because of the different shapes and sizes. It will also be shown that a combination of GB and RA was a good representation of a real mixture.

Three mixture combinations were designed to study the effect of superheating in HMA recycling by replacing real stone aggregates with glass beads. These combinations will be explained in detail in section 7.5.5.3.

Also an aging method was adopted to create artificial RA binder. The Rotating Cylinder Aging Test (RCAT) was used for this purpose. Two grades of bitumen were aged using different aging periods and their chemical and physical properties were determined. The properties of the artificially aged binder were compared with those of real RA binder. Based on the results an aging protocol was selected.

Once artificial RA aggregates were separated from virgin aggregates, their binders had to be extracted for further analysis. In case of real mixtures, a centrifugal extraction method along with a rotary evaporation setup is used to obtain sufficient binder for analysis. However, the current extraction and recovery setups are not suitable to recover small amounts of bitumen. Therefore the standard extraction and recovery method could not be used. A simple extraction and recovery method was devised based on solvent extraction and cabinet evaporation. The efficiency of this extraction and recovery approach was also investigated.

It was assumed that the aggregates were surrounded with different layers of binders. This assumption was based on results reported by Noureldin and Wood [84] and Huang et al [31] which will be discussed later. Inspired by their work, the effectiveness of separating the bituminous coating of aggregate particles into different layers was examined.

If a layered system indeed appears to exist then it should be determined how mixing of super-heated aggregates with cold RA affects the binder properties of the different layers. It would be an indication blending efficiency.

The following actions were therefore undertaken:

- an aging protocol was adopted;
- an extraction and recovery method was developed;
- the effectiveness and usefulness of a stage extraction method based on soaking in solvent was evaluated;
- three types of mixtures were produced;
- rheological and chemical properties of binders were compared.

7.2.1. Mixtures

In this study three mixtures were tested:

Mixture 1

Glass beads of 5mm (GB5) were coated with aged binder to create artificial RA. No filler is used in this mixture type to avoid any interference of filler presence in the binder analysis. Glass beads of 8mm (GB8) were used to represent the VA. In one experiment GB8 was superheated to 300 °C and in another experiment to 400 °C prior to mixing with GB5. These two temperatures were selected to study the effect of temperature. Mixture type1 is identified in this chapter with “300-” and “400-”. 50% superheated GB8 was mixed within 30 seconds with 50% pre-coated GB5. The flow chart for preparing mixture type1 and experiments is illustrated in Figure 7.1.

Mixture 2

Similar combinations of GB sizes, percentage and temperatures were also used to prepare mixture type 2. The only difference was that 1% virgin bitumen (VB) was also added during mixing. Mixtures of type 2 are identified by "300+" and "400+". The plus sign indicates the addition of VB where the minus sign in type 1 implicates no addition of bitumen. The flow chart of this experiment is also illustrated in Figure 7.1 .

Mixture 3

A real asphalt mixture was produced with 50% real RA. Only virgin aggregates were replaced by glass beads of different sizes. Filler, sand and virgin bitumen were added according to RAW2005. The used GB sizes were determined based on the mixture gradation requirements. GBs were superheated to 515°C prior to mixing; the real RA contained 4% moisture. The mixing time was set to 30 seconds. The flow chart of this experiment is also illustrated in Figure 7.2.

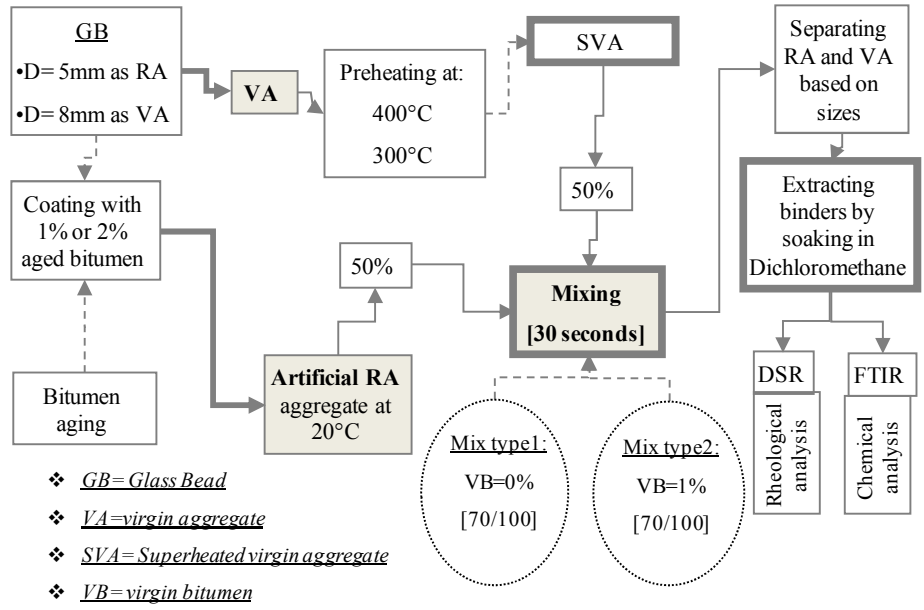

Figure 7.1 Experimental plan for mixtures 1&2

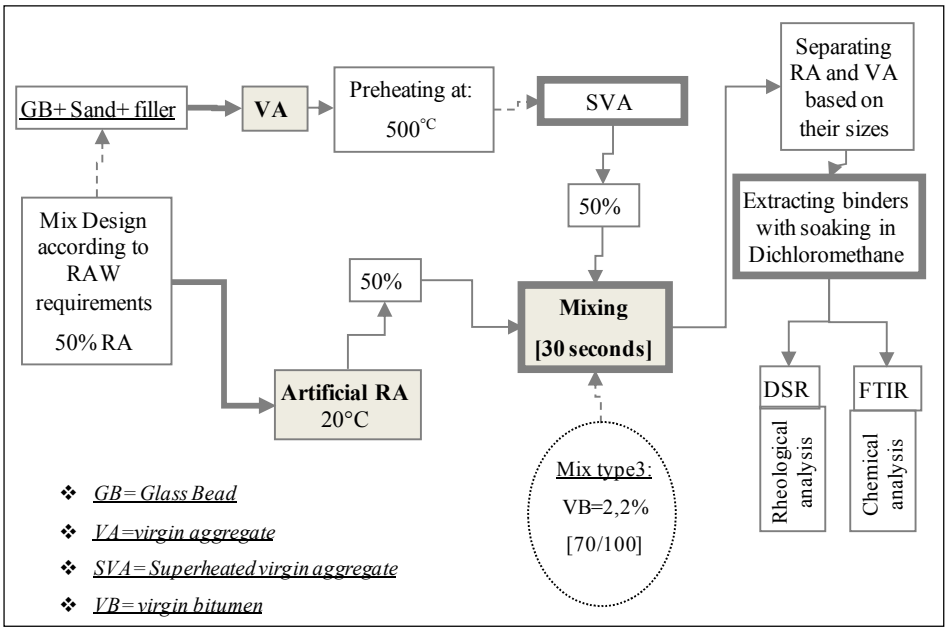

Figure 7.2 Mixing process of mixture 3

7.3. Materials and processes

As noted, artificial materials (GB and aged bitumen) were used to simulate real aggregates and RA binder. The material properties and preparation processes will be discussed in this section.

Three preliminary studies were required before conducting the main study on the effect of superheating. First of all the effectiveness and usefulness of stage extraction by soaking bituminous material in a solvent had to be investigated. Secondly, a convenient binder extraction and recovery method had to be developed. Thirdly, an appropriate aging protocol had to be established to obtain an artificial aged binder with properties as close as possible to those of a real RA binder.

In this section the development of these three processes as well as other material preparation techniques will be described. The mixture designs, mixing process and sample preparation will be discussed here as well.

7.3.1. Development of extraction and recovery method

In HMA recycling studies, binder extraction and recovery are essential processes in regaining the binder from RA. The binder is primarily needed for rheological analysis prior to designing a mixture. In addition a chemical analysis of RA binder or any aged binder was done to study the effect of aging on the original binder.

Extraction was firstly done by soaking an AC mixture into a solvent (such as Dichloromethane[18]) at ambient temperature to separate aggregate, sand, and filler from the binder. Secondly, the mineral fraction was physically separated from the binder solution in a centrifuge. These two steps of extraction are commonly practiced in the Netherlands according to NEN 3971 [85].

The bitumen is usually separated from the solvent via a rotary evaporation system at a rather high temperature (80, 150 and 175°C) according to EN12697-3 [86]. Those extraction and recovery setups are not suitable when small amounts of bitumen need to be recovered. Therefore another extraction and recovery method had to be developed.

A "simple" extraction and recovery method was developed in this research based on solvent extraction and cabinet evaporation. The efficiency of the extraction and recovery was also investigated. A similar method was used by Qiu in the LVO[19] project in 2012.

The method used here is referred to as the "Solution Spreading Extraction Method" (SSEM). The procedure is as follows:

- Step 1: a small amount of aggregate (about 50 grams) is washed manually in Dichloromethane by agitating manually for half an hour. 100 ml solvent is usually sufficient to get the aggregates clean.
- Step 2: the filler is separated from the bitumen in a desk centrifuge in the laboratory. The solution is filtered with a micro filter (0.6 micron) and centrifuging is done at 3700 rpm for 30 minutes.
- Step 3: the solution is carefully and gently taken from the centrifuge container to avoid remixing it with filler sediment.
- Step 4: the residual solution is spread on a surface of silicon paper with dimensions of 25×25 cm to facilitate the evaporation of the solvent at ambient temperature in a vacuum cabinet for 24 hours.

[18] Methylene Chloride (CH_2Cl_2)

[19] Levensduur verlengend onderhoud voor asfaltverhardingen

- Step 5: after 24 hours the residual thin binder film is brought into an oven at 50°C for 3 hours to ensure complete evaporation of the solvent.

The experimental design related to this preliminary study is shown in Figure 7.3. Two binders were tested being:

(1) 70/100 virgin bitumen (3.66 gr) + filler Wigro (4gr) + Dichloromethane (100 ml);

(2) RCAT163°C-24hr aged 70/100 bitumen (4.0 gram) + filler Wigro (4gr) + Dichloromethane (100 ml);

In the above mentioned solution, filler was poured in the solution of bitumen and solvent before centrifuging of the solvent.

After binder recovery, they were tested in a DSR to compare the properties of the SSEM extracted binder with the properties of the original bitumen. The DSR was conducted with a parallel plate geometry using plates with a diameter of 25mm and a 1mm thick layer of binder in between (Temperature range of 30-60C and frequency 0.05-50 Hz).

Master curves for the complex shear modulus G* were developed and these are shown in Figure 7.4. G* values at 20°C and various frequencies are also shown in Table 7.1. It turns out that the shear modulus of the binder extracted by means of the SSEM is in reasonable agreement with that of the original binder. Nevertheless the G* values are slightly lower after SSEM. This reduction might be because small amounts of solvent are still left in the binder. The reduction of 10-20% in G* values was observed for both the aged and virgin bitumen.

Table 7.1 Decrease in G values at 20°C after extraction*

Frequency	***0,1 Hz***	***1Hz***	***10Hz***	***20Hz***	***100Hz***
RCAT_Before extraction [MPa]	1,46	5,47	16,52	22,13	40,76
RCAT_After extraction [MPa]	1,10	4,42	14,27	19,46	37,20
Decrease in G* value	**-25%**	**-19%**	**-14%**	**-12%**	**-9%**
70/100_Before extraction [MPa]	0,15	1,01	5,37	8,43	21,75
70/100_After extraction [MPa]	0,11	0,78	4,33	6,89	18,36
Decrease in G* value	**-24%**	**-22%**	**-19%**	**-18%**	**-16%**

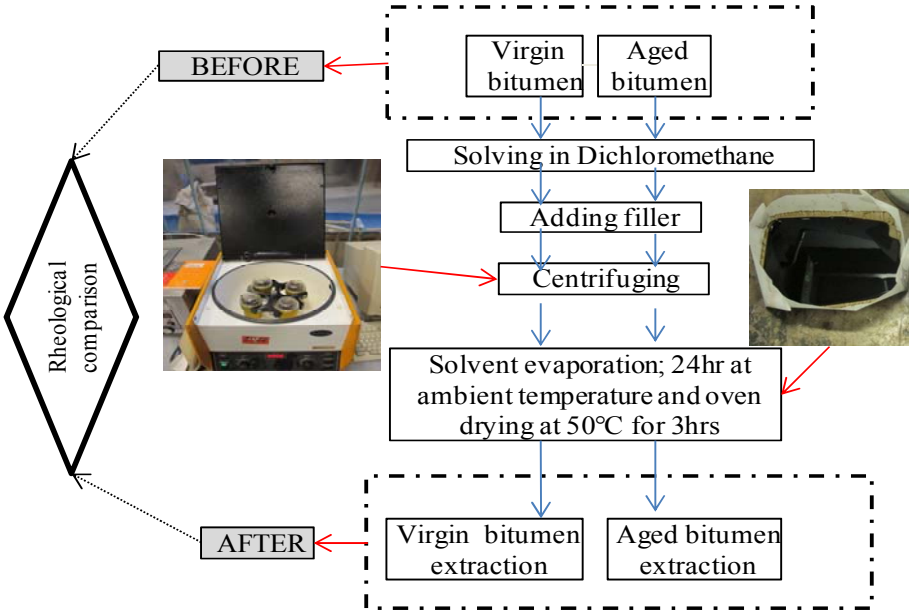

Figure 7.3 Flow chart of the research to study the effect of the solution spreading extraction method (SSEM)

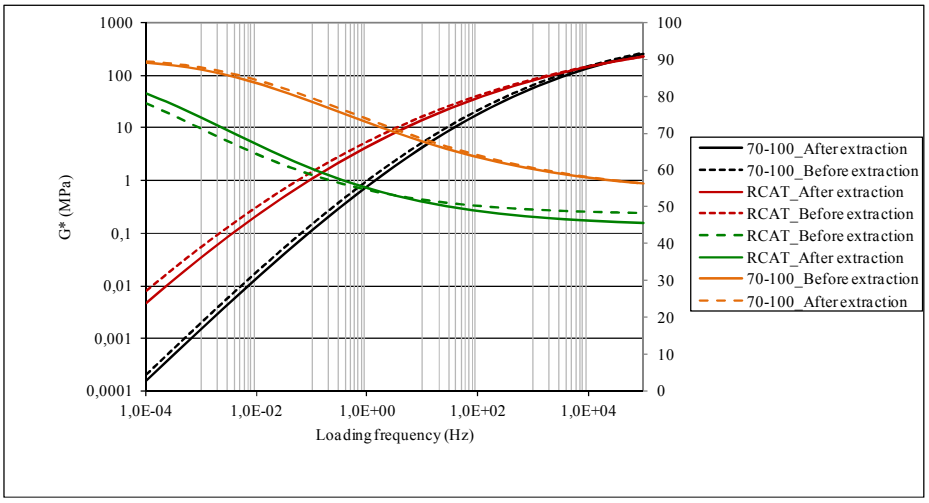

Figure 7.4 Comparison of G master curves (at 20°C) before and after extraction with SSEM.*

7.4. Stage Extraction

7.4.1. Background

Stage extraction has been practiced since 1980 by a number of researchers [87], [88]**.** It is a process of extracting binder from RA particles, layer by layer. It is repeatedly assumed that if RA aggregate is soaked in a solvent for a given period of time, the recovered binder corresponding to each soaking time is representing a layer of bitumen.

Noureldin and Wood (1987) conducted a test on a recycled mixture by applying a rejuvenator on RA aggregates [87] .They soaked RA aggregates in a solvent and took 4 binder solutions, each after a certain predetermined period of time. After recovery of the binder from each solution, they measured its penetration and viscosity. The penetration test results of the 4 imaginary layers are shown in Figure 7.5.

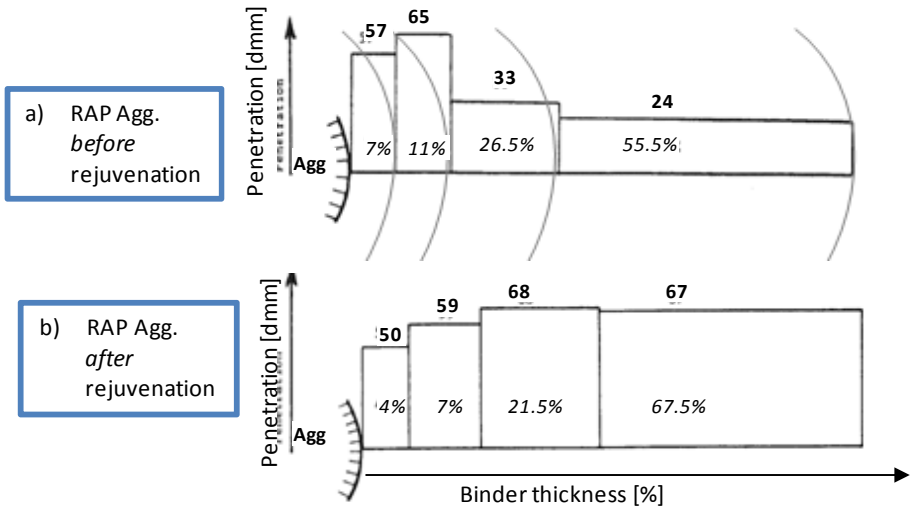

Figure 7.5 Penetration results obtained from imaginary layers on RA and rejuvenated RA binder by Noureldin and Wood [87]

They concluded that the outer (micro) layers are stiffer than the inside layers because of the exposure to the oxidation. They believed that the very inner layer is slightly harder than the next layer, because of the absorption of light fractions by the aggregate. A similar concept was used by Huang et al (2005) to extract four layers of binder as shown in Figure 7.6 [88].

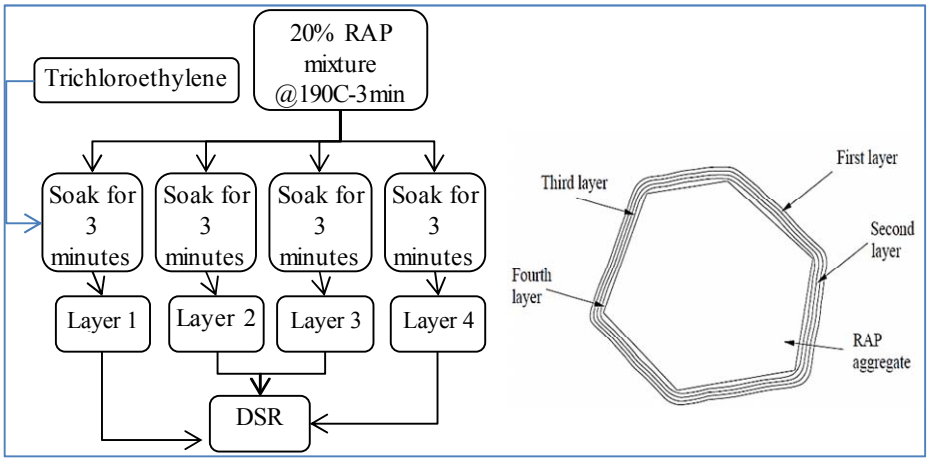

Figure 7.6 Process of stage extraction according to Huang et al (2005) [88]

After conducting DSR tests, they claimed that the inner layers are stiffer than the outer layers (see Figure 7.7), implying that inner layers are RA binders which are not completely blended with added virgin bitumen.

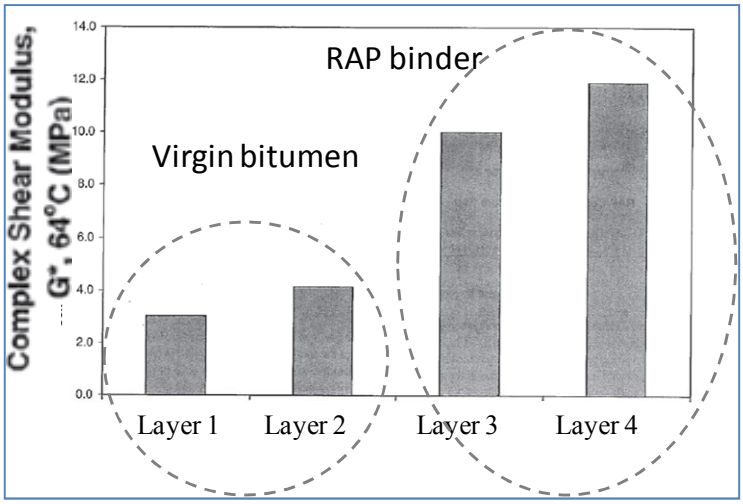

Figure 7.7 G values of imaginary layers of bitumen according to Huang et al (2005) [88]*

In both research experiments, only one variable was taken into account, namely the soaking time. It was assumed that the solvent will take an equally similar amount of binder from every aggregate particle. As will be shown

here-after, this assumption is only true if all the aggregate particles have the same size whereas the aggregate sizes in the mentioned experiments were ranging from 20 to 20,000µm. Later on it will be shown that the aggregate sizes have to be taken into account as extra variable.

The test program that was conducted here to examine the appropriateness of the stage extraction method therefore included aggregate size as an extra variable.

7.4.2. Extraction test in two layers

150 grams of RA aggregates were sieved into three fractions of 0-2mm, 2-5 mm and 5-11 mm. Each fraction was soaked in 50 ml Dichloromethane for 5 minutes at room temperature (see Figure 7.8). This binder solution was poured and stored in a separate container. The remaining aggregates were then thoroughly washed with another 50 ml Dichloromethane until the aggregates became apparently clean. The first and second solution was centrifuged for 30 minutes at a speed of 370 rpm to separate the fillers. After filtration, both solutions were recovered according to SSEM.

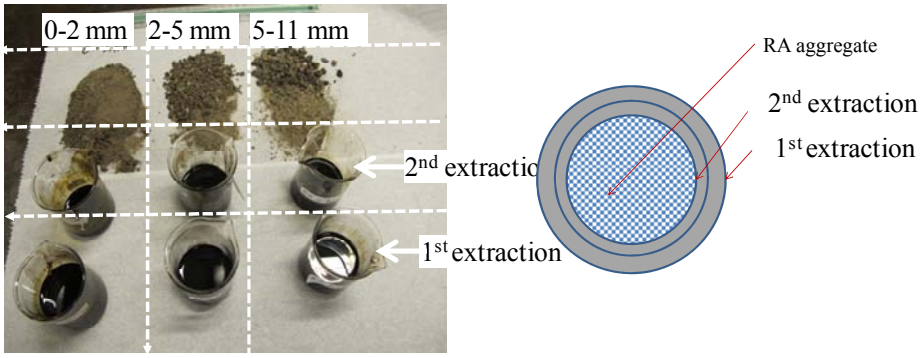

Figure 7.8 Extracting binder in two imaginary layers from different sizes of RA

The recovered binders were tested with the DSR to measure G* values at different temperatures and frequencies. The G* values of both recovered binders shifted to the reference temperature of 25°C are shown in Figure 7.9.

According to this figure, the effect of the size of the aggregates and the imaginary layers is considerable. The figure shows that the second extractions give slightly softer results than the first ones. However, the G^* values of both layers are almost the same for the binder recovered from the 2-5 mm fraction.

Figure 7.9 also shows that with respect to the effect of aggregate sizes, the binder extracted from the finer aggregates (0-2 mm) has an almost two times

higher shear stiffer than the binder extracted of the coarser aggregates (5-11 mm). Therefore it could be concluded that different sizes of aggregates may influence the properties of their binder films, with finer sizes causing a higher stiffness of the binder.

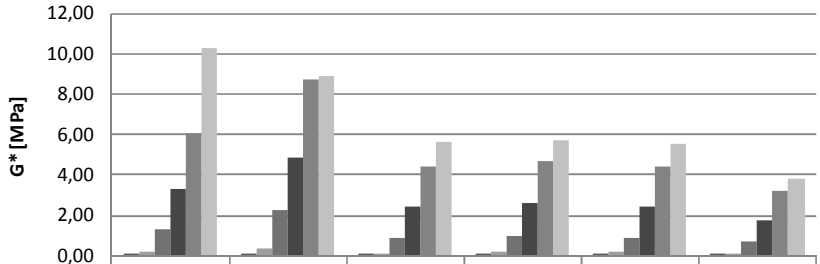

	0-2mm first extraction	0-2mm second extraction	2-5mm first extraction	2-5mm second extraction	5-11mm first extraction	5-11mm second extraction
0.001Hz	0,032	0,048	0,017	0,023	0,020	0,016
0.01Hz	0,218	0,326	0,135	0,166	0,152	0,115
0.1Hz	1,312	2,225	0,864	0,982	0,904	0,668
1Hz	3,301	4,886	2,404	2,595	2,430	1,780
4Hz	6,097	8,714	4,430	4,684	4,446	3,241
10	10,269	8,901	5,650	5,694	5,547	3,818

Figure 7.9 G values of imaginary layers around different aggregate sizes at the reference temperature of 25°C.*

Some differences between fine and coarse aggregates which could affect the aging of their film binder are:

- surface area; finer aggregate provides more available surface for short term aging and chemical interaction, the difference in absorption properties of fine and coarse aggregates,
- Possible influence of not removing all the filler, especially in the fine fraction.

Visual observation during manually washing of the aggregates, revealed the fact that not every aggregate size loses its binder at the same time. It took the finer fraction (0-2mm) almost double the time needed for the coarser fractions to get thoroughly cleaned. This is most probably because of the different binder contents of these aggregate fractions due to differences in their specific surface area (see also Table 7.5). Also, differences in texture and surface polarity between the coarse and fine aggregates might have had an influence.

As it was discussed in section 3.2.1, different fractions of RA aggregates have different volumetric properties due to the particles sizes and their mineral

properties. Volumetric properties of three RA fractions are presented in Figure 7.10 and Figure 7.11. The filler and bitumen content of the smaller fraction (0-2mm) is remarkably higher than those of the other two larger fractions. This may also explain the difference in the effort and the time required for extraction of each fraction.

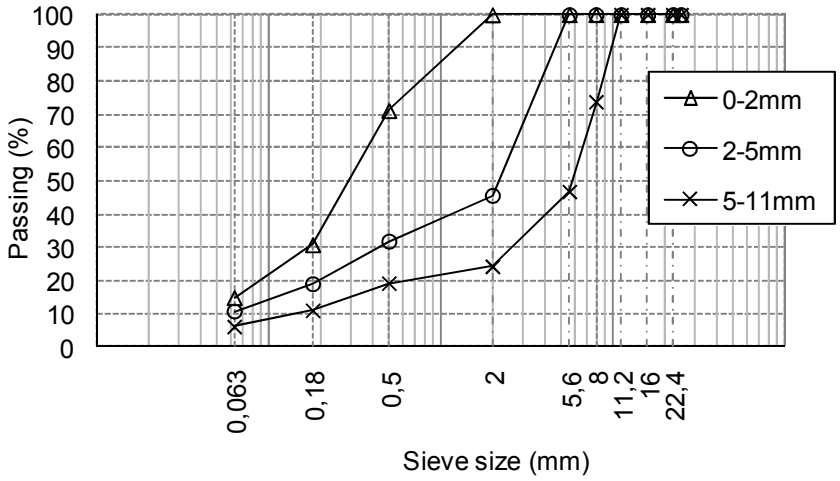

Figure 7.10 Aggregate gradation of different RA fractions

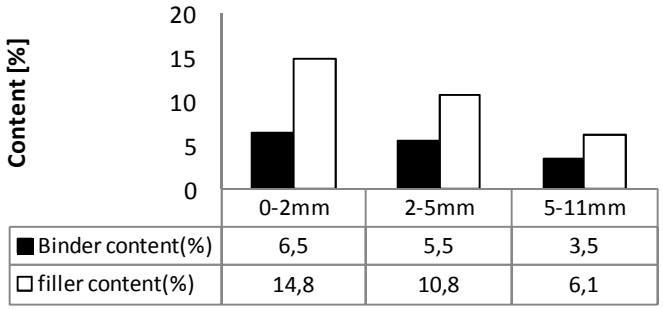

	0-2mm	2-5mm	5-11mm
■ Binder content(%)	6,5	5,5	3,5
□ filler content(%)	14,8	10,8	6,1

Figure 7.11 bitumen and filler content of different RA fraction sizes

The first conclusion is that a number of factors are influencing the properties of the binder recovered at different stages (as it was experienced in previous studies). The second conclusion is that there is indeed some evidence that a layered bitumen structure is present around the aggregate particles.

7.5. Material

7.5.1. Artificial RA binder

To make artificial RA binder (for GB coating), a short and long term aging method (STA and LTA) had to be adopted. According to the European norm a number of methods are available for accelerated bitumen aging such as RTFOT[20], PAV[21] and RCAT[22]. A summary of these aging testing methods is given in [33] (see Table 7.2). For a number of reasons, which will be described later on, the RCAT was selected for artificial ageing of binders in this research.

Table 7.2 Summary of bitumen aging methods [33]

	Test method	***T (°C)***	***Duration (min / hr)***	***Sample size (g)***	***Film thickness (mm)***	***Other features***	***Standard***
	Short-term aging						
1,	Thin Film Oven Test (TFOT)	163	5 hr	50	3,2	--	EN 12607-2
2,	Rolling Thin Film Oven Test (RTFOT)	163	75 min	35 x 8 bottles	1,25	15 rpm, air flow 4 l/min	EN 12607-1
3,	Rotating Cylinder Aging Test (RCAT)	163	235 min	500 - 550	--	5 rpm, air flow 4 l/min	NEN-EN15323
4,	German Rotating Flask Test (MGRFT)	165	150 min	100	--	flask rotation 20 rpm	DIN 52016
	Modified German Rotating Flask Test	165	210 min	200	--	flask rotation 20 rpm	DIN 52016
	Short-term aging						
1.	Pressure Aging Vessel Test (PAV), [POV]	90	20 hr			2.1 MPa pressure	EN-14769 (SHRP B-005)
2,	High Pressure Aging Test (HiPAT)	85	65 hr	50	3,2	2.1 MPa pressure	
3,	Rotating Cylinder Aging Test (RCAT)	85 / 90	240 / 144 hr	500 - 550	2,0	1 rpm, 4.5 l/hr Oxygen	BRRC method
4,	Modified German Rotating Flask Test	85	65 hr	200	--	flask rotation 20 rpm	DIN 52016
5,	Weatherometer aging * Combinations of light (UV), moisture (humidity, RH), and temperature	60	1000 hr	PA mixture	4.5% bitumen	Temp.+UV+humidity	New method - Simulation of field conditions

[20]Rolling Thin Film Oven Test [EN 12607-1]

[21] Pressure Aging Vessel [EN 14769]

[22] Rotating Cylinder Aging Test [EN 15325]

7.5.2. The rotating cylinder aging test (RCAT)

The RCAT accelerated aging method is developed by the Belgian Road Research Center (BRRC) to simulate both short term aging (STA) and long term aging (LTA) of bitumen. This method is suitable to age considerable amounts of bitumen (500 grams) to be used in further studies.

It consists of an oven for temperature control, a steel cylinder and a rotating system to maintain a constant rotation of the horizontally placed cylinder. A stainless steel roller is also freely rotating inside the cylinder to keep the film thickness constant. A constant flow of air or oxygen is blown into the rotating cylinder to accelerate the aging process (see Figure 7.12).

In this study, the available RCAT oven in the laboratory was not equipped with oxygen supply and therefore air was used in the process at a flow rate of 4.5 l/hr for a total duration of 24 hours. It should be emphasized that this aging protocol was adopted according to the availability of testing setup and it was not standard practice. Therefore the aging process at different times is studied as well here to characterize the bitumen properties during the adopted aging process in the RCAT.

The development of aging was monitored by taking samples of approximately 50grams at 0, 4, 8 and 24 hrs. These samples were used for penetration, $T_{R\&B}$, FTIR and DSR tests to study the progress of aging during the RCAT test. The results were compared with those obtained on a real RA binder which was taken as a reference.

Two grades of bitumen are used in this study, respectively a Q8 70/100 and a Q8 40/60. The test program is shown in Figure 7.13.

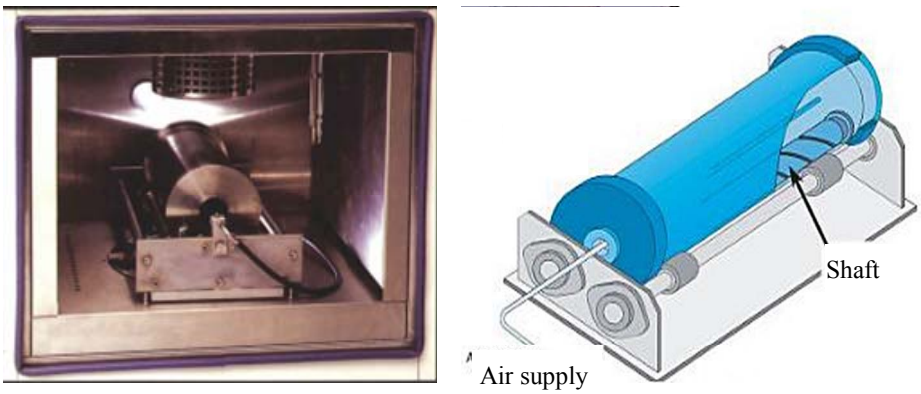

Figure 7.12 Rotating Cylinder Aging Test (RCAT) [33]

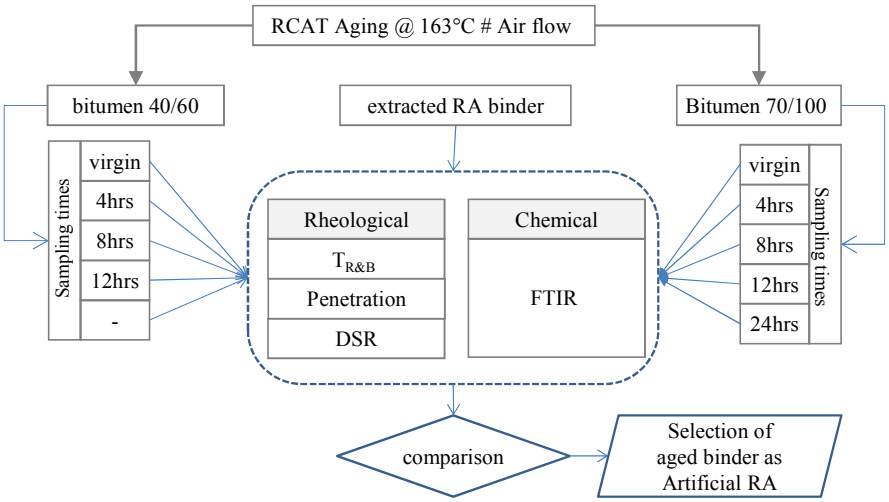

Figure 7.13 Flow chart of the process to compare artificially aged bitumen with properties of recovered real RA binder

A summary of the initially measured properties of the extracted RA binder is given in Table 7.3.

Table 7.3 Extracted RA binder properties

Properties	***Unit***	
Penetration @ 25°C (# @ 15°C)	0.1mm	21
Softening Point $T_{R\&B}$	°C	59
Penetration Index	( )	-0.8
Density, 25°C	kg/m3	1035

7.5.3. Rheological evaluation of aged binders

As mentioned earlier, penetration and softening point tests were carried out to determine the change of these rheological parameters as a function of aging time. The results are shown in Figure 7.14

A dynamic shear rheometer (AR2000ex) was used in the research to measure the complex shear modulus (G*) and the phase angle (δ) between shear stress and shear strain. The machine has a torque capacity of 0.2 Nm and is

equipped with an environmental test chamber. G* and δ values are measured at different temperatures (20-50°C) and loading frequencies (0,05-50Hz). The results were used to create master curves of the shear modulus (G*) and phase angle (δ).

The master curves of the aged binders and the virgin bitumen are illustrated in Figure 7.15 and Figure 7.16 respectively. DSR measurement results of a real RA binder are also given in both charts to compare the artificial aged binder with a real RA binder.

It can be concluded that RCAT aging of 70/100 bitumen at 163°C and 24hrs produces a binder that is closest to the real RA binder.

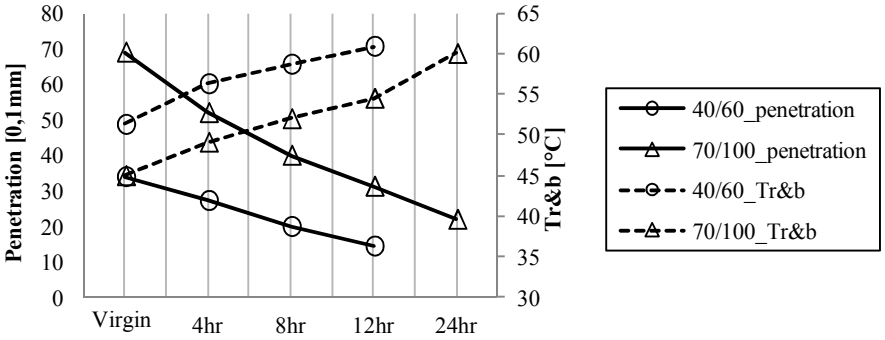

Figure 7.14 Penetration results at 25°C and softening points ($T_{r\&b}$) of binders aged with RCAT at 163°C

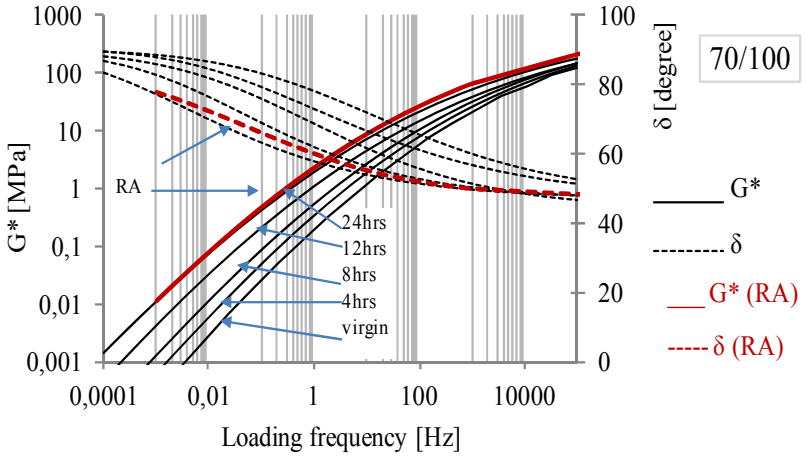

Figure 7.15 DSR master curves at 20°C after RCAT aging of 70/100 bitumen (red lines are for RA binder)

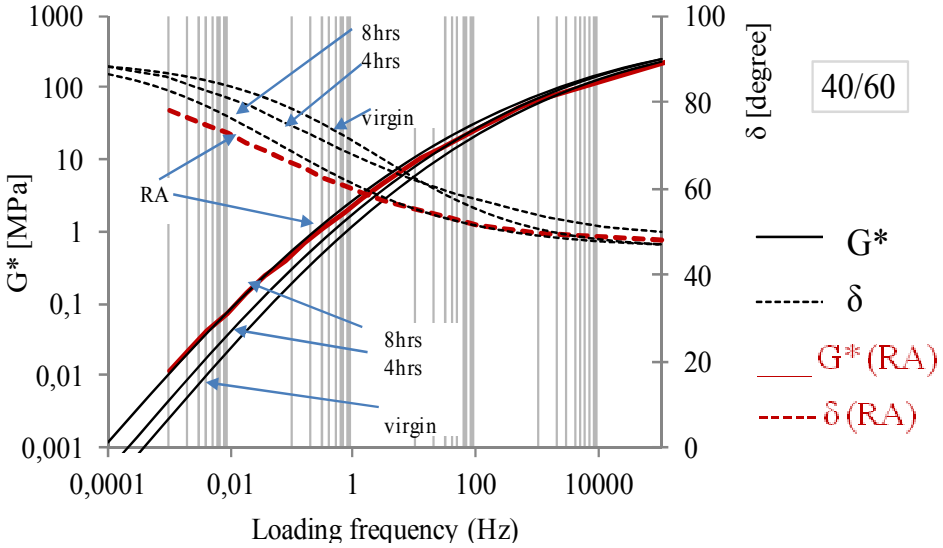

Figure 7.16 DSR master curves at 20°C on RCAT aging of 40/60 bitumen (red lines are for RA binder)

7.5.4. Glass beads

Glass beads are widely used in industry and research. In industry they are mainly used for blasting surfaces. In research, they are used to simulate particle flow in industrial processes. They are available in different sizes and even at micron sizes.

As mentioned before, the regular size and shape of GB's was the reason for using them in this study. However the smooth surface of GB's is a critical drawback in comparison with the natural, usually rough, micro surface of normal aggregates since smooth surfaces exhibit less adhesion than textured surfaces.

In this research, glass beads of different sizes were used to simulate RA and VA. Two sizes, 5 and 8mm, of Borosilicate glass beads were used in mixture type 1 & 2. In mixture type 3, sizes of 13mm and 20mm were used as well. They are identified as GB5, GB8, GB13 and GB20.

The GB's used in this research contain primarily silica and boron oxide which is making them more resistant to thermal shocks than any other common glasses. Table 7.4 shows the comparison between the chemical and physical properties of borosilicate glass beads and granite stones.

Table 7.4 Chemical and physical properties of borosilicate and granite stone

	Borosilicate GB		***Granite stone***	
Chemical composition	SiO_2	81,20 %	SiO_2	72%
	B_2O_3	12,40 %	Al_2O_3	14%
	Na_2O	2,93 %	K_2O	4%
Coefficient of thermal expansion	3×10^{-6} /°C at 20°C		5 × 10−6 /°C at 20°C	
Thermal conductivity	1.2-1.4 W/(m·K)		1.73-3.98 W/(m·K	
Melting point	$1600^{°C}$		1215 - 1260 °C	
Density	2230 kg/m^3		2700 kg/m^3	

The volumetric properties of GB5 and GB8 are presented in Table 7.5. The volumetric properties are needed to determine the required amount of binder to achieve the intended film thickness. The weight of the particles of each size was calculated by dividing the weight of a number of beads by that number. It turns out that 1% mass ratio of bitumen to GB results in 18 µm coating on 1000 grams of 5mm beads (this is without any filler added in the system). Therefore a mass ratio of bitumen to GB of 2% is needed to achieve 36 µm film thicknesses. The 36 µm film thickness was selected because this formed a stable bitumen coating around glass beads. This percentage was used later to prepare artificial RA with 5mm beads and aged bitumen.

Table 7.5 Glass bead properties and bitumen mass required obtaining a certain intended film thickness around the GB particles

Volumetric properties of GB	***Unit***	***GB5***	***GB8***
Specific density	[kg/mm3]	2.23×10^{-6}	2.23×10^{-6}
Diameter (2r)	[mm]	5	8
Surface area ($4\pi r^2$)	[mm2]	78.5	201.1
Volume ($4\pi r^3/3$)	[mm3]	65.4	267,9
Mass[kg]	kg	1,46E-4	5,98E-4
Nr of particles in 1 kg aggregate	[1/kg]	6855	1674
Total surface area of 1 kg aggregate	[mm2/kg]	538117	336323
Coating per 1.0 (% m/m) bitumen	[µm]	18	29

7.5.5. Mixtures

As mentioned before, three mixtures had to be prepared in the laboratory with artificial aggregates. The mixing procedure of each mix type is explained hereafter.

7.5.5.1. Mixture 1

In these mixtures, GB5 had to be covered with 2% (by weight) aged bitumen (RCAT163°C_70/100@24hrs) which was chosen during the preliminary aging tests which are discussed earlier. 2 kg of GB5 was premixed with 2% aged binder at 150°C to prepare the artificial RA. A Hobart pan mixer with a spiral dough hook (see Figure 7.17) was used to coat GB5 with aged binder within 3 minutes to ensure a homogenous coating. Since pure bitumen was used without any filler, it was important to carefully clean all mixing equipment prior to any mixing.

The pre-coated GB5 was cooled down with a fan ventilator, while it was spread on silicone paper on a table. After cooling with a fan ventilator for one hour, the mixture was stored for 3 hours at room temperature (23°C) and 24 hours in a climate room (15°C) to make it non-sticky enough to be broken into single particles by means of slight hammering (Figure 7.18). The separated particles were stored at -5°C to prevent them to stick together again.



Figure 7.17 Mixer setup and thermography of mixture

.



Figure 7.18 Hammering the cooled artificial RA to separate the particles at 15°C

Then 500 grams of GB8 (as virgin aggregate) was preheated to 300°C in an oven for three hours. After this the pre-coated GB5 particles (500gram at 15°C) were mixed in a pan mixer together with the GB8 particles for 30 seconds.

The heat exchange between the pre-heated bold G8 particles and the coated GB5 particles during mixing was measured by means of the infrared thermography method. As can be seen in Figure 7.17, the GB5 particles started to stick to each other as soon as they were added to the mixer, because of their pre-coating. For this reason manual agitation during 10 seconds by means of a steel spatula was done before mechanical mixing started; this improved mixing considerably.

Another similar mixture was prepared in which the GB8 was preheated to 400°C.

After mixing and cooling down, the particles of the mixture were separated by means of slight hammering.

A special sieve with openings of 6 mm was used to separate the GB5 particles from GB8. After the "sieving' a few small particles were still remaining on the sieve, and they had to be separated manually (see Figure 7.19).



Figure 7.19 Sieving and separating GB5 from GB8.

In the next step the binders covering the GB5 and GB8 particles were recovered by using the SSEM extraction and recovery method.

Initially it was intended to extract binders in two stages. However the GBs all binder as soon as they were soaked in the solvent. The two main reasons for causing the quick solving of the binders around the GBs are: lack of texture on the GB surface and the fact that pure bitumen (without filler, sand fraction) was used in the experiment.

Consequently only one stage extraction was applied on GB5 and GB8 for each mixture. The extracted binders are identified with the coding system explained in Table 7.6. These binders were used for further analysis.

Table 7.6 Coding system for extracted binders of GB5 and GB8 (mixture 1)

Mixture ID	Explanation
300-V5	Extracted binder from **GB5**; Mixture **1**; preheating temperature GB8 at **300°C**
300-V8	Extracted binder from **GB8**; Mixture 1; preheating temperature GB8 at **300°C**
400-V5	Extracted binder from **GB5**; Mixture **1**; preheating temperature GB8 at **400°C**
400-V8	Extracted binder from **GB8**; Mixture **1**; preheating temperature GB8 at **400°C**

7.5.5.2. Mixture 2

As mentioned in the experimental design section, mixture 2 was quite similar to mixture 1 in the sense of preheating temperature and mixing. The only two differences compared to mixture 1, were:

- GB5 is pre-coated at 150°C with 1% aged bitumen (where it was 2% in mixture type 1)
- then the same weight of super-heated GB8 particles (VA) and 1% virgin bitumen is added during 30 second of mixing time

Given the fact that both mix types contain 50% GB5 and 50% GB8, it turns out that the total binder content of all variations of mixtures 1 and 2 is 1% by total mass.

Other procedures such as preheating, storing, particle separation and binder extraction and recovery were similar to those used to prepare mixture 1. The identification system for the binders extracted from mixture 2 is shown in Table 7.7.

Table 7.7 Identification of binders extracted from GB5 and GB8 (Mixture 2)

Mixture ID	explanation
300+V5	Extracted binder from **GB5**; Mixture **2**; preheating temperature GB8 at **300°C**
300+V8	Extracted binder from **GB8**; Mixture **2**; preheating temperature GB8 at **300°C**
400+V5	Extracted binder from **GB5**; Mixture **2**; preheating temperature GB8 at **400°C**
400+V8	Extracted binder from **GB8**; Mixture **2**; preheating temperature GB8 at **400°C**

7.5.5.3. Mixture 3

In this mixture, some fractions of the virgin aggregates were replaced by different sizes of glass beads being; GB5, GB8, GB13 and GB20.

Firstly a mixture containing 50% RA was designed.

A 70/100 pen bitumen was used as virgin bitumen to be added during mixing. The target bitumen content of the mixture was set to 4.3% by mass (see section 3.2.4.1). Given the fact that the RA contained 4.3% bitumen, half of this amount (2.15% by mass) of virgin bitumen had to be added.

The modification of the aggregate gradation as well as the required GB's is presented in Table 7.8 and Figure 7.20. The other mixing conditions and materials are summarized below:

- RA 50%
- Virgin bitumen: 70/100
- Bitumen content: 4.3% (on 100% of aggregate by mass)
- Mixing time: 30 seconds
- Preheating temperature of virgin aggregates: 515 °C
- RA moisture content: 4%

The final mixture temperature was 170°C. The mixture was kept in an oven at 170 °C for 30 minutes before compacting it with a Marshall compaction hammer with 40 blows at each side. Normally 50 blows are applied on each side but because the glass beads could break during Marshall compaction, the number of blows was reduced to 40.

Table 7.8 Gradation adjustment for mixture 3

	Sieve opening (mm)	Cumulative % retained on each sieve		
		Target	Min.	Max.
Gradation Requirements	22.4	1.2	0	6
	16.0	13.5	-	-
	11.2	20	15	40
	8.0	40.2	-	-
	5.6	47.9	-	-
	2.0	57	54.0	60.0
	0.063	94.0	92.0	94.0
	< 0.063	6.0	-	-
Binder Requirements	Binder content		4.0%-5%	
	Penetration @ 25°C (# @ 15°C)		40-60	

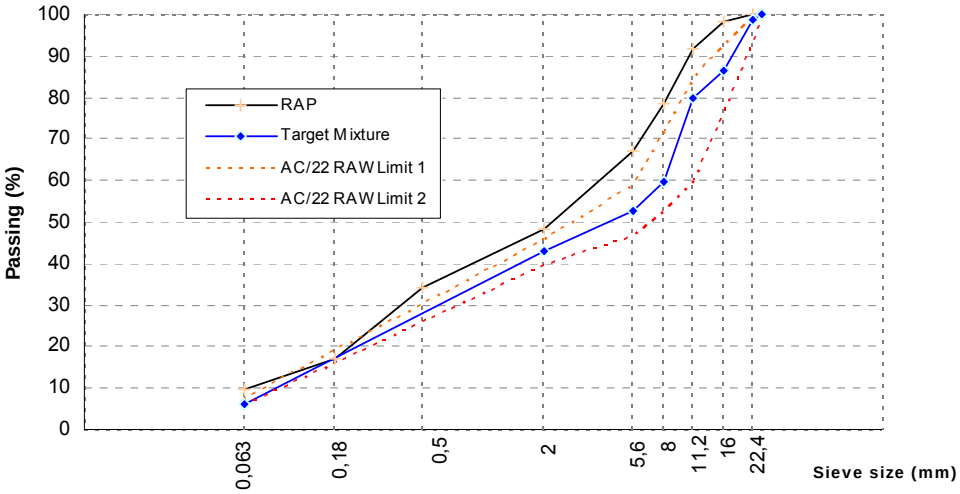

Figure 7.20 Gradation curve of the target mixture, the available RA and gradation limitations.

Table 7.9 Gradation adjustments for mixture 3

Size (mm)	***RA***	50 % RA (% m/m)	Virgin material (% m/m)	***Target***	***GB sizes intended to replace corresponding virgin aggregates***
> C22.4	0	0	**1,2**	1,2	**GB20**
C22.4 - C16	6	3	**9,2**	12,2	**GB20**
C16 - C11.2	11	5,5	**1,1**	6,6	**GB13**
C11.2 – C8	14	7	**13,2**	20,2	**GB8**
C8 - C5.6	9,2	4,6	**2,4**	7	**GB5**
C5.6 - C2	16,3	8,2	**1,7**	9,8	
River Sand (0/2)	35,7	17,9	**19,2**	37	
< 0.063	7,8	3,9	**2,1**	6	
Total (%)	100	50	**50**	100	
Bitumen	4,3	2,15	**2,35**	4,5	

The virgin materials, including the glass beads, as well as the final mixture are illustrated in Figure 7.21. The GB's could manually be separated from the loose mixture because of their shapes. The binder attached to the GB's and real aggregates were separately extracted and recovered for further analysis. In the remainder of the analysis, the binder extracted from the GB's is called "GB binder". The binder which is extracted from the mineral aggregates is called "Stone binder".

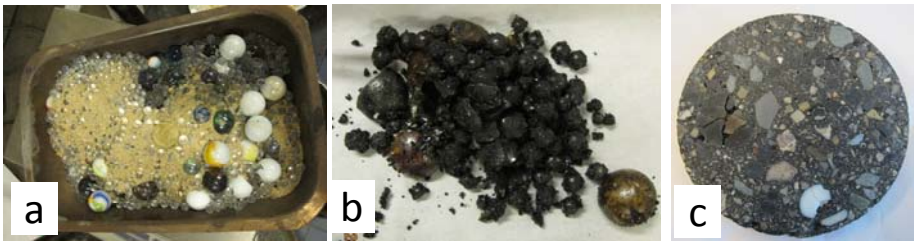

Figure 7.21 Materials and mixing process used in Mixture 3.Figure a: GB, sand and filler representing virgin aggregates; figure b: loose mixture after mixing with 50% RA; figure c: Marshall compacted specimen

7.6. Results and analysis

The extracted binders were used for rheological and chemical analyses. G* values were determined at different temperatures and frequencies by means of a Dynamic Shear Rheometer (DSR) using parallel plates with a diameter of 25 mm and thickness of 1 mm to create master curves. The same binders were used for ATR/FTIR analyses, the results of which will be presented for each mixture type. Peak area values in the FTIR spectra were utilized to determine the Carbonyl index (1700 cm-1) and Sulfoxide index (1039 mm-1) as indicators of chemical changes due to superheating.

It has to be noted once again that GB5 stands for glass bead (5mm) which was prepared as an artificial aggregate by pre-coating it with aged binder. Artificial virgin aggregates are represented by GB8 which are superheated prior to mixing at temperatures of 300°C and 400°. In mixture type1, GB5 was coated with 2% aged bitumen. GB5 in mixture type 2 is pre-coated with 1% aged bitumen and 1% virgin bitumen, which was added during mixing. Comparison of the binder content on each group of aggregates (GB5 and GB8) will give an indication of the amount of binder transfer from GB5 to GB8.

7.6.1. Mixture 1

Figure 7.22 shows that 0.8% of GB5 binder was transferred to GB8. This implies that 1.2% of the bitumen stayed at the GB5 particles. This can be explained as follows. Mixture 1 contained, in terms of weight, the same amount of GB8 and GB5 particles. This implies that the total surface area of the GB5 particles was 1.6 times larger than the total surface area of the GB8 particles (see also Table 7.5). Given the fact that the GB5 particles, with their total surface area of 1.6 times the GB8 particles, were carrying 1.5 times more bitumen in total than the GB8 particles, i , the GB5 and GB8 particles carried about the same amount of bitumen per unit of surface area. This amount was similar at both superheating temperatures. It shows that cold RA (GB5) could share to a large extent its binder with superheated aggregates even at short periods of mixing (30 seconds). Comparison between the shear modulus of GB5 and GB8 binders (at 300°C superheating temperature) shows no severe change or damage of the binder properties. However, superheating at 400°C has increased the G* value of the GB5 binder as well as that of the GB8 binder. G* values of the original aged binder (being RCAT_70/100@24hr) are also shown in the charts to compare with the binder before mixing.

Furthermore, the GB8 binder has become slightly stiffer than the GB5 binder. Direct exposure of the binder to superheated aggregates (400°C) is causing

the difference between the binders coating GB5 and GB8. At 300°C, the binder stiffness of GB8 is even lower than of the GB5 or artificial RA binder. This can be explained probably by measurement precision and accuracy.

FTIR was conducted on each extracted binder to study the chemical changes, particularly due to oxidation. The FTIR spectra related to mixture 1 are presented in Figure 7.23. The aging indexes of CO and SO are determined by calculating peak area values according [37] and are given in Table 7.10. A comparison of aging indices between the different groups of extracted binders (from mixture 1) is given in Figure 7.24. As can be seen, the binders of the 400°C mixtures are showing more oxidation compared to those of the 300°C mixtures. It is also evident that the binder coating GB8 has higher aging indices than the binder coating GB5, confirming the effect of direct exposure to superheated aggregates.

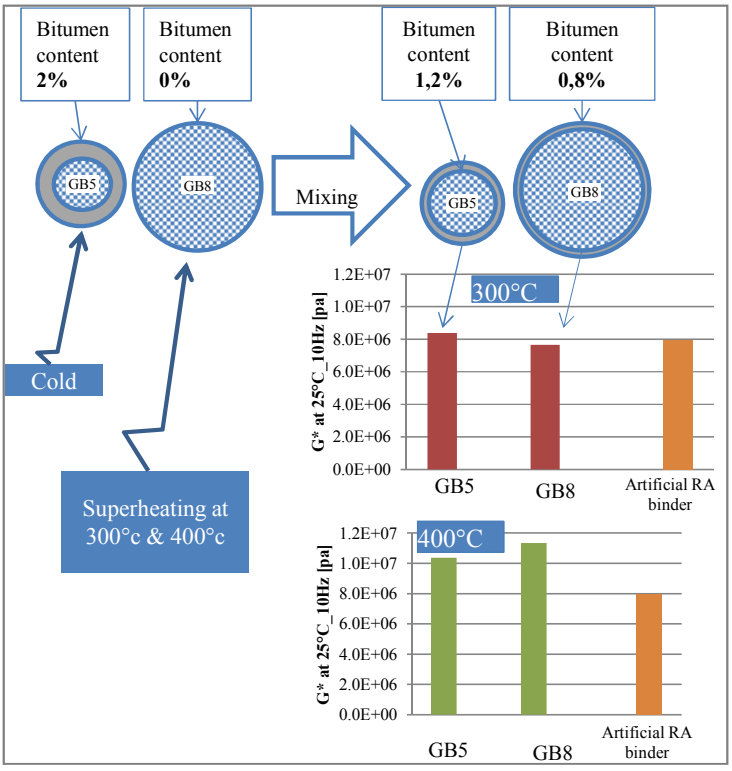

Figure 7.22 G results obtained on binders recovered from Mixture1*

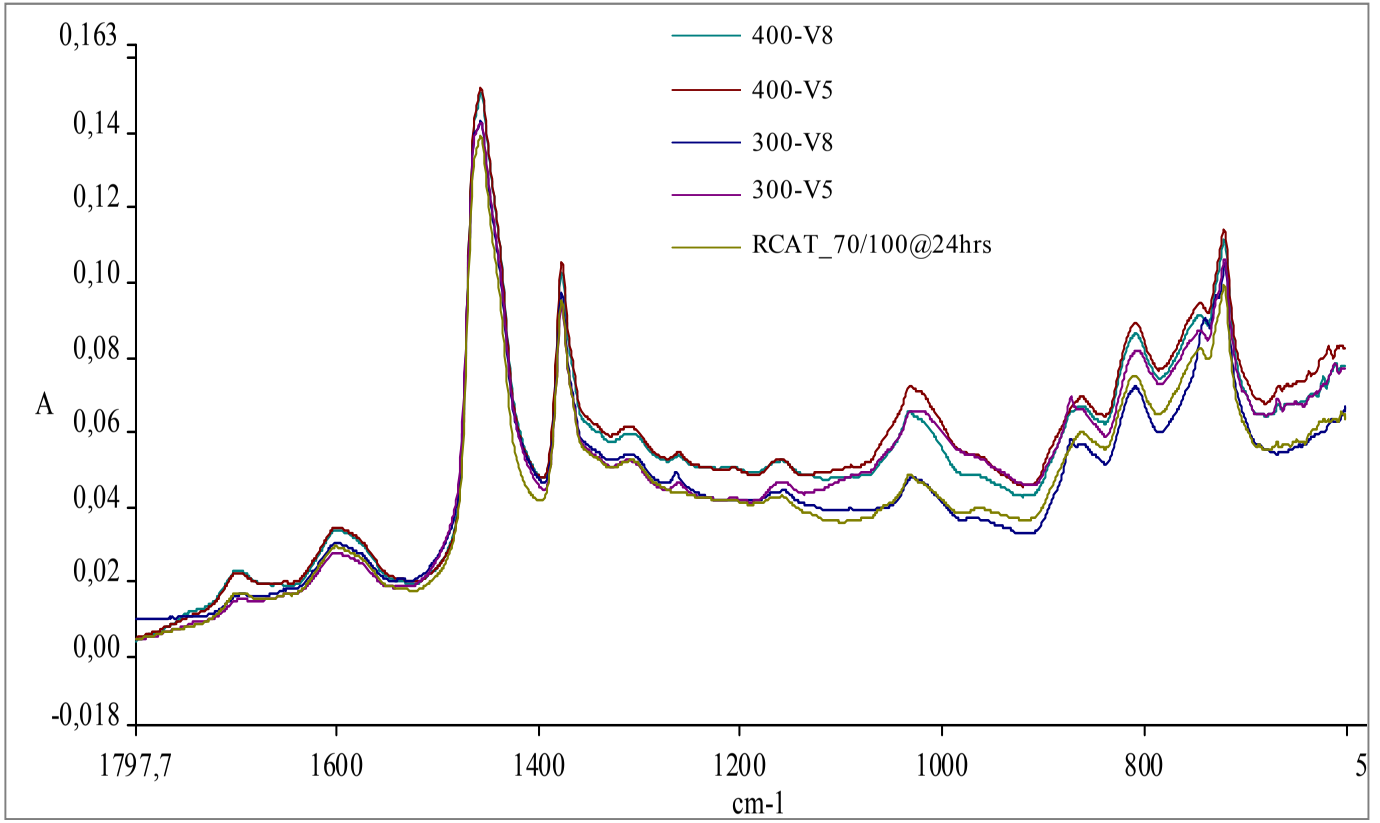

Figure 7.23 FTIR spectrums of binder from Mixture type1

Table 7.10 Peak area values in the FTIR spectra (mixture 1)

	A1030	***A1375***	***A1460***	***A1600***	***A1700***	***ISO***	***ICO***
300-V5	0,6407	0,9936	4,8442	0,5447	0,0558	0,110	0,010
300-V8	0,6786	1,1399	4,6757	0,7474	0,0898	0,117	0,015
400-V5	0,6266	0,9217	4,2226	0,5139	0,1093	0,122	0,021
400-V8	0,764	1,1313	4,8113	0,8059	0,107	0,129	0,018

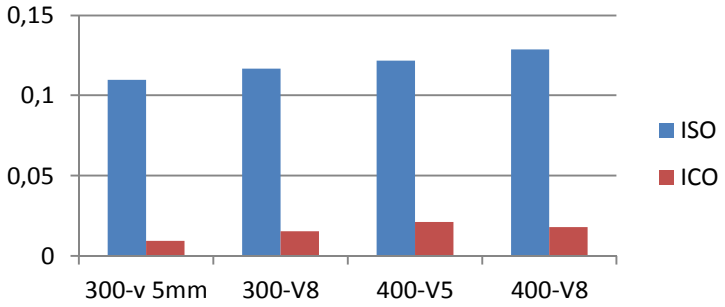

Figure 7.24 Aging indices mixture 1

7.6.2. Mixture 2

As can be seen from Figure 7.25, the GB8 particles are carrying the same amount of bitumen as the GB5 particles after being mixed with the GB5 particles carrying 1% of bitumen and the 1% added virgin bitumen. In contrary to what happened to mixture 1, the bitumen now seems NOT to be divided according to the surface area ratio of GB5 and GB8. It is however very difficult to say how much of the artificial aged binder on the GB5 particles was transferred to the GB8 particles. Although the G* values determined on the bitumen coming from the GB8 particles is slightly higher than those determined on the bitumen coming from the GB5 particles, this does not tell anything about the composition of the binder coming from the GB5 and GB8 particles. The only conclusion that perhaps can be made is that the superheated GB8 particles had almost the same effect in terms of aging on the bitumen that finally coated both glass beads sizes.

In Figure 7.25, the shear modulus of the binders extracted from GB5 and GB8 after mixing are compared with those of binders before mixing (virgin

bitumen and artificial aged bitumen). At both preheating temperatures, the G* values of the GB5 and GB8 binder are between those of the original binders. It shows the effect of blending between the two binders. At 300°C, the GB8 binder has become slightly stiffer than the GB5 binder, most probably because of the exposure to superheated particles (however, it is not sure what the virgin binder is doing). The same trend is observed in the other mixture where the superheating temperature was 400°C.

Increasing the superheating temperature from 300 to 400°C caused more aging on both the GB5 and GB8 binders.

The results can also be used to investigate the validity of the log (pen) rule, which is normally used in the Netherlands to determine the grade of virgin bitumen needed for recycling. The rule is:

$$A \times log\ (pen_{virgin}) + B \times log\ (pen_{RA}) = (A + B) \times log\ (pen_{mixture}) \qquad (7.1)$$

Where:

A	=	% of virgin bitumen
pen_{virgin}	=	penetration of the virgin bitumen added
B	=	% of bitumen coming from the reclaimed asphalt
pen_{RA}	=	penetration of the bitumen of the reclaimed asphalt
$pen_{mixture}$	=	penetration of the bitumen of the recycled mixture
$A+B$	=	100%

It is assumed that this rule is also applicable to determine the G*(at 25°C and 8 Hz) of the bitumen of the recycled mixture.

Since $G_{virgin}^* = 2.47 \times 10^6$ Pa and $G_{aged}^* = 8 \times 10^6$ Pa, one would expect the $G_{mixture}^*$ to be equal to 4.42×10^6 Pa. The figure shows that in case of the 300^0C pre-heated aggregates, the G* of the bitumen coming from GB5 equals 4.82×10^6 Pa and is 4.94×10^6 Pa for the bitumen coming from the GB8 particles. In this case it looks like the log (G*) rule seems to be valid. However it is clear that in case the virgin GB8 aggregate was pre-heated to 400 °C, the log (G*) rule is not valid. The G* of the bitumen from both the GB5 and GB8 particles is much higher. Obviously additional aging due to the super-heated aggregates must have occurred in this case.

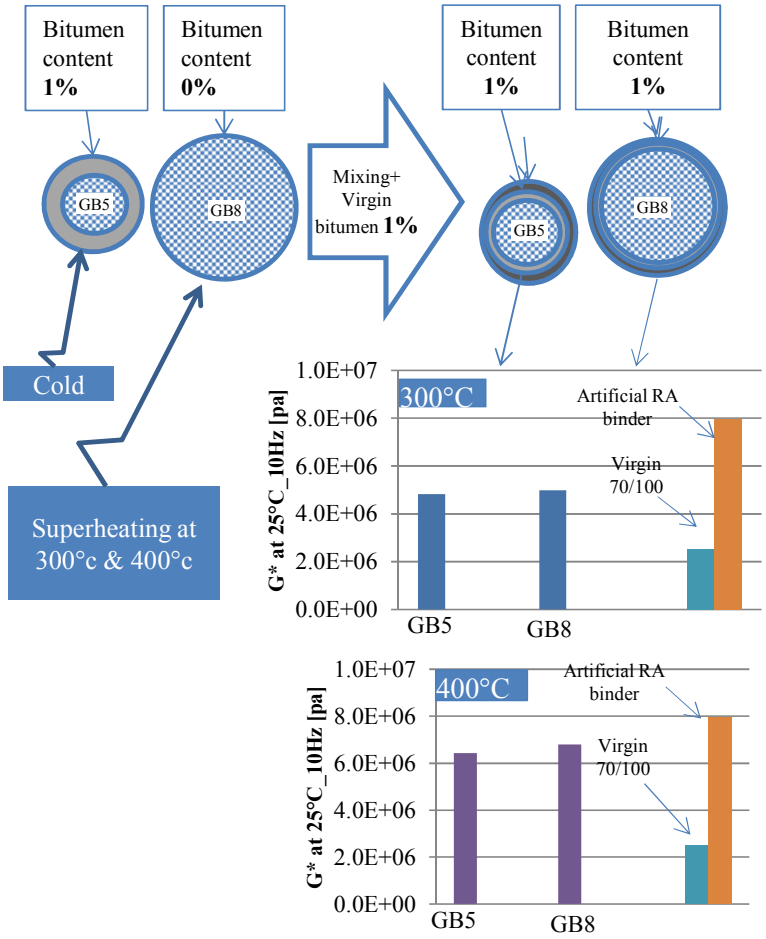

Figure 7.25 Values obtained on the binder recovered from the GB5 and GB8 particles in mixture 2

The effect of adding 1% virgin bitumen is shown in Figure 7.26, where a comparison is made between mixture type1 and 2.

Figure 7.27 shows the G* master-curves of all extracted binders in one chart. The FTIR spectra for the recovered bitumen from the GB5 and GB8 particles as well as those of the virgin and artificially aged binder are shown in Figure 7.28.

The aging indexes ICO and ISO are determined by calculating the peak area values and the results are shown in Table 7.11 and Figure 7.29. It can be seen that at 400°C the binders are showing slightly more oxidation compared to those of the 300°C mixtures. Since virgin bitumen is added to the mixture, no

meaningful relation could be seen between the aging indices of GB5 and GB8.

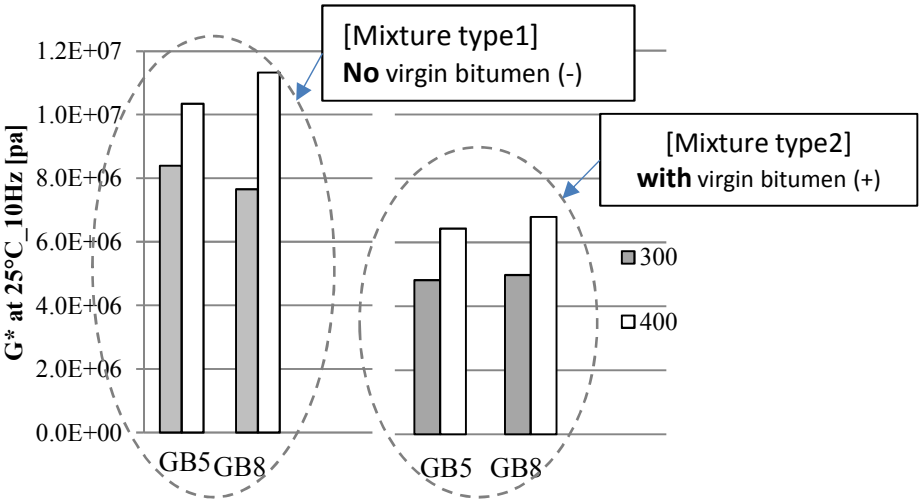

Figure 7.26 Comparison of G (25 C, 10 Hz) for recovered binders of mixtures 1 and 2*

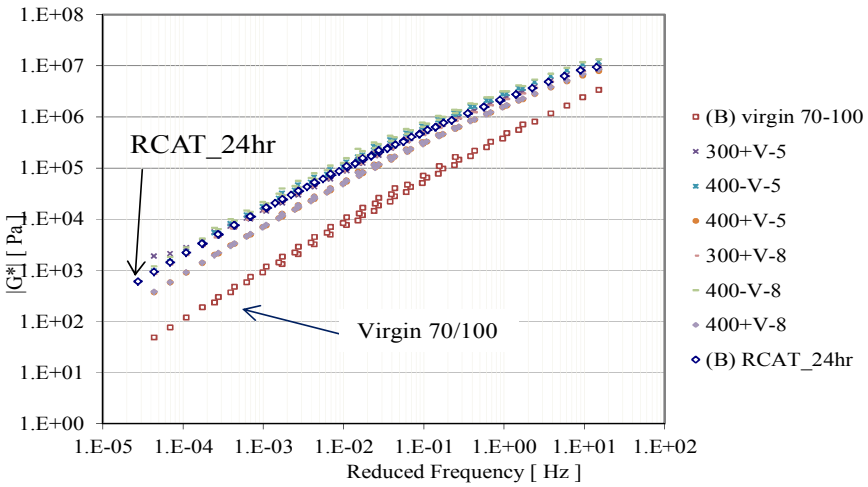

Figure 7.27 Master curve at 20°C for G^* values of the binders extracted from mixtures 1 and 2

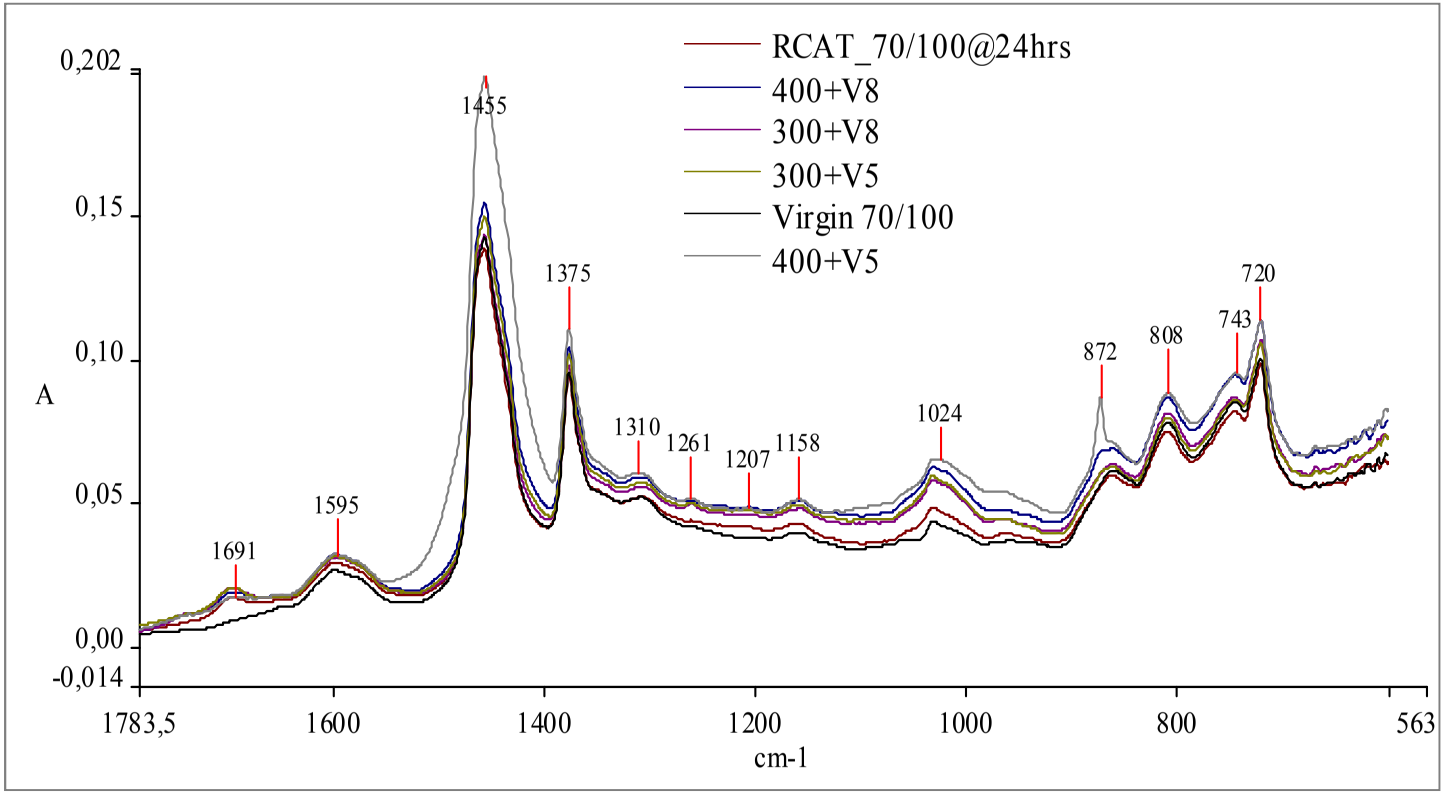

259

Figure 7.28 FTIR spectrums of binders from mixture 2

Table 7.11 Peak values in the FTIR spectra for mixture 2

	A1030	A1375	A1460	A1600	A1700	ISO	ICO
300+V5	0,675	1,156	4,871	0,721	0,151	0,112	0,025
300+V8	0,665	0,669	9,626	0,413	0,038	0,065	0,004
400+V5	0,417	0,878	3,594	0,486	0,041	0,093	0,009
400+V8	0,681	1,112	4,876	0,713	0,054	0,114	0,009

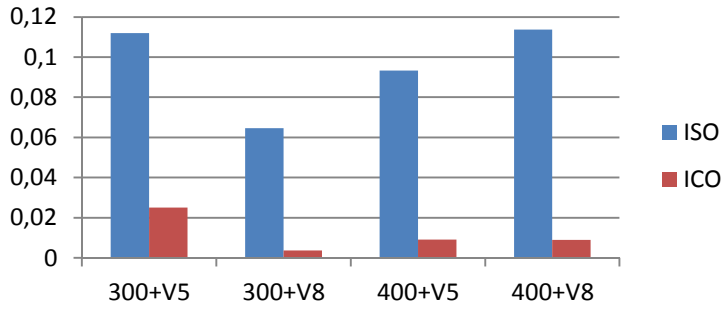

Figure 7.29 Aging indices mixture 2

7.6.3. Mixture 3

Binders were extracted from the GB and RA aggregates and were then tested in the DSR and FTIR. It has to be reminded that in the further analysis, binders extracted from the GB particles are identified as "GB binder" and the binder extracted from the rest of aggregates are called "Stone binder".

Shear modulus master curves of both binders are shown in Figure 7.30. Master curves of the original real RA binder and virgin 70/100 bitumen are also included to show the effect of superheating and blending after a mixing period of 30 seconds in a pan mixer. As shown in Figure 7.30, the GB binder has a higher G* than the binder extracted from the rest of the mixture (stone binder) implying the effect of direct exposure of the binder to virgin aggregates (GB) superheated to 515°C. The stone binder is relatively softer

which implies that it is less affected by the superheated aggregates. The stiffness of the stone binder is between the original RA and virgin bitumen.

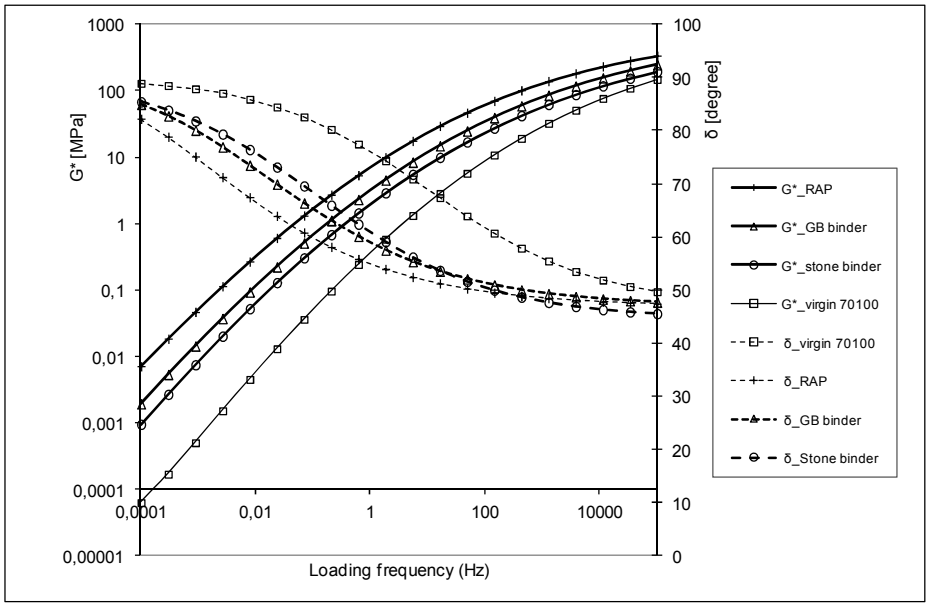

Figure 7.30 G Master curves of G* of extracted binders in mixture 3 at 25°C*

Table 7.12 gives more detailed information about the G* and δ values obtained at various frequencies. Furthermore penetration values are presented in this table which were calculated using the following equation which was developed by Saal and Labout [55]

$$Log\ (G^*_{0.4\,Hz;25℃;[MPa]}) = 2.923 - 1.9 \log\ (pen_{25℃:[dmm]}) \qquad (7.2)$$

In Table 7.12 the penetration value of the bitumen in mixture 3 is calculated by means of the log (pen) rule which was presented earlier. As one will observe, the penetration of the bitumen recovered from the stone is not too different from the penetration value calculated by means of the log (pen) rule. The penetration of the bitumen recovered from the GB particles is however much lower. All in all these results are showing that full blending of the RA and virgin binder as it is assumed in the log (pen) rule certainly did not occur. The table also shows that the G* of the GB binder is approximately 50% of that of the RA binder. The G* of the Stone binder is approximately 2/3 of the G* of the GB binder.

Table 7.12 G and δ values for the binders recovered from mixture 3 as well as penetration values for these binders calculated from G* (25°C) values.*

	RAP		***GB binder***		***Stone binder***		***virgin 70100***	
f [Hz]	G* [MPa]	δ [degree]	G* [MPa]	δ [degree]	G* [MPa]	δ [degree]	G* [MPa]	δ [degree]
0,01	0,323	66,6	0,113	72,7	0,064	75,7	0,006	85,6
0,4	**4,112**	**56,7**	**1,731**	**61,2**	**1,078**	**63,8**	**0,169**	**78,6**
1	7,089	54,9	3,118	58,9	1,979	60,9	0,361	76,1
10	23,578	51,7	11,566	54,3	7,678	54,7	2,033	68,9
20	32,302	51,0	16,372	53,2	11,010	53,3	3,250	66,7
100	61,836	49,7	33,789	51,3	23,418	50,5	8,780	61,7
*Predicted penetration								
	16		26		33		**88**	
** log pen rule based on 50% RA								
				38				

The FTIR spectrums of the binders are illustrated in Figure 7.31. The aging indices of ICO and ISO are determined by calculating the peak area values and the results are shown in Table 7.13. The indices of the Stone, GB, virgin and RA binder are compared in Figure 7.32. Higher values of ISO and ICO for the GB binder are indicating the effect of superheating on directly exposed binder.

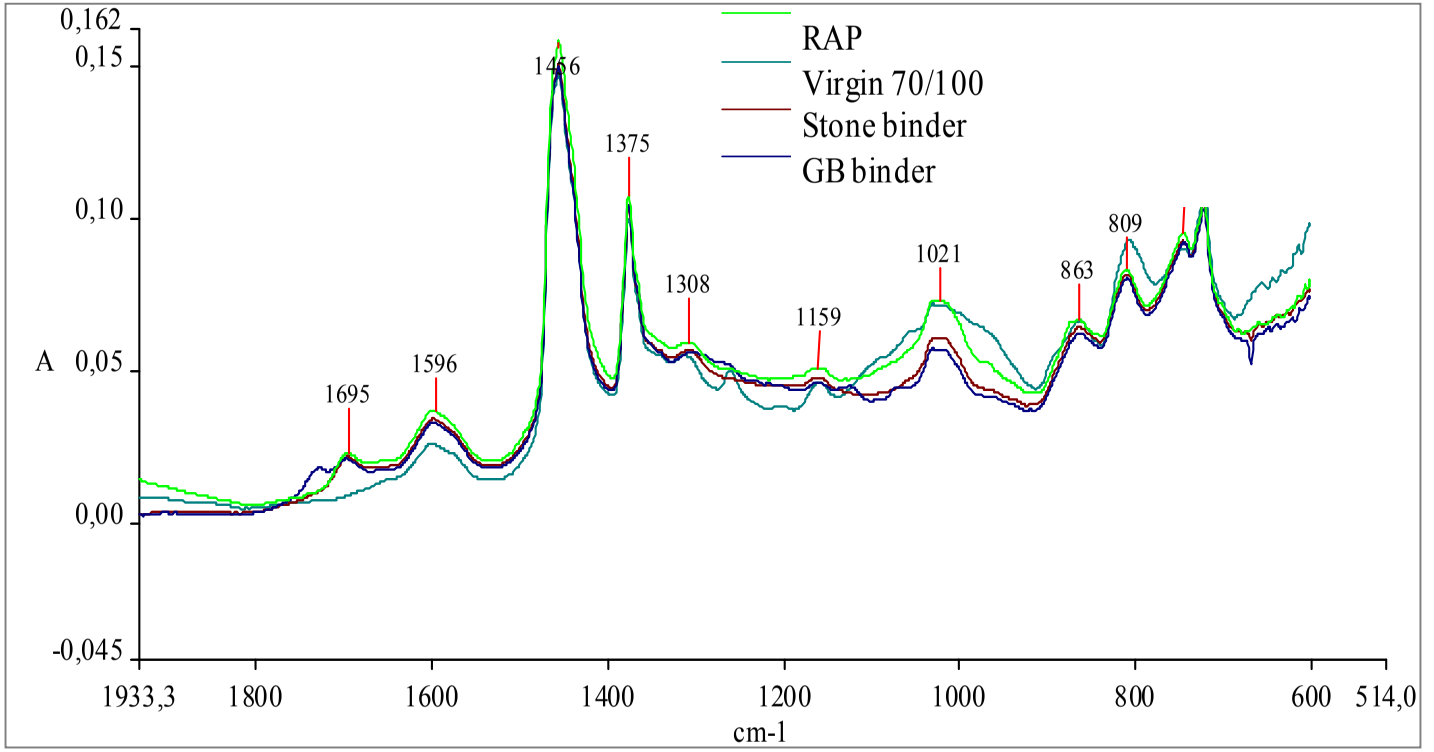

Figure 7.31 FTIR spectrums of binder from Mixture type 3

Table 7.13 Aging indices for mixture 3

`	***A1030***	***A1375***	***A1460***	***A1600***	***A1700***	***ISO***	***ICO***
Stone binder	0,656	1,044	4,191	0,721	0,122	0,125	0,023
GB binder	0,720	1,093	4,020	0,658	0,195	0,141	0,038
Virgin 70/100	0,442	1,064	4,450	0,546	-0,049	0,080	-0,009
RAP	0,817	1,092	4,625	0,796	0,104	0,143	0,018

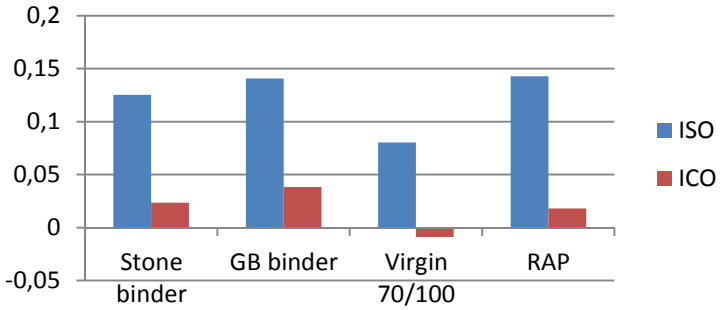

Figure 7.32 Aging indices mixture 3

7.7. Conclusions

Based on the presented research results, the following conclusions can be drawn.

1. Extraction of bitumen from asphalt mixtures is a delicate process. Great care should be given to the complete removal of the solvent and the filler.

2. Stage extraction which is done to determine the presence of a layered bitumen film around aggregate particles can only be successful if the extraction is done on particles of approximately the same size. It has been shown in this research that larger particles will lose their bitumen film more easy than the smaller particles. This implies that when stage extraction is done on a mixture consisting of different sized aggregates, one will first recover the bitumen around the coarse aggregates and in a later stage the bitumen around

the finer particles. Such a stage extraction will therefore tell nothing about the presence of a layered bitumen film around the various particle sizes.

3. G* measurements on the bitumen recovered by means of stage extraction from different particle sizes showed that the bitumen recovered from the finer particles had a higher G* than the G* of the bitumen recovered from the coarser particles.

4. The G* values obtained for the bitumen recovered from the first extraction (the outer bitumen layer around a particle) showed to be slightly higher than the G* values obtained for the bitumen from the second extraction (inner layer). The differences were however rather small and no clear trend could be discovered.

5. It can be concluded that the RCAT is a useful tool to artificial age virgin bitumen in such a way that its rheological properties are similar to the binders aged in the field.

6. The glass beads experiments showed to be very useful in getting an understanding of the transfer of RA binder from RA aggregates to (super)-heated virgin aggregates.

7. The experiments with the asphalt mixture where part of the virgin aggregates were replaced by glass beads showed that adding virgin binder to the mixture had a significant effect on the G* of the RA binder coating the RA particles (after separation and recovery)

8. Furthermore it can be concluded that the G* of the bitumen coating virgin aggregates in an RA mixture (in this case the glass beads) is not the same as the G* of the bitumen coating the RA aggregates.

9. Based on conclusion 7 it is concluded that full blending of RA and virgin binder does not occur.

10. In line with conclusion 8, experiments showed that the log (pen) rule which is often used to determine the required penetration of the virgin binder to obtain the desired penetration of the binder of the completed mixture was not applicable for the investigated mixture. It might however still be applicable for mixtures containing lower amounts of RA. Furthermore it should be noted that the experiments were especially designed to investigate the double barrel drum mixing. They therefore allow no conclusions to be made on the applicability of the log (pen) rule in case of pre-heating the RA material in a different way.

CHAPTER 8



RHEOLOGICAL STUDY ON POSSIBLE EFFECTS OF DIFFUSION ON BLENDING OF RA BINDER

8.1. Introduction

When RA is mixed with new soft grade bitumen and preheated virgin aggregates, the resulting binder in the recycled mixture is considered to be a full blended binder by most mix designers. The penetration of the binder in the recycled mixture e.g. is predicted by means of blending charts which use the penetration of the RA binder and the added virgin binder as input.

However, the question is to what extend the hypothesis of having a fully blended binder is true in practice, given the fact that the two binders contact each other in a complex mixture of stones and dust. In the previous chapter evidence against complete blending has been given.

Considering the HMA mixing process in a double drum mixer for example, superheated virgin aggregates are brought in contact with ambient, moist RA and first partly coated by RA binder when they are brought in contact with each other in the mixing chamber during the first 10-15 seconds of mixing. Secondly fillers and virgin bitumen (usually 70/100 or 160/220 pen) are brought into the mixing chamber. It is assumed that the virgin bitumen covers most aggregates as a separate layer. This implies that the binder after coating the aggregates may be considered as a multi- layer binder. Earlier, in chapters 3 and 7 the existence of multilayer binder systems was extensively discussed.

The main goal of mechanical mixing of virgin material with RA aggregates in a drum or pug mill mixer is to achieve a homogenous mixture with a homogeneously blended binder, however, there are still chances (or it is still possible) that some multi-layer binder system consisting of virgin bitumen and RA binder is created after mechanical mixing.

As soon as an interface between the two layers is created, diffusion will start dependent on the difference in molecular weight between the two binders.

Since a recycled mixture is a complex multi-phase composite at macro and micro scale, its visco-elastic properties such as shear modulus are significantly influenced by the effective modulus of the multi-layer bitumen system. In a composite, the effective modulus depends on the geometry of phases as well as on the volume and modulus of each phase. In the recycled mixture, the percentages of available RA and virgin binder should be considered as the volume fraction while the contact surface between the two binders in the mixture can be considered as their geometry. The thickness of the binder film is playing a key role in the effective modulus which is represented as volume fraction.

Given the fact that at high temperature diffusion is the highest, it can change the interface properties resulting in another layer with different properties which could contribute to the development of a multi-layer system. The possible creation of a blending zone between two binders is studied in chapter 9.

In this chapter, the effective visco-elastic properties of a multi-layer binder system are studied by means of rheological measurements. The multi-layer binder system (MLBS) is simulated by creating binder sandwiches of a number of thin binder films. The thickness of the binder films is controlled in such a way that a 50% volume fraction of RA binder and a 50% volume fraction of virgin bitumen is achieved.

The effective modulus of MLBS is compared with the modulus of RA and virgin binder. The comparison between effective modulus obtained in this way with that of a fully blended binder can give an indication to what extent diffusion in this particular experiment has contributed to blending.

The diffusion at binder/binder interfaces is also studied here during a long storage time at a given temperature with multiple G* measurements at specific time intervals. The degree of diffusion between two layers of bitumen could be measured by change in effective shear modulus because of mechanical changes of the interface zone.

8.1.1. Background on diffusion

Diffusion is a transport phenomenon between two phases by mass transport without any bulk movements.

A model is proposed by De Gennes [89] to explain the molecular movements of very long linear entangled macro-molecules melted in concentrated polymer solutions. It is known as reptation at which the molecular chains in a worm style move inside a cross linked polymeric gel (see Figure 8.1). According to Gennes it explains the viscous flow of amorphous polymers.

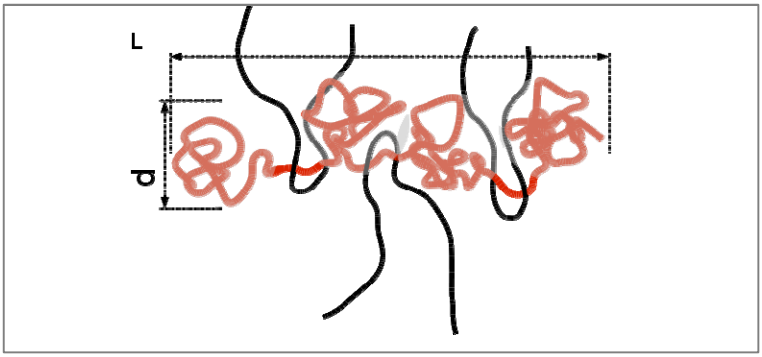

Figure 8.1. Reptation of molecular chain in the diffusing interface of epoxy

In hot mix asphalt recycling usually a rejuvenator or soft grade bitumen is used to reduce the stiffness of the aged RA binder. The performance of the HMA recycled mixture depends on the degree of blending between the two binders. Diffusion between a soft binder and an aged RA binder is one of the factors which possibly may contribute to blending and to the performance of the mixture.

With respect to bitumen diffusion, a number of influence factors are identified, like size and shape of the molecules and agglomerations, intermolecular forces, temperature and time [90]. Karlsson and Isacsson have investigated in [91] the influencing parameters on diffusion of rejuvenators in the bitumen. They highlighted the influence of temperature, time, viscosity, diffusant size and polarity on diffusion characteristics by examining the Stoke-Einstein equation. Based on this equation they derived a relation between temperature and diffusion rate using the heat energy activation approach resulting in:

$$D = k_1 . e^{k_2/T} \qquad (8.1)$$

Where k_1 and k_2 are constants and T is the absolute temperature in *Kelvin.*

Quite some research from the literature is particularly focused on bitumen diffusion [28], [87], [90], [92], [93]. The researchers were mostly focused on characterizing the diffusion between oily rejuvenators and RA binders by stage extraction of several imaginary layers to establish a relation between the viscosity of each layer and the extent of diffusion.

Diffusion of binders is also a hot topic in healing of fractured bituminous binders. Qiu has studied the crack closure through diffusion by means of a two piece healing (TPH) test setup in a DSR [94]. During the TPH test, the

healing process was mimicked by pressing two pieces of bitumen together in a parallel-plate system. The development of the complex shear modulus during the closure of the gap width and during healing rest periods was monitored and used as a healing indicator. Karlsson has utilized a two layer system of a soft and hard grade bitumen on top of each other and the resistance to shearing over the two layers was measured (see Figure 8.2) . He used the change in apparent viscosity to prove that diffusion took place and he also quantified it [90]. Then he justified his findings with ATR/FTIR analysis. In [90] layers of bituminous binders were applied on top of each other and the resistance to shearing was measured over the two layers. The change in shearing resistance (or apparent viscosity) due to diffusion was theoretically measurable, provided the difference in viscosity between the binders is sufficiently large. The change in apparent viscosity over time was in turn transformed to a diffusion coefficient. Figure 8.2 shows the principle Karlsson [90] used in his study. He prepared two layers of bitumen, and then he put them between the geometry plates of the DSR and pushed them together.

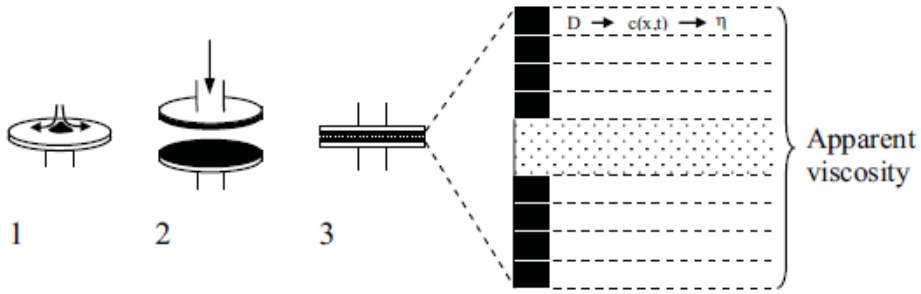

Figure 8.2 Concept of a multilayer experiment in the DSR by Karlsson [90].

Then he made calculations of diffusion coefficients based on Rheometer measurements by dividing the sample into 20 equally thick sub-layers. A diffusion coefficient, D, equal in all sub-layers, was assumed. For each sub-layer at a given time, the concentrations of the two binders were calculated. The determination of the diffusion coefficient based on the apparent viscosity is shown by Karlsson in Figure 8.3.

The use of the DSR for diffusion analyses was first developed by Hua Qui [95] with a multi-layer polymer sandwich (see Figure 8.4). The purpose of using several layers was to increase the contribution of the size of the interface area. He prepared thin polymer discs by cutting and polishing (as a mirror surface). The layers were brought on top of each other and placed between the DSR plates. The evolution of the shear modulus in time was

correlated to the diffusion coefficient. Therefore they could quantify the amount of diffusion in time.

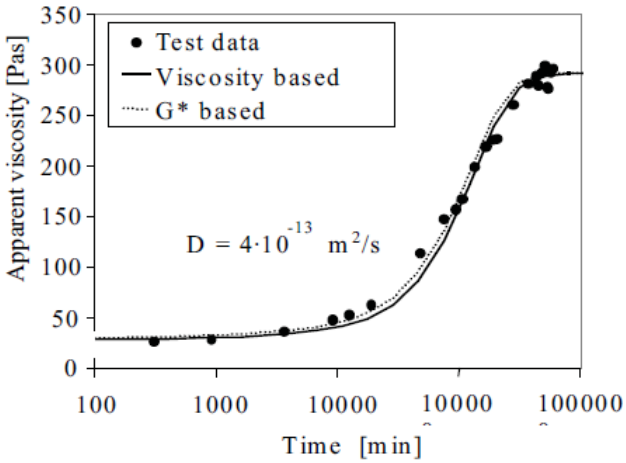

Figure 8.3 Determination of the diffusion coefficient through viscosity curve fitting over time by Karlsson [90]

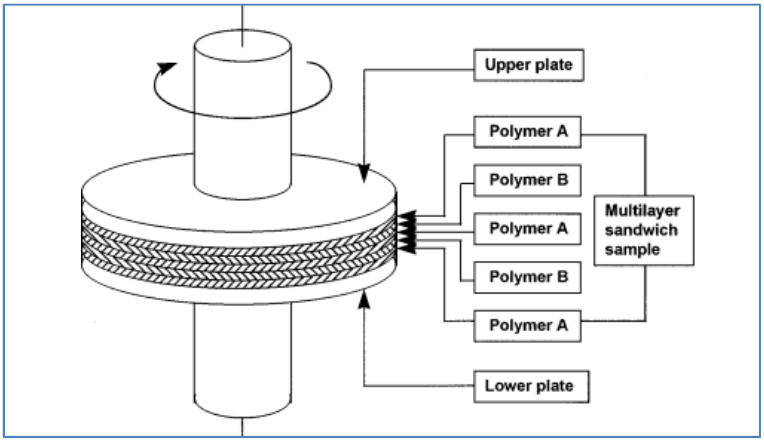

Figure 8.4 Determination of diffusion using a multi-layer polymer sandwich in DSR tests by Hua Qui (1999) [95]

8.2. MLBS setup and materials

As mentioned before, the focus in this study was on measuring the effective shear modulus of the MLBS. The contribution of diffusion in MLBS is also

taken into account. Two reference bitumens were used in the experiment; a 70/100 pen bitumen and an RA extracted binder.

The MLBS sandwiches were prepared by assembling thin films of binders on top of each other. A sufficient amount of pure bitumen was taken from a bitumen can by means of a spatula. Then it was pressed between two sheets of silicon paper at 60°C. The steel parallel plates were used to apply force on silicon papers by controlling the gap between the two plates. The thickness of the silicon papers was precisely measured with the DSR before preparing the binder films. The amount of bitumen was determined in such a way that the diameter of the resulting layer was5-10mm larger than the intended diameter of 25mm. The thickness of films depends on the number of layers which were supposed to be used to build up a sandwich.

For example, a two layer MLBS requires two films with a thickness of 500+20μm because the total thickness of each MLBS was set to 1000μm. This thickness was selected for comparison with the standard DSR testing for which at the used temperatures a 1 mm thickness is used. An extra thickness of 20 μm was necessary to fill the spaces between two layers and to compensate for the unevenness in film thickness once the binder layers were pressed on top of each other.

The binder film with silicon papers on both sides was stored at 5°C for at least 1hr. The reason for keeping the binders at a low temperature was to avoid deformation before they were assembled to MLBS sandwiches. Furthermore, the silicon papers can be removed easier when bitumen is cold and stiff.

When all the samples were ready, they were brought together by aligning their centers as illustrated in Figure 8.5.

The above described process was used to prepare samples of two and four layers of RA binder and 70/100 bitumen. The MLBS sandwiches were then placed directly between the two parallel plates of the DSR. They were preconditioned again for 5 minutes at 60°C before compressing them to the required final thickness of 1050μm. This thickness of each layer is required because the total thickness of the layers shouldn't exceed 1 mm in the DSR test to be in line with the standard test. Once the intended thickness was achieved, the excess binder around the DSR plates was trimmed off with a hot blade. Then the gap between the two plates was reduced to the final target thickness of 1000μm.

After this the MLBS was ready for shear modulus measurements at different time intervals using frequency sweep tests at each cycle at different temperatures (30°C, 40°C and 50°C).

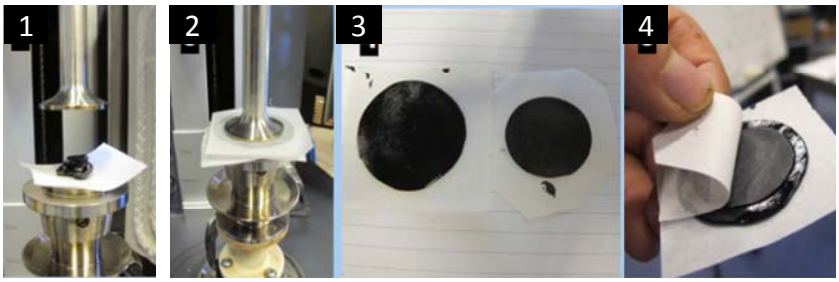

Figure 8.5. Process of preparing MLBS sandwiches for DSR testing. (1) required amount of bitumen is brought between two plates; (2) bitumen is pressed to the required thickness between two plates in the DSR geometry (3) bitumen films are prepared for each layer separately (4) layers are placed on each other

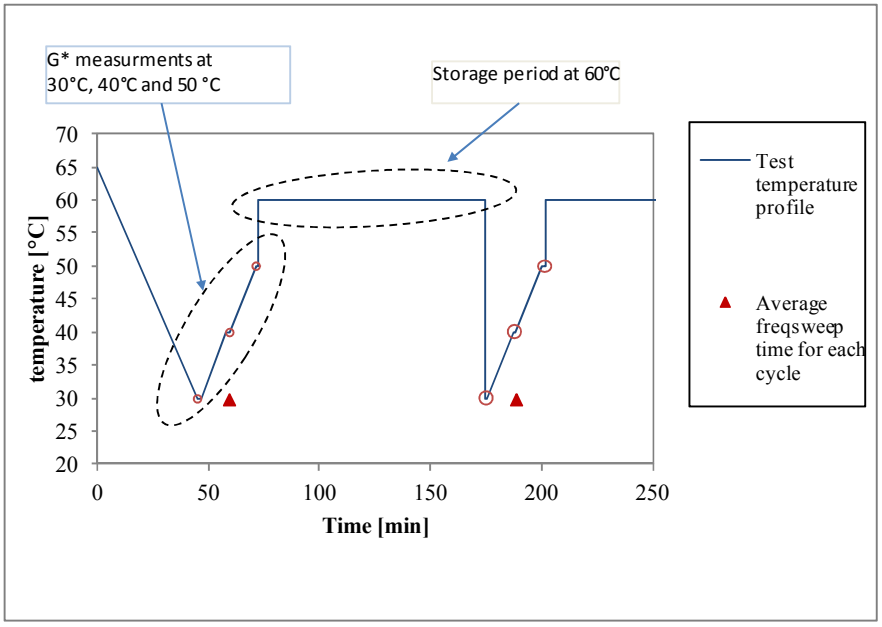

Figure 8.6 An example of the temperature profile during a diffusion test using the DSR

The first measurements (at 30°C, 40°C, 50°C) were done as soon as the MLBS was ready. Then the DSR remained in the idle mode at 60°C for 90 min. Then the sample was cooled down to 30°C and the second frequency sweep series took place at the three temperatures. After this the temperature of

the sample was increased to 60°C and again in the idle mode for 90 minutes. This procedure was repeated 10 times. Given the fact that the duration of a frequency sweep is 30 minutes, it turned out that each cycle of temperatures conditioning and measurement was 2hrs. The temperature profile of MLBS samples is illustrated in Figure 8.6. The triangle marks are showing the average time which is used further as corresponding time to each G* master curve.

The frequency sweep results were then used to construct a master curve for each cycle. The change in G* values and the master curve was related to the effect of diffusion.

In the DSR test, the shear load is applied from the upper plate while the bottom plate is fixed. The load cell and temperature sensors are connected to the lower plate. For the shear loading an oscillatory sinusoidal signal was used in strain controlled mode.

The order of stiff and soft layers would make sense when the shear stress propagates from the very first top layer. Therefore the two layer MLBS was also measured in reverse order where RA binder is at the bottom and 700/100 is on top. Gravity may have an influence on the diffusion when the soft binder is on top of the harder one since the concentration of molecule weight in the RA binder is higher than that in 70/100 bitumen.

Temperature conditioning of the DSR samples was done by air flow. This could initiate a problem since the rim of the binder sample (at the plate edge) could get aged when exposed to air flow at a rather high temperature of 60°C. Consequently an uncertainty arose about whether this aging is affecting the shear modulus. There is also the possibility that the G* increases due to physical hardening being the rearrangement of molecules in a thixotropic material like bitumen. Another possibility could be the crystallization of wax, especially, in softer bitumen in the temperature region between 60 to 30°C. To prove that the changes of G* are only influenced by diffusion, a single layer test was also conducted. The shear modulus of the original binders (RAP and virgin binder) were measured as single layers with a thickness of 1000 µm using the same temperature profile and the same number of cycles as shown in Figure 8.6.

Not only MLBS sandwiches were made; also other combinations of two and four binders were created in the DSR to study the effect of layer arrangements. They are called HLF (two half circle binder specimens) and QRT (four quarter binder specimens). The preparation of these specimens is shown in Figure 8.7. This figure shows that layers are prepared in a similar way as the previously mentioned layers. HLF segments are created by folding a 500µm film as shown in Figure 8.7c. The QRT segments are prepared by

folding a 250µm film two times. It turned out that the final thickness of QRT and HLF reaches 1000µm, before placing them between the plates in the DSR. A single time frequency sweep was performed on these samples and not the long time temperature conditioning for diffusion testing. The QRT and HLF tests were only done to compare the effective modulus of different combinations of 50% RA and 50% virgin bitumen when they are not fully blended.

Another sample of fully blended 50% RA and 50% virgin 70/100 binder was prepared by mixing 100 grams of each at 150°C for 50 minutes in a shear mixer. This blended binder was then measured in the same DSR setup to create G* master curves at 25°C. These master curves were compared with those obtained on other combinations.

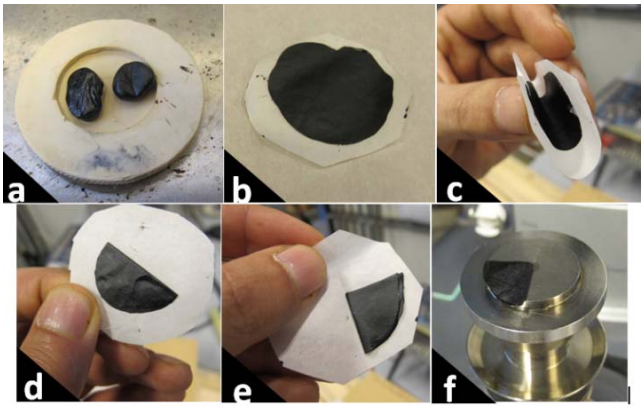

Figure 8.7. Preparing QRT (e) and HLF (d) binder combinations

8.2.1. Results and discussion on diffusion

A summary of the diffusion tests is given in Table 8.1. The results of test 1, 2 and 3, 4 and 5 are summarized in Figure 8.8 to Figure 8.12. Each figure consists of:

- an illustration of test setup and arrangement,
- temperature profile of the test,
- a chart showing the development of G* (*at 30°C)* due to diffusion at different frequencies,
- master curves of effective shear modulus at 25 °C in comparison with original layers.

Table 8.1 Summary of long term diffusion tests at 60°C

Test No.	***Name***	***Test duration***	***combination***	***Results***
1	RA top- 70/100 bottom	19hr	2 layers (each 500µm)	Figure 8.8
2	70/100 top- RA bottom	15hr	2 layers (each 500µm)	*Figure 8.9*
3	Four layers	66hr	4 layers (each 250µm)	*Figure 8.10*
4	Single RA layer	19hr	1 layer (each 1000µm)	Figure 8.11
5	Single 70/100 layer	19hr	1 layer (each 1000µm)	Figure 8.12

In each figure (Figure 8.8 to Figure 8.12) the slope of the G* value at 30°C is given from the linear regression at each temperature separately. A summary of the G* slope at different temperatures is shown in Table 8.2. The slope values could be interpreted as a comparative indication of diffusion in time. They are also compared in Figure 8.13.

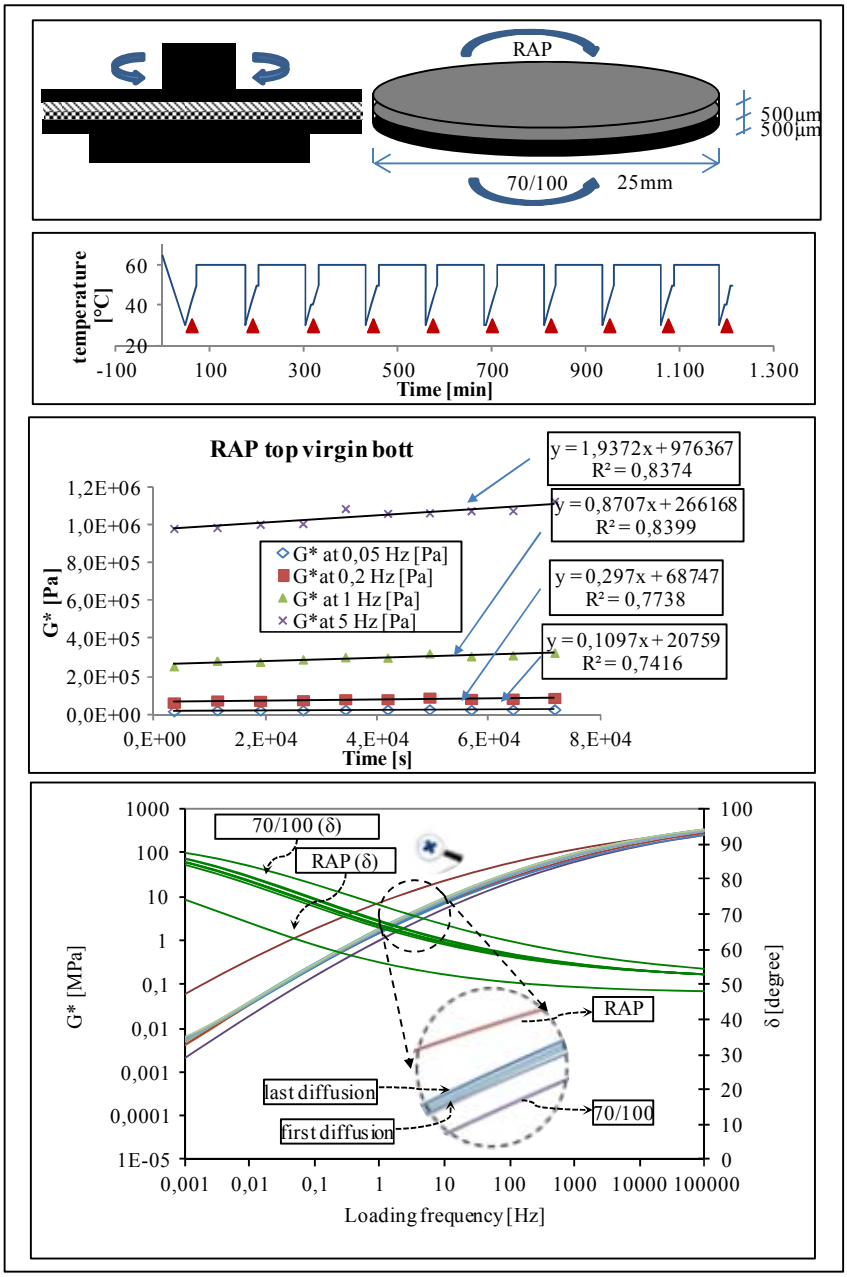

Figure 8.8 Two layer MLBS diffusion results [RA on top and virgin binder at the bottom] (G Mastercurves are at 25°C)*

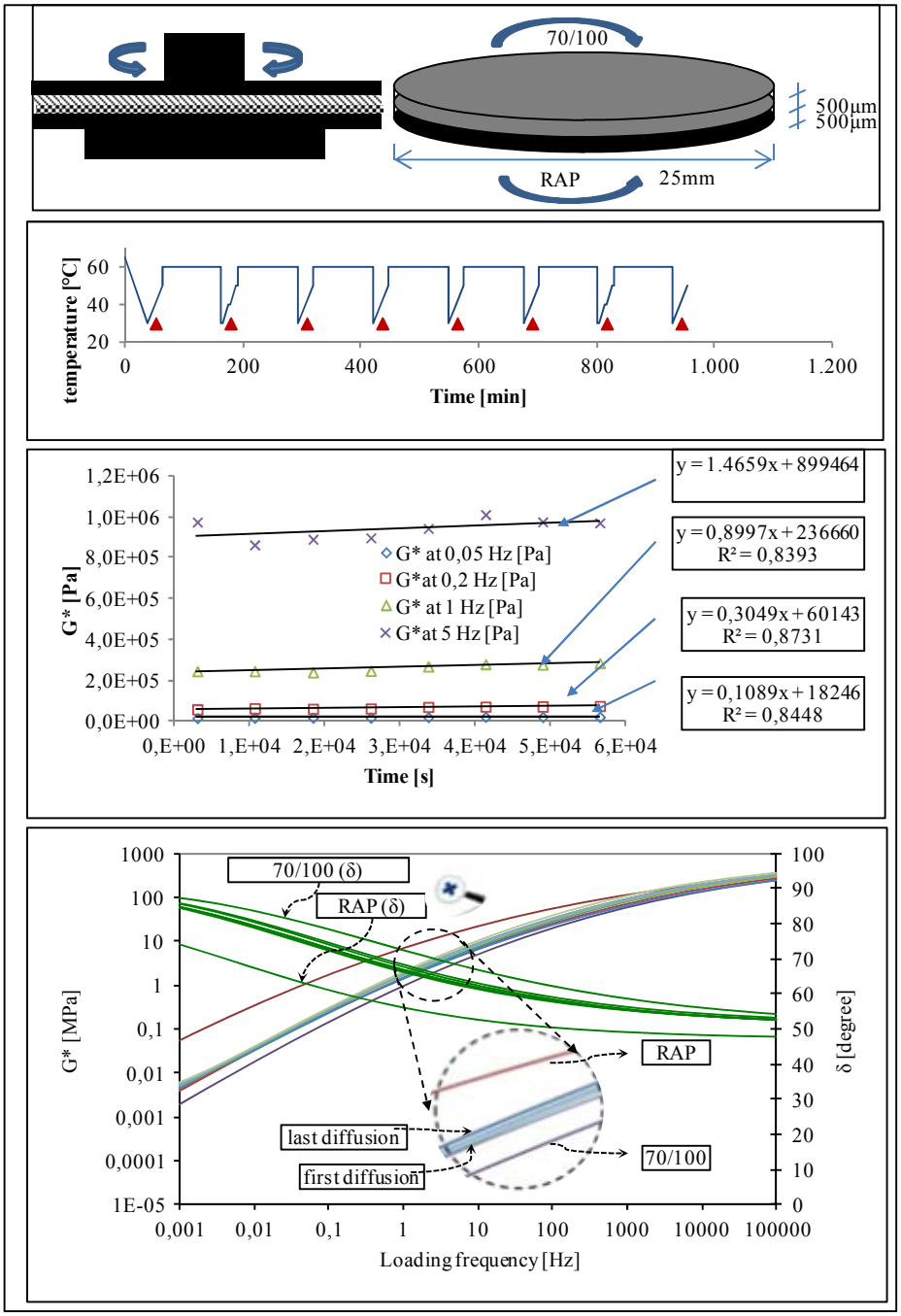

Figure 8.9 Two layer MLBS diffusion results [70/100 on top and RA binder at the bottom] (G Mastercurves are at 25°C)*

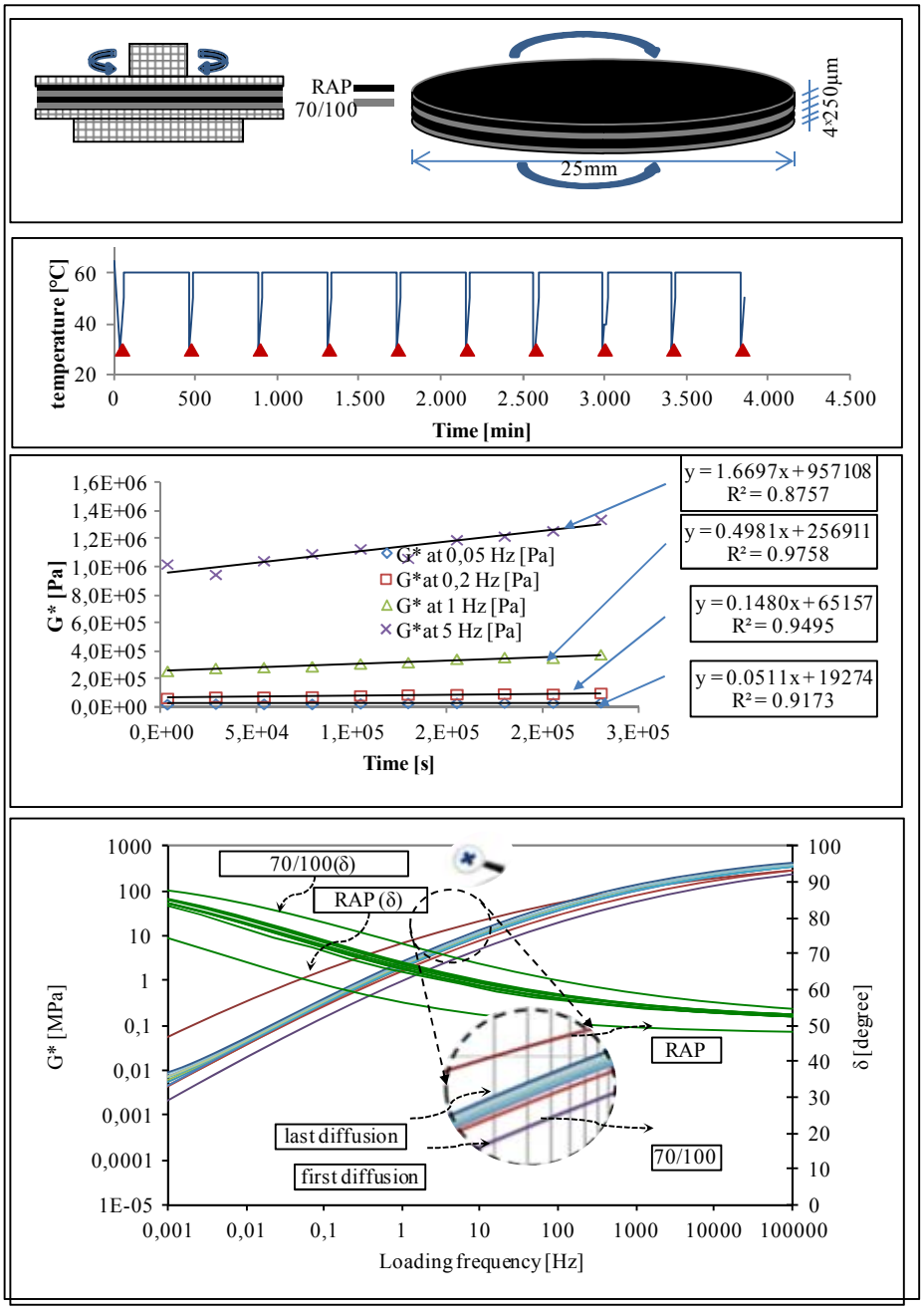

Figure 8.10 The four layers MLBS diffusion results (G Mastercurves are at 25°C)*

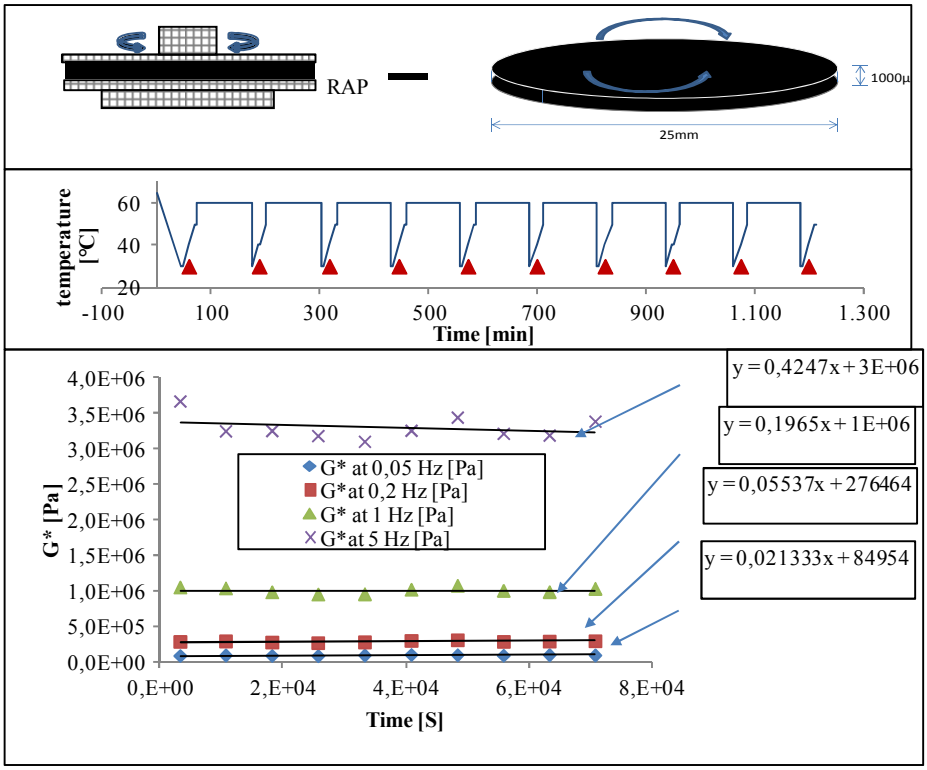

Figure 8.11 Single layer of RA

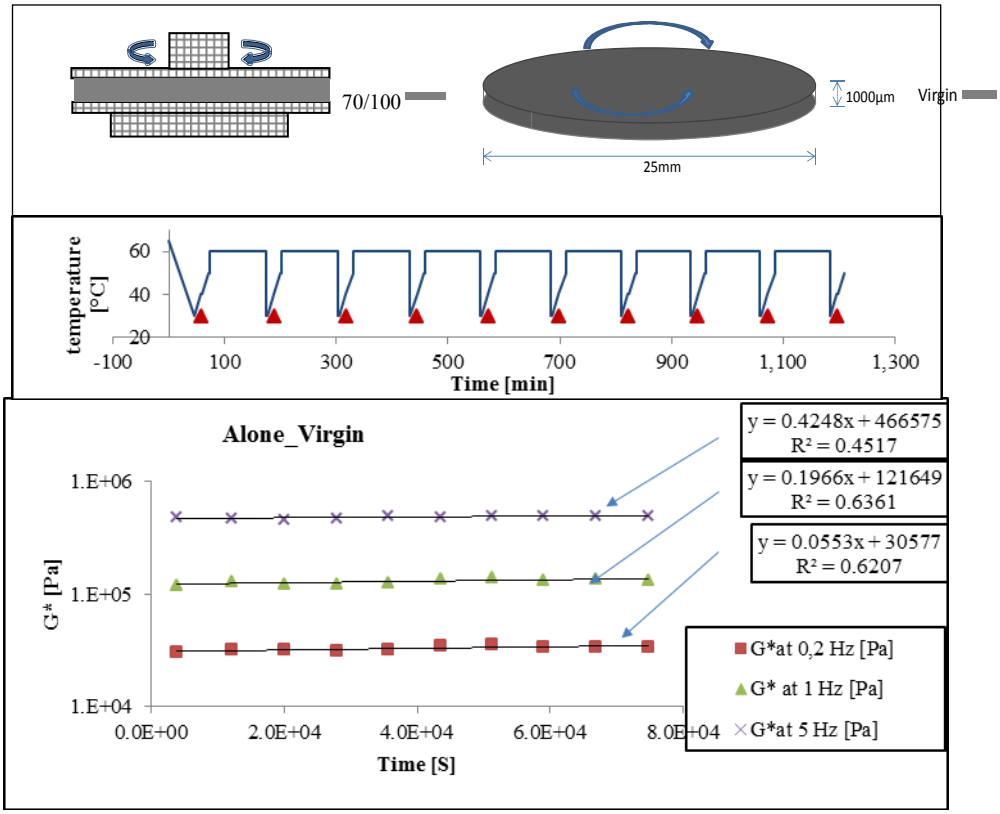

Figure 8.12 Single layer of virgin 70/100

Table 8.2 Summary of the slope of the time vs G values obtained during the long term diffusion tests at 60°C*

Test No.	*Test description*	*0,05Hz*	*0,2Hz*	*1Hz*	*5Hz*
1	RA top- 70/100 bottom	0.109683	0.296989	0.870715	1.937234
2	70/100 top- RA bottom	0.108937	0.304944	0.899704	1.465895
3	Four layers	0.051121	0.148003	0.498109	1.669782
4	Single RA layer	0.1048	0.2405	0.4464	0.5215
5	Single 70/100 layer	0.021338	0.055307	0.196583	0.424763

As can be seen in Figure 8.13, the slope values of G* (at 5Hz) are in the range of 1.5-2 for the MLBS samples while they are in the range of 0.4-0.5 for the

single binders. It indicates that approximately around 30% of the G* increment belongs to either aging or physical hardening (or wax crystallization). The rest is attributed to the effect of diffusion at the interfaces. The average slopes of test 4 and 5 (which belong to the single layer test) are deducted from the slopes of the multiple layer test in order to have a corrected slope because of the effect of aging. The corrected slopes are shown in Figure 8.14. Then the corrected slope values are used to predict the G* values after 70000 seconds. These values are compared with the initial value in the early stages of diffusion (1000s) in Table 8.3. It is assumed that the increase in G* showed in this table is only the effect of diffusion because the effect of aging was removed by correction. The diffusion effect in test 3 (four layers) is similar to the other two layers test, while it was expected to be more because of more interfaces between layers. No explanation could be found for this result.

Given the fact that the conditioning temperature was only 60°C, one can assume that all slope values related to the diffusion will increase when determined from test results obtained at higher temperatures. This is important since the 60°C temperature is far away from the mixing and storage temperatures in practice which are around 160-170°C. It was therefore first tried to conduct these tests by conditioning the MLBS samples at 170°C by casting them in silicon liquid. Unfortunately the thickness of the binder layer could not be controlled at that temperature. A temperature of 60°C was the highest temperature at which a stable arrangement could be achieved.

Table 8.3 G values in the beginning of the tests and after 70000 s (after correction of the aging effect)*

Test nr.	***G* values [Pa] at t=1000 s***				***G* values [Pa] at t=70000 s***			
	0,05Hz	*0,2Hz*	*1Hz*	*5Hz*	*0,05Hz*	*0,2Hz*	*1Hz*	*5Hz*
1	20806	68896	266717	977831	24022	79183	304614	1078854
2	18292	60300	237238	900639	21457	71136	277135	969139
3	19262	65157	257088	958305	18438	65164	269274	1040874

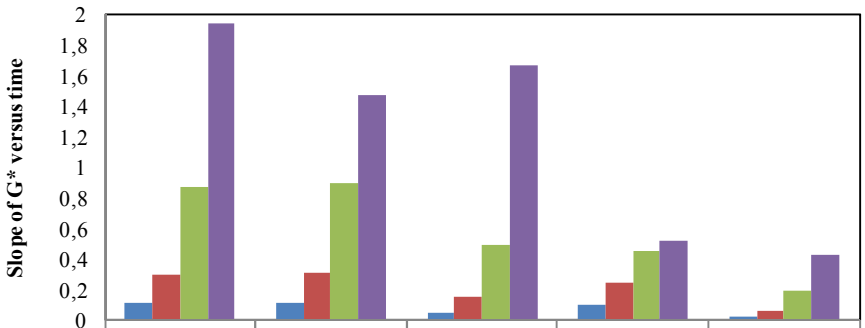

	1	2	3	4	5
0,05Hz	0,109683	0,108937	0,051121	0,1048	0,021338
0,2Hz	0,296989	0,304944	0,148003	0,2405	0,055307
1Hz	0,870715	0,899704	0,498109	0,4464	0,196583
5Hz	1,937234	1,465895	1,669782	0,5215	0,424763

Figure 8.13 Comparison of G slope as an indication of diffusion (without the correction of aging); storage temperature 60°C (1,2,3,4,5, are the test number)*

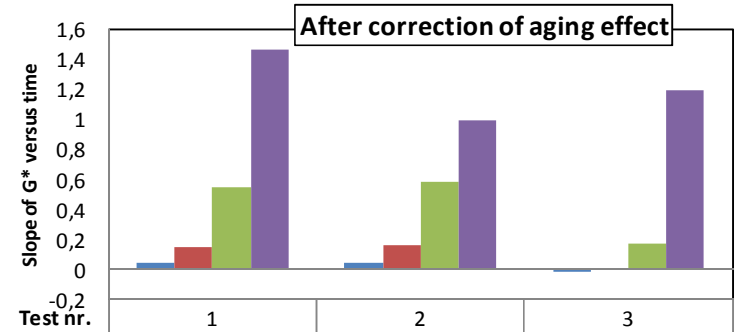

Test nr.	1	2	3
0,05Hz	0,046614	0,045868	-0,011948
0,2Hz	0,1490855	0,1570405	9,95E-05
1Hz	0,5492235	0,5782125	0,1766175
5Hz	1,4641025	0,9927635	1,1966505

Figure 8.14 Comparison of G slope as an indication of diffusion (after the correction of the effect of aging); storage temperature 60°C*

8.2.2. Results and discussion on effective shear modulus

As mentioned, extra combinations of virgin and RA binders were tested being QRT, HLF and BLD. They are illustrated in Figure 8.15. As mentioned, BLD stands for full blend of RA and virgin binder which are tested as a single layer having a thickness of 1000µm thickness.

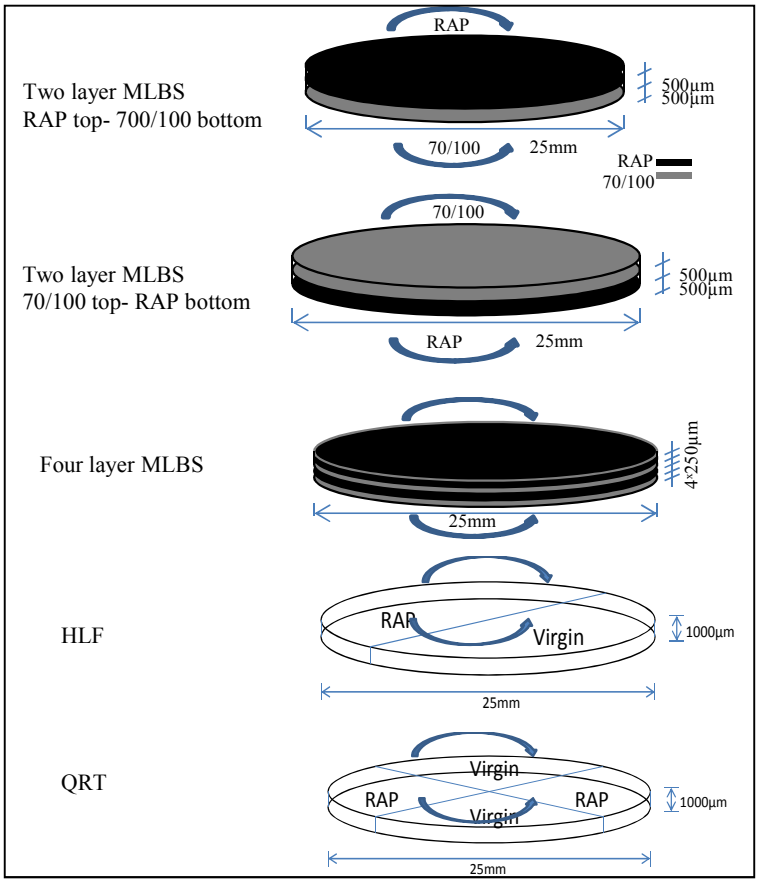

Figure 8.15 DSR test on multiple binder combinations in horizontal and vertical series

According to the master curves shown in Figure 8.16 and the comparisons presented in Figure 8.17, almost all horizontal combinations of binder fractions have a lower effective shear modulus in comparison to the effective shear modulus of the full blended binder. However, the difference is not (that) significant.

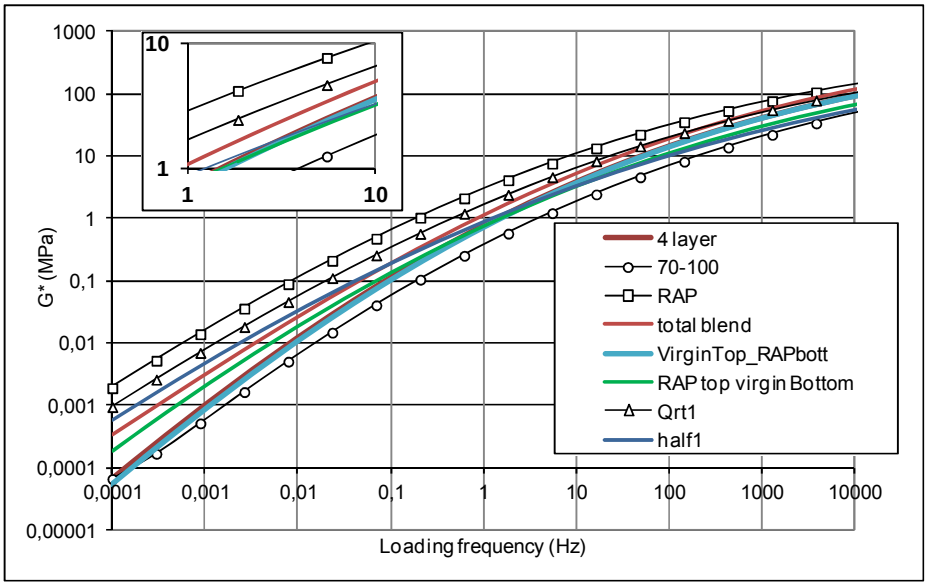

Figure 8.16 Effective shear modulus master curves of the multiple binder combinations in horizontal and verticalseries

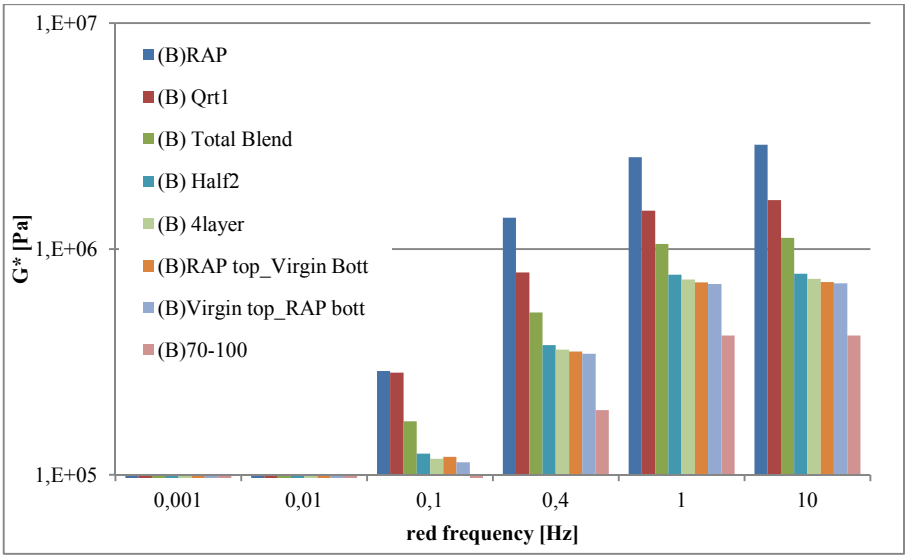

Figure 8.17 Comparison of effective G values at 20°C (the values are obtained immediately after preparation of the samples)*

8.3. Conclusions

Based on the results of the research into the possible effects of diffusion on the effective shear modulus of composite binders the following conclusions are drawn:

1. A test setup and material preparation method was developed that allows quantification of diffusion at binder-binder interfaces using rheological tools. The technique consists of measuring the dynamic shear modulus as a function of time for MLBS sandwiches.
2. Since conditioning of the samples was done by airflow the continuous increase in shear modulus of MLBs sandwiches in time could be partly explained by either aging, physical hardening or crystallization of waxes. The influences of aging and physical hardening were estimated to be approximately 30% of the total increment.
3. The long term diffusion could be predicted by the slope of the G* vs time relationships after correction for aging and physical hardening. However, more research is needed to determine the magnitude of the effect of aging and physical hardening
4. The effective modulus of the two layer MLBS is slightly higher when RA is on top, because the shear force is propagating from the top layers, given the fact that the upper plate is oscillating in the DSR set-up. The diffusion rate (defined in this research as the slope of G* as function of time) is higher when the RA binder is on top, most probably because of the influence of gravity.
5. The temperature for determining the influence of time on diffusion was 60°C because of limitations of the test setup. Nevertheless some diffusion was measured at this temperature. It is expected that the diffusion rate will be significantly higher at temperatures above 100°C.
6. The comparison of the effective modulus between different arrangements of pure bitumen showed minimal differences between all those arrangements for fully blended binder. Given the fact that a HMA mixture is usually at high temperature for quite some time (taking the mixing, storage and construction period in to account it will mostly be more than 3 hours), the minimal difference could be to some extend compensated by diffusion.

8.4. Recommendation

- The test was only done on bitumen. A similar study on multiple mastic layers is very important as a complementary study. This would give more realistic information on blending between RA mastic and virgin mastics.

CHAPTER 9



MORPHOLOGY OF THE BLENDING INTERFACES OF RA BINDER

9.1. Introduction [1]

Hot mix asphalt recycling mostly requires addition of softer bitumen or a rejuvenator to soften the stiffer RA binder. The RA binder is already hardened due to aging in the pavement during its service life. The grade of the soft bitumen to be added in the recycled asphalt mixture is usually determined by blending charts or equations such as the log-pen rule, assuming that the RA binder is homogeneously and completely blended with the virgin bitumen during the mixing process. Several laboratory and field studies have shown however that this latter assumption is seldom completely valid. In some cases designers even consider RA to act as black rock (no blending). This issue will also become very important when considering asphalt production at lower temperatures.

Non homogenous and partial blending of RA with soft virgin bitumen could decrease the fatigue life [31] or improve it [96]. These contradicting results indicate the necessity of investigating the degree of blending between RA binder and virgin bitumen. Figure 9.1 shows an example how RA binder, which is covering the RA aggregates, might be blended with the virgin binder that is covering the virgin aggregates. The question however is whether this hypothetical model (shown in Figure 9.1) is correct and how we can use it to measure the blending degree.

[1] This chapter is based partly on [100]

Quite some research has been done to determine the degree of blending by means of two different approaches, the so called mechanistic and the interface detection approach. In the mechanistic approach it is tried to indirectly determine the amount of blending by comparing rheological properties of RA mixtures and ideal mixtures in which extracted RA binder is already blended with virgin bitumen prior to mixing [97].

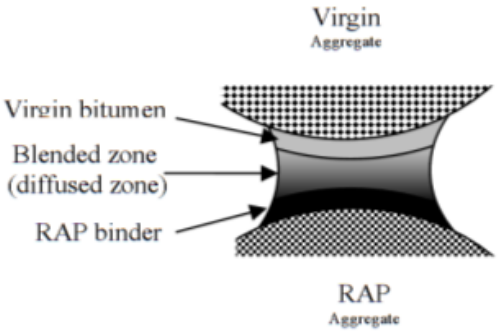

Figure 9.1: Model of blended zone between RA and virgin aggregate [100]

with interface detection and morphology studies, blending measurements are mainly based on studying the diffusion between two binders or between binder and rejuvenator. Stage extraction, DSR, and FTIR-AR tests are often used to determine the degree of blending.

In this chapter the aim is to investigate if it is possible to detect two binders in a mixture which are chemically and physically different. Rheology, density and molecular microstructure were analyzed with laboratory equipment such as nano computed tomography (nano CT scanning), nano-indentation (NI), and optical microscopy.

Nano-tomography scanning and optical microscopy were done on three different groups of samples. Nano-indentation was conducted to evaluate the difference in the surface stiffness of aggregate-binder interfaces. Nano CT scanning techniques were used to observe slight differences in density at the interface between two binders. Optical microscopy was conducted on thin sections of an asphalt mixture to detect the interface zone between two binders.

Optical microscopy was selected to observe the distribution of virgin bitumen and RA binder and the coating thickness of RA aggregates after mixing. Nano indentation and Nano CT-scanning were used to observe the interface and blending zone of two binders.

9.2. Morphology research Methodology

9.3. Nano indentation

In the nano-indentation test, mechanical properties of the surface are measured by analyzing the surface response to the penetration of a tip (Berkovich tip) with defined shape penetrating into the material. The indentation process consists of a loading, holding and unloading phase (Figure 9.2). The displacement versus force curve obtained by controlling the force or displacement is plotted during the indentation. The initial slope of the curve in the unloading part of the curve is used to determine the stiffness of the material [98]. The hardness of the surface is obtained from the maximum force and the contact area. Equations 9.1 and 9.2 are expressing the hardness and stiffness respectively.

$$H = \frac{P_{\max}}{A_c} \qquad (9.1)$$

$$S = \frac{dP}{dh}\Big|_{h=h_{\max}} = \frac{2}{\sqrt{\pi}} M \sqrt{A_c} \qquad (9.2)$$

Where, P_{max} is the maximum indentation force, S the initial slope of the unloading phase and A_c the projected contact area.

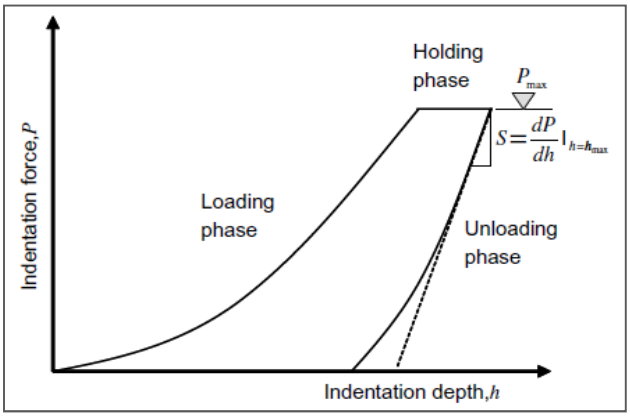

Figure 9.2: Indentation depth vs. loading [99]

9.4. Nano computed tomography scanning

It was assumed that nano CT scanning can be used for visualizing the interface between two binders of different densities. Similar to other forms of tomography and micro tomography, Nano computed tomography uses X-Rays to create cross-sections from a 3D- object. These cross-sections can be used to create a 3D model without destroying the original sample. The X-Ray beams carry various wavelengths and energies (polychromatic). As the X-rays pass through the scanned object, the signal is attenuated by scattering and absorption. The attenuation μ of these X-rays inside the object is energy dependent and therefore it is not a constant. The grey values are a combination of the local object density and the local average attenuation coefficient. By using X-ray filters it is possible to reduce the contribution of the parameter μ and finally get a good idea of the density of the object. For most samples the density will provide an idea of the internal structure.

The major difference between nano CT scanning and other types of X-Ray tomography techniques is their pixel size in the cross-section images. With this kind of equipment, cross-sections with pixel sizes in the nanometer range are possible. The minimum possible pixel size is 400 nm. However the accuracy depends on the size of the scanned object. As a rough estimation, the pixel size is approximately 1000 times smaller than the original dimension.

For instance, scanning a sample of 0.5 mm diameter can result in 500 nm pixels.

9.5. Materials and specimen preparation

9.5.1. Material Preparation for nano CT scanning

Two types of bitumen were used to prepare the samples for nano tomography scanning; a pen 20/30 (bulk density 1044 kg/m3) and pen 160/220 (bulk density 1019 kg/m3) were used. Three different samples were prepared and scanned by nano tomography (Figure 9.3);

Sample CT1 - Glass beads of 1mm and 2mm were coated with soft and hard bitumen and they were mixed at 130 °C to allow the two binders to be blended.

Sample CT2 - Soft and hard bitumen were poured in a plastic cylinder of 5mm diameter on top of each other to produce a column of the two bitumens. They were heated up to 100 °C and 150 °C respectively, in order to be soft enough to pour them in the cylinder. Then the samples were kept in an oven at 50 °C for 30 minutes and after that at room temperature.

Sample CT3 – a metal tracer (Tetrabromobisphenol A 97%) was initially mixed (0.2 % mass) into a soft bitumen (pen 160/220) at 150°C with a high shear mixer at 2500 rpm. After mixing the soft bitumen was poured on top of the hard binder (pen 20/30) in a 5mm diameter cylinder. The purpose of using the tracer was to detect it by nano CT scanning to get in this way an indication of diffusion.

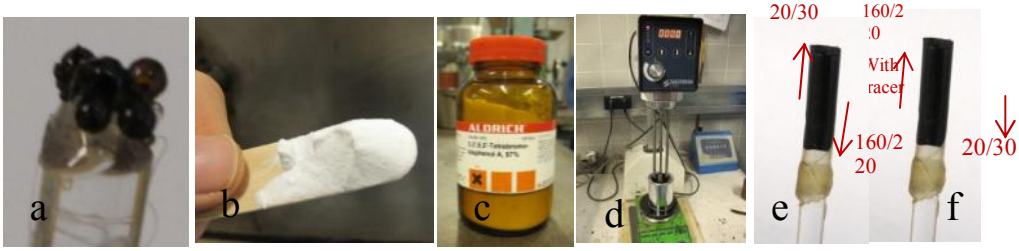

Figure 9.3: (a) Sample CT1, (b and c) Tetrabromobisphenol, (d) shear mixer (e) sample CT2, and (f) sample CT3

9.5.2. Material preparation for nano indentation and optical microscopy

Mixtures were designed with standard mono-sized glass beads and mono-sized river sand as aggregates. Pen 20/30 bitumen was used to simulate the RA binder. The soft binder was a 160/220 pen bitumen.

50% of the aggregates were coated with a layer of approximately 20µm soft binder and the rest was coated with the hard bitumen at the minimum coating thickness presented in Table 9.1 prior to mixing. The required amount of bitumen to coat the aggregate was determined by calculating the specific surface area of the aggregates.

Different sizes of glass beads and sieved river sand were used to make 7 specimens (BL1:BL7). BL3 was used for nano-indentation and the other specimens were used to prepare thin sections for optical microscopy. The aggregate sizes of each mixture are listed in Table 9.1.

Table 9.1: Aggregate sizes in each mixture

Specimen ID	***Type and size of aggregate coated with soft bitumen (160/220)***	***Type and size of aggregate coated with hard bitumen (20/30)***
BL1	GB 2mm	GB 2mm
BL2	GB 1mm	GB 2mm
BL3	GB 1mm	GB 1mm
BL4	4-2mm	S 1-2mm
BL5	1-2mm	4-2mm
BL6	S 0.5-1mm	S 0.5-1mm
BL7	S 0.5mm	S 0.5-1mm

S: Sand, GB: Glass Bead

Since the mixtures consist of mono-size aggregates and no filler was added, they were not strong enough to sustain sawing and polishing. Therefore they were molded in a paper cup without compaction and then they were

impregnated with epoxy to get a stable sample. The impregnated samples could be cut, polished, etc.

A seperate sample (BL-0) was made of granite stone slices. One side of each stone was covered with a thin layer of hard and the other with soft bitumen. Then they were placed on top of each other in such a way that the soft bitumen was exposed to the hard bitumen. Since the first step was to find out if it was possible to see a clear zone between the two binders, they were just kept at 50ºC for an hour in an oven. Although this fairly low temperature and relatively short period of time will not allow full blending between the two binders, it was expected that at least a limited blending area in the interface zone between the two binders could be detected.

All samples were cut to 30×40 mm sizes. Then they were polished with several rough and soft sand papers to achieve smooth surfaces. All samples were cooled in ice water at 0 ºC during cutting and polishing to prevent smearing of the bitumens. Other samples were polished with sand paper and rollers to make thin slices (30µm) for optical microscopy. Figure 9.4 illustrates a section of BL3 and a cut sample of BL0 which were used for nano-indentations in this research.

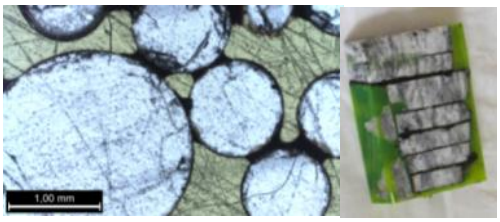

Figure 9.4:BL3 (left: cross section of glass beads coated with bitumen, green surfaces are epoxy used for impregnation) and BL0 (right: layers of stones bonded with bitumen)

9.6. Experiments and results

9.6.1. Light polarized microscopy imaging

Thin sections were made by grinding a slice of the mixture which was glued on a glass slide, until it reached a thickness of about 30 microns. Most

minerals become transparent at this thickness and can therefore be studied with a light polarized microscope by light transmission. Thin film sections (with a thickness of 30µm) were made from BL1-BL7. Some images from BL4 and BL6 are shown in Figure 9.5. Images a, b and c are taken from BL4 at different scales to find out if it is possible to detect the soft and hard binder layers. Since aggregates consist of different minerals, one can differentiate them by their colors in the images. But in the binder zone, as it is enlarged in the BL-4 and BL-6, it is not possible to separate soft binder from hard binder. There is a slight difference at the stone-binder interface zone, but this is probably because of a lower binder thickness around the stones.

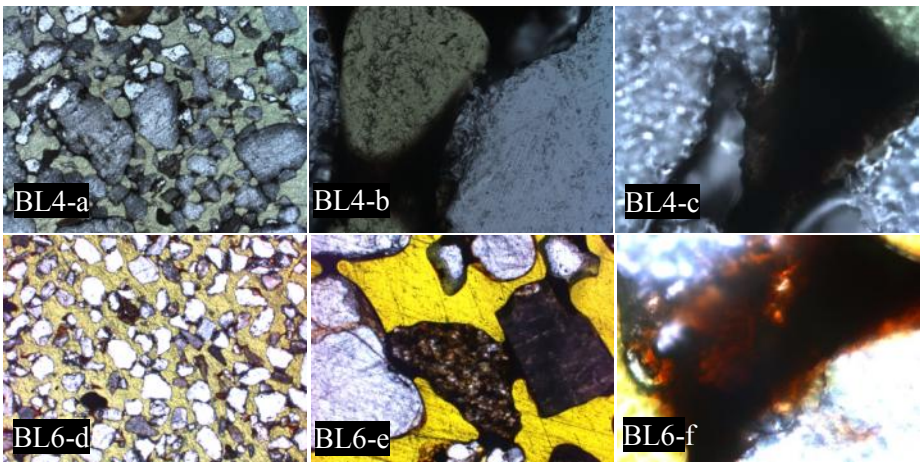

Figure 9.5: Optical Microscopy images of thin sections; BL4 (a, b and c), BL6 (d, e and f).

9.6.2. Nano indentation results

All indentation tests were done with a G200-Nanoindentor instrument using a Berkovich tip. A special setup was attached beneath the sample holder to maintain the surface temperature at -10°C during the indentations. First indentations were done on a selected line on BL-3 (see Figure 9.6). The indentations started from a point on the glass bead and ended on the binder. This was done to observe properties of the aggregate and binder interfaces. 100 indentations were done with a distance of 3µm between each indentation.

The maximum penetration was in all cases 200 nm; the possible effect of an indentation on the neighboring indentation points was not taken into account.

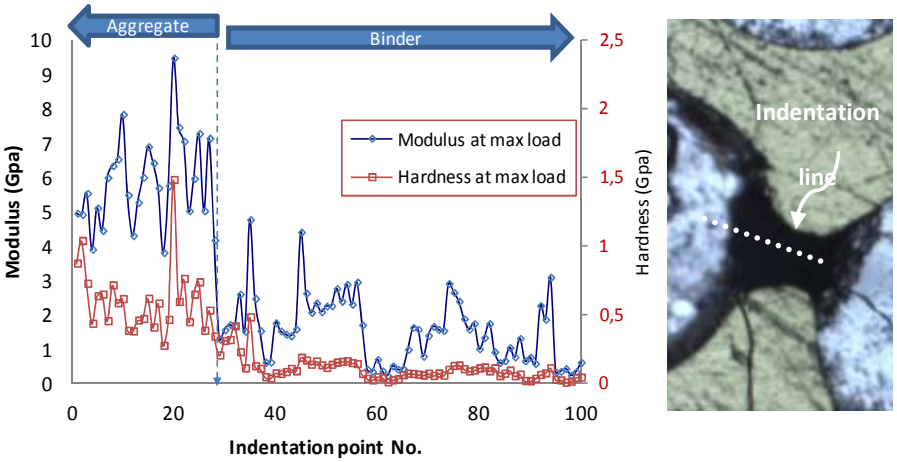

Figure 9.6: Modulus and hardness on a glass-bitumen interface (BL-3)

In analyzing the data attention it should be kept in mind that the binder behavior is viscoelastic and the stone can be considered an elastic material. The software default calculation method was used to analyze the indentations made on both the aggregate and the binder (Equations 9.1 and 9.2). The software calculates the modulus at the maximum load.

According to Figure 9.6, most modulus values are in the same range until point 30. They are between 4 and 8 GPa. From point 30 the modulus values suddenly drop to less than 2 GPa. This zone, which is as wide as 45 micron, is probably the interface between the binder and the glass.

Figure 9.7 shows a model of the binder film thickness around the aggregate at the surface of the mixture. It shows that the measured modulus values may also be influenced by the aggregate modulus below the indentation point due to the differences of binder film thickness at each point.

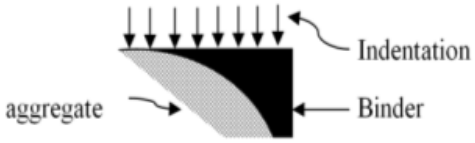

Figure 9.7: Binder film thickness above the aggregate while surveying the surface of a cut sample with the nano indenter.

In the zone between points 35 to 100, repetitively an increase and decrease in the modulus is observed within almost every 20 indentation points (every 60 μm). Repetitive rise and fall in the modulus curve could suggest the presence of hard areas with higher molecular weight micelles (or crystalline phase from wax) which is dissolved in a softer and lower molecular weight medium as is hypothesized in [13]. Peak values of harder areas are between 2 and 3 GPa. Away from the peak values (on the micelles) the modulus decreases gradually to less than 0.5 GPa. Also, stiffness and hardness peak values are decreasing from left to right. If the properties of each binder are known separately, then it is possible to recognize the interface or border between the two bitumens.

Another indentation test was done on a stone-binder-stone interface for BL-0. Nano indentations were again done at -10 °C with a maximum penetration depth of 500nm. 150 points were indented every 3μm. The modulus results are shown in Figure *9.8.* In this figure the modulus of the binder zone is shown separately below the main chart.

Nano-indentation on BL-0 was done in a different sequence. As described earlier, BL-0 consists of parallel granite stone sheets. It was done on a line starting from one stone and ending on the other stone by passing the bituminous “bridge” consisting of soft and hard binder.

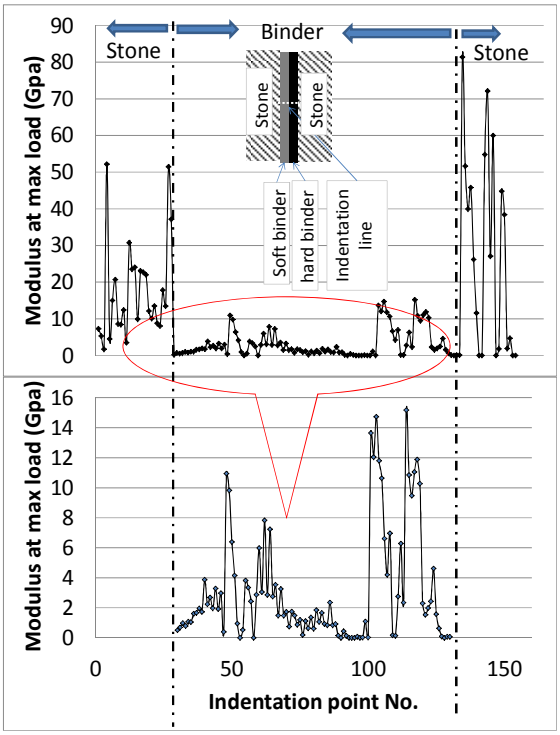

Figure 9.8: Modulus results obtained from nano-indentation on a stone-binder-stone interface in BL-0 (below: data obtained on the binder zone at a lower modulus scale)

Three different zones are detectable in Figure *9.8*. The two stone zones can be recognized from their high modulus, and consist of points 1-30 and points 130-150. The third zone is the binder zone with a total thickness of 300µm. This zone consists of points 31-129. The modulus values of the stone zone are between 25 and 70 GPa. In the binder zone one can see a periodic rise and fall at every 20 points. There is also a region (points no. 100-125) in which the modulus is less than the stone modulus and much higher than the values for the bitumen obtained in the area from points 30-99.

This could indicate the hard bitumen but this is not sure because the values in the 100-125 area are very high for bitumen, even for hard bitumen. Because of this it is not clear whether the "jump" in modulus at position 100 indicates the interface between the two types of bitumen.

9.6.3. Nano computed tomography imaging results

9.6.3.1. Sample CT-1

By analyzing images obtained from CT scanning on sample 1 (Figure 9.9), one can measure the bitumen film thickness around the glass beads but with this imaging it was not possible to distinguish between soft binder and hard binder.

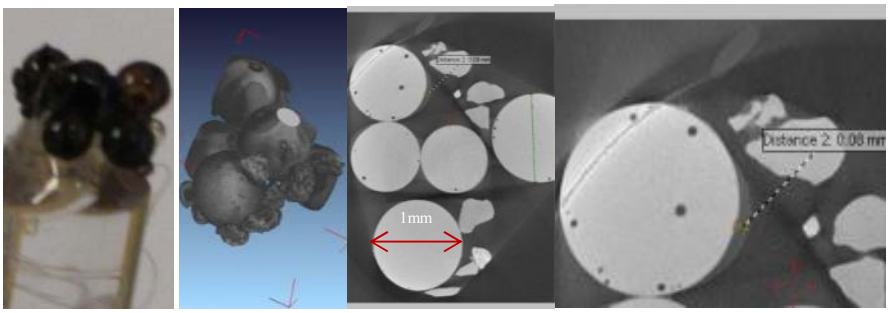

Figure 9.9: CT scan imaging of CT-1

9.6.3.2. Sample CT2:

CT scan images of sample 2 (Figure 9.10) clearly illustrate the interface between two binders. Usually the gray value of lower density materials in CT scan images, are higher than those of more heavy materials, therefore their CT images are darker. In spite of its lower density, the soft binder is illustrated in a lighter color (lower gray values) which indicates it as a denser one. The same result was obtained after filtering images to correct for the beam hardening effect. Unfortunately the reason for this phenomenon could not be found in this research.

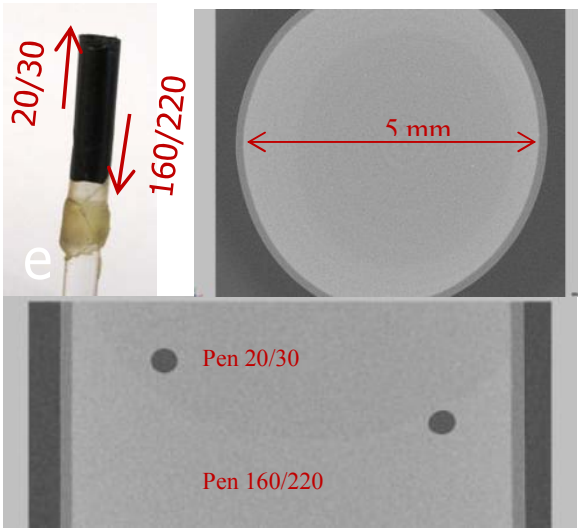

Figure 9.10- CT scan image of sample 2

9.6.3.3. Sample CT3

As it was explained earlier, a bromide based metal tracer was mixed with the soft binder in order to trace the soft binder and to visualize its possible diffusion and blending into the hard bitumen. Contrary to the previous sample (SampleCT2), the bitumen was poured on top of the soft bitumen (Figure 9.11). Images in Figure 9.11 clearly illustrate the interface between soft and hard binder again but the tracer was not detectable in the soft binder (on top). This might be because of the low melting point of the tracer. Shear mixing was carried out at 150 °C - 170 °C, and probably the tracer was melted in the bitumen (See Table 9.2 for physical properties of the tracer). Because of melting the concentration of this substance may become so low that it is not detectable. However, the exact reason could not be identified in this research.

Increasing the percentage of the tracer in the soft bitumen could have been helpful in detecting the tracer in soft and hard bitumen. (It is also important to discuss the value of adding such a tracer, probably a very large molecule compared to the molecules in the bitumen, etc.)

Table 9.2: Physical Properties of Tetra Bromobisphenol A

Properties	***Molar mass***	***Density***	***Melting point***	***Boiling point***
values	543.9 g.mol-1	2,12 g·cm−3 (20 °C)	178 °C	250 °C

Despite the fact that the top bitumen is lighter than the bottom bitumen, these images show that the top bitumen (soft) is lighter in color than the lower bitumen (hard). We don't know what the reason is in spite of the distinction that is made by the images.

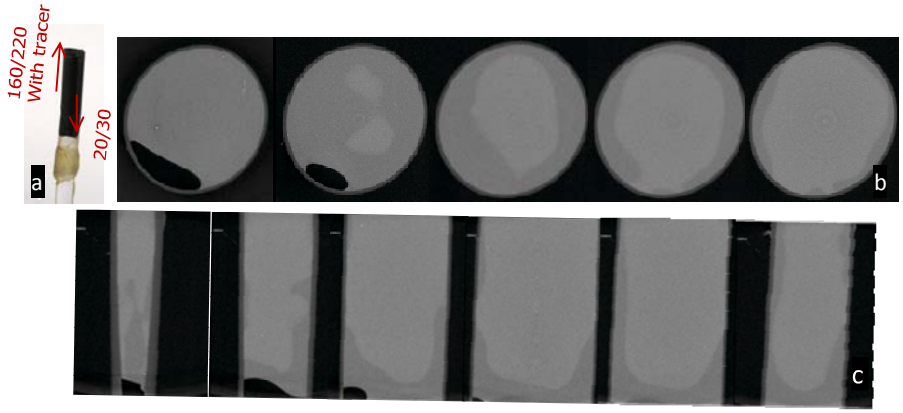

Figure 9.11: Evolution of CT scanning imaging in sample 3: (a) illustrates the arrangement of bitumens on top of each other in the sample holder, (b) a top view of CT-scanning images from top to bottom (c) side view of CT-scanning images

Zooming into the CT scan images in both samples (CT1 and CT2) which were obtained from samples 2 and 3 shows some kind of string structured texture in the bitumen which more or less looks like the microstructure of bitumen as observed in ESEM images as was illustrated in chapter 6 (see Figure 6.9). These strings are identified with different gray values as illustrated in Figure 9.12. More CT-scan imaging should be carried out on smaller sized samples in order to achieve a better resolution. Then conclusions can be drawn whether these string shapes are related to the bitumen microstructure or that they are due to inappropriate resolution of the images.

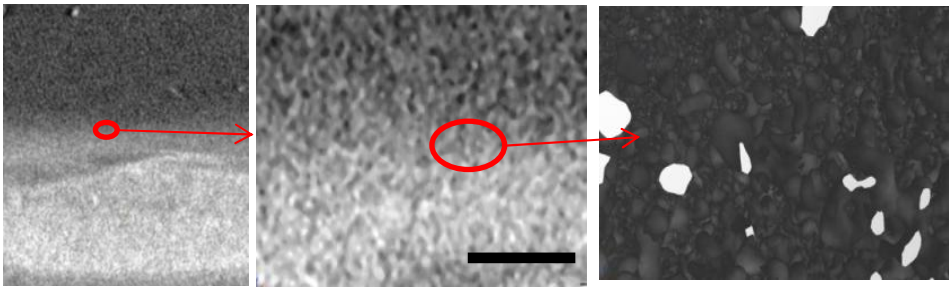

Figure 9.12: High resolution CT images on the interface zone between two bitumens. The interface between the two bitumens is the area in which the colour of the pixel has been changed from light to dark.

9.7. Conclusions

The following conclusions have been drawn based on the results reported in this Chapter;

1. The results of the indentation tests successfully showed the interface between binder and aggregates based on the huge difference in their modulus values. Detecting the interface between two binders was not possible.
2. Modulus values in the binder zones as determined by means of nano-indentation showed a continuous increase and decrease for each 60µm. The peak values could represent the denser and harder functional groups of bitumen molecules such as asphaltenes (or crystallized areas) and low modulus values could be due to the softer phases of molecules.
3. Although polarized optical microscopy was successfully used to study the stone-binder interfaces, it was not possible to separate the soft binder from the harder one.
4. It was not possible to differentiate between two different binders in the mixture (with aggregate) with nano tomography scanning images , while it was very clearly possible to detect the binder from the aggregates. Also film thickness can be determined by using these images.
5. Nano tomography imaging was successfully used in indicating the interfacial zone in a column of two binders on top of each other. Contrary to the fact that the hard binder is denser in reality, grey

values (in CT images) indicated it as the lighter one. Not enough observations were done to explain the reason of this phenomenon in bitumen CT scanning at Nano and Micro level. This phenomenon was not found before.

6. Nano CT scanning images at a higher resolution seem to indicate a string shape network of higher density material in analogy to the hypothesis of the colloid theory of bitumen. This phenomenon has to be studied in much more detail on smaller sized samples in order to make sure that this observation is directly related to the microstructure of bitumen and not because of measurement issues.
7. Tracers were not detectable in the images, probably because they were melted in the bitumen during shear mixing. Tracer detection should be investigated in more detail when using higher amounts and lower mixing temperatures (less than 150°C).

CHAPTER 10



GENERAL CONCLUSIONS AND RECOMMENDATIONS

The focus of this dissertation was on the influence of high percentages of RA in hot mix asphalt produced using two different mixing plants and a standard laboratory mixing process on the mechanical characteristics of the mixture. The effects of moisture and superheating of the virgin aggregates were highlighted. This dissertation was organized in two main parts. The first part discussed the effect of mixing conditions on the mechanical properties of mixtures while in the second part, the focus was on blending of virgin and recycled binder when mixed together In this chapter the main conclusions from both parts of the study. At the end recommendations are given based on the experience and findings in this research.

10.1. Conclusions on Part 1

1. According to what was found in the literature, almost every HMA mixture can be made by replacing a major portion of the virgin materials by RA. However the preheating of RA and handling of the moisture conditions of the RA makes producing a mixture containing RA different from producing a mixture using virgin materials. Among all HMA plants, the double barrel drum mixer has the capability of using cold and moist recycled material in which thermal energy is transferred via virgin aggregates; this implies that the level of preheating should be selected in accordance with the RA content and its moisture content.
2. The mechanical properties of HMA containing a high percentage of RA are primarily affected by its binder stiffness which is directly dependent on the percentage of RA and its preheating and moisture conditions. The stiffness of the HMA mixture with a high amount of RA could be possibly affected by the interaction between and the blending of the two binders.

3. Mixture designs of HMA with high amounts of RA are mainly based on blending charts for the binder in which the presumption is that the virgin and RA binders are fully blended. The log-pen rule is also based on the same assumption. This rule may not correctly predict the penetration of the binder in the recycled mixture.
4. Thermal analysis of HMA with cold RA by means of TMIT as used in this dissertation is found to be very helpful in visualizing the mixing efficiency in the lab as well as in the real plant. It was used in this research to determine the optimum mixing time in the lab. TMIT analyses on mixtures produced with the double drum showed that mixing at short mixing times with 50% RA and 4% moisture resulted in a much better homogeneity than what was expected from TMIT analyses on similar mixtures produced in the laboratory.
5. TMIT could also detect thermal segregation occurring during construction of the pavement. It showed that the feeding system used during construction did not improve the pavement quality in terms of homogeneity in temperature. Inhomogeneity in temperature can result in inhomogeneity of pavement compaction which very well could result in premature cracking and raveling.
6. Based on the results of "Phase I" it is concluded that the amount of RA as well as the moisture content of the RA do not have a negative effect on the mechanical properties of the investigated recycled mixtures when compared to those of a reference mixture made of virgin materials. The presence of high moisture content in laboratory mixing conditions seems to reduce the stiffness of the mixture with 60% RA. Also the IT fatigue life has been increased probably due to lower stiffness values. It showed the importance of studying the influence of mixing conditions in the real plant in Phase 2 of this Part 1 of the dissertation. In the laboratory experiment a shorter mixing period (in laboratory conditions) and higher air voids content resulted in lower IT fatigue life. However the question remains whether that was because of the higher air voids content or shorter mixing time.
7. In Phase II of the experimental study the quality of HMA with 50% RA produced by means of an Astec double drum mixer (A) and a batch plant (BB) with parallel drum was evaluated. The mixture properties were compared with the mixture produced in the lab (L).

8. Three mixtures with the same materials and similar volumetric properties were produced in an ASTEC double drum (indicated by A), a batch plant with parallel drum (indicated by BB) and in the Laboratory (L). Additionally, another mixture was prepared in the batch plant (B) in which PRAP was added with the same amount (25%) as normal RA. By means of 4PB stiffness tests, mixture L was found to be stiffer than A and BB and mixture A was found to be the softest mixture. The higher stiffness of L might be explained by extra aging of the RA binder during the preheating time in the oven. The lower stiffness of mixture A might be because of the effect of foaming during mixing of superheated aggregates and cold and moist RA aggregates. However no effort has been made in this research to study this phenomenon in greater depth.
9. In the BB mixtures, RA was preheated during a shorter period of time in a parallel drum dryer. Furthermore, mixture A has the lowest stiffness which is most probably due to the system of cold and moist RA feeding in the double drum system. The results of 4PB fatigue test (displacement controlled) appear to be influenced by the initial stiffness values of the mixture. Consequently, mixture L showed the lowest fatigue life while mixture A and BB had almost similar fatigue lines. However mixture A was slightly more resistant to fatigue loading.
10. The Medani/Molenaar model was applied to predict the fatigue behaviour of three mixtures based on material properties. It was found to be a reasonably accurate model in prediction of 4PB fatigue life of recycled mixtures containing high amounts of RA.
11. From the monotonic uniaxial compression and tension tests it was found that the tensile and compression strength of the tested mixture are temperature and time dependent. This behavior was used to a make master curves of each at certain temperatures. This allows the strength of the material to be determined at any temperature and strain rate.
12. The tension and compression master curves for mixtures A, BB, and L do not show significant differences. This is to some extent remarkable because of the quite different preheating and mixing process. Also the stiffness and fatigue resistance of mixture L is quite different. It should however be noted that all three mixtures were made of the same materials and had the same composition. The slope of the tension and compression master curves of mixture L was a little bit steeper than for mixtures BB and A which is indicating a slightly more brittle behavior of the laboratory produced mixture.

13. A model was developed to estimate the fatigue endurance limit (FEL). This model requires only initial stiffness values, temperature and loading frequency. It is a simple tool to predict the FEL of recycled mixtures with high amounts of RA. This model was used to calculate the FEL for each mixture at each loading condition. According to FEL calculations, the endurance limit of mixture "A" was higher than the FEL for BB and L. The FEL was 124, 107 and 56 μm/m for mixtures A, BB and L respectively. When relating the studies of Phase I with the Phase II studies, it should be mentioned that mixture SM and L experienced similar mixing conditions. Similar preheating and moisture conditions were used with PW and BB and the same with UPG and A. However, the amount of RA was not the same in the two phases. Summarizing the stiffness values obtained in the two phases shows that mixture "A" from the real plant like UPG with 4% moisture has relatively lower stiffness than the others. The order of resistance to fatigue life (high to low) in Phase I was UPG, PW and UPG. The same trend of fatigue life was observed in Phase II as: A, BB, L.

10.2. Conclusions on Part 2

1. From the literature survey, various techniques were found useful to observe the bitumen microstructure. Examples were nano-indentation and atomic force microscopy. However limited studies were found on the microstructural characterization and interaction between virgin and RA binder in terms of blending and diffusion.
2. Stage extraction was used to recover the binder from aggregate fractions that differed in size. G* measurements showed that the bitumen recovered from the finer particles had a higher G* than the G* of the bitumen recovered from the coarser particles. The G* of first extraction (the outer bitumen layer around a particle) was slightly higher than the G* values obtained on the bitumen from the second extraction (inner layer).
3. The experiments with the asphalt mixture, where part of the virgin aggregates were replaced by glass beads, showed that adding virgin binder to the mixture had a significant effect on the G* of the RA binder coating the RA particles (after recovery). It can be concluded that the G* of the bitumen coating virgin aggregates in an RA mixture (in this case the glass beads) is not the same as the G* of the bitumen coating the RA aggregates. Therefore it is evident that full blending of RA and virgin binder does not occur.

4. The so-called Log (pen) rule was not applicable for the investigated mixture. It might however still be applicable for mixtures containing lower amounts of RA.
5. The MLBS sandwich method was developed to quantify the diffusion that might occur between two binders at 60°C. The effective modulus of different arrangements of bitumen was measured. The measurement showed small differences between all those arrangements and that of a fully blended binder system. Given the fact that a HMA mixture is usually at high temperature for quite some time (taking the mixing, storage and construction period into account, it will mostly be more than 3 hours), the small difference could be compensated by diffusion.
6. Based on the large difference in stiffness, the interface between binder and aggregates could be observed by means of nano indentation, however the interface between two binders could not be determined by this technique. With polarized microscopy it was also not possible to detect the interface between two binders.
7. Nano tomography imaging was used in characterizing the interfacial zone in a column in which two binders were placed on top of each other. Nano CT scanning images at a high resolution indicated a string shape network of higher density material in analogy to the hypothesis of the colloid theory of bitumen. This phenomenon has to be studied in much more detail on samples of much smaller size in order to make sure that this observation is directly related to the microstructure of bitumen and not because of measurement issues.
8. An overall and general conclusion is that blending of RA binder and virgin bitumen may not occur in real asphalt plants. However a HMA mixture is such a forgiving mixture that this lack of blending is not really visible when determining the material properties. Factors such as production, storage, transportation and conditions during laying and compaction seem to mask any effect of incomplete blending.

10.3. Recommendations

Although much has been learned about HMA recycling using high amounts of RA from the research described in this dissertation, it did not solve all the questions and queries. Aspects which certainly need to be investigated are the following.

1. The effect of preheating RA on blending should be investigated. Preheating of RA in a parallel drum to 130°C, which is normal practice in the Netherlands, reduces the need to preheat the virgin aggregates to

very high temperatures and because of the smaller temperature difference a better blending could be obtained.

2. The influence of the foaming effect during mixing superheated virgin aggregates and cold and moist RA in the double drum mixer has to be studied.
3. Bio products like oils extracted from seeds and vegetables are currently used to rejuvenate RA binder and mixtures of 100% RA rejuvenated with such products are already produced. Research on the blending of such products and the RA binder is needed to understand why such products are effective and when such products are not going to be effective.
4. Because of environmental reasons, warm and half-warm asphalt mixtures with high RA percentages will be used extensively in the near future.. Knowledge about blending of the RA binder with e.g. foamed bitumen is not available at the moment but is essential in order to be able to understand the critical factors determining the quality of such mixtures.
5. Blending seems to be an important issue but the question still is what the effect is of partly blending on the mechanical characteristics of mixtures with high RA percentages and their durability.
6. The micro-structural mechanisms controlling blending of old and new bitumen at their mixing interfaces should be studied because it will provide information to select the right type of virgin binder given the present RA binder.
7. Fractionizing RA into a number of fractions will certainly enhance control on the homogeneity and quality of the recycled mixture. Especially when more than 50% RA will be used in HMA, fractionizing of the RA is highly recommended.
8. Since the quality of plant produced HMA mixtures strongly depends on the temperature control of the final mixture, it is proposed to implement real time TMIT control in asphalt plants. Application of this technique in real time mode needs to be automatized which seems to be possible with electronics and software available in the market. The application of TMIT during the pavement construction phase was found to be a helpful tool in visualizing the thermal homogeneity of the pavement during construction. It is therefore recommended to use them on pavers in order to enhance quality control.

Bibliography

[1] J. A. EPPS, D. N. Little, R. J. Holmgreen and R. L. Terrel, "Guidelines for Recycling Pavement materials," National Highway Cooperative Research Program, USA, 1980.

[2] VBW, 65 Jaar Asfalt in Nederlands, Breukelen: Vereniging Bevordering van Werken in Asfalt, 1988.

[3] EAPA, "Asphalt in figures," 2011. [Online]. Available: http://www.eapa.org/asphalt.php. [Accessed January 2012].

[4] F. L. Roberts, P. S. Kandhal, E. Ray Brown and D. Y. Lee, "Hot mix asphalt materials, mixture design, and construction," NAPA Research and Education, Lanham, 1996.

[5] NAPA, "Asphalt History," [Online]. Available: http://www.hotmix.org. [Accessed 2011].

[6] C. Lange, "Hot Mix Asphalt Production," Council for Scientific and Industrial Research (CSIR), 2006. [Online]. Available: www.csir.co.za.

[7] P. Lavin, Asphalt pavements: a practical guide to design, production and maintenance for engineers and architects, New York and London: CRC press (Taylor & Francis), 2003.

[8] E. R. Brown, Hot-Mix Asphalt Paving Handbook, American Association of State Highway and Transportation Officials, 2000.

[9] P. N. Sharrat, Handbook of batch process design, Blackie Academic professional, 1997.

[10] D. WhiteOak and J. Read, The Shell Bitumen Handbook, London: Thomas Telford Ltd, 2003.

[11] The Asphalt Handbook- Mannual series MS4, Asphalt Institute, 1989.

[12] J. Brock, "Milling and Recycling (T-127)," Astec Industry, Co, Chattanooga, 1994.

[13] P. Kandhal, "Recycling of Asphalt pavements- An overview," *Association of Asphalt Paving Technology,* vol. 66, pp. 686-696, 1997.

[14] Astec, "Astec double barrell drum mixer," *Hot mix magazine,* vol. 7, no. 3, pp. 6-8, 2002.

[15] T. W. Kennedy, R. B. McGennis and N. H. Predoehl, "Asphalt Mixture Segregation; Diagnostics and Remedies," *Association of Asphalt Paving Technology,* vol. 56, pp. 304-329, 1987.

[16] M. Gardiner and E. Brown, "Segregation in Hot Asphalt pavements," National cooperative highway Research Program, Report 441, Washington DC, 2000.

[17] S. cross and E. Brown, "Effect of Segregation on Performance of Hot Mix Asphalt," Highway Research Center, Auburn University, Auburn, 1992.

[18] J. D. Brock, J. G. May and G. Rengar, "Segregation; Causes and Cures," Astec Idustries, Technical paper T-117, USA, 2003.

[19] B. A. Vallerga, C. L. Monismith and K. Granthem, "A study of some factors influencing the weathering of paving asphalt," *AAPT,* vol. 26, 1957.

[20] F. Finn, "Factors involved in the desing of asphaltic pavement surfaces," NCHRP, Report 39, 1967.

[21] J. Brock, "Light Oils in Asphalt," Astec Industries Inc, Technical paper T-116, Chatanooga, 1996.

[22] D. White Oak and D. Fordyce, "Asphalt workability, its measurment, and how it can be modified," in *Shell bitumen review*, London, Shell International Petroleum Company Ltd, 1989, pp. 14-17.

[23] S. Haas, "Drum dryer mixer in North Dakota," *AAPT,* vol. 34, pp. 41-47, 1974.

[24] M. Smiljanic, J. Stefanovic, H. J. Neumann, I. Rahimaian and J. Jovanovic, "Aging of Asphalt on Paved Roads — Characterization of Asphalt Extracted from the Wearing Courses of the Belgrade-Nis Highway," *Journal of Erdol and Kohl,* vol. 46, no. 6, 1993.

[25] G. R. Kemp and N. H. Predoehl, "A Comparison of Field and Laboratory Environments on Asphalt Durability," *AAPT,* vol. 50, pp. 492-537, 1981.

[26] L. Grunberg and A. H. Nissan, "Mixing Law for Viscosity," *Nature,* vol. 164, pp. 799-800, 1949.

[27] ASTM, "Standard Practice for Preparation of Viscosity Blends for Hot

Recycled Bituminous Materials," ASTM D4887-99 , 2003.

[28] S. H. Carpenter and J. R. Wolosick, "Modifier Influence in the characterization of Hot-Mix Recycled Material," *Transportation Research Record,* vol. 777, pp. 15-22, 1980.

[29] R. S. McDaniel, H. Soleimani and R. Micheal Anderson, "Recommended Use of Reclaimed Asphalt Pavement in the Superpave Mix Design Method," National Cooperative Highway Research Program, NCHRP 9-12, 2000.

[30] J. W. H. Oliver, "The influence of the binder in RAP on recycled asphalt properties," *Road Materials and Pavement Design,* vol. 2, pp. 311-325, 2001.

[31] B. Huang, G. Li, D. Vukosavljedic, X. Shu and B. K. Egan, "Laboratory investigation of Mixing Hot-Mix Asphalt with Reclaimed Asphalt Pavement," *Transportation Research Record,* vol. 1929, 2005.

[32] J. D. Stepens, J. Mahoney and C. Dippold, "Determination of The PG Binder Grade to Use in a RAP Mix," University of Connecticut and the Connecticut Department of Transportation, Report JHR00-278, 2001.

[33] T. H. Hagos, The Effect of Aging on Binder Properties of Porous Asphalt Concrete, Delft: Delft University of Technology, PhD dissertation, 2008.

[34] B. L. Buur, C. J. Glover, R. R. Davison and J. Bullin, "New apparatus and Procedure for the Extraction and Recovery of Asphalt Binder from Pavement mixture," *Transportation Research Record,* vol. 1391, pp. 20-29, 1993.

[35] A. Chacho, "Investigating the effect of different lab mixing procedures on the mechanical characteristics by using more RAP in asphalt mixtures," Master Thesis, Delft University of Technology, Delft, 2012.

[36] G. M. Merine, "Developement of a mix desing method in the laboratory for mixes with recycled asphalt pavement in a drum mix facility," MSc thesis, Delft University of Technology, Delft, 2009.

[37] W. Van den Bergh, The Effect of Aging on the Fatigue and Healing Properties of Bituminous Mortars, Delft, 2011.

[38] M. F. Woldekidan, Response Modeling of Bitumen, Bituminous Mastic and Mortar, Delft: PhD dissertation, 2011.

[39] C. Y. Gheung, Mechanical behaviour of bitumens and bituminous mixtures., PhD Dissertation, University of Cambridge, Engineering department, 1995.

[40] J. Groenendijk, Accelerated testing and surface cracking of asphaltic concrete pavements, the Netherlands, Delft: PhD Dissertation, Delft University of technology, 1998.

[41] K. M. B. Jansen, Thermomechanical modeling and characterization of polymers, Delft: PhD dissertation, Delft University of Technology, 2006.

[42] T. O. Medani and R. M. Huurman, "Superposition principle to determine properties of bituminous mixtures in the time-temperature domain," in *Bearing Capacity of Roads, Railways, and Airfields (BCRA)*, Trondheim, Norway, 2005.

[43] H. U. Bahia, D. I. Hanson, M. Zeng, H. Zhai, M. A. Khatri and R. Anderson, "Characterisation of Modified Asphalt Binders in Superpave Mix Design," Rep. No. 459. National Academy Press, Washington DC, 2001.

[44] R. M. Huurman and A. C. Pronk, "A detailed FEM simulation of a 4-point bending test device," in *Four point bending*, London, Taylor & Francis Group, 2012, pp. 3-12.

[45] "Bitumenous mixtures-Test methods for hot mix asphalt-part 26: Stiffness," EN 12697-26, 2004.

[46] T. O. Medani, "Design Principles of Surfacings on Orthotropic Steel Bridge Decks" PhD thesis, Delft: Delft University of Technology, 2006.

[47] S. M. J. G. Erkens and M. R. Poot, "Determining and Modeling Asphalt Concrete Response (ACRe)," *Heron,* vol. 45, no. 3, pp. 219-236, 2000.

[48] S. M. J. G. Erkens and M. Poot, "The Uniaxial Test Asphalt Concrete Response (ACRe)," Delft University of Technology, Report No. 7-10-117-7, Delft, 2001.

[49] S. M. J. G. Erkens, Asphalt Concrete Response (ACRe), Determination, Modeling and prediction, Delft: PhD Dissertation, Delft Universtiy of Technology, 2002.

[50] NEVUL, NEVUL Nederlandse Vereniging Van Fabrikanten En Importeurs Van Vulstof Voor Bitumineuze Werken, Venray, Nederland, 2010.

[51] K. A. Willoughby, "Construction Related asphalt concrete pavement temperature and density differentials," *Construction,* pp. 68-67, 2002.

[52] R. William, "Hot-Mix Asphalt Segregation: Measurement and Effects," *Transportation Research Board,* no. 1543-1, pp. 97-105, 1996.

[53] M. Stroup-Gardiner, "Using Infrared Thermography to Detect and Measure segregation in Hot Mix Asphalt Pavement," *International Journal of Pavement Engineering,* vol. 1, no. 4, pp. 265-284, 2000.

[54] S. Miller, Hot mix asphalt construction: Towards a more professional approach, PhD dissertation: University of Twente.

[55] R. N. J. Saal and J. W. A. Labout, "Rheological Properties of Asphalt," *Journal of Rheology,* Vols. 2, chapter9, no. Edirich, pp. 363-400, 1958.

[56] Shell, Shell Pavement Design Manual—Asphalt Pavements and Overlays for. Road Traffic, London: Shell International Petroleum Company, Ltd, 1978.

[57] F. Bonnaure, G. Gest, A. Gravoir and P. Uge, "A New Method of Predicting the Stiffness of Asphalt Paving Mixtures," *Proceedings of AAPT,* vol. 46, pp. 64-105, 1977.

[58] T. O. Medani and A. A. A. Molenaar, "A Simplified Procedure for Estimation of Fatigue and Crack Growth Characteristics of Asphalt Mixes," *Road Materials and Pavement Design,* vol. 1, no. 4, 2000.

[59] P. M. Muraya, Permanent deformation of asphalt mixes, Delft: Delft university of technology, PhD dissertation, 2007.

[60] Y. R. Kim, M. N. Guddati, B. S. Underwood, T. Y. Yun, V. Subramanian and V. Savadatti, "Development of a Multiaxial Viscoelastoplastic Continuum Damage Model for Asphalt Mixtures," FHWA, 2009.

[61] D. C.S. and D. Zhang, "Viscoplastic Model for Geologic Materials with Generalized Flow Rule," *International Journal for Numerical and Analytical Methods in Geomechanics,* vol. 11, p. 603–620, 1987.

[62] J. Uzan, M. Perl and A. Sides, "Viscoelastoplastic Model for Predicting Performance of Asphalt Mixtures," *Transportation Research Record 1043,* p. 78–79, 1985.

[63] G. R. Chehab, Y. R. Kim, R. A. Schapery, M. Witczack and R. Bonaquist, "Characterization of Asphalt Concrete in Uniaxial Tension Using a Viscoelastoplastic Model," *Asphalt Paving Technology, AAPT,* vol. 72, p. 315–355, 2003.

[64] R. A. Schapery, "Nonlinear Viscoelastic and Viscoplastic Constitutive Equations with Growing Damage," *International Journal of Fracture,* vol. 97, p. 33–66, 1999.

[65] A. Scarpas, R. Al-Khoury, C. Van Gurp and S. M. J. G. Erkens, "Finite Element Simulation of Damage Development in Asphalt Concrete Pavements," in *International Conference on Asphalt Pavements*, University of Washington, Seattle, WA, 1997.

[66] N. Gibson, A Viscoelastoplastic Continuum Damage Model for the Compressive Behavior of Asphalt Concrete, University of Maryland, College Park,: PhD dissertation, 2006.

[67] N. Li, "Asphalt Mixture Fatigue Testing- Influence of Test Type and Specimen Size" PhD Thesis, Delft: Delft University of Technology, 2013.

[68] B. D. Prowell, R. E. Brwon, R. M. Anderson and J. S. Daniel, "Validating the Fatigue Endurance Limit for Hot Mix Asphalt," National Cooperative Highway Research Program (Report 646), Washington, 2010.

[69] N. Li, A. A. A. Molenaar and M. F. C. Van de Ven, "Estimation of fatigue endurance limit of HMAC for perpetual pavements," *Journal of Wuhan University of Technology-Mater. Sci. Ed.,* vol. 25, no. 4, pp. 645-649, 2010.

[70] P. Redelius, "Relation between Bitumen chemistry and performance," in *International conference of RILEM*, Zurich, 2011.

[71] F. J. Nellensteyn, "The Constitution of Asphalt," *Inst. Petrol. Technology,* vol. 10, pp. 311-325, 1924.

[72] J. C. Peterson, "Binder Characterization and evaluation," Washington D.C, 1994.

[73] C. J. Mack, "Colloid Chemistry of Asphalts,," *Physic Chemistry,* vol. 36, pp. 2901-2914.

[74] J. W. Labout, "Constitution of Asphaltic Bitumen," *The Properties of Asphaltic Bitumen,* Vols. Pfeiffer, J.Ph. (Ed.). Elsevier, Amsterdam, 1950.

[75] C. Van der Poel, "A General System Describing the Viscoelastic Properties of Bitumens and Its Relation to Routine Test Data," *Applied Chemistry,* vol. 4, pp. 221-236, 1954.

[76] J. P. Pfeiffer and R. N. J. Saal, "Asphaltic Bitumen as Colloidal System," *Physics Chemistry,* vol. 44, pp. 139-149.

[77] T. F. Yen, J. G. Erdman and S. S. Pollack, "Investigation of the Structure of Petroleum Asphaltenes by X-Ray Diffraction,," *Analytic Chemistry,* vol. 33, pp.

1587-1594, 1961.

[78] K. H. Altgelt and O. L. Harle, "The Effect of Asphaltenes on Asphalt Viscosity," *Industrial & Engineering Chemistry, Prod. R&D,,* vol. 14, pp. 240-246, 1975.

[79] J. C. Peterson and P. M. Harnsberger, "Asphalt aging: Dual oxidation Mechanism and its relationship with asphalt composition".

[80] I. Ishai, B. Brule and J. Vaniscote, "Some rheological and physio-chemical aspects of long term asphalt duribility," *AAPT,* vol. 66, 1988.

[81] K. A. Stangl and R. Jager, "Microstructure-based identification of bitumen performance," *Road Material Pavement Design,* no. EATA, Warwickshire, UK, 2006.

[82] A. Jäger, R. Lackner and J. Eberhardsteiner, "Identification of viscoelastic properties by means of nanoindentation taking the real tip geometry into account," *Meccanica 42,* vol. 42, no. 3, pp. 293-306, 2007.

[83] J. Masson, V. Leblond and J. Margeson, "Bitumen morphologies by phase detection atomic force microscopic," *Journal of Microscopy,* vol. 221, no. 17-29, 2006.

[84] A. S. Noureldin and L. E. Wood, "Rejuvenator Diffusion in Binder Film for Hot-Mix Recycled Asphalt Pavement," *Transportation Research Record ,* no. 1115, pp. 51-61, 1989.

[85] "NEN 3971(1991): Recovery of bitumen from asphalt for qualitative testing purposes.," 1991.

[86] "NEN 12697-3: Bituminous mixtures - Test methods for hot mix asphalt - Part 3: Bitumen recovery: Rotatory evaporator," 2005.

[87] A. S. Noureldin and L. E. Wood, "Rejuvenator diffusion in binder film for hot-mix recycled asphalt pavement," *Transportation research Record 1115,* pp. 51-61, 1987.

[88] B. Huang, G. Li, D. Vukosavljevic, X. Shu and B. K. Egan, "Laboratory investigation of mixing hot mix asphalt with reclaimed asphalt pavement," *Transportation Research Record,* no. 1929, pp. 37-45, 2005.

[89] P. G. de Gennes, "Reptation of a polymer chain in the presence of fixed Obstacles," *Journal of ChemPhys,* vol. 55, no. 2, pp. 572-579, 1971.

[90] R. Karlsson and U. Isacsson, "Investigations on Bitumen Rejuvenator Diffusion and Structural Stability," *AAPT,* vol. 72, 2003.

[91] R. Karlsson and U. Isacsson, "Laboratory studies of diffusion in bitumen using markers," *Material science,* vol. 38, pp. 2835-2844, 2003.

[92] Van Der Kooj, J.; Verburg, H. A., "Mixing of High peneteration Bitumen with aged bitumen during Hot Mix Recycling of Porous Asphalt," in *Euroasphalt & Eurobitume Congress*, 1996.

[93] J. W. H. Oliver, "Diffusion of Oils in Asphalts," *Australian Road Research Board,* no. Report No. 9, 1975.

[94] J. Qui, Self Healing of Asphalt Mixtures Towards a Better Understanding of the Mechanism, Delft universtiy of technology: PhD Dissertation, 2012.

[95] H. Qui and M. Bousmina, "New technique allowing the quantification of diffusion at polymer/polymer interfaces using rheological analysis: Theoretical and experimental results," *Journal of Rheology,* vol. 43, pp. 551-568, 1999.

[96] A. A. A. Molenaar, M. Mohajeri and M. F. C. Van de Ven, "Design of recycled asphalt mixtures using a double drum mixer".

[97] I. L. Al-Qadi, S. H. Carpenter, G. Roberts, H. Ozer and Q. Aurangzeb, "Determination of usable residual asphalt binder in RAP," Illinois center for transportation, Research report ICT-R27-11, 2009.

[98] W. C. Oliver and G. M. Pharr, "An improved technique for determining hardness and elastic modulus using load and displacement sensing indentation," *Journal of material research,* vol. 2, pp. 1564-1581, 1992.

[99] M. Vandamme and F. Ulm, "Viscoelastic solutions for conical indentation," *Internation Journal of Solids and Structures,* vol. 43, pp. 3142-3165, 2006.

[100] M. Mohajeri, A. A. A. Molenaar and M. F. C. Van de Ven, "Experimental Study into the Fundamental Understanding of Blending between Reclaimed Asphalt Binder and Virgin Bitumen using Nano-indentation and Nano-computed Tomography," *Road Material Pavement Design,* vol. 15, no. 2, pp. 372-384, 2014.

Appendices

Appendix A Volumetric properties of Specimen

$$\rho_{bssd} = \frac{m_1}{m_3 - m_2} \times \rho_w$$

where

ρ_{bssd} is the bulk density (SSD), in kilograms per cubic metre (kg/m^3);

m_1 is the mass of the dry specimen, in grams (g);

m_2 is the mass of the specimen in water, in grams (g);

m_3 is the mass of the saturated surface-dried specimen, in grams (g);

ρ_w is the density of the water at test temperature, in 0,1 kilogram per cubic metre.

(Water density in 25°C= 997.1 kg/m³

$$V_m = \frac{\rho_m - \rho_b}{\rho_m} \times 100 \ \% \ (v/v)$$

where

V_m is the air voids content of the mixture, in 0,1 percent (v/v);

ρ_m is the maximum density of the mixture, in kilograms per cubic metre (kg/m^3);

ρ_b is the bulk density of the specimen, in kilograms per cubic metre (kg/m^3).

$$VMA = V_m + B \times \rho_b / \rho_B \ \% \ (v/v)$$

where

VMA is the voids content in the mineral aggregate in 0,1 % (v/v)

V_m is the air voids content of the specimen in 0,1 % (v/v);

B is the binder content of the specimen (in 100% mixture), in 0,1 % (m/m);

ρ_b is the bulk density of the specimen, in 1 kilogram per cubic metre (kg/m^3);

$$VFB = ((B \times \rho_b / \rho_B) / VMA) \times 100 \ \% \ (v/v)$$

where

VFB is the percentage of the voids in the mineral aggregate filled with binder in 0,1 % (v/v);

*Table A. 1 Volumetric properties of the **gyratory** compacted specimens*

	specimen	*m1 Dry Wt. (gr)*	*m2 Subm. Wt. (gr)*	*m3 Surface Dry Wt.*	*Bulk Density (kg/m³)*	*Max density (kg/m³)*	*Vm (%)*	*VMA (%)*	*VFM (%)*
SM0	SM0-1	985,1	586,0	985,8	2457	2526	2,7%	13,4%	79,6%
	SM0-2	960,0	566,6	960,9	2428	2526	3,9%	14,5%	73,0%
	SM0-3	957,5	568,5	958,5	2448	2526	3,1%	13,7%	77,5%
	SM0-4	988,6	584,6	989,5	2435	2526	3,6%	14,2%	74,5%
SM30	SM30-1	942,6	556,6	943,0	2432	2507	3,0%	13,6%	78,0%
	SM30-2	948,5	564,4	948,9	2460	2507	1,9%	12,6%	84,9%
	SM30-3	927,0	546,6	927,4	2427	2507	3,2%	13,7%	76,8%
	SM30-4	937,9	554,3	938,5	2434	2507	2,9%	13,5%	78,4%
SM60	SM60-1	972,2	571,9	972,6	2419	2490	2,8%	13,3%	78,8%
	SM60-2	988,1	583,2	989,0	2428	2490	2,5%	13,0%	81,0%
	SM60-3	939,0	554,0	940,0	2426	2490	2,6%	13,1%	80,4%
	SM60-4	952,9	560,8	953,3	2421	2490	2,8%	13,3%	79,2%
Pw30	PW30-1	979,5	580,3	979,8	2445	2507	2,5%	13,1%	81,0%
	PW30-2	936,7	555,7	936,9	2450	2507	2,3%	12,9%	82,4%
	PW30-3	906,8	535,5	907,5	2431	2507	3,1%	13,6%	77,6%
	PW30-4	1184,0	677,7	1186,0	2323	2507	7,4%	17,5%	57,8%
PW60	PW60-1	1001,1	588,5	1001,4	2417	2490	2,9%	13,4%	78,4%
	PW60-2	1044,7	616,3	1045,2	2429	2490	2,4%	13,0%	81,2%
	PW60-3	1055,4	621,9	1056,4	2422	2490	2,7%	13,2%	79,5%
	PW60-4	963,6	570,4	964,1	2440	2490	2,0%	12,6%	84,3%
UPG030	UPG030-1	989,4	584,2	990,0	2431	2507	3,0%	13,6%	77,7%
	UPG030-2	974,2	574,9	974,4	2431	2507	3,0%	13,6%	77,8%
	UPG030-3	1009,4	594,6	1010,2	2422	2507	3,4%	13,9%	75,5%

	UPG030-4	981,8	579,9	982,3	2433	2507	3,0%	13,5%	78,1%
UPG060	UPG060-1	1023,6	603,9	1024,3	2427	2490	2,5%	13,0%	80,9%
	UPG060-2	1005,4	593,4	1005,7	2431	2490	2,3%	12,9%	81,8%
	UPG060-3	979,0	582,9	979,5	2461	2490	1,1%	11,8%	90,4%
	UPG060-4	993,3	587,3	993,9	2436	2490	2,2%	12,7%	83,1%
UPG430	UPG430-1	953,2	563,5	954,1	2433	2507	2,9%	13,5%	78,3%
	UPG430-2	951,4	568,1	952,1	2470	2507	1,5%	12,2%	87,9%
	UPG430-3	952,7	560,4	953,3	2418	2507	3,6%	14,1%	74,7%
	UPG430-4	966,8	574,1	967,6	2449	2507	2,3%	13,0%	82,2%
UPG460	UPG460-1	1001,4	590,9	1002,1	2428	2490	2,5%	13,0%	81,1%
	UPG460-2	1010,3	588,5	1010,8	2385	2490	4,2%	14,6%	71,3%
	UPG460-3	988,6	584,3	989,0	2436	2490	2,2%	12,8%	83,0%
	UPG460-4	1060,9	626,4	1060,6	2436	2490	2,1%	12,7%	83,1%

*Table A. 2 Volumetric properties of the **Marshall** compacted specimens*

	specimen	***m1 Dry Wt. (gr)***	***m2 Subm. Wt. (gr)***	***m3 Surface Dry Wt.***	***Bulk Density (kg/m³)***	***Max density (kg/m³)***	***Vm (%)***	***VMA (%)***	***VFM (%)***
SM0	SM0-1	1210,8	710,6	1212	2408	2527	4,7%	15,2%	69,1%
	SM0-2	1204,1	706,25	1206	2404	2527	4,8%	15,3%	68,3%
	SM0-3	1202,5	711,47	1206	2426	2527	4,0%	14,5%	72,5%
	SM0-4	1199,1	708,7	1200	2432	2527	3,8%	14,3%	73,8%
SM30	SM30-1	1139,5	665,1	1142	2383	2507	5,0%	15,3%	67,6%
	SM30-2	1190,2	698,5	1193	2398	2507	4,4%	14,8%	70,5%
	SM30-3	1194,3	701,85	1196	2410	2507	3,9%	14,3%	73,1%
	SM30-4	1189,9	699,55	1192	2411	2507	3,8%	14,3%	73,1%

SM60	SM60-1	1195,4	701,2	1199	2395	2490	3,8%	14,2%	73,3%
	SM60-2	1196,1	700,7	1198	2400	2490	3,6%	14,0%	74,4%
	SM60-3	1186,8	694,5	1188	2396	2490	3,7%	14,2%	73,6%
	SM60-4	1169,9	684,5	1172	2394	2490	3,8%	14,2%	73,1%
PW30	PW30-1	1196,3	703,3	1199	2406	2507	4,0%	14,5%	72,1%
	PW30-2	1186,6	692,4	1189	2381	2507	5,0%	15,4%	67,3%
	PW30-3	1164,7	683,4	1168	2396	2507	4,4%	14,9%	70,1%
	PW30-4	1189,6	699,25	1193	2402	2507	4,2%	14,7%	71,3%
PW60	PW60-1	1191,9	698,6	1193	2402	2490	3,5%	14,0%	74,7%
	PW60-2	1108,8	652	1112	2403	2490	3,5%	13,9%	75,1%
	PW60-3	1196,6	703,35	1199	2409	2490	3,2%	13,7%	76,3%
	PW60-4	1194,1	693,45	1199	2353	2490	5,5%	15,7%	65,1%
UPG030	UPG030-1	1196,7	703,54	1199	2406	2507	4,0%	14,5%	72,2%
	UPG030-2	1201,5	707,5	1203	2416	2507	3,6%	14,1%	74,3%
	UPG030-3	1194,4	705,75	1196	2430	2507	3,1%	13,6%	77,5%
	UPG030-4	1210,8	716,6	1212	2435	2507	2,9%	13,5%	78,7%
UPG060	UPG060-1	1203,4	710,3	1204	2430	2490	2,4%	13,0%	81,6%
	UPG060-2	1209,2	714,26	1211	2430	2490	2,4%	13,0%	81,4%
	UPG060-3	1207,3	713,2	1208	2432	2490	2,3%	12,9%	82,0%
	UPG060-4	1215,9	716,25	1217	2420	2490	2,8%	13,3%	78,9%
UPG430	UPG430-1	1195,7	707,7	1198	2433	2507	3,0%	13,6%	78,1%
	UPG430-2	1206	712,15	1208	2427	2507	3,2%	13,8%	76,7%
	UPG430-3	1201,7	708,35	1203	2422	2507	3,4%	13,9%	75,6%
	UPG430-4	1209,2	711,89	1210	2418	2507	3,5%	14,1%	74,8%
UPG460	UPG460-1	1174,3	687,45	1176	2397	2490	3,7%	14,1%	73,7%
	UPG460-2	1180,9	692,3	1182	2404	2490	3,4%	13,9%	75,3%
	UPG460-3	1200	703,72	1201	2407	2490	3,3%	13,8%	76,0%
	UPG460-4	1206,2	711,38	1211	2408	2490	3,3%	13,8%	76,1%

Table A. 3 Volumteric properties of Beams from Doubld Drum (A)

specimen	m1 Dry Wt. (gr)	m2 Subm. Wt. (gr)	m3 Surface Dry Wt.	Bulk Density (kg/m³)	Max density (kg/m³)	Vm (%)	VMA (%)	VFM (%)
A01	2672,7	1554,9	2675,7	2378	2495	4,9%	15,2%	68,0%
A02	2678,3	1568,2	2680,5	2401	2495	4,0%	14,4%	72,5%
A03	2696,3	1576,2	2699,1	2394	2495	4,2%	14,6%	71,1%
A04	2664,7	1564,5	2667,7	2408	2495	3,7%	14,1%	74,1%
A05	2624,1	1532,7	2626,5	2392	2495	4,3%	14,7%	70,7%
A06	2657	1549	2659,2	2386	2495	4,5%	14,9%	69,5%
A07	2664,1	1556,1	2666,4	2392	2495	4,3%	14,7%	70,7%
A08	2674,1	1564,6	2676,6	2398	2495	4,1%	14,5%	71,8%
A09	2697,7	1575,6	2699,9	2392	2495	4,3%	14,7%	70,8%
A10	2667,7	1560,2	2669,9	2397	2495	4,1%	14,5%	71,7%
A11	2703,4	1582,3	2705,7	2399	2495	4,0%	14,5%	72,2%
A12	2648,2	1547,6	2650,3	2395	2495	4,2%	14,6%	71,2%

Table A. 4 Volumetric properties of Cylinders from Double Drum (A)

specimen	m1 Dry Wt. (gr)	m2 Subm. Wt. (gr)	m3 Surface Dry Wt.	Bulk Density (kg/m³)	Max density (kg/m³)	Vm (%)	VMA (%)	VFM (%)
A01	1083,6	633,1	1084,1	2400	2495	3,8%	14,3%	73,2%
A02	1084,5	631,2	1085,1	2386	2495	4,4%	14,7%	70,4%
A03	1085,7	633,2	1086,2	2394	2495	4,1%	14,5%	71,9%
A04	1088	634,5	1088,5	2393	2495	4,1%	14,5%	71,9%
A05	1089,2	636,9	1089,7	2402	2495	3,7%	14,2%	73,8%

A06	1083,8	634,7	1084,2	2408	2495	3,5%	14,0%	75,0%
A07	1078,7	628,6	1079,2	2391	2495	4,2%	14,6%	71,3%
A08	1074,1	625,2	1074,7	2386	2495	4,4%	14,7%	70,5%
A09	1076,4	628,3	1076,9	2396	2495	4,0%	14,4%	72,5%
A10	1076,7	627,6	1077,2	2392	2495	4,1%	14,5%	71,5%
A11	1201,4	705,6	1202,1	2417	2495	3,1%	13,6%	77,0%
A12	1196,9	700,5	1197,5	2405	2495	3,6%	14,1%	74,4%
A13	1186,3	689,6	1185,7	2388	2495	4,3%	14,7%	70,8%
A14	1185	690,5	1187,1	2383	2495	4,5%	14,8%	69,8%
A15	1183,9	688,5	1184,7	2383	2495	4,5%	14,9%	69,7%
A16	1180,8	687,3	1181,6	2386	2495	4,4%	14,8%	70,3%
A17	1182,4	687,3	1183,2	2381	2495	4,6%	14,9%	69,4%
A18	1182,8	687,4	1183,4	2382	2495	4,5%	14,9%	69,5%
A19	1185,7	691,3	1186,3	2392	2495	4,1%	14,5%	71,6%
A20	1200,1	703,9	1200,7	2413	2495	3,3%	13,8%	76,0%
A21	1124,07	653,85	1124,85	2383	2495	4,5%	14,8%	69,9%
A22	1132,17	655,21	1133,06	2366	2495	5,2%	15,4%	66,6%
A23	1142,7	663,21	1143,85	2374	2495	4,8%	15,2%	68,1%
A24	1130,23	658,88	1131,13	2390	2495	4,2%	14,6%	71,2%
A25	1145,26	666,09	1146,7	2380	2495	4,6%	15,0%	69,2%
A26	1166,42	680,62	1167,17	2394	2495	4,0%	14,4%	72,0%
A27	1146,88	671,52	1147,73	2405	2495	3,6%	14,1%	74,4%
A28	1139,62	663,04	1140,37	2384	2495	4,4%	14,8%	70,0%
A29	1154,6	674,92	1155,32	2400	2495	3,8%	14,2%	73,3%
A30	1151,1	672,44	1151,68	2399	2495	3,9%	14,3%	73,0%

Table A. 5 Volumteric properties of Beams from Batch Plant (B)

specimen	*m1 Dry Wt. (gr)*	*m2 Subm. Wt. (gr)*	*m3 Surface Dry Wt.*	*Bulk Density (kg/m³)*	*Max density (kg/m³)*	*Vm (%)*	*VMA (%)*	*VFM (%)*
B01	2701,4	1588,2	2703,7	2418	2495	3,1%	13,6%	77,4%
B02	2690	1580	2692,6	2414	2495	3,2%	13,7%	76,5%
B03	2710,9	1592	2713,4	2414	2495	3,2%	13,7%	76,4%
B04	2829,6	1661	2831,8	2413	2495	3,3%	13,8%	76,2%
B05	2790,2	1642	2792,3	2422	2495	2,9%	13,4%	78,3%
B06	2656	1557	2658	2409	2495	3,4%	13,9%	75,2%
B07	2783	1630	2785,2	2406	2495	3,6%	14,0%	74,5%
B08	2738,7	1603	2741,8	2402	2495	3,7%	14,2%	73,6%
B09	2727,3	1609	2730	2430	2495	2,6%	13,2%	80,1%
B10	2674,5	1581	2677,4	2436	2495	2,4%	13,0%	81,7%
B11	2815,7	1653	2818,4	2413	2495	3,3%	13,8%	76,1%
B12	2780,83	1639	2783,1	2427	2495	2,7%	13,3%	79,5%

Table A. 6 Volumetric properties of Cylinders from Batch Plant (B)

specimen	*m1 Dry Wt. (gr)*	*m2 Subm. Wt. (gr)*	*m3 Surface Dry Wt.*	*Bulk Density (kg/m³)*	*Max density (kg/m³)*	*Vm (%)*	*VMA (%)*	*VFM (%)*
BB-1	1207,5	713,9	1208,6	2438	2495	2,3%	12,9%	82,2%
BB-2	1195,0	701,3	1196,1	2412	2495	3,3%	13,8%	75,9%
BB-3	1191,9	699,4	1192,6	2414	2495	3,3%	13,8%	76,3%
BB-4	1185,6	696	1187	2412	2495	3,3%	13,8%	75,8%
BB-5	1184,9	693,1	1185,7	2402	2495	3,7%	14,2%	73,8%

BB-6	1187,5	695,8	1188,3	2408	2495	3,5%	14,0%	75,0%
BB-7	1189,9	695,4	1191,7	2394	2495	4,0%	14,4%	72,1%
BB-8	1195,3	699,9	1196,4	2404	2495	3,6%	14,1%	74,2%
BB-9	1192,7	697,9	1193,6	2403	2495	3,7%	14,1%	73,9%
BB-10	1192,7	700,1	1194,1	2411	2495	3,4%	13,8%	75,7%
BB-11	1150,5636	673,5	1151,6	2404	2495	3,7%	14,1%	74,1%
BB-12	1153,5609	674,3	1154,6	2399	2495	3,9%	14,3%	73,0%
BB-13	1148,4655	670,5	1149,5	2395	2495	4,0%	14,4%	72,2%
BB-14	1144,4691	666,9	1145,5	2388	2495	4,3%	14,7%	70,9%
BB-15	1162,3529	682	1163,4	2412	2495	3,3%	13,8%	75,8%
BB-16	1158,7562	681,6	1159,8	2420	2495	3,0%	13,5%	77,8%
BB-17	1124,9866	657,4	1126	2398	2495	3,9%	14,3%	72,8%
BB-18	1138,1747	663,9	1139,2	2392	2495	4,1%	14,5%	71,5%
BB-19	1129,7823	659,4	1130,8	2394	2495	4,1%	14,5%	72,0%
BB-20	1151,0631	673,9	1152,1	2404	2495	3,6%	14,1%	74,2%
BB-21	1152,1	675,82	1153,83	2407	2495	3,5%	14,0%	74,9%
BB-22	1148,95	671,74	1150,68	2396	2495	4,0%	14,4%	72,4%
BB-23	1149,51	671,92	1150,64	2398	2495	3,9%	14,3%	72,9%
BB-24	1157,87	677,64	1158,79	2404	2495	3,7%	14,1%	74,0%
BB-25	1162,54	682,74	1163,37	2416	2495	3,2%	13,7%	76,8%
BB-26	1161,65	682,87	1163,05	2416	2495	3,2%	13,7%	76,9%
BB-27	1149,24	670,49	1150,28	2392	2495	4,1%	14,5%	71,7%
BB-28	1144,28	667,1	1145,72	2388	2495	4,3%	14,7%	70,8%
BB-29	1158,45	677,56	1160,1	2398	2495	3,9%	14,3%	72,8%
BB-30	1154,03	677,56	1155,76	2410	2495	3,4%	13,9%	75,6%

Table A. 7 Volumetric properties of Beams from Laboratory (L)

specimen	*m1 Dry Wt. (gr)*	*m2 Subm. Wt. (gr)*	*m3 Surface Dry Wt.*	*Bulk Density (kg/m³)*	*Max density (kg/m³)*	*Vm (%)*	*VMA (%)*	*VFM (%)*
L01	2799,40	1651,00	2804,26	2424	2495	2,8%	13,4%	78,8%
L02	2770,30	1631,00	2775,50	2417	2495	3,1%	13,6%	77,2%
L03	2761,30	1626,47	2768,67	2414	2495	3,2%	13,7%	76,5%
L04	2643,90	1561,38	2649,05	2428	2495	2,7%	13,3%	79,6%
L05	2719,30	1617,27	2724,67	2452	2495	1,7%	12,4%	86,2%
L06	2757,50	1638,08	2762,77	2449	2495	1,9%	12,5%	85,1%
L07	2735,70	1628,70	2748,87	2439	2495	2,2%	12,8%	82,5%
L08	2721,30	1613,93	2732,62	2429	2495	2,6%	13,2%	80,1%
L09	2874,20	1701,75	2879,93	2436	2495	2,4%	12,9%	81,8%
L10	2823,30	1671,72	2829,40	2436	2495	2,4%	13,0%	81,6%
L11	2745,80	1613,72	2751,55	2410	2495	3,4%	13,9%	75,5%
L12	2727,60	1608,80	2733,53	2422	2495	2,9%	13,5%	78,2%

Table A. 8 *Volumetric Volumetric properties of Cylinders (L)*

specimen	*m1 Dry Wt. (gr)*	*m2 Subm. Wt. (gr)*	*m3 Surface Dry Wt.*	*Bulk Density (kg/m³)*	*Max density (kg/m³)*	*Vm (%)*	*VMA (%)*	*VFM (%)*
L01	2799,40	1651,00	2804,26	2424	2495	2,8%	13,4%	78,8%
L02	2770,30	1631,00	2775,50	2417	2495	3,1%	13,6%	77,2%
L03	2761,30	1626,47	2768,67	2414	2495	3,2%	13,7%	76,5%

L04	2643,90	1561,38	2649,05	2428	2495	2,7%	13,3%	79,6%
L05	2719,30	1617,27	2724,67	2452	2495	1,7%	12,4%	86,2%
L06	2757,50	1638,08	2762,77	2449	2495	1,9%	12,5%	85,1%
L07	2735,70	1628,70	2748,87	2439	2495	2,2%	12,8%	82,5%
L08	2721,30	1613,93	2732,62	2429	2495	2,6%	13,2%	80,1%
L09	2874,20	1701,75	2879,93	2436	2495	2,4%	12,9%	81,8%
L10	2823,30	1671,72	2829,40	2436	2495	2,4%	13,0%	81,6%
L11	2745,80	1613,72	2751,55	2410	2495	3,4%	13,9%	75,5%
L12	2727,60	1608,80	2733,53	2422	2495	2,9%	13,5%	78,2%

Appendix B Details of stiffness values (Phase I)

Table B. 1 Stiffness values [MPa] (at Phase I)

T[°C]	*f[Hz]*	*SM0*	*SM30*	*SM60*	*PW30*	*PW60*	*UPG030*	*UPG060*	*UPG430*	*UPG460*
5	1	12865	14040	13734	14395	14929	14196	14851	15043	12285
	2	14019	15070	15234	15339	15766	15151	16233	16050	13049
	4	15831	16442	16832	17121	17543	16853	17820	18423	15249
	8	17422	18641	18431	18345	19522	18081	19667	19916	17728
	12	16664	18369	18505	18580	24399	19688	20038	19403	17401
10	1	8306	9463	10210	9673	10222	9816	11176	9868	9108
	2	10377	11103	11291	10980	11403	11426	13045	11417	10235
	4	11235	12504	12753	12210	12675	12917	14399	13083	11672
	8	13069	14510	14372	14073	14810	14585	15347	14916	13637
	12	14285	14934	15046	14739	15772	15778	13547	15324	13486
15	1	6010	7660	8123	7327	7873	6547	7864	6854	6372
	2	7489	8949	9288	8512	9257	7819	9022	8032	7556
	4	8995	10666	10973	10166	10559	9321	10797	9790	9186
	8	10100	12216	12632	11568	12172	10950	12521	11704	10266
	12	10650	13089	13313	11808	12936	11524	13635	12540	10471
23	1	1496	2986	3512	3318	3686	2786	3642	2917	2561
	2	2835	3682	4303	4084	4449	3457	4447	3615	3252
	4	3501	4879	5622	5220	5574	4899	5624	4741	4225
	8	5620	6066	6688	6494	6858	5708	7269	6112	5864
	12	5895	6992	7487	7510	7535	6401	8269	6884	6240
35	1	575	922	1088	1000	1095	760	1045	858	666
	2	716	1156	1378	1259	1370	984	1352	1133	897
	4	996	1497	1803	1660	2100	1293	1775	1443	1377
	8	1357	2079	2448	2230	2545	1805	2460	2051	1688
	12	1710	2482	2873	2631	2951	2105	2876	2368	1946

Appendix C Details of stiffness values (Phase II)

*Table C. 1 stiffness values [MPa] of Mixture **A***

T [°C]	***F [Hz]***	***A01***	***A02***	***A03***	***A04***	***A05***	***A06***	***A07***	***A08***	***A09***	***A10***	***A11***	***A12***	***avg***
5	1Hz	9732	10474	12200	12441	10441	11188	10030	9696	11000	11075	11800	11128	10934
	2Hz	10200	11500	13100	13500	11400	11900	11100	11400	12500	12200	13100	12200	12008
	4Hz	11500	12800	14600	15400	12800	14300	12000	12500	14000	13700	14600	13900	13508
	8Hz	13200	14000	16300	17200	13700	15300	13300	14100	15500	15500	16500	15000	14967
10	1Hz	6790	8790	7940	8890	8380	7940	7800	8400	8310	7810	8680	8190	8160
	2Hz	7750	9920	9000	9990	8780	8630	8940	9650	9180	8760	9750	9200	9129
	4Hz	8980	11500	10200	11300	10200	9750	9450	11200	10400	10200	11400	10700	10440
	8Hz	10700	13600	11600	13300	11600	11200	11200	12800	11700	11700	13300	12300	12083
15	1Hz	4810	5270	5330	5380	5420	5110	5350	5880	5300	5240	5600	5230	5327
	2Hz	5500	6200	5990	6350	6100	5900	6310	6360	6260	6100	6600	5930	6133
	4Hz	6590	6820	7180	7470	7200	6950	7320	7390	7510	6900	7650	6620	7133
	8Hz	7810	8220	8550	8960	8410	7960	8490	8890	9140	8370	9080	7970	8488
20	1Hz	2870	3050	3190	3140	3030	3130	3550	3770	3150	3020	3380	3160	3203
	2Hz	3610	3580	3890	3700	3650	3640	3940	4310	3770	3600	4090	3490	3773
	4Hz	4000	4380	4950	4480	4620	4450	4680	4930	4540	4280	4740	4440	4541
	8Hz	5210	5810	6330	5690	5680	5330	5800	6380	5540	5370	6170	5400	5726
35	1Hz	768	765	952	781	896	850	857	616	755	619	788	772	785
	2Hz	872	830	1160	856	853	930	886	740	707	763	812	915	860
	4Hz	1010	1080	1210	1120	1010	1070	1050	972	923	863	1010	958	1023
	8Hz	1090	1190	1770	1370	1220	1250	1320	1080	1290	973	1150	1110	1234

*Table C. 2 Initial stiffness values [MPa] of Mixture **B***

T [°C]	***f [Hz]***	***B01***	***B02***	***B03***	***B04***	***B05***	***B06***	***B07***	***B08***	***B09***	***B10***	***B11***	***B12***	***Bavg***
5	1Hz	14968	14733	14894	14855	16192	17059	15504	13938	13290	14244	14533	14022	14853
	2Hz	15961	15167	15854	15987	16977	18007	16951	15637	14633	15408	15725	15001	15942
	4Hz	17305	16404	17509	17295	18303	19626	18522	17523	16194	16887	17059	16422	17421
	8Hz	18791	18218	19059	18465	19574	20321	19882	19878	18074	18415	18601	17968	18937
10	1Hz	10943	10720	10413	10810	11471	12418	11283	10140	9667	10989	10574	10246	10806
	2Hz	12046	11361	11490	11977	12417	13495	12702	11714	10837	12192	11781	11202	11934
	4Hz	13032	12326	12749	12997	13482	14754	13922	13170	12168	13087	12820	12554	13088
	8Hz	14775	14212	14371	14405	15281	15858	15515	15511	14099	14887	14512	13875	14775
15	1Hz	8090	7942	7792	8008	8454	9198	8358	7512	7163	8109	7834	7610	8006
	2Hz	9213	8683	8767	9154	9531	10315	9708	8953	8376	9263	9004	8584	9129
	4Hz	10153	9591	9795	10114	10494	11484	10835	10249	9468	10342	9976	9702	10184
	8Hz	11940	11493	11535	11650	12148	12825	12547	12544	11402	12090	11736	11475	11949
20	1Hz	5257	5003	4041	5045	5635	5811	5271	4727	4502	5212	4934	5041	5040
	2Hz	6277	5587	4527	5898	6522	6665	6264	5765	5384	6071	5799	5862	5885
	4Hz	7005	6490	5342	6854	7618	7805	7355	6947	6404	7075	6757	6946	6883
	8Hz	8680	8083	6934	8195	9155	9034	8836	8834	8018	8694	8256	8196	8410
35	1Hz	963	941	920	948	1055	1090	990	889	848	941	928	864	948
	2Hz	1163	1080	1059	1139	1273	1284	1208	1113	1041	1093	1120	1055	1136
	4Hz	1305	1223	1205	1291	1507	1467	1384	1308	1207	1313	1273	1095	1298
	8Hz	1664	1570	1527	1592	1891	1754	1715	1715	1558	1594	1604	1414	1633

Table C. 3 stiffness values [MPa] of Mixture ***BB***

T [°C]	***F [Hz]***	***BB01***	***BB02***	***BB03***	***BB04***	***BB05***	***BB06***	***BB07***	***BB08***	***BB09***	***BB10***	***BB11***	***BB12***	***BBavg***
5	1Hz	12521	12370	13808	14209	12638	12987	12752	12493	12128	13526	13497	14785	13143
	2Hz	13617	13637	14693	14956	13695	13325	13408	12890	13158	14586	15235	15648	14071
	4Hz	14959	14462	15984	16609	15135	14581	14871	14015	14483	15668	16465	17254	15374
	8Hz	16606	16420	17735	18133	16674	16398	17521	15863	15976	17287	18276	19342	17186
10	1Hz	7994	8531	9163	9428	8913	8683	8755	8578	8408	9259	9294	10180	8932
	2Hz	8990	9655	10059	10240	10054	9599	9753	9377	9379	10336	10825	11119	9949
	4Hz	10277	10669	11382	11827	11126	10802	10975	10344	10472	11800	12163	12745	11215
	8Hz	11769	12241	12892	13181	12673	12363	13264	12009	11854	13543	13956	14770	12876
15	1Hz	5090	5351	5787	5955	5783	5870	5799	5681	5443	6432	6248	6843	5857
	2Hz	6116	6423	6762	6883	6661	6799	6676	6419	6373	7481	7605	7810	6834
	4Hz	6929	7452	7814	8120	7845	7772	7818	7369	7259	8623	8673	9088	7897
	8Hz	8388	9006	9338	9547	9106	9298	9748	8827	8673	10202	10373	10978	9457
20	1Hz	3494	3434	3840	3950	3898	3943	3902	3823	3801	3864	4030	4411	3866
	2Hz	4174	4350	4596	4678	4784	4614	4664	4485	4541	4489	4958	5092	4619
	4Hz	4978	5036	5439	5651	5423	5681	5562	5243	5343	5372	5849	6127	5475
	8Hz	6336	6296	6782	6934	6889	6798	7250	6566	6522	6612	7213	7632	6819
35	1Hz	919	783	943	970	721	861	787	771	869	936	948	1037	879
	2Hz	967	865	986	1004	942	921	925	890	932	995	1057	1085	964
	4Hz	1164	1073	1211	1256	1077	1038	1058	1000	1251	1158	1311	1372	1164
	8Hz	1254	1298	1366	1396	1261	1352	1381	1255	1351	1343	1475	1558	1357

*Table C. 4 Initial stiffness values [MPa] of Mixture **L***

T [°C]	***F [Hz]***	***L01***	***L02***	***L03***	***L04***	***L05***	***L06***	***L07***	***L08***	***L09***	***L10***	***L11***	***L12***	***Lavg***
5	1Hz	13325	12449	12332	13121	12925	13007	11909	12239	11665	12151	11246	13017	12449
	2Hz	15440	13499	14604	15329	14390	14202	12650	13098	12792	13338	12115	13771	13769
	4Hz	16821	15105	15589	16504	15571	16002	13642	14524	14342	14893	13555	14896	15120
	8Hz	18234	16018	16567	17045	17051	17279	14852	15772	15887	16205	14944	16221	16340
10	1Hz	10714	10000	9911	10545	10727	10614	9801	10073	9779	9860	9275	10735	10170
	2Hz	11776	11047	11510	12080	11824	11666	10393	10761	10837	10837	4946	5594	10273
	4Hz	13252	12095	12375	13100	13038	12994	11248	11975	12095	12088	11217	12328	12317
	8Hz	14813	13812	13836	14235	14634	14594	12644	13427	13774	13539	12723	13811	13820
15	1Hz	7149	6640	6598	7019	7325	7243	6692	6877	6601	6458	6169	7138	6826
	2Hz	8132	7594	7931	8323	8323	8366	7385	7646	7550	7363	6919	7864	7783
	4Hz	9393	8682	8823	9340	9403	9410	8130	8655	8617	8531	7956	8743	8807
	8Hz	11113	10311	10356	10654	11046	10970	9525	10114	9908	9989	9267	10058	10276
20	1Hz	4288	4267	4094	4354	4462	4471	4105	4218	4116	4066	3865	4470	4231
	2Hz	5089	4902	5037	5285	5352	5403	4761	4929	4996	4812	4552	5172	5024
	4Hz	6154	5865	5866	6208	6356	6363	5499	5853	6000	5705	5434	5971	5940
	8Hz	7601	7248	7176	7382	7694	7937	6765	7183	7369	7057	6723	7297	7286
35	1Hz	935	957	906	963	895	1058	899	923	992	910	899	1039	948
	2Hz	1080	1056	1077	1128	1135	1247	1058	1095	1071	1193	1052	1191	1115
	4Hz	1284	1311	1266	1338	1403	1414	1223	1299	1312	1313	1221	1337	1310
	8Hz	1572	1638	1551	1595	1738	1838	1553	1647	1772	1582	1567	1698	1646

CURRICULUM VITAE



Mohamad Mohajeri

Date of birth: 1-4-1979
Place of birth: Shar-e-Rey, Tehran, Iran
Email: mohajeri_me@yahoo.com

EDUCATIONS

- (2008-2013), PhD Candidate. Delft University of technology, Faculty of civil engineering. Section of Road and Railway engineering (Dissertation title: Hot Mix Asphalt Recycling)
- (2004–2007), M.Sc. Urban & Regional Planning, Tehran University, Tehran, Iran.
- (1998- 2003), B.Sc. Civil Engineering, Department of civil Engineering, Technical university of Khaje Nasiredin Toosi, Tehran, Iran.
- 1994-1998, High School Diploma. Bagherloloom High School. Tehran, Iran.

PUBLICATIONS

- (2014) M. Mohajeri, A.A.A. Molenaar, M.F.C. Van de Ven. "Blending of Virgin and RA Binder in Mixtures with High Amounts of RA" Book chapter in "Advances in Asphalt Materials: Road and Pavement Construction" expected publishing date: Dec of 2014, Publisher Woodhead publishing.
- (2014) A.A.A. Molenaar, M.Mohajeri, M.F.C.van de Ven. "Hot Recycled Asphalt Mixtures containing High Percentages of Reclaimed Asphalt". Proc. 9th Malaysion Road Conference. Nov. 2014, Kuala Lumpur, Malaysia
- (2014) A.A.A. Molenaar, M. Mohajeri, , M.F.C. Van de Ven. "Hot mix asphalt recycling in the Netherlands" Transportation Research CIRCULAR number E-C188, Application of Reclaimed Asphalt Pavement and Recycled Asphalt Shingles in Hot-Mix Asphalt National and International Perspectives on Current Practice, January 12, 2014 Washington, D.C." Number E-C188 October Washington, D.C.
- (2014) M. Mohajeri, A.A.A. Molenaar, M.F.C. Van de Ven. "Experimental Study into the Fundamental Understanding of Blending between Reclaimed Asphalt Binder and Virgin Bitumen using Nano-indentation and Nano-Computed Tomography", Journal of Road Material and Pavement Design (RMPD), Volume 15, Issue 2, 2014
- (2013) S. N. Nahar, M. Mohajeri, A. J. M. Schmets, A. Scarpas1, M. F. C. van de Ven, "First Observation of Blending-Zone Morphology at Interface of Reclaimed Asphalt Binder and Virgin Bitumen" Journal of the Transportation Research Board. Volume 2370 / Asphalt Materials and Mixtures 2013. Vol. 1 pages 1-9. DOI. 10.3141/2370-01

- (2013) M. Mohajeri, A.A.A. Molenaar, M.F.C. Van de Ven. "Temperature Segregation during Mixing and Laying of Asphalt Mixtures". 15th International Flexible Pavements Conference, Australian Asphalt Pavement Association (AAPA), Sept 2013, Queensland, Australia
- (2012) M. Mohajeri, A.A.A. Molenaar, M.F.C. Van de Ven. "Fundamental Study on Blending between Reclaimed Asphalt Binder and Virgin Bitumen using Nano-indentation and Nano Computed tomography' 2nd International Symposium on Asphalt Pavements and environment ISAP Fortaleza, Brazil. Oct 2012.
- (2012) M. Mohajeri, A.A.A. Molenaar, M.F.C. Van de Ven "Cracking Resistance of Recycled Asphalt Mixtures in relation to Blending of RA and Virgin Binder" 7th RILEM International Conference on Cracking in Pavements, June 20-22, 2012, Delft, Netherlands.
- (2011) M. Mohajeri, A.A.A. Molenaar, M.F.C. Van de Ven "Design of Recycled Asphalt Mixtures Using a Double Drum Mixer", The 10th Conference on Asphalt Pavements for Southern Africa 11-14 September 2011.
- (2011) M. Mohajeri, A.A.A. Molenaar, M.F.C. Van de Ven "Design of Recycled Asphalt Mixtures" .14th AAPA International Flexible Pavements Conference Sydney, 25–28 September

WORK EXPERIENCES

- (Aug 2013- Current) Head of Laboratory and R&D in Gebr. Van der Lee Road Building Contractors
- (2008-2013) PhD candidate in Delft university of technology, faculty of civil engineering and geosciences, section of Road engineering.
- (2004-2008) R&D and QC manager (part time) ,in Vima Co, Tehran, Iran.
- (2002-2003) Research engineer, in Clinic Construction Co, Tehran, Iran.
- (2001-2002) Research engineer, (part time) Vand Chimie Co, Tehran, Iran.

AWARDS

- (2013) K. B. Wood Award for the best paper in Transportation Research Board annual meeting, Washington, USA, (together with S. N. Nahar, M. Mohajeri, A. J. M. Schmets, A. Scarpas1, M. F. C. van de Ven)
- (2010) Poster prize (2nd) in12th PhD Symposium of The Research School Integral Design of Structures, 2 - 3 December 2010, Zeist, the Netherlands